Leveraging Low-Frequency Isotope Data for Modeling Catchment-Scale Transit Time Distributions

Dissertation

submitted to obtain the degree of

Doctor of Natural Sciences

(Dr. rer. nat.)

at the Faculty of

Biology, Chemistry and Earth Sciences

of the University of Bayreuth

presented by

Arianna Borriero

from Arzignano - Italy

Bayreuth, 2023

This doctoral thesis was prepared at the Department of Hydrogeology of the Helmholtz-Centre for Environmental Research from June 2020 until December 2023 and was supervised by Prof. Dr. Jan Fleckenstein.

This is a full reprint of the thesis submitted to obtain the academic degree of Doctor of Natural Sciences (Dr. rer. nat.) and approved by the Faculty of Biology, Chemistry and Geosciences of the University of Bayreuth.

Form of the thesis: cumulative thesis

Date of submission: 06.12.2023

Date of defence: 14.05.2024

Acting dean: Prof. Dr. Cyrus Samimi

Doctoral committee:

Prof. Dr. Jan Fleckenstein (reviewer)
Prof. Dr. Stefan Peiffer (reviewer)
Prof. Dr. Johanna Pausch (chair)
Prof. Dr. Efstathios Diamantopoulos

Acknowledgment

I once believed that this day would never have come. During these difficult years, I faced feelings of professional and personal worthlessness, doubting whether I could make it or even deserve a doctorate. An inner drive led me to the end of this journey, and here I am, writing these lines to express my gratitude for the exceptional support of my supervisors, colleagues, friends and family.

Jan, thank you for your valuable guidance, constant supervision, and strong support over these years, not only scientifically but also on a personal level. Rohini, thank you for your contagious enthusiasm, enduring assistance in navigating me through challenges, and firm trust in me and our work. Tam, thank you for your patient assistance and scientific and technical support, which has been crucial in the completion of my doctorate. Andreas, thank you for joining my supervision during these last months. Your outstanding contribution played an essential role in this journey. Stefanie, thank you for starting this journey with me and accompanying me later from afar. You have all been an immense pillar of support and I am extremely grateful for your supervision and the scientific passion you have conveyed.

Thanks to the entire Department of Hydrogeology for the friendships we developed, with special mention to fellow doctoral candidates for sharing happy and sad moments and for the mutual support we gave each other. Thanks to all the peers met at UFZ, in Delft, during conferences and summer schools. Exchanging similar difficulties has made me feel less lonely and wrong over the years.

Thanks to Joshua, for being my anchor and support at times when my strengths wavered. Thanks to Alessia, for making me realize what matters in life. Thanks to all my friends, near and far, for bringing a smile back to my face in the hardest moments.

Mom and Dad, thank you for always being by my side and teaching me that success is falling nine times and getting back up ten.

The most significant lesson from this doctorate goes beyond science but it regards valuable insights about life. I will apply what I have learned to shape my future.

Table of Contents

Abstract **1**

Zusammenfassung **3**

1 Introduction **7**

Introduction **7**

1.1 Addressing Water Challenges at Catchment-Scale 7

1.2 Revealing Catchment Dynamics using Transit Time Distributions 8

1.3 Significance of TTDs in Water Quality Models 9

1.4 Isotope Hydrology to Estimate TTDs 11

2 Research Question & Study Overview **13**

3 Materials & Methods **17**

3.1 Study Site 17

3.2 Data 18

3.3 StorAge Selection Functions 19

3.3.1 Parameterization and Interpolation 21

3.3.2 Young Water Fraction 22

3.3.3 Instream Nitrate Concentrations 23

4 Key Findings & Discussions **25**

4.1 Uncertainty Analysis in TTD-based Models 25

4.2 Alternative Ways to Simulate TTDs 27

4.3 Validating Nitrate-Derived TTDs Using Isotopes 28

5 Synthesis and Outlook **31**

5.1 Synthesis 31

5.2 Water Transit Time across Studies 31

5.3 Implications on Water Quality 32

5.4 Outlook 33

References **35**

Declaration of Contributions **51**

Study 1 51

Study 2 52

Study 3 52

Manuscripts **55**

Study 1 56

Supplemental Material Study 1 72

Study 2 75

Supplemental Material Study 2 88

Study 3 97

Supplemental Material Study 3 114

List of publications **123**

Abstract

Ensuring adequate water quantity and quality is essential for the well-being of both humans and ecosystems, particularly in the face of global challenges such as climate change and population growth. To this aim, it is crucial to understand how water and solutes move across rivers, lakes and groundwater at the catchment-scale. The Transit Time Distribution (TTD) of streamflow allows conceptualizing the complexity of water flow patterns within a catchment, thus revealing the catchment's functioning and export dynamics of pollutants such as nitrates (NO_3^-). While TTDs cannot usually be measured directly, they can be inferred from transport models calibrated to stable water isotope data (e.g. $\delta^{18}O$). However, the generally limited availability of high-frequency $\delta^{18}O$ data challenges global-scale analysis, encouraging the targeted use of low-frequency $\delta^{18}O$ data already available at a broader spatial coverage.

The aim of this thesis is to explore the potential of low-frequency $\delta^{18}O$ data for modeling TTDs at the catchment-scale, in order to gain insights into hydrological processes and NO_3^- export patterns. Study 1 quantifies the uncertainty in simulated TTDs resulting from different choices in spatio-temporal interpolation techniques of low-frequency $\delta^{18}O$ data and model parameterization. Study 2 proposes alternative methods for simulating TTDs making use of low-frequency $\delta^{18}O$ data, with a focus on the young water fraction, i.e. water younger than approximately three months (F_{yw}). Study 3 integrates $\delta^{18}O$ data into a NO_3^--based water quality model to enhance the simulation of TTDs.

In all studies, TTDs were modeled using StorAge Selection (SAS) functions with $\delta^{18}O$ data. Studies 1 and 3 investigated a mesoscale German catchment within the Bode River Basin, while Study 2 explored 23 sites in the same region. Monte Carlo experiments were conducted to calibrate SAS parameters and simulate TTDs. The water median transit time (TT_{50}) derived from the TTD was used as a proxy for streamflow water age, and its uncertainty was assessed with the 95% prediction uncertainty method (95PPU).

In Study 1, the impact of different methodological choices on the 95PPU of TT_{50} was investigated. This involved assessing the effect of temporal interpolation methods (step function vs. sine interpolation) and spatial representation choices (single-location vs. spatial interpolation with kriging) of precipitation $\delta^{18}O$ data, and SAS parameterizations

(time-invariant vs. time-variant functions). Sine interpolation led to both over- and underestimation of $\delta^{18}O$ data compared to the measured $\delta^{18}O$, hampering the interpretability of the resulting TT_{50}. Conversely, the step function preserved the maxima in the values of precipitation $\delta^{18}O$ data, thus likely improving the reliability of the simulated TT_{50}. Using precipitation $\delta^{18}O$ data from a single location oversimplified the representation of $\delta^{18}O$ within the catchment compared to spatial interpolation using kriging. Time-invariant functions resulted in relatively small variations in TT_{50}, while time-variant functions yielded pronounced fluctuations. The knowledge of catchment-specific water dynamics is crucial for the choice of the appropriate SAS parameterization.

In Study 2, the effect of calibrating time-invariant SAS parameters with and without F_{yw} on the 95PPU in TT_{50} was assessed. F_{yw} values were derived from fitting monthly $\delta^{18}O$ data in precipitation and streamflow with sine-waves. The F_{yw} values, exhibiting large variability among the study sites (0.02 - 0.26), had different effects on reducing the 95PPU. Catchments releasing more young water ($F_{yw} \geq 0.10$) experienced an effective reduction in the 95PPU, while catchments discharging less young water ($F_{yw} \leq 0.05$) had a more moderate reduction in the 95PPU. Consequently, F_{yw} values significantly improved the predictability of TTD-based models, especially in catchments with a tendency towards young water release.

In Study 3, three different targets — instream NO_3^-, $\delta^{18}O$ and both datasets — were employed to calibrate SAS parameters and understand their impacts on the 95PPU of TT_{50}. A relatively similar pattern of simulated TT_{50} was observed across the different targets, suggesting that NO_3^- and $\delta^{18}O$ data hold comparable information to describe transport processes. While calibration to NO_3^- led to a greater 95PPU of TT_{50} and parameter equifinality, calibration to both datasets enhanced parameter identifiability and reduced the 95PPU. Consequently, the inclusion of $\delta^{18}O$ data enhanced the description of hydrological transport in the NO_3^- model.

In summary, these studies leveraged the high spatial coverage of low-frequency isotope data to enhance the understanding of TTDs of streamflow in the absence of high-frequency measurements. This thesis quantified challenges (Study 1) and highlighted opportunities (Study 2) related to the use of low-frequency isotopic measurements and integrated them into water quality modeling (Study 3) to improve the representation of hydrological, thus NO_3^- transport. Overall, this work advocates a shift in perspective from "how could we obtain more data?" to "what meaningful insights can be derived from existing data?" until more comprehensive datasets become available. This step is crucial for advancing current and future challenges in water quantity and quality-related research and management, particularly relevant given the escalating extremes in climate conditions and the rising water pollution in the era of global change.

Zusammenfassung

Die Sicherstellung einer ausreichenden Wassermenge und -qualität ist von entscheidender Bedeutung für das Wohlergehen von Menschen und Ökosystemen, insbesondere angesichts globaler Herausforderungen wie Klimawandel und Bevölkerungswachstum. Daher ist es wichtig zu verstehen, wie sich Wasser und gelöste Stoffe in Flüssen, Seen und Grundwasser auf der Einzugsgebietsebene bewegen. Die Transitzeitverteilung (TTD) von Wasser im Fluss ermöglicht es, die Komplexität von Fließwegen innerhalb eines Einzugsgebiets und somit seine Funktionsweise sowie die Dynamik des Schadstoffaustrags, zum Beispiel von Nitrat (NO_3^-), zu beschreiben. TTDs können nicht direkt gemessen werden, sondern erfordern eine Modellierung mit Hilfe von Tracerdaten wie stabilen Wasserisotopen (z. B. $\delta^{18}O$). Die begrenzte Verfügbarkeit von zeitlich hochaufgelösten $\delta^{18}O$-Daten stellt jedoch eine Herausforderung für globale Analysen dar, was den gezielten Einsatz von niederfrequenten $\delta^{18}O$-Daten mit größerer räumlicher Abdeckung nahelegt.
Ziel dieser Arbeit ist es, das Potenzial niederfrequenter $\delta^{18}O$-Daten zur Modellierung von TTDs auf Einzugsgebietsebene zu untersuchen, um Erkenntnisse in hydrologische Prozesse und NO_3^--Exportmuster zu gewinnen. Studie 1 quantifiziert die Unsicherheit in den simulierten TTDs, die sich aus der Wahl der räumlichen und zeitlichen Interpolationsverfahren für die $\delta^{18}O$-Daten und der Modellparametrisierung ergeben. In Studie 2 werden alternative Methoden zur Simulation von TTDs mit niederfrequenten $\delta^{18}O$-Daten vorgestellt, indem der Anteil jungen Wassers (F_{yw}), d. h. Wasser, das jünger als drei Monate ist, Anwendung findet. In Studie 3 werden $\delta^{18}O$-Daten in ein NO_3^--basiertes Wasserqualitätsmodell integriert, um die Simulationen von TTDs zu verbessern.
In allen Studien wurden TTDs mit Hilfe von StorAge Selection (SAS) Funktionen mit niederfrequenten $\delta^{18}O$ Daten modelliert. Die Studien 1 und 3 untersuchten ein mesoskaliges deutsches Einzugsgebiet im Einzugsgebiet der Bode, während Studie 2 23 Standorte in derselben Region untersuchte. Es wurden Monte-Carlo-Experimente durchgeführt, um die SAS-Parameter zu kalibrieren und die TTDs zu simulieren. Der Median der Verweilzeitverteilung (TT_{50}), abgeleitet aus der TTD, wurde als Indikator für das Alter des Wassers im Fluss verwendet, und Unischerheiten wurde mittels einer 95%-Vorhersageunsicherheit (95PPU) bestimmt.

In Studie 1 wurden die Auswirkungen verschiedener methodischer Entscheidungen auf die 95PPU von TT_{50} untersucht, indem Methoden der zeitlichen Interpolation der δ^{18}O-Daten (Stufenfunktion vs. Sinusinterpolation), und der räumlichen Repräsentation von Niederschlagsdaten (Einzelstandort vs. räumliche Interpolation mit Kriging) und der SAS-Parametrisierungen (zeitlich konstante vs. variable Funktionen) bewertet wurden. Die Sinusinterpolation führte sowohl zu über- als auch zu unterschätzten δ^{18}O-Werten im Vergleich zu den gemessenen Werten, was die Interpretierbarkeit der resultierenden TT_{50} beeinträchtigte. Die Stufenfunktion gibt die Maxima in den gemessenen δ^{18}O-Daten exakt wieder, was die Verlässlichkeit des simulierten TT_{50}-Wertes verbesserte. Die Verwendung von δ^{18}O-Niederschlagsdaten eines einzigen Standorts vereinfachte die Repräsentation von δ^{18}O-Werten innerhalb des Einzugsgebiets im Vergleich zur räumlichen Interpolation mittels Kriging zu stark. Zeitlich konstante SAS-Funktionen führten zu relativ geringen Schwankungen von TT_{50}, während zeitlich variable Funktionen zu großen Schwankungen führten. Die einzugsgebietsspezifische Funktionsweise ist daher entscheidend für die Wahl einer geeigneten SAS-Parametrisierung.
In Studie 2 wurde der Effekt einer Kalibrierung zeitlich konstanter SAS-Parameter mit und ohne F_{yw} auf die Unsicherheit in TT_{50} bewertet. Die F_{yw} wurden aus der Interpolation monatlicher δ^{18}O-Daten in Niederschlag und Abfluss mit Sinuswellen abgeleitet. Die F_{yw}-Werte, mit großer Variabilität zwischen den Untersuchungsstandorten (0,02-0,26), hatten unterschiedliche Auswirkungen auf die Verringerung der 95PPU. Einzugsgebiete mit viel jungem Wasser ($F_{yw} \geq 0{,}10$) erfuhren eine effektive Reduzierung des Unsicherheitsintervalls, während Einzugsgebiete mit weniger jungem Wasser ($F_{yw} \leq 0{,}05$) eine moderatere Reduzierung des Unsicherheitsintervalls aufwiesen. Dies unterstreicht die Bedeutung größerer F_{yw}-Werte für eine deutliche Verringerung der Unsicherheit von TT_{50} und die Verbesserung von TTD-basierten Modellen.
In Studie 3 wurden drei verschiedene Zielgrößen - NO_3^-, δ^{18}O und beide Datensätze gleichzeitig – zur Kalibrierung der SAS-Parameter verwendet, um die Auswirkungen auf die 95PPU von TT_{50} zu verstehen. Es wurde ein relativ ähnliches Muster der simulierten TT_{50} für die verschiedenen Zielgrößen beobachtet, was darauf hindeutet, dass NO_3^-- und δ^{18}O-Daten vergleichbare Informationen zur Beschreibung von Transportprozessen enthalten. Die Kalibrierung nur mit NO_3^- führte jedoch zu einer größeren Unsicherheit und Parameteräquifinalität. Die Kalibrierung mit beiden Datensätzen hingegen verbesserte die Identifizierbarkeit der Parameter und reduzierte die 95PPU. Folglich verbesserte die Berücksichtigung von δ^{18}O-Daten die Beschreibung des hydrologischen Transports im NO_3^--Modell.
Insgesamt nutzte diese Arbeit die große räumliche Abdeckung von Niederfrequenz-Isotopendaten, um das Verständnis von TTDs in Einzugsgebieten zu verbessern, wenn

Hochfrequenzdaten fehlen. In dieser Arbeit wurden die Herausforderungen quantifiziert (Studie 1) und die Chancen hervorgehoben (Studie 2), die mit der Verwendung von niederfrequenten Isotopenmessungen und ihrer Integration in die Wasserqualitätsmodellierung verbunden sind (Studie 3), um die Darstellung des hydrologischen Transports und damit des NO_3^--Transports zu verbessern. Allgemein plädiert diese Arbeit für einen Perspektivwechsel von "Wie könnten wir mehr Daten bekommen?" zu "Welche sinnvollen Erkenntnisse lassen sich aus den vorhandenen Daten ableiten?", bis umfassendere Datensätze zur Verfügung stehen. Dieser Ansatz ist, von entscheidender Bedeutung für die Bewältigung aktueller und zukünftiger Herausforderungen in der Forschung und Bewirtschaftung im Zusammenhang mit der Wassermenge und -qualität. Dies ist besonders wichtig angesichts der zunehmenden extremeren klimatischen Bedingungen und der zunehmenden Wasserverschmutzung im Zeitalter des globalen Wandels.

Chapter 1

Introduction

1.1 Addressing Water Challenges at Catchment-Scale

Sufficient water quantity and good water quality are crucial for the well-being of humans and ecosystems. Adequate water supply is essential for all living forms (Berghuijs et al., 2014; Seager et al., 2007) while ensuring safe water is critical to prevent deficiencies in water quality (Onda et al., 2012). Maintaining these aspects below critical levels is fundamental, otherwise the crossing of natural planetary boundaries is at risk (Steffen et al., 2015), causing harmful consequences for human health and the aquatic ecosystem (Diaz and Rosenberg, 2008; Jenny et al., 2020; Vörösmarty et al., 2010). To avoid these adverse situations, it is necessary to prioritize water resources protection and management to ensure good conditions in terms of water quantity and quality (European Environment Agency et al., 2018, 2021). In this regard, various regulations, such as the Water Framework Directive of the European Union, have been established to address several water management objectives by guaranteeing both qualitative and quantitative aspects of water resources (EU, 2000). Despite these efforts, the global water crisis, driven by climate change and human population growth, still poses significant challenges (Vitousek et al., 1997; Jury and Vaux, 2007).

To comprehensively address water challenges, it is necessary to not only quantify water volume but also explore how water moves through terrestrial landscapes, including rivers, lakes and groundwater. This knowledge is essential for gaining hydrological insights related to the transport of substances such as pollutants, sediments, and nutrients (Hrachowitz et al., 2016; Kirchner et al., 2000). However, an appropriate spatial scale is needed to explore these hydrological processes, and the catchment-scale offers a practical

perspective to gain the fundamental knowledge needed for effective water management and protection strategies (Sivapalan, 2006; Wagener et al., 2007).
A catchment is defined as the landscape element routing all precipitation water toward a specific location, which is typically the outlet of a stream network. However, only a portion of the precipitation that falls reaches the outlet and contributes to the streamflow because processes such as tree canopies, evaporation of water that settles on the surface and plant transpiration can reduce the amount of precipitation that reaches the stream network. Precipitation that is not affected by these processes is called effective precipitation, and it can take different routes through distinct flow paths within the catchment before contributing to the streamflow (McGuire and McDonnel, 2006). The generation of such flow paths depends on the catchment's heterogeneity in terms of geology, topography, wetness conditions, hydraulic soil properties and vegetation index (McGuire et al., 2005). For example, water may travel rapidly through macropores in wet and shallow soils formed via root holes or cracks (Tromp-van Meerveld and McDonnell, 2006), and slowly through dry soil, thus facilitating deep flow paths that reach the groundwater (Jasechko et al., 2016). These flow paths, once generated, significantly influence the overall export of solutes from the catchment.
Understanding these complex dynamics within a catchment is a primary concern for hydrologists. Nonetheless, the inherent complexity of catchments poses challenges for an accurate understanding of water movement. Therefore, a practical tool is needed to effectively conceptualize water transport processes at the catchment-scale.

1.2 Revealing Catchment Dynamics using Transit Time Distributions

The water transit time (TT) of streamflow is a valuable tool for gaining insights into the catchment-scale hydrological behavior. TT of streamflow represents the time elapsed from the entry of a water parcel into the catchment through precipitation to its exit via streamflow, thus informing on the duration that water parcels spend within the catchment. As such, TT allows for the understanding of runoff generation processes (Hrachowitz et al., 2016), the contact time of water with the soil matrix which influences biogeochemical reactions (McClain et al., 2003), and the hydrological connectivity within the catchment (Jencso et al., 2009). Even more crucial metric is the transit time distribution (TTD) of streamflow, which effectively represents the entire spectrum of TTs in streamflow, offering an ensemble view of water parcels at the catchment outlet (Botter et al., 2010; Rinaldo et al., 2011; van der Velde et al., 2012).

While early studies have often assumed time-invariant TTDs for steady-state systems (Rinaldo et al., 2006), experiments have shown that TTDs are time-variant due to the variability in meteorological forcing (Botter et al., 2010; Hrachowitz et al., 2010; Heidbüchel et al., 2020) and the activation and/or deactivation of flow paths in response to varying hydrological conditions (Ambroise, 2004; Heidbüchel et al., 2013). Time-variant TTDs of streamflow can be classified either as "backward" or "forward" depending on whether they refer to the time water parcels have entered the catchment as precipitation or have left the catchment as streamflow (Benettin et al., 2015a). Backward distributions are more commonly used in hydrological studies as they provide insights into the streamflow age by quantifying the contribution of past precipitation to a water sample collected at the outlet at a specific time (Botter et al., 2011; Harman, 2015; van der Velde et al., 2012). Similar to TTD, the residence time distribution (RTD) describes the age distribution of water currently stored within the catchment. TTD and RTD are identical only when the composition of streamflow matches that of the water in storage, a condition often referred to as "well-mixed".

A fundamental challenge with TTD applications is that TTDs are not directly measurable quantities in the real world, but they require estimation with some modeling approaches. In recent years, StorAge Selection (SAS) functions have emerged as an innovative approach to represent the relationship between TTDs and RTDs, and estimating time-variant TTDs based on non-stationary assumptions (Botter et al., 2011; van der Velde et al., 2012; Rinaldo et al., 2015). SAS functions play a crucial role in characterizing whether a catchment tends to discharge streamflow composed of young water (i.e. water entered the catchment as precipitation recently) or old water (i.e. water entered the catchment as precipitation a long time ago). This knowledge is crucial for inferring water ages in streamflow, thus providing modelers with a novel framework for simulating TTDs. SAS functions approach has proven effective in simulating TTDs and water release dynamics across various settings, including lysimeters (Asadollahi et al., 2020, 2022; Kim et al., 2016), hillslopes (Kim et al., 2022; Kim and Harman, 2022; Pangle et al., 2017), lakes (Smith et al., 2018) and at the catchment-scale (Benettin et al., 2015b, 2017a; Harman, 2015).

1.3 Significance of TTDs in Water Quality Models

Due to the link between hydrology and biogeochemistry (Hrachowitz et al., 2016), the significance of TTDs and SAS functions goes beyond their role in understanding water quantity. They also offer valuable insights into the export of instream dissolved solutes, thereby playing a key role in water quality modeling (Cirmo and McDonnell, 1997). The

incorporation of TTDs into water quality models advances the representation of solute transport as TTDs allow for the quantification of velocity, i.e. the actual water speed, as opposed to celerity, i.e. the speed of a pressure pulse (Ilampooranan et al., 2019). This distinction is crucial given that TTDs and water velocities provide meaningful information about the actual distribution of flow paths in a catchment, beyond hydrology's traditional focus on the typically pressure-driven hydrologic response and hydrograph. Consequently, TTD-based water quality models are promising in simulating dissolved solutes in catchments and predicting future solute trajectories under changing climate and land use (Beck, 1987).

A central focus within water quality models is nitrogen (N). While N is essential for living organisms, it represents a significant source of diffuse water pollution largely due to the excessive use of fertilizers and manure in agriculture (Bouraoui and Grizzetti, 2014; Galloway et al., 2004). Microbial processes in the soil play a crucial role in converting organic and inorganic N compounds into nitrate (NO_3^-), which is a harmful water pollutant (Erisman et al., 2013). Elevated NO_3^- concentration threats water quality, making it unusable for drinking purposes, and harms the aquatic ecosystem (Abbott et al., 2019; Knobeloch et al., 2000; Le Moal et al., 2019; Smith, 2003). Despite efforts such as the Nitrate Directive of the European Union to reduce fertilizer application (EU, 1991), high NO_3^- concentration persists in surface water and groundwater (Bodirsky et al., 2014; Bouraoui and Grizzetti, 2014), partly due to legacy effects resulting from the accumulation of N in the subsurface and long TTs of NO_3^- through the catchment (Van Meter and Basu, 2017). This situation causes time lags in NO_3^- concentration between diffuse and point-source N inputs and the NO_3^- at the catchment outlet (Meals et al., 2010). Consequently, there is a gap between implemented measures aimed at reducing NO_3^- concentrations and actual improvements, which calls for further actions to enhance water quality status (Basu et al., 2022).

Denitrification is the primary process responsible for the permanent removal of NO_3^- in water, involving the conversion of NO_3^- to gaseous N by bacteria (Burgin and Hamilton, 2007). This biogeochemical reaction is crucial for the natural attenuation of NO_3^- pollution. Denitrification is significantly influenced by the duration water remains in contact with the soil matrix, as prolonged contact yields more efficient denitrification (McClain et al., 2003). Therefore, simulating TTDs and water ages plays a key role in understanding NO_3^- removal via denitrification. This knowledge is essential for implementing effective NO_3^- management strategies (Cirmo and McDonnell, 1997; Kumar et al., 2020) and understanding time delays in NO_3^- transport within catchments (Van Meter et al., 2018).

1.4 Isotope Hydrology to Estimate TTDs

Modeling TTDs using SAS functions for applications in water quantity and quality does not follow a direct modeling approach. Instead, TTDs are derived through inverse modeling, meaning that they are estimated using tracer concentrations observed in the streamflow. Tracer concentrations serve as calibration constraints for SAS model parameters, and once these parameters are calibrated, they can be employed to estimate TTDs. Therefore, measurements of tracer concentrations that parameterize TTD-based models play a crucial role in overcoming equifinality issues typical of modeling (Beven, 2006).

Common tracers used to infer TTDs are stable water isotopes, which are atoms of the same element with different amounts of neutrons in their nucleus. Stable water isotopes are naturally occurring in the water cycle, thereby they provide valuable insights into hydrological water transport (Jasechko, 2019). Key stable water isotopes include hydrogen (e.g. ^{1}H and ^{2}H) and oxygen (e.g ^{16}O and ^{18}O), which are conservative tracers as they do not react. Stable water isotopes are commonly represented as isotopic ratios such as ^{1}H/^{2}H and ^{16}O/^{18}O. The deviation of these isotopic ratios in a given sample from the Vienna Standard Mean Ocean Water, an international standard established by the International Atomic Energy Agency, provides values of δ^{2}H and δ^{18}O. These values are referred to as signatures of stable water isotopes of hydrogen and oxygen, respectively, and are typically used in hydrological applications.

Stable water isotope analysis involves utilizing mass spectrometry on water samples collected from precipitation and streamflow (Ghosh and Brand, 2003). Recognizing the critical role of samples in hydrology (Beven, 2006), effective modeling of TTDs requires well-executed spatial and temporal collection of water samples since water and solute export dynamics are reflected in the measured sampled data. The impact of sampling frequency and length of tracer data time series on understanding the catchment's hydrological behavior has been widely discussed (McGuire and McDonnel, 2006; Benettin et al., 2022). However, one of the primary challenges to date is the lack of extensive sampling campaigns with an appropriate spatial distribution that span over decades at a high frequency (e.g. daily or sub-daily) as these campaigns encounter limitations due to cost and logistical constraints (von Freyberg et al., 2022). While some well-equipped catchments, such as the Bode region in Germany (Wollschläger et al., 2017) and the Plynlimon in Wales (Neal et al., 2013), have abundant data, the majority of catchments worldwide lack sufficient historical data due to limited monitoring instrumentation (Tetzlaff et al., 2018). Low-frequency isotope measurements are therefore more widely available on a global scale compared to high-frequency data.

To overcome challenges in less-equipped catchments, strategies for estimating TTDs include reconstruction in space of stable water isotope data in precipitation from nearby monitoring stations (Bowen and Revenaugh, 2003). This method is also valuable for enhancing the understanding of ungauged basins (Hrachowitz et al., 2013; Seibert and Beven, 2009; Soulsby and Tetzlaff, 2008). Additionally, strategies for reconstructing stable water isotope data over time involve using temporal smoothing functions (Allen et al., 2019; Buzacott et al., 2020) to capture typical seasonal isotopic variations driven by temperature changes, i.e. more negative (or positive) values of stable water isotope signatures in winter (or summer). An approach to infer specific aspects of the TTD from low-frequency stable water isotope data involves the concept of the young water fraction (F_{yw}), representing the proportion of streamflow with a TT younger than approximately 2–3 months (Kirchner, 2016*a*). F_{yw} is derived from the ratio of seasonal isotopic amplitudes in precipitation and streamflow and can be estimated from sparsely sampled stable water isotopes covering 2-3 years only (Benettin et al., 2022). Serving as a robust descriptor under spatially heterogeneous and non-stationary conditions (Kirchner, 2016*b*), F_{yw} is a proxy for fast hydrological behavior and rapid solute transport dynamics (Benettin et al., 2017b). Consequently, F_{yw} has been widely applied for water age quantification and catchments inter-comparison (Jasechko et al., 2016).

To date, datasets on F_{yw} (Jasechko et al., 2016) and stable water isotope (Allen et al., 2019) are gradually expanding. Additionally, the European Union's COST Action WATSON (https://watson-cost.eu/, last access: 16-10-2023) is building a comprehensive database containing stable isotope data collected in Europe, to simplify future searches for users of existing datasets. Despite these initiatives to improve the availability of stable water isotope data, the wider global accessibility of low-frequency measurements, compared to high-frequency stable water isotope data, suggests that researchers and water managers should leverage the use of low-frequency data to address the limitations of missing intense monitoring campaigns. Currently, further efforts are needed to explore the benefits of low-frequency data in the context of TTD-based modeling. Understanding how to strategically employ low-frequency stable water isotopes in modeling applications related to water quantity and quality is crucial for decision-making in the water resources and NO_3^- management until more complete datasets become available. This objective requires a shift in perspective from "how could we obtain more data?" to "what meaningful insights can be derived from existing data?".

Chapter 2

Research Question & Study Overview

Stable water isotopes are crucial in catchment-scale transport models and the subsequent estimation of TTDs. However, limited access to high-frequency sampling in many areas worldwide has led to the more global accessibility of low-frequency stable water isotope data. Considering such context, this thesis addresses the question:
Can low-frequency stable water isotope data provide valuable insights into catchment-scale TTDs?
To answer this question, a dataset of δ^{18}O time series covering a few years at monthly frequency was employed across all three studies in this thesis. While Studies 1 and 3 focused on a mesoscale catchment, Study 2 expanded its analysis to multiple contrasting catchments. Each study contributes to the overarching objective of understanding TTDs using low-frequency δ^{18}O data, although they explore distinct aspects, such as challenges and opportunities related to the use of coarse datasets of δ^{18}O. The specific sites, data and methodologies of each study are summarized in Figure 1 and further detailed in the following, providing a comprehensive overview of the individual aims and analytical approaches.

In Study 1, I converted low-frequency measured δ^{18}O data in precipitation into high-frequency time series to meet specific modeling requirements. Additionally, δ^{18}O data in precipitation were collected at different locations. While these δ^{18}O data served as input time series for model simulations, the conversion from low to high-frequency and variation in collection locations can introduce uncertainty in the simulated TTDs. To explore this uncertainty, I developed two contrasting techniques for both the temporal reconstruction and the spatial representation of δ^{18}O data in precipitation. For the reconstruction of high-frequency temporal data, one technique captured the typical δ^{18}O seasonality, while the other emphasized individual δ^{18}O measurements. Regarding

Dissertation	Study	Site	Data	Methods
Leveraging Low-frequency Isotope Data For Modeling Catchment-scale Transit Time Distributions	*Uncertainty in Water Transit Time Estimation with StorAge Selection Functions and Tracer Data Interpolation*	Mesoscale catchment	• P, Q and ET timeseries • $\delta^{18}O$ measurements in P and Q	• SAS functions • Spatio-temporal interpolations • TTDs
	Can the Young Water Fraction Reduce Predictive Uncertainty in Water Transit Time Estimations?	Multiple mesoscale and headwater catchments	• P, Q and ET timeseries • $\delta^{18}O$ measurements in P and Q	• SAS functions • TTDs • F_{yw}
	The Value of Instream Stable Water Isotope and Nitrate Concentration Data for Calibrating a Travel-Time based Water Quality Model	Mesoscale catchment	• P, Q and ET timeseries • $\delta^{18}O$ measurements in P and Q • NO_3^- measurements in Q	• SAS functions • TTDs • Da number

Figure 1: Study design of the thesis and the three studies it comprises. P, Q and ET are precipitation, streamflow and evapotranspiration, respectively; SAS functions refer to the StorAge Selection functions; TTDs represent the transit time distributions; F_{yw} is the young water fraction; and Da stands for the Damköhler number.

the spatial representation of $\delta^{18}O$ data in precipitation, I considered collection at a single location and multiple locations within the catchment. Thorough a comprehensive uncertainty analysis, I compared the simulated TTDs of a mesoscale catchment using these two temporal interpolation and spatial representation techniques for $\delta^{18}O$ data. The goal was to gain a deep understanding of how choices in model input data can impact the simulated TTDs. Ultimately, I examined the implications the implications of these choices for studies related to water quantity and quality.

In Study 2, I presented a novel method to constrain model parameters for simulating TTDs by leveraging the use of the F_{yw}. This approach differs from the traditional calibration methods for TTD-based model parameters, which typically involve calibration against a time series of instream tracer data. Specifically, I calculated values of F_{yw} across diverse catchments from the fitting of seasonal cycles observed in low-frequency $\delta^{18}O$ data in precipitation and streamflow collected for 2-3 years. By calibrating the parameters against F_{yw} values, I aimed to determine whether F_{yw} values could help constrain SAS parameters and the simulation of TTDs. I tested the effectiveness of F_{yw} as a calibration tool for TTDs through a "proof of concept" experiment by using time series of instream $\delta^{18}O$ data. Furthermore, I ranked the analyzed catchments based on the efficiency of F_{yw} in constraining model parameters and deriving TTDs. With this study, I contributed to advancing the understanding of the hydrological functioning and water quality status in the study catchments by employing a new calibration technique,

which proved especially beneficial when dealing with limited availability of tracer data.

In Study 3, I further expanded my investigations into water quality by simulating TTDs through the calibration of model parameters with reactive solute concentrations, specifically NO_3^-. While NO_3^- concentrations offer insights into both biogeochemical and transport mechanisms, $\delta^{18}O$ data provide more accurate information about hydrological transport and TTDs due to their nature as conservative tracers. In other words, relying solely on model parameters calibrated against NO_3^- concentrations can lead to an inaccurate representation of TTDs, as the calibration may be affected by potential interactions and compensations between transport and reaction-related parameters inherent within the model. To evaluate the suitability of NO_3^- concentrations for informing about water transport and TTDs, I separately validated TTDs using low-frequency $\delta^{18}O$ data as a means to infer transport processes. With this work, I contributed valuable insights into the interplay between hydrological transport and biogeochemical reactions within the study catchment and explored whether the integration of stable water isotopes in water quality models for NO_3^- is beneficial.

Within this thesis, Studies 1 and 2 collectively address challenges and opportunities posed by low-frequency isotopic measurements, by employing numerical modeling, data reconstruction, model calibration with traditional and alternative procedures, uncertainty analysis, and statistical techniques for catchment classification. On the other hand, Study 3 employs numerical modeling not only to understand hydrological processes but also biogeochemical reactions, specifically NO_3^- removal via denitrification. This thesis aims to provide insights into the use of low-frequency isotope data and it encourages researchers to maximize their utility in understanding TTDs for tackling the absence of high-frequency measurements. The ultimate goal is to enhance the understanding of catchment functioning in order to foster catchment-scale water and NO_3^- management strategies despite limited isotope data.

Chapter 3

Materials & Methods

3.1 Study Site

The study sites of this thesis are located in the Bode River Basin, a mesoscale catchment with an area of 3,178 km^2 at Staßfurt gauging station (Fig. 2). The Bode River Basin drains into the Elbe River and represents a well-studied area integrated within the TERENO (TERrestrial ENvironmental Observatories; Wollschläger et al. 2017) network of the Helmholtz Association. Specifically, both Studies 1 and 3 focus on the mesoscale Upper Selke catchment situated in the southern part of the Bode River Basin (Fig. 2). On the other hand, Study 2 extends its spatial scale to include 22 additional diverse catchments located within the region (Fig. 2).

The Bode region extends from the Harz Mountains to the Central German Lowlands, thereby the study catchments are characterized by high diversity in size, land use, vegetation, soil, geology and climate. The size of the catchments ranges between 0.11 km^2 and 200 km^2, without considering the Bode catchment at Staßfurt. The altitude varies from 14 to 1139 m above mean sea level (m.a.s.l.), while the mean slope ranges from 2% to 19%. The headwater region is largely dominated by coniferous and broadleaf forests, while the lowland areas are mainly used for agriculture. The soil consists of Cambisols, Luvisols, Leptosols and Gleysols in the Harz Mountains, and Chernozems in the central lowland (Wollschläger et al., 2017). The geology is characterized by Palaeozoic rocks in the mountainous catchments (Frühauf and Schwab, 2008), whereas the lowlands are dominated by Mesozoic and late Palaeozoic rocks covered by Tertiary and Quaternary sediments (Schuberth, 2008). Geological composition in the Harz Mountains results in a shallow groundwater system with relatively fast flow paths, while deep sedimentary aquifers dominate the lowland region (Yang et al., 2018).

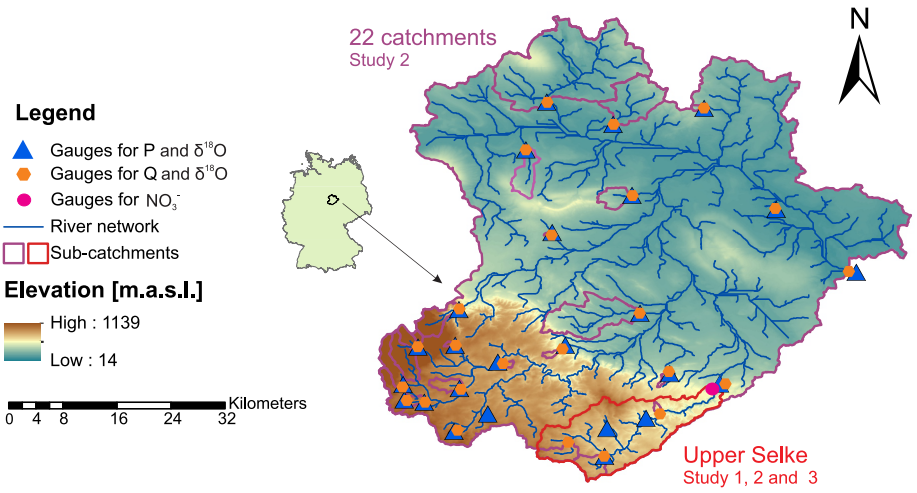

Figure 2: Bode region with its catchments (red polygon for Studies 1, 2 and 3, purple polygons for Study 2), sampling points for precipitation and $\delta^{18}O$ in precipitation (blue triangles), sampling points for streamflow and $\delta^{18}O$ in streamflow (orange hexagons), sampling points for NO_3^- in streamflow (pink dots), the river network (blue lines) and the elevation gradient in meters above sea level (colored map). The location of the Bode region in Germany is shown in the center.

3.2 Data

In well-studied catchments, such as those in the Bode River Basin, extensive data from various sources and studies have contributed to a substantial amount of knowledge (Dupas et al., 2017; Musolff et al., 2021; Nguyen et al., 2021, 2022; Yang et al., 2018; Winter et al., 2021, 2022). This thesis uses a dataset that is described in the following.

At all gauging stations of the study catchments, daily precipitation (P) and actual evapotranspiration (ET) time series from 2013 to 2022 were supplied by the German Weather Service (DWD). On the other hand, daily streamflow (Q) time series from 2013 to 2022 were provided by the State Office of Flood Protection and Water Management of Saxony-Anhalt (LHW). For catchments with incomplete continuous measurements during the study period, daily Q and ET time series were simulated using the mesoscale Hydrologic Model (mHM; Kumar et al. (2013); Samaniego et al. (2010); Zink et al. (2017)). Time series of Q and ET were calibrated and evaluated from multiple stations in the Bode region (Mueller et al., 2016). Average annual P, ET and Q across the study sites were 795 (542 - 1311), 610 (494 - 802) and 202 (52 - 601) mm, respectively, with the mountainous catchments experiencing higher annual P and Q than the lowland area.

Monthly oxygen isotope data ($\delta^{18}O$) for precipitation and streamflow from 2013 to 2015 were taken from Lutz et al. (2018). Streamflow $\delta^{18}O$ data were grab samples collected at the catchments' outlet mainly during non-event flow conditions, while precipitation $\delta^{18}O$ data were sampled at different locations in the Bode region (Fig. 2). Precipitation $\delta^{18}O$

data were subsequently spatially interpolated using kriging with altitude as external drift and weighted with spatially distributed monthly precipitation specific to each catchment, to obtain values of $\delta^{18}O$ in precipitation representative of the entire catchment. Lastly, daily instream NO_3^- concentration from 2013 to 2022 was obtained from a water quality sensor operated by the Helmholtz - Centre for Environmental Research, using an in-situ UV-VIS-based probe. In Figure 3, the time series of hydroclimatic, tracer and solute data is presented for the Upper Selke as an illustrative example. More detailed information on the datasets can be found in Studies 1, 2 and 3.

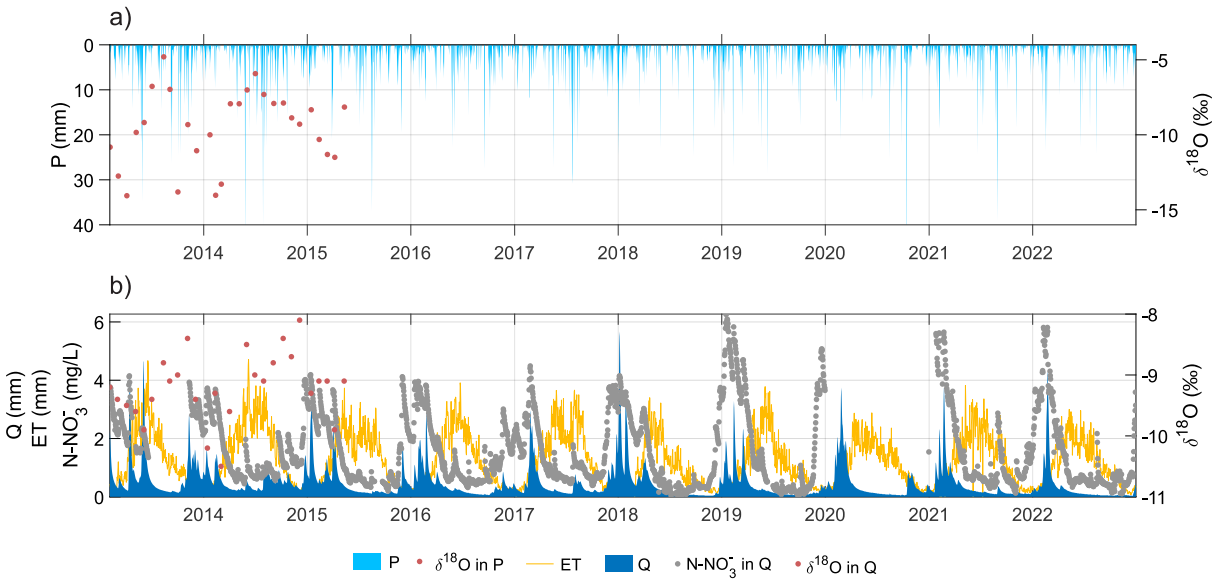

Figure 3: Time series of (a) precipitation and $\delta^{18}O$ data in precipitation, and (b) actual evapotranspiration, streamflow, NO_3^- and $\delta^{18}O$ data in streamflow in the Upper Selke catchment.

3.3 StorAge Selection Functions

The overall research design of this thesis is based on the modeling framework of the StorAge Selection (SAS) functions (Botter et al., 2011; Rinaldo et al., 2015; van der Velde et al., 2012), which represent a novel approach for simulating time-variant TTDs. The peculiarity of the SAS functions lies in their ability to relate the water age distribution in storage and outflows. For example, considering a catchment where new water (i.e. precipitation) enters, while some water, that entered the system earlier, leaves (i.e. streamflow and evapotranspiration), all the water remaining in the catchment can exhibit a wide range of water ages. This allows the expression of each water parcel in the system with a water age balance, a reinterpretation of the mass balance, describing the evolution of the water depending on inputs, outputs and aging (Benettin et al., 2022). SAS functions play

a crucial role in this water age balance as they represent statistical summaries describing how the water within the catchment contributes to streamflow or evapotranspiration. The water age balance with the SAS functions is expressed as (Botter et al., 2011; Harman, 2015; van der Velde et al., 2012):

$$\frac{\partial S_T(T,t)}{\partial t} + \frac{\partial S_T(T,t)}{\partial T} = P(t) - Q(t) \cdot \Omega_Q(S_T,t) - ET(t) \cdot \Omega_{ET}(S_T,t) \tag{3.1}$$

where P(t) [L^3T^{-1}], Q(t) [L^3T^{-1}] and ET(t) [L^3T^{-1}] are precipitation, streamflow and evapotranspiration time series, respectively; $S_T(T,t)$ [L^3] is the age-ranked storage (i.e. volume of water in storage ranked from youngest to oldest, Harman 2015); lastly, $\Omega_Q(S_T,t)$ [-] and $\Omega_{ET}(S_T,t)$ [-] are the cumulative SAS functions for Q and ET, respectively. The solution of Eq. 3.1 allows the derivation of the TTD of streamflow [T^{-1}] as (Benettin and Bertuzzo, 2018):

$$p_Q(T,t) = \frac{\partial \Omega_Q(S_T,t)}{\partial S_T} \cdot \frac{\partial S_T}{\partial T}. \tag{3.2}$$

TTDs can be skewed with long tails (Kirchner et al., 2001), mainly due to the challenge of identifying older water components (Benettin et al., 2017a). Hence, in this study I explored the median transit time, TT_{50} [T], a commonly used metric for streamflow water age that overcomes the poor identifiability of older water. TT_{50} represents the time at which 50% of the water has left the catchment as streamflow and is calculated from the cumulative TTD reaching a value equal to 0.5 (i.e. 50% probability).

To calculate TTD with Eq. 3.2, hydrological fluxes and SAS functions need to be defined. While hydrological fluxes are typically known from monitoring campaigns or simulated via hydrological models, SAS functions cannot be directly observed, but are defined through the calibration of their parameters. The calibration process is commonly done against time series of isotope data in streamflow and involves (i) computing the TTD of streamflow (Eq. 3.2) with multiple values of SAS parameters set a priori, (ii) simulating instream isotope data and, when measured instream isotope data are available, (iii) finding the best values of the SAS parameters while minimizing the difference between simulated and measured isotope data. In detail, instream isotope data, such as instream $\delta^{18}O_Q$ [-], are modeled as (Benettin and Bertuzzo, 2018):

$$\delta^{18}O_Q(T,t) = \int_0^\infty \delta^{18}O_S(T,t) p_Q(T,t) dT \tag{3.3}$$

where $\delta^{18}O_S(T,t)$ [-] is the isotopic signature of a water parcel in storage.

In all three studies, the calibration of SAS functions is the primary means for simulating time series of TT_{50}. For Studies 1 and 2, I used the tran-SAS transport model (Benettin

and Bertuzzo, 2018), while I employed the mHM-SAS transport model in Study 3 (Nguyen et al., 2021). Although a common modeling framework is shared across these studies, each of them employs unique methodologies, as detailed in the subsections below, to address specific research questions.

3.3.1 Parameterization and Interpolation

The form of the SAS functions is unknown, hence it is commonly parameterized using probability distributions. The two most commonly used distributions are the power law (Asadollahi et al., 2020; Benettin et al., 2017a) and the beta distribution (van der Velde et al., 2012). These distributions are based on specific parameters that contain information on various water release patterns, including young and/or old water release and a well-mixed system. These patterns can be either constant or vary over time, resulting in time-invariant or time-variant SAS functions and parameters. The time-variant nature of the SAS functions is driven by the wetness of the catchment, meaning that the preference for releasing young or old water depends on when the catchment is wet or dry. To date, there is no common agreement on which parameterization should be used, therefore a pragmatic approach is to choose one and estimate its parameters via the calibration process described in Section 3.3 (Harman, 2015).

Furthermore, SAS functions rely on continuous isotope data in precipitation (Benettin et al., 2022), emphasizing the need to fill data gaps (e.g. missing daily data between monthly measurements). To reconstruct missing δ^{18}O data, various temporal interpolation methods can be employed, including the step function, where values between consecutive samples are assumed to be the same as the last sample, and sine interpolation, which captures the seasonal variations often observed in δ^{18}O data (Feng et al., 2009). Additionally, the choice of input δ^{18}O data in precipitation for SAS models depends on whether precipitation data are collected at a single catchment location, in this study referred to as "raw" δ^{18}O data, or at multiple locations. In the latter case, spatial interpolation techniques, such as kriging, are utilized to assess the isotopic signature variability in precipitation samples.

In Study 1, I explored the uncertainty in simulated TTDs by employing twelve different model setups. These setups involved a range of SAS function parameterizations, including power law time-invariant (PLTI), power law time-variant (PLTV) and beta time-invariant (BETATI). Also, the setups considered various temporal interpolations and spatial distributions of δ^{18}O data in precipitation, as those discussed above. I conducted Monte-Carlo experiments to calibrate SAS model parameters against instream δ^{18}O time series and simulate the associated TT_{50}. Calibration involved minimizing the differences between

simulated and measured instream δ^{18}O, assessed using the Kling-Gupta efficiency (KGE; Gupta et al., 2009), a highly used metric for evaluating model performance. To quantify the uncertainty in the simulated TT_{50}, I applied the 95% prediction uncertainty method (95PPU; Abbaspour et al., 2004), by calculating the 2.5% and 97.5% percentiles within the cumulative distribution of the time series of the TT_{50} values.
While Studies 2 and 3 are based on the same SAS methodology as Study 1, they maintain a consistent setup made of SAS functions parameterized with a BETATI distribution, step function for temporal interpolation and δ^{18}O in precipitation spatially interpolated using kriging. This allows us to fix the model input and structure while addressing other aspects of the TTD-based models for Studies 2 and 3, as shown below.

3.3.2 Young Water Fraction

The F_{yw} has emerged as an innovative metric for deriving a fraction of the streamflow water age that is younger than a specific threshold, leveraging low-frequency and short-term isotope data. Values of F_{yw} can be estimated by fitting the seasonal cycles of measured δ^{18}O data in precipitation ($\delta^{18}O_P$ [-]) and streamflow ($\delta^{18}O_Q$ [-]) with sinusoids as (Kirchner, 2016*a*):

$$\delta^{18}O_P(t) = a_P cos(2\pi ft) + b_P sin(2\pi ft) + k_P \tag{3.4}$$

$$\delta^{18}O_Q(t) = a_Q cos(2\pi ft) + b_Q sin(2\pi ft) + k_Q \tag{3.5}$$

where a and b [-] are the cosine and sine coefficients of the sinusoids, f [T^{-1}] is the cycle frequency and k [-] is the vertical displacement of the sinusoid. Values of f and k are derived from the available monthly δ^{18}O data, while a and b are determined using the iteratively reweighted least squares regression, which is a method commonly employed to limit the influence of outliers (Lutz et al., 2018; Stockinger et al., 2016; von Freyberg et al., 2018). Following this, F_{yw} [-] can be calculated as the ratio of the amplitude of the seasonal cycles in the δ^{18}O in streamflow (A_Q [-]) and precipitation (A_P [-]) as (Kirchner, 2016*a*):

$$F_{yw} = \frac{A_Q}{A_P} = \frac{\sqrt{a_Q^2 + b_Q^2}}{\sqrt{a_P^2 + b_P^2}}. \tag{3.6}$$

F_{yw} values range from 0 to 1, indicating the dominance of young (or old) water in streamflow when F_{yw} is closer to 1 (or 0). The uncertainty in F_{yw} estimates can be expressed as a standard error (SE), calculated from a Gaussian error propagation (von Freyberg et al., 2018).

The link between F_{yw} and TTD is challenged due to the stationary nature of F_{yw} in contrast to time-variant TTDs simulated with SAS functions. To ensure comparability between F_{yw} and TTD, it is possible to calculate the marginal TTD [-], intended as a time-average of all TTDs (Eq. 3.2), as follows (Benettin et al., 2022; Botter et al., 2010):

$$< p_Q(T) >= \frac{1}{t} \int_0^t p_Q(T,t)dt. \tag{3.7}$$

The marginal TTD can be assessed with a specific water age $T = \tau_{yw}$ [T], where τ_{yw} represents the threshold for young water (e.g. with $\tau_{yw} = 10$ days, I calculate a value for F_{yw} corresponding to the water in streamflow younger than 10 days). The typical range for τ_{yw} falls between 42 and 94 days (i.e. 2-3 months), based on the shape parameter α of the assumed gamma TTD (Kirchner, 2016*a*).
Unlike the traditional approach of calibrating SAS function parameters against time series of instream $\delta^{18}O$ data (Study 1), Study 2 uses F_{yw} as a constraint for calibrating SAS parameters and simulating TT_{50}. Specifically, I compared values of F_{yw}, obtained by fitting measured monthly $\delta^{18}O$ data (Eq. 3.6) with the simulated marginal TTD (Eq. 3.7) for each of the 23 study catchments. I conducted a Monte-Carlo experiment and whenever the simulated marginal TTD, calculated for a set of predefined SAS parameters (i.e. prior parameters), matched the value of $F_{yw} \pm$ SE, I identified a set of acceptable SAS parameters (i.e. posterior parameters) for simulating the associated TT_{50} values (i.e. posterior solution of TT_{50}). I clustered the catchments with the same F_{yw} values and efficacy in F_{yw} to constrain the modeled TT_{50}. To account for uncertainty in the τ_{yw} value, I considered a range of [42-94] days in the calculation of the marginal TTD. Evaluation of simulated TT_{50} uncertainty and model performance used the 95PPU method and the KGE coefficient, respectively, as in Study 1.

3.3.3 Instream Nitrate Concentrations

SAS functions are not limited to conservative tracers such as $\delta^{18}O$ data but also apply to reactive solutes such as NO_3^- concentrations. In the case of NO_3^-, it can transform within the catchment and, for example, biogeochemically degrade through denitrification, a process governed by a first-order reaction constant. By including a first-order constant in Eq. 3.3, previously used for deriving instream $\delta^{18}O$ data, it is possible to estimate the instream concentration of NO_3^- [ML^{-3}] as (Nguyen et al., 2021):

$$\mathrm{NO_3^-}_Q(T,t) = \int_0^\infty \mathrm{NO_3^-}_S(T,t)\mathrm{e}^{-kT} p_Q(T,t)dT \tag{3.8}$$

where $NO_3^-{}_S$ [ML^{-3}] represents the NO_3^- concentration in the storage and k [T^{-1}] is the first order denitrification rate parameter.
Instead of focusing solely on $\delta^{18}O$ (Studies 1 and 2), Study 3 simulated instream NO_3^- concentration and TT_{50} of streamflow by calibrating SAS parameters in a Monte-Carlo approach against time series of NO_3^- concentration (i.e. Experiment 1). This mirrors the methodology of Study 1 but with a focus on reactive solutes rather than conservative tracers. In addition, in two further Monte-Carlo experiments, SAS parameters were calibrated to simulate TT_{50} of streamflow against $\delta^{18}O$ data (i.e. Experiment 2) and both NO_3^- and $\delta^{18}O$ data (i.e. Experiment 3). With these three experiments, I aimed to explore the effect of using different target variables for model calibration by evaluating differences and similarities among calibrated SAS parameters and simulated TT_{50}. Also, I aimed to understand the interaction, or correlation, between transport (i.e. SAS function parameters) and reaction-related parameters (i.e. denitrification rate), and assess if simulated TT_{50} derived from model calibration against NO_3^- concentrations (Experiment 1), is the same as TT_{50} derived with $\delta^{18}O$ data (Experiments 2 and 3). To further reveal the interaction between transport and reaction, the Damkőhler number (Da) was calculated as the ratio between TT_{50} and the inverse of the denitrification rate (Ocampo et al., 2006). The distribution of SAS model parameters across experiments was analyzed using kernel distributions. As in Studies 1 and 2, uncertainty in TT_{50} and model performance were evaluated using the 95PPU method and KGE coefficient.

Chapter 4

Key Findings & Discussions

4.1 Uncertainty Analysis in TTD-based Models

The comprehensive uncertainty analysis of Study 1 is the first attempt ever to explore the impact of various choices in model input and structure on simulated TT_{50} time series. I identified the (i) temporal interpolation of $\delta^{18}O$ in precipitation, (ii) non-spatially interpolated $\delta^{18}O$ in precipitation, (iii) selection between time-variant and time-invariant SAS functions and (iv) dry flow conditions as primary sources of uncertainty for TT_{50} in the Upper Selke.

When reconstructing high-frequency $\delta^{18}O$ in precipitation from monthly samples via interpolation, sine interpolation effectively captured the seasonality of the observed $\delta^{18}O$ data but smoothed detailed characteristics (Allen et al., 2019; Feng et al., 2009; McGuire and McDonnel, 2006), causing an underestimation and an overestimation of high and low values in $\delta^{18}O$ data, respectively (Fig. 3 of Study 1). This smoothing effect might conceal a more pronounced hydrological response of the system (Hrachowitz et al., 2011), hence simulated TT_{50} relying on sine interpolation should be interpreted carefully (Fig. 4g-l). In contrast, step function interpolation preserved the maxima in the values of monthly $\delta^{18}O$ in precipitation (Fig. 3 of Study 1), improving the fit of simulated instream $\delta^{18}O$ to measured data (Fig. 4a–f in Study 1) and enhancing overall model performance (Fig. 5 in Study 1). This suggests a more robust simulation of TT_{50} time series (Fig. 4a-f). However, combining step function with raw $\delta^{18}O$ resulted in a larger 95PPU (Fig. 4d-f), reflecting the importance of a comprehensive uncertainty range exploration beyond the sole goodness of fit. The spatial representation of $\delta^{18}O$ in precipitation had minimal influence on the pattern of TT_{50} (Fig. 4) as TT_{50} time series were similar with both raw $\delta^{18}O$ and $\delta^{18}O$ spatially interpolated using kriging. However, interpolating $\delta^{18}O$ in precipitation from various locations using kriging was able to reduce the 95PPU in TT_{50} (Fig. 4a-c and g-i), possibly due to the substantial elevation gradient in the Upper Selke

which makes measurements from a single location overly simplistic as representative of the entire area. The choice of time-invariant functions such as PLTI and BETATI resulted in moderate fluctuations in the 95PPU of TT_{50}, whose mean value was around 250 days (Fig. 4a, c, d, f, h, i, k and l). This behavior might result from the assumption of a constant water selection preference over time. In contrast, time-variant SAS functions such as PLTV (Fig. 4b, e, h and k), yielded pronounced seasonal fluctuations in the 95PPU of TT_{50}, which were linked to the catchment wetness leading to shorter (or longer) TT_{50} when the catchment was wet (or dry) during storm events (or low-flow periods) (Berghuijs and Allen, 2019; Jasechko et al., 2016). Moreover, the 95PPU of TT_{50} was exceptionally large during low-flow conditions, ranging at most between 259 and 1009 days (Fig. 4e). The large 95PPU during low-flow conditions is likely due to the water moving through drier soil zones, which causes erratic flow behavior with varying flow directions and patterns influenced by soil moisture's impact on conductivity. As a result, wet areas may be patchy, with water flowing at specific locations only, posing challenges in constraining older water ages. This large 95PPU during dry conditions may limit PLTV's effectiveness in understanding flow and solute transport during dry conditions.

In summary, Study 1 showcased the crucial role of spatiotemporal interpolations of $\delta^{18}O$ data and SAS parameterization in affecting the outcomes of TTD-based models. Regarding $\delta^{18}O$ data interpolation, the study suggests that, in the absence of high-frequency measurements in precipitation, reconstructing high-frequency time series from low-frequency data can serve as a viable approach to address the limitations of a coarse input dataset. However, it emphasizes the need to acknowledge uncertainties introduced by such choices. The significance of this uncertainty becomes evident in the highly different 95PPUs of simulated TT_{50} observed across the twelve tested setups (Fig. 4).

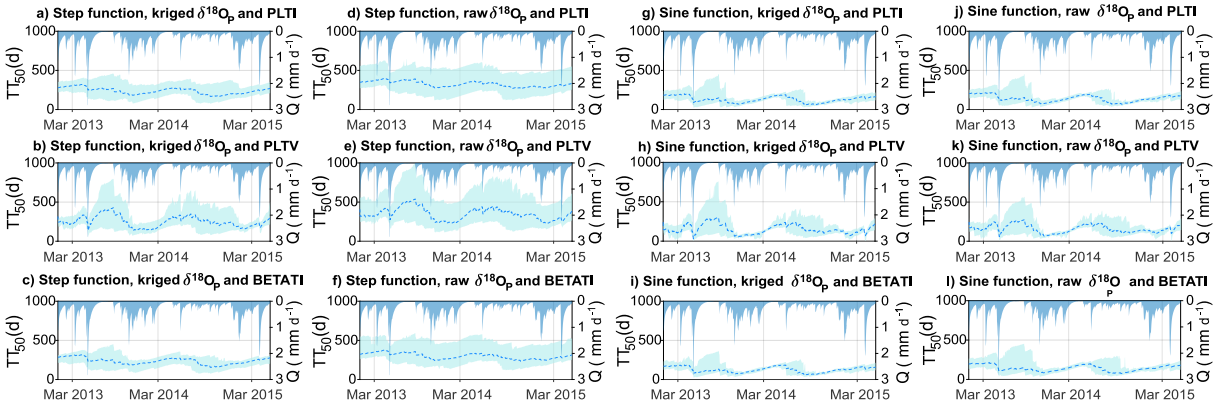

Figure 4: Predicted TT_{50} of streamflow; the light blue line and the shaded area represent the ensemble mean of all possible solutions and their range according to the 95PPU, respectively.

4.2 Alternative Ways to Simulate TTDs

Study 2 leverages the metric of F_{yw} to constrain model parameters and simulations of TTD-based models. The calculation of F_{yw} at 23 study sites revealed a significant range from 0.02 to 0.26, indicating that 2-26% of streamflow is composed of water from the past 2-3 months (Fig. 5). Using these values of F_{yw} as the only constraint for TTD-based modeling effectively reduced the equifinality in the model simulations, narrowing the 95PPU of the simulated TT_{50} from the prior to the posterior solution in most catchments. However, this reduction in the 95PPU was site-specific (Fig. 6 in Study 2). Catchments with $0.10 \leq F_{yw} \leq 0.26$, experienced a notable reduction in the 95PPU of TT_{50}, from 76% to 92% between prior and posterior solution (Fig. 6 of Study 2). This resulted in a narrower posterior 95PPU skewed toward smaller values, with the mean of the TT_{50} time series averaging approximately around 1 year across the catchments (Figs. 6a and S6 of Study 2). The largest F_{yw} values were observed in lower-altitude mountainous catchments (Fig. 5), likely influenced by rapid runoff through shallow flow paths during wet conditions and soil saturation (Lutz et al., 2018; Sprenger et al., 2019). Larger F_{yw} values were also observed in lowland areas (Fig. 5), where artificial drainage could trigger fast runoff into the stream network (Musolff et al., 2015; Danesh-Yazdi et al., 2016; Lutz et al., 2018). Catchments with $F_{yw} \leq 0.05$ had a more moderately reduced 95PPU from 46% to 50% between prior and posterior solution of TT_{50} (Fig. 6 of Study 2). This resulted in a larger 95PPU and longer TT_{50} values up to 12.5 years (Figs. 10c and S6 in Study 2). Smaller F_{yw} values were predominantly observed in mountainous catchments (Fig. 5), potentially due to the highly permeable soil of the Harz mountains, inducing rapid vertical infiltration and, in turn, activation of deep flow paths (Jasechko et al., 2016).

These results indicate that smaller F_{yw} values were less effective in constraining TTD-based models. The challenge of accurately representing old water components, characterizing the catchments of the poor cluster, may be attributed to the strong attenuation in the instream $\delta^{18}O$ data used to derive F_{yw}, thus making it difficult to quantify old water ages. On the contrary, the use of larger F_{yw} values successfully reduced uncertainty in the 95PPU of simulated TT_{50} from prior to posterior solution. This was further supported by improved model performance in terms of KGE values in the posterior solution compared to the prior solution (Figs. 9 and S5 of Study 2). Overall, in cases where only limited $\delta^{18}O$ data are available, relatively large values of F_{yw} can represent a practical and cost-effective tool for constraining TTD-based models. This aligns with previous studies highlighting the benefits of incorporating F_{yw} as an alternative constraint in model calibration (Lutz et al., 2018; Callı et al., 2023).

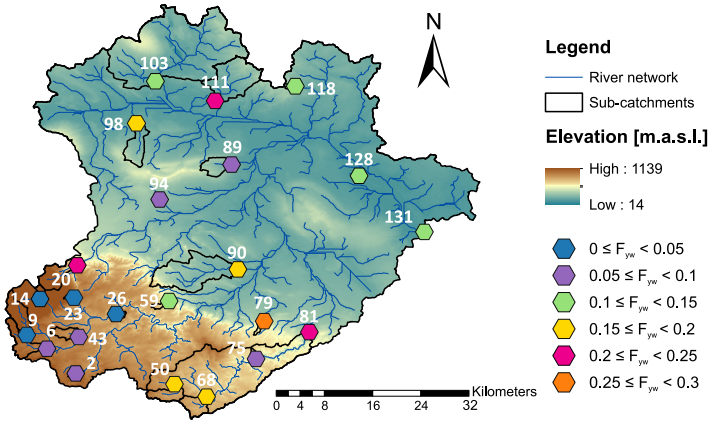

Figure 5: F_{yw} values obtained from the sine-wave approach in 23 catchments (black polygons) with their corresponding identification number, the river network (blue lines), and elevation in meters above sea level (colored map).

4.3 Validating Nitrate-Derived TTDs Using Isotopes

Study 3 simulated TT_{50} of streamflow obtained from model calibration against NO_3^- concentration (Experiment 1), low-frequency $\delta^{18}O$ data (Experiment 2) and both datasets (Experiment 3). Despite the different target variables for calibration, the 95PPUs of TT_{50} across all three experiments were comparable, ranging from 0 to 15 months in Experiment 1 (Fig. 6a), and from 0 to 11 months in Experiment 2 (Fig. 6b) and 3 (Fig. 6c). This indicates that NO_3^- and $\delta^{18}O$ data contain similar information for describing hydrological transport in the study catchment. All experiments showed seasonal variations in TT_{50} time series, with a significant decrease during high flows in winter and spring, and a gradual increase during low flows in summer and early autumn (Fig. 6). The impact of the 2018-2019 drought was evident (Winter et al., 2023), with TT_{50} peaking during and after the drought years (Fig. 6). The analysis of SAS parameters α (Fig. 6a of Study 3), describing transport processes within the catchment, yielded comparable calibrated values across all experiments, indicating a major release of young water from the catchment (i.e. $\alpha < 1$ and $\beta \geq 1$). However, Experiment 1 showed a greater interaction between α and the denitrification rate (Table S4 in Study 3), leading to equifinality issues (Figs. 6a and 7 in Study 3). This interaction was reduced in Experiment 3 when incorporating $\delta^{18}O$ data in model calibration (Table S4 in Study 3), thus resulting in a better description of hydrological transport as evident from the narrower range in α (Figs. 6a and 7 of Study 3) and 95PPU of TT_{50} time series (Fig. 6c) compared to Experiment 1. Analysis of the Da number highlights the dominance of transport as the primary driving force for NO_3^- removal during high-flow conditions, with Da < 1 (Fig. 8 in Study 3). Thus, during

high-flow conditions, there was a chemo-dynamic accretion pattern of the Upper Selke (Musolff et al., 2015; Ebeling et al., 2021), characterized by rapid NO_3^- release during storm events (Fig. 3 of Study 3). In contrast, during low-flow periods with Da > 1, denitrification became the primary driver of NO_3^- removal (Fig. 8 in Study 3). The Da number served as a key indicator to reveal the dynamic shift between transport and biogeochemical processes based on flow conditions, enhancing the understanding of NO_3^- export dynamics within the catchment (Ocampo et al., 2006).

Overall, Study 3 demonstrated the similarity of the transport parameter α and the temporal dynamic of TT_{50} values in the Upper Selke derived by calibrating the model using instream NO_3^- and $\delta^{18}O$ time series, separately and simultaneously. However, the absolute values differed, and employing a transport model with both low-frequency $\delta^{18}O$ data and NO_3^- concentrations reduced the interaction between transport and reaction parameter. This was beneficial as it improved the description of hydrological transport. Hence, I argue that incorporating $\delta^{18}O$ data in water quality models for NO_3^- can enhance the robustness of transport description.

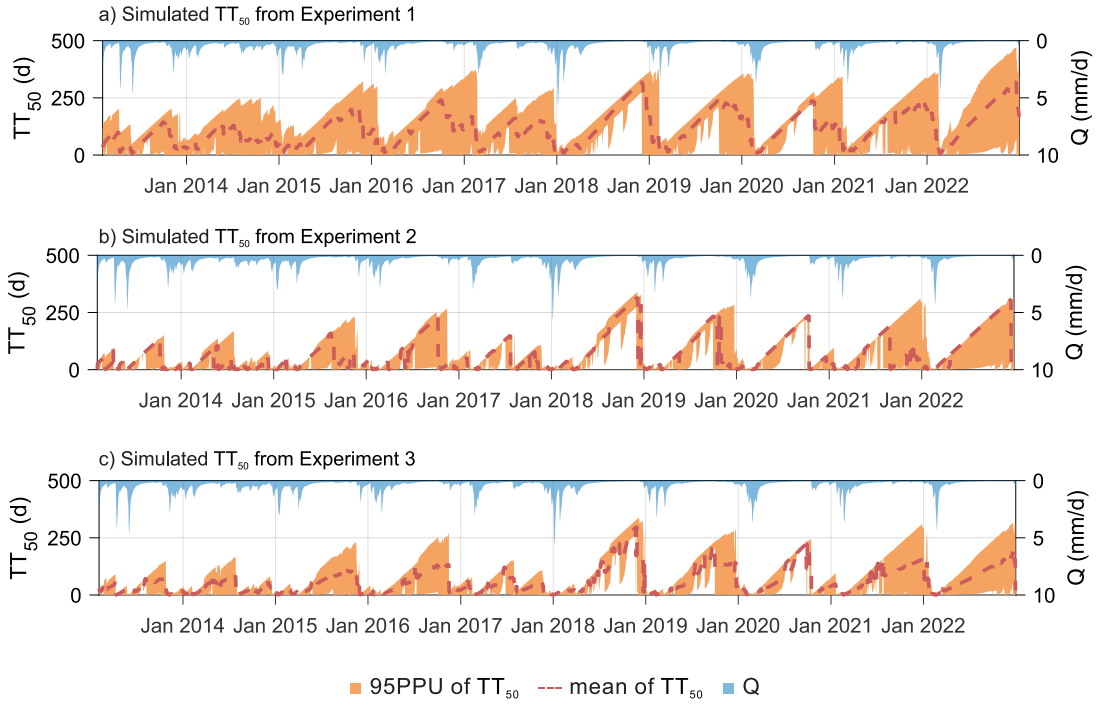

Figure 6: 95PPU of TT_{50} obtained by model calibration with (a) Experiment 1, (b) Experiment 2 and (c) Experiment 3; the dashed line is the ensemble mean derived from all solutions and the dark blue area is the streamflow time series.

Chapter 5

Synthesis and Outlook

5.1 Synthesis

This thesis leverages the use of low-frequency isotope data to gain valuable insights into TTDs and, in turn, underlying hydrological processes and solute export dynamics at the catchment-scale. Firstly, the thesis addresses challenges related to low-frequency isotope data, analyzing uncertainties arising from spatio-temporal interpolations of low-frequency $\delta^{18}O$ data in precipitation and SAS functions parameterization in TTD-based models. Secondly, the thesis explores alternative methods for simulating TTDs with low-frequency $\delta^{18}O$ data, highlighting the effectiveness of using the F_{yw}. Lastly, the thesis validates NO_3^--derived TTDs using low-frequency $\delta^{18}O$ data, providing insights into both hydrological and biogeochemical processes.

5.2 Water Transit Time across Studies

The studies focused on simulating TT_{50} time series across multiple catchments, including the common site of the Upper Selke. Results across the three studies reveal consistent patterns in the TT_{50} time series of the Upper Selke showing fluctuations dependent on the hydrological state of the system. However, the magnitude of these fluctuations varies, being more or less pronounced depending on the use of time-variant and -invariant SAS functions, respectively. There are differences in absolute values of TT_{50} between Studies 1 and 2 compared to Study 3, averaging around 1 year and approximately 4 months throughout the study period, respectively. This difference can be attributed to the different models used in Studies 1 and 2 (tran-SAS; Benettin and Bertuzzo, 2018) compared to Study 3 (mHM-SAS; Nguyen et al., 2021), which have different structure, parameters and input data, potentially impacting the study outcomes. This aligns with the primary

message of Study 1. Moreover, the results indicate consistent values of SAS parameters in the Upper Selke across the three studies, suggesting a predominant release of young water which often indicates the activation of shallow, fast flow paths (Mulholland et al., 1990; Tetzlaff et al., 2007) such as lateral flow via macro pores (Tromp-van Meerveld and McDonnell, 2006). This can enable rapid routing of water to the catchment outlet (Berghuijs and Allen, 2019), and indicate the catchment's short-term responsiveness along with rapid solute transport. Despite the differences in the absolute values of TT_{50} between Studies 1 and 2 compared to Study 3, the outcomes for the Upper Selke in all three studies suggest the same water release dynamics and fluctuations of TT_{50} based on the streamflow time series. This emphasizes the robustness of employing low-frequency $\delta^{18}O$ data in TTD-based models in drawing the same conclusions, even when different methodological approaches are used. Additionally, the results for the Upper Selke regarding water release dynamics found in this thesis align with other studies in the region (Nguyen et al., 2021, 2022; Winter et al., 2021, 2022).
Study 2 also identified other catchments with short TT_{50}, likely reflecting similar hydrological processes such as those described above. However, other sites showed longer TT_{50}, suggesting deep, long flow paths retaining water for a decade (Hrachowitz et al., 2010; Jasechko et al., 2016; Jasechko, 2019). This implies slow catchment drainage with long-term memory of past inputs (de Lavenne et al., 2022). Such different water release behaviors highlight varying degrees of hydrological connectivity (Blume and van Meerveld, 2015) influenced by specific hydro-meteorological forcing and activation of source areas (Kim et al., 2016).

5.3 Implications on Water Quality

The findings of this thesis provide valuable insights for water quality management. The analysis of the 95PPU of TT_{50} time series in all studies is crucial, as a large 95PPU indicates significant variations in the simulated TT_{50} values, which directly impacts solute export dynamics, especially for reactive solutes such as NO_3^-. For example, TT_{50} influences the NO_3^- exposure time to the soil matrix (McClain et al., 2003), thus affecting biogeochemical reactions such as denitrification (Kumar et al., 2020; Otero et al., 2009; Smith et al., 2009). A larger F_{yw} and shorter values of TT_{50} indicate rapid solute transport, which limits the time for denitrification and natural attenuation of contaminants (Ocampo et al., 2006; Rivett et al., 2008; Jawitz et al., 2020). Conversely, a smaller F_{yw} and larger values of TT_{50} are associated with old water release, which improves the efficacy of denitrification leading to reduced instream NO_3^- concentration. Nonetheless, a major release of old water may also cause delayed solute export responses (Dupas et al.,

2016; Van Meter et al., 2017), contributing to long-term issues of diffuse NO_3^- pollution (Basu et al., 2022; Lutz et al., 2022).
Water quality modelers can utilize these findings to enhance the understanding of the catchment's functioning, thus supporting planning, design, and/or operational decisions for effective water and NO_3^- management strategies (Zessner, 2021). Recognizing uncertainties in TTD-based models arising from model input is crucial, as they can impact the conclusions of water quality studies for management purposes (Study 1). The effectiveness of relatively large values of F_{yw} in reducing uncertainty in model simulations at sites with shorter TT_{50} is promising, as these are typically the sites with elevated instream solute concentration, prone to pollution and characterized by high water quality vulnerability (Study 2). Finally, the comparison of TTDs of water quality models calibrated to instream NO_3^- concentrations against simulated TTDs with $\delta^{18}O$ data is a valuable way to assess water quality models' effectiveness in describing hydrological processes (Study 3).

5.4 Outlook

Follow-up research could further explore and validate the uncertainty analysis of TT_{50} time series (Study 1). For example, alternative methods for temporal interpolation, such as Generalized Additive Models (GAM; Buzacott et al., 2020) based on smoothing functions might offer another approach to evaluate the uncertainty in TT_{50} due to input tracer data reconstruction. Similarly, considering the gamma SAS parameterization (Harman, 2015) could insights into model structure uncertainty. Additionally, gaining a more comprehensive understanding of catchment functioning, including evapotranspiration and catchment storage, could be valuable for future studies to enhance the accuracy of TTD uncertainty characterization and determine which model setup is most plausible for the specific catchment.
Moreover, research should leverage the global availability of F_{yw}. A study by Jasechko et al. (2016), which calculated F_{yw} in 254 catchments worldwide using $\delta^{18}O$ data, identified a correlation with topographic gradient (i.e. smaller F_{yw} at higher altitude), indicating potential for regionalizing F_{yw} across diverse regions and climates. This regionalization could yield estimates of F_{yw} in ungauged areas, similar to deriving $\delta^{18}O$ data in precipitation through spatial interpolation with measurements from nearby monitoring stations (Bowen and Revenaugh, 2003). Future studies could build extensive datasets containing F_{yw} or sinusoidal cycles of $\delta^{18}O$ data in precipitation (Allen et al., 2019) employed to calculate F_{yw}, to enhance the use of F_{yw} as a helpful tool for supporting SAS-based models.

However, further studies are needed to evaluate and exploit the possibilities associated with F_{yw} regionalization.
The proposed use of low-frequency $\delta^{18}O$ data as a validation tool for water quality models gives room for further understanding of how different calibration targets produce comparable outcomes in simulated TTDs. This can be especially explored in catchments with diverse hydrological and geophysical settings compared to the Upper Selke. While the findings in the Upper Selke emphasized similarities in TTDs and SAS model parameters when using both NO_3^- and $\delta^{18}O$ data, catchments discharging predominantly old water may show different TTDs and transport mechanisms when inferred with NO_3^- or $\delta^{18}O$ data. Hence, future studies should check whether NO_3^- and $\delta^{18}O$ data hold similar or different information for model calibration and transport processes description across contrasting catchments.
To address the aforementioned open questions, a low-frequency isotopic dataset can be employed and provide valuable insights into hydrological processes. While low-frequency measurements may contain less information compared to high-frequency data, they are generally characterized by greater global availability. This broader accessibility of data allows for the exploration and comparison of numerous catchments, contributing to an enhanced understanding of their functioning. Notably, the studies in this thesis are based on low-frequency data, and the applied methodologies have proven successful in exploring catchment-scale TTDs and their associated uncertainty. Consequently, these methods can be transferred to other catchments, for which low-frequency data are also available, thus promoting a comprehensive understanding of catchment-scale TTDs and solute transport across diverse sites. This approach highlights the importance of shifting the research focus from “how could we obtain more data?” to “what meaningful insights can be derived from existing data?” until more high-frequency datasets become available. This change in perspective highlights the need for optimizing the use of available resources for enhanced water quantity and quality management, particularly crucial given increasingly extreme weather conditions and water pollution due to global change.

References

Abbaspour, K. C., Johnson, C. A. and van Genuchten, M. T. (2004), 'Estimating Uncertain Flow and Transport Parameters Using a Sequential Uncertainty Fitting Procedure', *Vadose Zone Journal* **3**(4), 1340–1352.
URL: *https://doi.org/10.2136/vzj2004.1340*

Abbott, B. W., Bishop, K., Zarnetske, J. P., Hannah, D. M., Frei, R. J., Minaudo, C., Chapin III, F. S., Krause, S., Conner, L., Ellison, D., Godsey, S. E., Plont, S., Marçais, J., Kolbe, T., Huebner, A., Hampton, T., Gu, S., Buhman, M., Sayedi, S. S., Ursache, O., Chapin, M., Henderson, D., K. and Pinay, G. (2019), 'A water cycle for the Anthropocene', *Hydrol. Process.* **3**3, 3046–3052.
URL: *https://doi.org/10.1002/hyp.13544*

Allen, S. T., Jasechko, S., Berghuijs, W. R., Welker, J. M., Goldsmith, G. R. and Kirchner, J. W. (2019), 'Global sinusoidal seasonality in precipitation isotopes', *Hydrol. Earth Syst. Sci.* **2**3, 3423–3436.
URL: *https://doi.org/10.5194/hess-23-3423-2019*

Ambroise, B. (2004), 'Variable 'active' versus 'contributing' areas or periods: a necessary distinction', *Hydrol. Process.* **1**8, 1149–1155.
URL: *https://doi.org/10.1002/hyp.5536*

Asadollahi, M., Nehemy, M. F., McDonnell, J. J., Rinaldo, A. and Benettin, P. (2022), 'Toward a Closure of Catchment Mass Balance: Insight on the Missing Link From a Vegetated Lysimeter', *Water Resour. Res.* **5**8, e2021WR030698.
URL: *https://doi.org/10.1029/2021WR030698*

Asadollahi, M., Stumpp, C., Rinaldo, A. and Benettin, P. (2020), 'Transport and Water Age Dynamics in Soils: A Comparative Study of Spatially Integrated and Spatially Explicit Models', *Water Resour. Res.* **5**6, e2019WR025539.
URL: *https://doi.org/10.1029/2019WR025539*

Basu, N. B., Van Meter, K. J., Byrnes, D. K., Van Cappellen, P., Brouwer, R., Jacobsen, B. H., Jarsjö, J., Rudolph, D. L., Cunha, M. C., Nelson, N., Bhattacharya, R., Destouni, G. and Olsen, S. B. (2022), 'Managing nitrogen legacies to accelerate water quality improvement', *Nat. Geosci.* **1**5, 97–105.
URL: *https://doi.org/10.1038/s41561-021-00889-9*

Beck, M. B. (1987), 'Water quality modeling: A review of the analysis of uncertainty', *Water Resour. Res.* **2**3, 1393–1442.
URL: *https://doi.org/10.1029/WR023i008p01393*

Benettin, P., Bailey, W., S., Rinaldo, A., Likens, G. E., McGuire, K. J. and Botter, G. (2017b), 'Young runoff fractions control streamwater age and solute concentration dynamics', *Hydrol. Process.* **3**1, 2982–2986.
URL: *https://doi.org/10.1002/hyp.11243*

Benettin, P. and Bertuzzo, E. (2018), 'tran-SAS v1.0: a numerical model to compute catchment-scale hydrologic transport using StorAge Selection functions', *Geosci. Model Dev.* **1**1, 1627–1639.
URL: *https://doi.org/10.5194/gmd-11-1627-2018*

Benettin, P., Kirchner, J. W., Rinaldo, A. and Botter, G. (2015b), 'Modeling chloride transport using travel time distributions at Plynlimon, Wales', *Water Resour. Res.* **5**1, 3259–3276.
URL: *https://doi.org/10.1002/2014WR016600*

Benettin, P., Rinaldo, A. and Botter, G. (2015a), 'Tracking residence times in hydrological systems: forward and backward formulations', *Hydrol. Process.* **2**9, 5203–5213.
URL: *https://doi.org/10.1002/hyp.10513*

Benettin, P., Rodriguez, N. B., Sprenger, M., Kim, M., Klaus, J. Harman, C. J., der Velde, Y., Hrachowitz, M., Botter, G., McGuire, K. J., Kirchner, J., Rinaldo, A. and McDonnell, J. J. (2022), 'Transit Time Estimation in Catchments: Recent Developments and Future Directions', *Water Resour. Res.* **5**8, e2022WR033096.
URL: *https://doi.org/10.1029/2022WR033096*

Benettin, P., Soulsby, C., Birkel, C., Tetzlaff, D., Botter, G. and Rinaldo, A. (2017a), 'Using SAS functions and high-resolution isotope data to unravel travel time distributions in headwater catchments', *Water Resour. Res.* **5**3, 1864–1878.
URL: *https://doi.org/10.1002/2016WR020117*

Berghuijs, W. R. and Allen, S. T. (2019), 'Waters flowing out of systems are younger than the waters stored in those same systems', *Hydrol. Process.* **3**3, 3251–3254.
URL: *https://doi.org/10.1002/hyp.13569*

Berghuijs, W. R., Woods, R. A. and Hrachowitz, M. (2014), 'A precipitation shift from snow towards rain leads to a decrease in streamflow', *Nat Clim Change* **4**, 583–586.
URL: *https://doi.org/10.1038/nclimate2246*

Beven, K. (2006), 'A manifesto for the equifinality thesis', *J. Hydrol.* **3**20, 18–36.
URL: *https://doi.org/10.1016/j.jhydrol.2005.07.007*

Blume, T. and van Meerveld, H. J. (2015), 'From hillslope to stream: methods to investigate subsurface connectivity', *WIREs Water* **2**, 177–198.
URL: *https://doi.org/10.1002/wat2.1071*

Bodirsky, B. L., Popp, A., Lotze-Campen, H., Dietrich, J. P., Rolinski, S., Weindl, I., Schmitz, C., Müller, C., Bonsch, M., Humpenöder, F., Biewald, A. and Stevanovic, M. (2014), 'Reactive nitrogen requirements to feed the world in 2050 and potential to mitigate nitrogen pollution', *Nat Commun* **5**, 3858.
URL: *https://doi.org/10.1038/ncomms4858*

Botter, G., Bertuzzo, E. and Rinaldo, A. (2010), 'Transport in the hydrologic response: Travel time distributions, soil moisture dynamics, and the old water paradox', *Water Resour. Res.* **4**6, W03514.
URL: *https://doi.org/10.1029/2009WR008371*

Botter, G., Bertuzzo, E. and Rinaldo, A. (2011), 'Catchment residence and travel time distributions: The master equation', *Geophys. Res. Lett.* **3**8, L11403.
URL: *https://doi.org/10.1029/2011GL047666*

Bouraoui, F. and Grizzetti, B. (2014), 'Modelling mitigation options to reduce diffuse nitrogen water pollution from agriculture', *Sci. Total Environ.* **4**68–469, 1267–1277.
URL: *https://doi.org/10.1016/j.scitotenv.2013.07.066*

Bowen, G. J. and Revenaugh, J. (2003), 'Interpolating the isotopic composition of modern meteoric precipitation', *PNAS* **3**9, 1299.
URL: *https://doi.org/10.1029/2003WR002086*

Burgin, A. J. and Hamilton, S. K. (2007), 'Have we overemphasized the role of denitrification in aquatic ecosystems? a review of nitrate removal pathways', *Front Ecol Environ.* **5**, 89–96.
URL: *https://doi.org/10.1890/1540-9295(2007)5[89:HWOTRO]2.0.CO;2*

Buzacott, A. J. V., van der Velde, Y., Keitel, C. and Vervoort, R. W. (2020), 'Constraining water age dynamics in a south-eastern Australian catchment using an age-ranked storage and stable isotope approach', *Hydrol. Process.* **3**4, 4384–4403.
URL: *https://doi.org/10.1002/hyp.13880*

Callı, K. O., Bittner, D., Liu, Y., Callı, S. S., Mielsen, L. A. Bense, V. and Hartmann, A. (2023), 'Revealing the positive influence of young water fractions derived from stable isotopes on the robustness of karst water resources predictions', *J. Hydrol.* **6**21, 129549.
URL: *https://doi.org/10.1016/j.jhydrol.2023.129549*

Cirmo, C. P. and McDonnell, J. J. (1997), 'Linking the hydrologic and biogeochemical controls of nitrogen transport in near-stream zones of temperate-forested catchments: a review', *J. Hydrol.* **1**99, 88–120.
URL: *https://doi.org/10.1016/S0022-1694(96)03286-6*

Danesh-Yazdi, M., Foufoula-Georgiou, E., Karwan, D. L. and Botter, G. (2016), 'Inferring changes in water cycle dynamics of intensively managed landscapes via the theory of time-variant travel time distributions', *Water Resour. Res.* **5**2, 7593–7614.
URL: *https://doi.org/10.1002/2016WR019091*

de Lavenne, A., Andréassian, V., Crochemore, L., Lindström, G. and Arheimer, B. (2022), 'Quantifying multi-year hydrological memory with Catchment Forgetting Curves', *Hydrol. Earth Syst. Sci.* **2**6, 2715–2732.
URL: *https://doi.org/10.5194/hess-26-2715-2022*

Diaz, R. J. and Rosenberg, R. (2008), 'Spreading Dead Zones and Consequences for Marine Ecosystems', *Science* **3**21, 926–929.
URL: *https://doi.org/10.1126/science.1156401*

Dupas, R., Jomaa, S., Musolff, A., Borchardt, D. and Rode, M. (2016), 'Disentangling the influence of hydroclimatic patterns and agricultural management on river nitrate dynamics from sub-hourly to decadal time scales', *Sci. Total Environ.* **5**71, 791–800.
URL: *https://doi.org/10.1016/j.scitotenv.2016.07.053*

Dupas, R., Musolff, A., Jawitz, J. W., Rao, P. S. C., Jäger, C. G., Fleckenstein, J. H., Rode, M. and Borchardt, D. (2017), 'Carbon and nutrient export regimes from headwater catchments to downstream reaches', *Biogeosciences* **1**4, 4391–4407.
URL: *https://doi.org/10.5194/bg-14-4391-2017*

Ebeling, P., Kumar, R., Weber, M., Knoll, L., Fleckenstein, J. H. and Musolff, A. (2021), 'Archetypes and Controls of Riverine Nutrient Export Across German Catchments',

Water Resour. Res. **57**, e2020WR028134.
URL: *https://doi.org/10.1029/2020WR028134*

Erisman, J. W., Galloway, J. N., Seitzinger, S., Bleeker, A., Dise, N. B., Petrescu, A. M., Leach, A. M. and de Vries, W. (2013), 'Consequences of human modification of the global nitrogen cycle', *Phil. Trans. R. Soc. B.* **3**68, 20130116.
URL: *https://doi.org/10.1098/rstb.2013.0116*

EU, C. (1991), 'Directive 91/676/eec. Council Directive of 12 december 1991 concerning the protection of waters against pollution caused by nitrates from agricultural sources', *Official Journal of European Community* **L** 375, 1–8.

EU, C. (2000), 'Directive 2000/60/EC of the European Parliament and of the Council of 23 october 2000 on establishing a framework for Community action in the field of water policy', *Official Journal of European Community* **L** 327, 1–73.

European Environment Agency, Kristensen, P., Kampa, E., Vöolker, J., Stein, U. and Mohaupt, V. (2021), 'Drivers of and pressures arising from selected key water management challenges - a European overview', *Technical report.* .
URL: *https://data.europa.eu/doi/10.2800/059069*

European Environment Agency, Zal, N., Whalley, C., Christiansen, T., Kristensen, P. and Nery, F. (2018), 'European waters. Assessment of status and pressures', *Technical report.* .
URL: *https://www.eea.europa.eu/publications/state-of-water*

Feng, X., Faiia, A. M. and Posmentier, E. S. (2009), 'Seasonality of isotopes in precipitation: Ac global perspective', *J. Geophys. Res* **1**14, D08116.
URL: *https://doi.org/10.1029/2008JD011279*

Frühauf, M. and Schwab, M. (2008), '5.6.2 Landschaftscharakter und Oberflächengestalt', *In: Bachmann GH et al (eds) Geologie von Sachsen-Anhalt* .

Galloway, J. N., Dentener, F. J., Capone, D. G., Boyer, E. W., Howarth, R. W., Seitzinger, S. P., Asner, G. P., Cleveland, C. C., Green, P. A., Holland, E. A., Karl, D. M., Michaels, A. F., Porter, J. H., Townsend, A. R. and V oosmarty, C. J. (2004), 'Nitrogen Cycles: Past, Present, and Future', *Biogeochemistry* **7**0, 153–226.
URL: *https://doi.org/10.1007/s10533-004-0370-0*

Ghosh, P. and Brand, W. A. (2003), 'Stable isotope ratio mass spectrometry in global climate change research', *Int. J. Mass Spectrom.* **2**28, 1–33.
URL: *https://doi.org/10.1016/S1387-3806(03)00289-6*

Gupta, H. V., Kling, H., Yilmaz, K. K. and Martinez, G. F. (2009), 'Decomposition of the mean squared error and NSE performance criteria: Implications for improving hydrological modelling', *J. Hydrol.* **3**77, 80–91.
URL: *https://doi.org/10.1016/j.jhydrol.2009.08.003*

Harman, C. J. (2015), 'Time-variable transit time distributions and transport: Theory and application to storage-dependent transport of chloride in a watershed', *Water Resour. Res.* **5**1, 1–30.
URL: *https://doi.org/10.1002/2014WR015707*

Heidbüchel, I., Troch, P. A. and Lyon, S. W. (2013), 'Separating physical and meteorological controls of variable transit times in zero-order catchments', *Water Resour. Res.* **4**9, 7644–7657.
URL: *https://doi.org/10.1002/2012WR013149*

Heidbüchel, I., Yang, J., Musolff, A., Troch, P., Ferré, T. and Fleckenstein, J. H. (2020), 'On the shape of forward transit time distributions in low-order catchments', *Hydrol. Earth Syst. Sci.* **2**4, 2895–2920.
URL: *https://doi.org/10.5194/hess-24-2895-2020*

Hrachowitz, M., Benettin, P., van Breukelen, B. M., Fovet, O., Howden, N. J. K., Ruiz, L van der Velde, Y. and Wade, A. J. (2016), 'Transit times — the link between hydrology and water quality at the catchment scale', *WIREs Water* **3**, 629–657.
URL: *https://doi.org/10.1002/wat2.1155*

Hrachowitz, M., Savenije, H. H. G., Blöschl, G., McDonnell, J. J., Sivapalan, M., Pomeroy, J. W., Arheimer, B., Blume, T., Clark, M. P., Ehret, U., Fenicia, F., Freer, J. E., Gelfan, A., Gupta, H. V., Hughes, D. A., Hut, R. W., Montanari, A., Pande, S., Tetzlaff, D., Troch, P. A., Uhlenbrook, S., Wagener, T., Winsemius, H. C., Woods, R. A., Zehe, E. and Cudennec, C. (2013), 'A Decade of Predictions in Ungauged Basins (PUB) — a review', *Hydrological Sciences Journal* **5**8, 1198–1255.
URL: *https://doi.org/10.1080/02626667.2013.803183*

Hrachowitz, M., Soulsby, C., Tetzlaff, D. and Malcolm, I. A. (2011), 'Sensitivity of mean transit time estimates to model conditioning and data availability', *Hydrol. Process.* **2**5, 980–990.
URL: *https://doi.org/10.1002/hyp.7922*

Hrachowitz, M., Soulsby, C., Tetzlaff, D., Malcolm, I. A. and Schoups, G. (2010), 'Gamma distribution models for transit time estimation in catchments: Physical interpretation

of parameters and implications for time-variant transit time assessment', *Water Resour. Res.* **4**6, W10536.
URL: *https://doi.org/10.1029/2010WR009148*

https://watson-cost.eu/ (last access: 16-10-2023), 'WATer isotopeS in the critical zONe: from groundwater recharge to plant transpiration'.
URL: *https://watson-cost.eu/*

Ilampooranan, I., Van Meter, K. J. and Basu, N. B. (2019), 'A Race Against Time: Modeling Time Lags in Watershed Response', *Water Resour. Res.* **5**5, 3941–3959.
URL: *https://doi.org/10.1029/2018WR023815*

Jasechko, S. (2019), 'Global Isotope Hydrogeology — Review', *Reviews of Geophysics* **57**, 835–965.
URL: *https://doi.org/10.1029/2018RG000627*

Jasechko, S., Kirchner, J. W., Welker, J. M. and McDonnell, J. J. (2016), 'Substantial proportion of global streamflow less than three months old', *Nature Geosci* **9**, 126–129.
URL: *https://doi.org/10.1038/ngeo2636*

Jawitz, J., Desormeaux, A. M., Annable, M. D., Borchardt, D. and Dobberfuhl, D. (2020), 'Disaggregating Landscape-Scale Nitrogen Attenuation Along Hydrological Flow Paths', *JGR Biosciences* **1**25, e2019JG005229.
URL: *https://doi.org/10.1029/2019JG005229*

Jencso, K. G., McGlynn, B. L., Gooseff, M. N., Wondzell, S. M., Bencala, K. E. and Marshall, L. A. (2009), 'Hydrologic connectivity between landscapes and streams: Transferring reach- and plot-scale understanding to the catchment scale', *Water Resour. Res.* **4**5, W04428.
URL: *https://doi.org/10.1029/2008WR007225*

Jenny, J.-P., Anneville, O., Arnaud, F., Baulaz, Y., Bouffard, D., Domaizon, I., Bocaniov, S. A., Chèvre, N., D. M., Dorioz, J.-M., Dunlop, E. S., Dur, G., Guillard, J., Guinaldo, T., Jacquet, S., Jamoneau, A., Jawed, Z., Jeppesen, E., Krantzberg, G., Lenters, J., Leoni, B., Meybeck, M., Nava, V., Nõges, T., Nõges, P., Patelli, M., Pebbles, V., P. M.-E., Rasconi, S., Ruetz, C. R., Rudstam, L., Salmaso, N., Sapna, S., Straile, D., Tammeorg, O., Twiss, M. R., Uzarski, D. G., Ventelä, A.-M., Vincent, W. F., Wilhelm, S. W., Wangberg, S.-A. and Weyhenmeyer, G. A. (2020), 'Scientists' Warning to Humanity: Rapid degradation of the world's large lakes', *J. Great Lakes Res.* **4**6, 686–702.
URL: *https://doi.org/10.1016/j.jglr.2020.05.006*

Jury, W. A. and Vaux, H. J. (2007), 'The Emerging Global Water Crisis: Managing Scarcity and Conflict Between Water Users', *Adv. Agron.* **9**5, 1–76.
URL: *https://doi.org/10.1016/S0065-2113(07)95001-4*

Kim, M. and Harman, C. J. (2022), 'Transit Times and StorAge Selection Functions in Idealized Hillslopes With Steady Infiltration', *Water Resour. Res.* **5**8, e2019WR025917.
URL: *https://doi.org/10.1029/2019WR025917*

Kim, M., Pangle, L. A., Cardoso, C., Lora, M., Volkmann, T. H. M., Wang, Y., Harman, C. J. and Troch, P. A. (2016), 'Transit time distributions and StorAge Selection functions in a sloping soil lysimeter with time-varying flow paths: Direct observation of internal and external transport variability', *Water Resour. Res.* **5**2, 7105–7129.
URL: *https://doi.org/10.1002/2016WR018620*

Kim, M., Volkmann, T. H. M., Wang, Y., Meira Neto, A. A., Matos, K., Harman, C. J. and Troch, P. A. (2022), 'Direct Observation of Hillslope Scale Storage Selection Functions in Experimental Hydrologic Systems: Geomorphologic Structure and Preferential Discharge of Old Water', *Water Resour. Res.* **5**8, e2020WR028959.
URL: *https://doi.org/10.1029/2020WR028959*

Kirchner, J. W. (2016*a*), 'Aggregation in environmental systems – Part 1: Seasonal tracer cycles quantify young water fractions, but not mean transit times, in spatially heterogeneous catchments', *Hydrol. Earth Syst. Sci.* **2**0, 279–297.
URL: *https://doi.org/10.5194/hess-20-279-2016*

Kirchner, J. W. (2016*b*), 'Aggregation in environmental systems – Part 2: Catchment mean transit times and young water fractions under hydrologic nonstationarity', *Hydrol. Earth Syst. Sci.* **2**0, 299–328.
URL: *https://doi.org/10.5194/hess-20-299-2016*

Kirchner, J. W., Feng, X. and Neal, C. (2000), 'Fractal stream chemistry and its implications for contaminant transport in catchments', *Nature* **4**03, 524–527.
URL: *https://doi.org/10.1038/35000537*

Kirchner, J. W., Feng, X. and Neal, C. (2001), 'Catchment-scale advection and dispersion as a mechanism for fractal scaling in stream tracer concentrations', *J. Hydrol.* **2**54, 82–101.
URL: *https://doi.org/10.1016/S0022-1694(01)00487-5*

Knobeloch, L., Salna, B., Hogan, A., Postle, J. and Anderson, H. (2000), 'Blue babies and nitrate-contaminated well water', *Environ. Health Perspect.* **1**08, 675–678.
URL: *https://doi.org/10.1289/ehp.00108675*

Kumar, R., Heße, F., Rao, P. S. C., Musolff, A., Jawitz, J. W., Sarrazin, F., Samaniego, L., Fleckenstein, J. H., Rakovec, O., Thober, S. and Attinger, S. (2020), 'Strong hydroclimatic controls on vulnerability to subsurface nitrate contamination across Europe', *Nat Commun* **1**1, 6302.
URL: *https://doi.org/10.1038/s41467-020-19955-8*

Kumar, R., Samaniego, L. and Attinger, S. (2013), 'Implications of distributed hydrologic model parameterization on water fluxes at multiple scales and locations', *Water Resour. Res.* **4**9, 360–379.
URL: *https://doi.org/10.1029/2012WR012195*

Le Moal, M., Gascuel-Odoux, C., Ménesguen, A., Souchon, Y., Étrillard, C., a. A., Moatar, F., Pannard, A., Souchu, P., Lefebvre, A. and Pinay, G. (2019), 'Eutrophication: A new wine in an old bottle?', *Sci. Total Environ.* **6**51, 1–11.
URL: *https://doi.org/10.1016/j.scitotenv.2018.09.139*

Lutz, S. R., Ebeling, P., Musolff, A., Nguyen, T. V., Sarrazin, F. J., Van Meter, K. J., Basu, N. B., Fleckenstein, J. H., Attinger, S. and Kumar, R. (2022), 'Pulling the rabbit out of the hat: Unravelling hidden nitrogen legacies in catchment-scale water quality models', *Hydrol. Processes* **3**6, e14682.
URL: *https://doi.org/10.1002/hyp.14682*

Lutz, S. R., Krieg, R., Müller, C., Zink, M., Knöller, K., Samaniego, L. and Merz, R. (2018), 'Spatial Patterns of Water Age: Using Young Water Fractions to Improve the Characterization of Transit Times in Contrasting Catchments', *Water Resour. Res.* **5**4, 4767–4784.
URL: *https://doi.org/10.1029/2017WR022216*

McClain, M. E., Boyer, E. W., Dent, C. L., Gergel, S. E., Grimm, N. B., Groffman, P. M., Hart, S. C., Harvey, J. W., Johnston, C. A., Mayorga, E., McDowell, W. H. and Pinay, G. (2003), 'Biogeochemical Hot Spots and Hot Moments at the Interface of Terrestrial and Aquatic Ecosystems', *Ecosystems* **6**, 301–312.
URL: *https://doi.org/10.1007/s10021-003-0161-9*

McGuire, K. J. and McDonnel, J. J. (2006), 'A review and evaluation of catchment transit time modeling', *J. Hydrol.* **3**30, 543–563.
URL: *https://doi.org/10.1016/j.jhydrol.2006.04.020*

McGuire, K. J., McDonnell, J. J., Weiler, M., Kendall, C., McGlynn, B. L., Welker, J. M. and Seibert, J. (2005), 'The role of topography on catchment-scale water residence time', *Water Resour. Res.* **4**1, W05002.
URL: *https://agupubs.onlinelibrary.wiley.com/doi/10.1029/2004WR003657*

Meals, D. W., Dressing, S. A. and Davenport, T. E. (2010), 'Lag Time in Water Quality Response to Best Management Practices: A Review', *J. Environ. Qual.* **3**9, 85–96.
URL: *https://doi.org/10.2134/jeq2009.0108*

Mueller, C., Zink, M., Samaniego, L., Krieg, E., Merz, R., Rode, M. . and Knöller, K. (2016), 'Discharge Driven Nitrogen Dynamics in a Mesoscale River Basin As Constrained by Stable Isotope Patterns', *Environ. Sci. Technol.* **5**0(17), 9187–9196.
URL: *https://doi.org/10.1021/acs.est.6b01057*

Mulholland, P., Wilson, G. and Jardine, P. (1990), 'Hydrogeochemical Response of a Forested Watershed to Storms: Effects of Preferential Flow Along Shallow and Deep Pathways', *Water Resour. Res.* **2**6, 3021–3036.
URL: *https://doi.org/10.1029/WR026i012p03021*

Musolff, A., Schmidt, C., Selle, B. and Fleckenstein, J. H. (2015), 'Catchment controls on solute export', *Adv. Water Resour.* **8**6, 133–146.
URL: *https://doi.org/10.1016/j.advwatres.2015.09.026*

Musolff, A., Zhan, Q., Dupas, R., Minaudo, C., Fleckenstein, J. H., Rode, M., Dehaspe, J. and Rinke, K. (2021), 'Spatial and Temporal Variability in Concentration-Discharge Relationships at the Event Scale', *Water Resour. Res.* **5**7, e2020WR029442.
URL: *https://doi.org/10.1029/2020WR029442*

Neal, C., Reynolds, B., Kirchner, J., Rowland, P., Norris, D., Sleep, D., Lawlor, A., Woods, C., Thacker, S., Guyatt, H., Vincent, C., Lehto, K., Grant, S., Williams, J., Neal, M., Wickham, H., Harman, S. and Armstrong, L. (2013), 'High-frequency precipitation and stream water quality time series from Plynlimon, Wales: an openly accessible data resource spanning the periodic table', *Hydrol. Process.* **2**7, 2531–2539.
URL: *https://doi.org/10.1002/hyp.9814*

Nguyen, T. V., Kumar, R., Lutz, S. R., Musolff, A., , J. and Fleckenstein, J. H. (2021), 'Modeling Nitrate Export From a Mesoscale Catchment Using StorAge Selection Functions', *Water Resour. Res.* **5**7, e2020WR028490.
URL: *https://doi.org/10.1029/2020WR028490*

Nguyen, T. V., Kumar, R., Musolff, A., Lutz, S. R., Sarrazin, F., Attinger, S. and Fleckenstein, J. H. (2022), 'Disparate Seasonal Nitrate Export From Nested Eeterogeneous Subcatchments Revealed With StorAge Selection Functions', *Water Resour. Res.* **5**8, e2021WR030797.
URL: *https://doi.org/10.1029/2021WR030797*

Ocampo, C. J., Oldham, C. E. and Sivapalan, M. (2006), 'Nitrate attenuation in agricultural catchments: Shifting balances between transport and reaction', *Water Resour. Res.* **4**2, W01408.
URL: *https://doi.org/10.1029/2004WR003773*

Onda, K., LoBuglio, J. and Bartram, J. (2012), 'Global Access to Safe Water: Accounting for Water Quality and the Resulting Impact on MDG Progress', *Int. J. Environ. Res. Public Health* **9**(3), 880–894.
URL: *https://doi.org/10.3390/ijerph9030880*

Otero, N., Torrentó, C., Soler, A., Menció, A. and Mas-Pla, J. (2009), 'Monitoring groundwater nitrate attenuation in a regional system coupling hydrogeology with multi-isotopic methods: The case of Plana de Vic (Osona, Spain)', *Agric Ecosyst Environ.* **1**33, 103–113.
URL: *https://doi.org/10.1016/j.agee.2009.05.007*

Pangle, L. A., Kim, M., Cardoso, C., Lora, M., Meira Neto, A. A., Volkmann, T. H. M., Wang, Y., Troch, P. A. and Harman, C. J. (2017), 'The mechanistic basis for storage-dependent age distributions of water discharged from an experimental hillslope', *Water Resour. Res.* **5**3, 2733–2754.
URL: *https://doi.org/10.1002/2016WR019901*

Rinaldo, A., Benettin, P., Harman, C. J., Hrachowitz, M., McGuire, K. J., van der Velde, Y., Bertuzzo, E. and Botter, G. (2015), 'Storage selection functions: A coherent framework for quantifying how catchments store and release water and solutes', *Water Resour. Res.* **5**1, 4840–4847.
URL: *https://doi.org/10.1002/2015WR017273*

Rinaldo, A., Beven, K. J., Bertuzzo, E., Nicotina, L., Davies, J., Fiori, A., Russo, D. and Botter, G. (2011), 'Catchment travel time distributions and water flow in soils', *Water Resour. Res.* **4**7, W07537.
URL: *https://doi.org/10.1029/2011WR010478*

Rinaldo, A., Botter, G., Bertuzzo, E., Uccelli, A., Settin, T. and Marani, M. (2006), 'Transport at basin scales: 1. Theoretical framework', *Hydrol. Earth Syst. Sci.*

10, 19–29.
URL: *https://doi.org/10.5194/hess-10-19-2006*

Rivett, M. O., Buss, S. R., Morgan, P., Smith, J. W. N., and Bemment, C. D. (2008), 'Nitrate attenuation in groundwater: A review of biogeochemical controlling processes', *Water Research* **4**2, 4215–4232.
URL: *https://doi.org/10.1016/j.watres.2008.07.020*

Samaniego, L., Kumar, R. and Attinger, S. (2010), 'Multiscale parameter regionalization of a grid-based hydrologic model at the mesoscale', *Water Resour. Res.* **4**6, W05523.
URL: *https://doi.org/10.1029/2008WR007327*

Schuberth, K. (2008), '2 Geomorphologischer Überblick', *In: Bachmann GH et al (eds) Geologie von Sachsen-Anhalt* p. 689.

Seager, R., Ting, M., Held, I., Kushnir, Y., Lu, J., Vecchi, G., Huang, H. P., Harnik, N., Leetmaa, A., Lau, N. C., Li, C., Velez, J. and Naik, N. (2007), 'Model projections of an imminent transition to a more arid climate in southwestern North America', *Science* **3**16, 1181–1184.
URL: *https://doi.org/10.1126/science.1139601*

Seibert, J. and Beven, K. J. (2009), 'Gauging the ungauged basin: how many discharge measurements are needed?', *Hydrol. Earth Syst. Sci.* **1**3, 883–892.
URL: *https://doi.org/10.5194/hess-13-883-2009*

Sivapalan, M. (2006), 'Pattern, Process and Function: Elements of a Unified Theory of Hydrology at the Catchment Scale', *In Encyclopedia of Hydrological Sciences (eds M.G. Anderson and J.J. McDonnell)* .
URL: *https://doi.org/10.1002/0470848944.hsa012*

Smith, A., Tetzlaff, D. and Soulsby, C. (2018), 'On the Use of StorAge Selection Functions to Assess Time-Variant Travel Times in Lakes', *Water Resour. Res.* **5**4, 5163–5185.
URL: *https://doi.org/10.1029/2017WR021242*

Smith, J. W. N., Surridge, B. W. J., Haxton, T. H. and Lerner, D. N. (2009), 'Pollutant attenuation at the groundwater–surface water interface: A classification scheme and statistical analysis using national-scale nitrate data', *J. Hydrol.* **3**69, 392–402.
URL: *https://doi.org/10.1016/j.jhydrol.2009.02.026*

Smith, V. H. (2003), 'Eutrophication of freshwater and coastal marine ecosystems a global problem', *Environ. Sci. Pollut. Res.* **1**0, 126–139.
URL: *https://doi.org/10.1065/espr2002.12.142*

Soulsby, C. and Tetzlaff, D. (2008), 'Towards simple approaches for mean residence time estimation in ungauged basins using tracers and soil distributions', *J. Hydrol.* **3**63, 60–74.
URL: *https://doi.org/10.1016/j.jhydrol.2008.10.001*

Sprenger, M., Stumpp, C., Weiler, M., Aeschbach, W., Allen, S. T., Benettin, P., Dubbert, M., Hartmann, A., Hrachowitz, M., Kirchner, J. W., McDonnell, J. J., Orlowski, N., Penna, D., Pfahl, S., Rinderer, M., Rodriguez, N., Schmidt, M. and Werner, C. (2019), 'The Demographics of Water: a Review of Water Ages in the Critical Zone', *Reviews of Geophysics* **57**, 800–834.
URL: *https://doi.org/10.1029/2018RG000633*

Steffen, W., Richardson, K., Rockström, J., Cornell, S. E., Fetzer, I., Bennett, E. M., Biggs, R., Carpenter, S. R., de Vries, W., de Wit, C. A., Folke, C., Gerten, D., Heinke, J., Mace, G. M., Persson, L. M., Ramanathan, V., Reyers, B. and Sörlin, S. (2015), 'Planetary boundaries: Guiding human development on a changing planet', *Science* **3**47, 1259855.
URL: *https://doi.org/10.1126/science.1259855*

Stockinger, M. P., Bogena, H. R., Lücke, A., Diekkrüger, B., Cornelissen, T. and Vereecken, H. (2016), 'Tracer sampling frequency influences estimates of young water fraction and streamwater transit time distribution', *J. Hydrol.* **5**41, 952—-964.
URL: *https://doi.org/10.1016/j.jhydrol.2016.08.007*

Tetzlaff, D., Malcolm, I. A. and Soulsby, C. (2007), 'Influence of forestry, environmental change and climatic variability on the hydrology', *J. Hydrol.* **3**46, 93–111.
URL: *https://doi.org/10.1016/j.jhydrol.2007.08.016*

Tetzlaff, D., Piovano, T., A., P., Smith, A., K., C. S., Marsh, P., Wookey, P. A., Street, L. E. and Soulsby, C. (2018), 'Using stable isotopes to estimate travel times in a data-sparse Arctic catchment: Challenges and possible solutions', *Hydrol. Process.* **3**2, 1936–1952.
URL: *https://doi.org/10.1002/hyp.13146*

Tromp-van Meerveld, H. J. and McDonnell, J. J. (2006), 'Threshold relations in subsurface stormflow: 1. a 147-storm analysis of the Panola hillslope', *Water Resour. Res.* **4**2, W02410.
URL: *https://doi.org/10.1029/2004WR003778*

van der Velde, Y., Torfs, P. J. J. F., van der Zee, S. E. A. T. M. and Uijlenhoet, R. (2012), 'Quantifying catchment-scale mixing and its effect on time-varying travel time

distributions', *Water Resour. Res.* **4**8, W06536.
URL: *https://doi.org/10.1029/2011WR011310*

Van Meter, K. J. and Basu, N. B. (2017), 'Time lags in watershed-scale nutrient transport: an exploration of dominant controls', *Environ. Res. Lett.* **1**2, 084017.
URL: *https://doi.org/10.1088/1748-9326/aa7bf4*

Van Meter, K. J., Basu, N. B. and Van Cappellen, P. (2017), 'Two centuries of nitrogen dynamics: Legacy sources and sinks in the Mississippi and Susquehanna River Basins', *Global Biogeochemical Cycles* **3**1, 2–23.
URL: *https://doi.org/10.1002/2016GB005498*

Van Meter, K. J., Van Cappellen, P. and Basu, N. B. (2018), 'Legacy nitrogen may prevent achievement of water quality goals in the Gulf of Mexico', *Science* **3**60, 427–430.
URL: *https://doi.org/10.1126/science.aar4462*

Vitousek, P. M., Mooney, H. A., Lubchenco, J. and Melillo, J. M. (1997), 'Human Domination of Earth's Ecosystems', *Science* **2**77, 494–499.
URL: *https://doi.org/10.1126/science.277.5325.494*

von Freyberg, J., Allen, S. T., Seeger, S., Weiler, M. and Kirchner, J. W. (2018), 'Sensitivity of young water fractions to hydro-climatic forcing and landscape properties across 22 Swiss catchments', *Hydrol. Earth Syst. Sci.* **2**2, 3841–3861.
URL: *https://doi.org/10.5194/hess-22-3841-2018*

von Freyberg, J., Rücker, A., Zappa, M., Schlumpf, A., Studer, B. and Kirchner, J. W. (2022), 'Four years of daily stable water isotope data in stream water and precipitation from three Swiss catchments', *Sci Data* **9**, 46.
URL: *https://doi.org/10.1038/s41597-022-01148-1*

Vörösmarty, C. J., McIntyre, P. B., Gessner, M. O., Dudgeon, D., Prusevich, A., Green, P., Glidden, S., Bunn, S. E., Sullivan, C. A., Liermann, C. R. and Davies, P. M. (2010), 'Global threats to human water security and river biodiversity', *Nature* **4**67, 555–561.
URL: *https://doi.org/10.1038/nature09440*

Wagener, T., Sivapalan, M., Troch, P. and Woods, R. (2007), 'Catchment Classification and Hydrologic Similarity', *Geogr. Compass* **1**, 901–931.
URL: *https://doi.org/10.1111/j.1749-8198.2007.00039.x*

Winter, C., Lutz, S. R., Musolff, A., Kumar, R. Weber, M. and Fleckenstein, J. H. (2021), 'Disentangling the Impact of Catchment Heterogeneity on Nitrate Export Dynamics

From Event to Long-Term Time Scales', *Water Resour. Res.* **57**, e2020WR027992.
URL: *https://doi.org/10.1029/2020WR027992*

Winter, C., Nguyen, T. V., Musolff, A., Lutz, S. R., Rode, M., Kumar, R., and Fleckenstein, J. H. (2023), 'Droughts can reduce the nitrogen retention capacity of catchments', *Hydrol. Earth Syst. Sci.* **27**, 303–318.
URL: *https://doi.org/10.5194/hess-27-303-2023*

Winter, C., Tarasova, L., Lutz, S. R., Musolff, A., Kumar, R. and Fleckenstein, J. H. (2022), 'Explaining the Variability in High-Frequency Nitrate Export Patterns Using Long-Term Hydrological Event Classification', *Water Resour. Res.* **5**8, e2021WR030938.
URL: *https://doi.org/10.1029/2021WR030938*

Wollschläger, U., Attinger, S., Borchardt, D., Brauns, M., Cuntz, M., Dietrich, P., Fleckenstein, J. H., Friese, K., Friesen, J., Harpke, A., Hildebrandt, A., Jäckel, G., Kamjunke, N., Knöller, K., Kögler, S., Kolditz, O., Krieg, R., Kumar, R., Lausch, A., Liess, M., Marx, A.and Merz, R., Mueller, C., Musolff, A., Norf, H., Oswald, S. E., Rebmann, C., Reinstorf, F., Rode, M., Rink, K., Rinke, K., Samaniego, L., Vieweg, M., Vogel, H. J., Weitere, M., Werban, U., M., Z. and Zacharias, S. (2017), 'The Bode hydrological observatory: a platform for integrated, interdisciplinary hydro-ecological research within the TERENO Harz/Central German Lowland Observatory', *Environ. Earth Sci.* **7**6, 29.
URL: *https://doi.org/10.1007/s12665-016-6327-5*

Yang, X., Jomaa, S., Zink, M., Fleckenstein, J. H., Borchardt, D. and Rode, M. (2018), 'A New Fully Distributed Model of Nitrate Transport and Removal at Catchment Scale', *Water Resour. Res.* **5**4, 5856–5877.
URL: *https://doi.org/10.1029/2017WR022380*

Zessner, M. (2021), 'Monitoring, Modeling and Management of Water Quality', *Water* **1**3, 1523.
URL: *https://doi.org/10.3390/w13111523*

Zink, M., Kumar, R., Cuntz, M. and Samaniego, L. (2017), 'A high-resolution dataset of water fluxes and states for Germany accounting for parametric uncertainty', *Hydrol. Earth Syst. Sci.* **2**1, 1769–1790.
URL: *https://doi.org/10.5194/hess-21-1769-2017*

Declaration of Contributions

Study 1

Title:	Uncertainty in water transit time estimation with StorAge Selection functions and tracer data interpolation
Status:	Published in Hydrology and Earth System Sciences
DOI:	10.5194/hess-27-2989-2023
Authors:	Arianna Borriero, Rohini Kumar, Tam V. Nguyen, Jan H. Fleckenstein, Stefanie R. Lutz

Own contribution:

Study concept and design:	60 %
Data analysis:	100 %
Preparation of figures and tables:	100 %
Interpretation of the results:	80 %
Preparation of the manuscript:	90 %

Contribution of authors:

AB conducted the model simulations, carried out the analysis, interpreted the results, prepared the figures and wrote the original draft of the paper. AB, SRL and RK designed and conceptualized the study. SRL and RK provided data for model simulations. TVN provided technical support for modeling and helped organize the structure and content of the manuscript. AB, SRL, RK, and TVN conceived the methodology and experimental design. All co-authors helped AB interpret the results. All authors contributed to the review, final writing, and finalization of this work. AB is the corresponding author.

Study 2

Title:	Can the Young Water Fraction Reduce Predictive Uncertainty in Water Transit Time Estimations?
Status:	Published in Journal of Hydrology
DOI:	10.1016/j.jhydrol.2024.132238
Authors:	Arianna Borriero, Tam V. Nguyen, Stefanie R. Lutz, Jan H. Fleckenstein, Andreas Musolff, Rohini Kumar

Own contribution:

Study concept and design:	60 %
Data analysis:	100 %
Preparation of figures and tables:	100 %
Interpretation of the results:	90 %
Preparation of the manuscript:	90 %

Contribution of authors:

AB conducted the model simulations, carried out the analysis, interpreted the results, prepared the figures and wrote the original draft of the paper. AB, SRL and RK designed and conceptualized the study. SRL and RK provided data for model simulations. AB, SRL, RK and TVN conceived the methodology and experimental design. All co-authors helped AB interpret the results. All authors contributed to the review, final writing, and finalization of this work. AB is the corresponding author.

Study 3

Title:	The Value of Instream Stable Water Isotope and Nitrate Concentration Data for Calibrating a Travel-Time based Water Quality Model
Status:	Published in Hydrological Processes
DOI:	10.1002/hyp.15154
Authors:	Arianna Borriero, Andreas Musolff, Rohini Kumar, Jan H. Fleckenstein, Stefanie R. Lutz, Tam V. Nguyen

Own contribution:

Study concept and design:	70 %
Data analysis:	100 %
Preparation of figures and tables:	100 %
Interpretation of the results:	90 %
Preparation of the manuscript:	100 %

Contribution of authors:

AB conducted the model simulations, carried out the analysis, interpreted the results, prepared the figures and wrote the original draft of the paper. AB, AM, TVN and RK designed and conceptualized the study. TVN provided the support for modeling. AM, TVN, RK and SRL provided data for model simulations. AB, AM, TVN and RK conceived the methodology and experimental design. All co-authors helped AB interpret the results. All authors contributed to the review, final writing and finalization of this work. AB and TVN are the corresponding authors.

Manuscripts

Hydrol. Earth Syst. Sci., 27, 2989–3004, 2023
https://doi.org/10.5194/hess-27-2989-2023

Hydrology and Earth System Sciences
Open Access
EGU

Uncertainty in water transit time estimation with StorAge Selection functions and tracer data interpolation

Arianna Borriero[1], Rohini Kumar[2], Tam V. Nguyen[1], Jan H. Fleckenstein[1,3], and Stefanie R. Lutz[4]

[1]Department of Hydrogeology, Helmholtz Centre for Environmental Research – UFZ, Leipzig, Germany
[2]Department of Computational Hydrosystems, Helmholtz Centre for Environmental Research – UFZ, Leipzig, Germany
[3]Bayreuth Centre of Ecology and Environmental Research, University of Bayreuth, Bayreuth, Germany
[4]Copernicus Institute of Sustainable Development, Department of Environmental Sciences,
Utrecht University, Utrecht, the Netherlands

Correspondence: Arianna Borriero (arianna.borriero@ufz.de)

Received: 10 June 2022 – Discussion started: 26 July 2022
Revised: 22 June 2023 – Accepted: 2 July 2023 – Published: 14 August 2023

Abstract. Transit time distributions (TTDs) of streamflow are useful descriptors for understanding flow and solute transport in catchments. Catchment-scale TTDs can be modeled using tracer data (e.g. oxygen isotopes, such as δ^{18}O) in inflow and outflows by employing StorAge Selection (SAS) functions. However, tracer data are often sparse in space and time, so they need to be interpolated to increase their spatiotemporal resolution. Moreover, SAS functions can be parameterized with different forms, but there is no general agreement on which one should be used. Both of these aspects induce uncertainty in the simulated TTDs, and the individual uncertainty sources as well as their combined effect have not been fully investigated. This study provides a comprehensive analysis of the TTD uncertainty resulting from 12 model setups obtained by combining different interpolation schemes for δ^{18}O in precipitation and distinct SAS functions. For each model setup, we found behavioral solutions with satisfactory model performance for in-stream δ^{18}O (KGE $>$ 0.55, where KGE refers to the Kling–Gupta efficiency). Differences in KGE values were statistically significant, thereby showing the relevance of the chosen setup for simulating TTDs. We found a large uncertainty in the simulated TTDs, represented by a large range of variability in the 95 % confidence interval of the median transit time, varying at the most by between 259 and 1009 d across all tested setups. Uncertainty in TTDs was mainly associated with the temporal interpolation of δ^{18}O in precipitation, the choice between time-variant and time-invariant SAS functions, flow conditions, and the use of nonspatially interpolated δ^{18}O in precipitation. We discuss the implications of these results for the SAS framework, uncertainty characterization in TTD-based models, and the influence of the uncertainty for water quality and quantity studies.

1 Introduction

Understanding how catchments store and release water of different ages has significant implications for flow and solute transport, as water ages encapsulate information about flow paths' characteristics (McGuire and McDonnel, 2006; Botter et al., 2011), the contact time of solutes with the soil matrix (Benettin et al., 2015a; Hrachowitz et al., 2016), and vulnerability assessment (Kumar et al., 2020). This plays an important role in water resources protection and management, and it requires a tool that can effectively describe catchment-scale transport processes (Rinaldo and Marani, 1987). The age of water in outflows is commonly referred to as transit time (TT), i.e. the time that elapses between the entry of a water parcel into the catchment via precipitation and its exit via streamflow or evapotranspiration. Accordingly, the transit time distribution (TTD) describes the whole spectrum of transit times in outflows (Botter et al., 2005; Van der Velde et al., 2010). Early studies have often assumed simplified steady-state transport models, resulting in time-invariant TTDs (Niemi, 1977; Rinaldo et al., 2006). However, experimental simulations have shown that TTDs are time-variant due to the variability in meteorological forcing (Botter et al.,

Published by Copernicus Publications on behalf of the European Geosciences Union.

2010; Hrachowitz et al., 2010; Heidbüchel et al., 2020) and the activation/deactivation of flow paths in response to varying hydrologic conditions (Ambroise, 2004; Heidbüchel et al., 2013). Recent research has introduced new models for representing time-variant TTDs, for example, allowing for the estimation of TTDs without making prior assumptions about their shape (Kirchner, 2019; Kim and Troch, 2020) or with the parameterization of the StorAge Selection (SAS) functions (Rinaldo et al., 2015; Harman, 2019). SAS functions describe how catchments selectively remove water of different ages from storage for outflows, and they have led to a new framework of nonstationary transport models based on water age, which have been successfully applied in various studies (Benettin et al., 2015b; Queloz et al., 2015; Kim et al., 2016; Lutz et al., 2017; Wilusz et al., 2017; Nguyen et al., 2021).

Model-based TTDs are subjected to uncertainty, which limits their ability with respect to decision support. In general, model prediction uncertainty stems from model inputs, structure, and parameters (Beven and Freer, 2001). As TTDs are not directly observable, conservative environmental tracers (e.g. oxygen isotopes, such as δ^{18}O) in inflow and outflows are commonly used to infer water ages (Hrachowitz et al., 2013; Birkel and Soulsby, 2015; Stockinger et al., 2015). Long-term, high-frequency tracer data with an appropriate spatial distribution are generally recommended for a sufficient understanding of TTD dynamics across a wide range of fast and heterogeneous hydrological behaviors (Kirchner et al., 2004; Danesh-Yazdi et al., 2016; von Freyberg et al., 2017). Therefore, a lack of appropriate tracer data coverage can hamper our understanding of TTD dynamics at the desired resolution (McGuire and McDonnel, 2006). Additionally, uncertainty in the driving hydroclimatic fluxes, such as precipitation, discharge, and evapotranspiration, could propagate into the uncertainty in the modeling results. Further uncertainty emerges from the model structure due to the difficulty in representing physical processes because of our incomplete knowledge of complex reality (Ajami et al., 2007). Finally, specification of model parameters is also an important source of uncertainty (Beven, 2006; Kirchner, 2006), as the best-fit parameters may suffer from equifinality (Schoups et al., 2008).

A few studies have investigated the uncertainty in the estimated TTDs with SAS models. Danesh-Yazdi et al. (2018) and Jing et al. (2019) analyzed the effect of interactions between distinct flow domains, external forcing, and recharge rate on the resulting TTDs. Several works (Benettin et al., 2017; Wilusz et al., 2017; Rodriguez et al., 2018, 2021) have explored model parameter uncertainty and suggested that additional types of tracers, data on physical characteristics of the catchment, and parsimonious parameterization may help to further reduce parametric uncertainty in the SAS models. More recently, Buzacott et al. (2020) investigated how gap-filling of the δ^{18}O record in precipitation propagated uncertainty into the simulated mean water transit time (MTT), i.e. the average time it takes for water to leave the catchment (McDonnel et al., 2010).

Despite the studies cited above, there are other aspects that are particularly significant for SAS modeling and cause uncertainty in the simulated TTDs that have not yet been thoroughly investigated. First, isotope data are generally sparse globally in space and time (von Freyberg et al., 2022), due to laborious and costly sampling campaigns limited to well-equipped areas (Tetzlaff et al., 2018). As SAS models require continuous time series of input tracer data, different methods for temporal interpolation could be used to reconstruct isotope values in precipitation; consequently, the interpolated input data are subject to uncertainty. Furthermore, the input data of SAS models are influenced by whether the tracer data in precipitation are collected at a single location within the catchment or at multiple locations. In the latter scenario, there is a need to account for the spatial variability in the tracer composition in precipitation, which is commonly done via spatial interpolation. Choosing data from one approach (i.e. tracer data from a single location) over the other (i.e. tracer data spatially interpolated based on multiple locations, including stations outside the catchment boundaries) can potentially result in different resulting TTDs. Finally, SAS functions, employed to model TTDs, must be parameterized, and their functional forms need to be specified a priori. Commonly used forms are the power law (Benettin et al., 2017; Asadollahi et al., 2020), beta (van der Velde et al., 2012; Drever and Hrachowitz, 2017), and gamma (Harman, 2015; Wilusz et al., 2017) distributions. However, there is no general agreement on which SAS function should be used, as the hydrological processes that control the patterns and dynamics of the subsurface vary across catchments. Therefore, the most convenient approach is to simply rely on a specific parameterization over another and estimate its parameters (Harman, 2015). All of these aspects, related to model input, structure, and parameters, induce uncertainty in the simulated TTDs. To date, the role of these individual uncertainty sources and their combined effect on the modeled TTDs have not been adequately discussed.

This study bridges the aforementioned gaps by specifically exploring the combined effect of tracer data interpolation and model parameterizations on the simulated TTDs. We investigated TTD uncertainty using an SAS-based catchment-scale transport model applied to the upper Selke catchment, Germany. We evaluated TTDs resulting from 12 model setups obtained by combining distinct interpolation techniques of δ^{18}O in precipitation and parameterizations of SAS functions. For each model setup, we searched for behavioral parameter sets (i.e. those providing acceptable predictions) based on model performance for in-stream δ^{18}O, and we evaluated the sources of uncertainty and their combined effects in the modeled TTDs. Overall, our results provide new insights into the uncertainty characterization of TTDs, particularly in the absence of high-frequency tracer data, and the

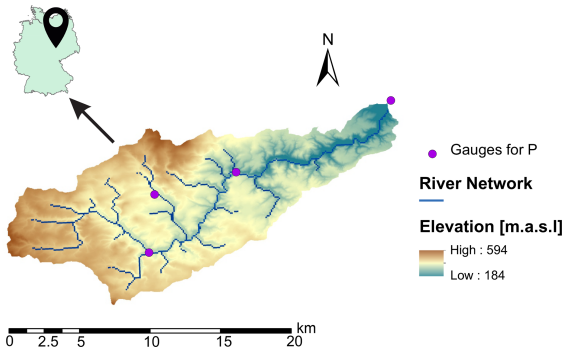

Figure 1. The upper Selke catchment, showing precipitation sampling points (purple dots), the river network (blue lines), and the elevation (in meters above sea level) as a colored map. The inset presents the location of the upper Selke catchment in Germany.

use of SAS functions as well as the implications of TTDs' uncertainty on water quantity and quality studies.

2 Study area and data

The upper Selke catchment is located in the Harz Mountains in Saxony-Anhalt, central Germany (Fig. 1). The study site is part of the Bode region, an intensively monitored area within the TERENO (TERrestrial ENvironmental Observatories; Wollschläger et al., 2017) network. The catchment has a drainage area of 184 km^2, the altitude ranges between 184 and 594 m above mean sea level, and the mean slope is 7.65 %. Land use is dominated by forest (broadleaf, coniferous, and mixed forest) and agricultural land (winter cereals, rapeseed, and maize), representing 72 % and 21 % of the catchment, respectively. The soil is largely composed of Cambisols and the underlying geology consists of schist and claystone, resulting in a predominance of relatively shallow flow paths (Dupas et al., 2017; J. Yang et al., 2018).

Daily hydroclimatic and monthly tracer data in the upper Selke catchment were available for the period between February 2013 and May 2015. Precipitation (P) was taken from the German Weather Service, whereas discharge (Q) and evapotranspiration (ET) were simulated data obtained from the mesoscale Hydrological Model (mHM; Samaniego et al., 2010; Kumar et al., 2013), as continuous measurements were not available for the given outlet and period. A thorough evaluation of mHM performance for past measurements has been conducted in previous studies (Zink et al., 2017; X. Yang et al., 2018; Nguyen et al., 2021). The average annual P, Q, and ET are 703, 108, and 596 mm, respectively. The area is characterized by high flow during November–May (average $Q = 0.88\,\mathrm{m}^3\,\mathrm{s}^{-1}$) and low flow during June–October (average $Q = 0.42\,\mathrm{m}^3\,\mathrm{s}^{-1}$). Evapotranspiration is higher in June (109 mm per month) and lower in December (10 mm per month). The average monthly temperature ranges from −0.7 °C in January to 17 °C in July. The δ^{18}O values in precipitation ($\delta^{18}O_P$) and in streamflow ($\delta^{18}O_Q$) at a monthly resolution were taken from Lutz et al. (2018) and are displayed in Fig. 2. Values of $\delta^{18}O_P$ were used in the form of "raw" (i.e. values collected at the catchment outlet) and "processed" (i.e. values collected at multiple locations and spatially interpolated using kriging) data (see Sect. 3.2 for more details). The variability in $\delta^{18}O_P$ was larger than that in $\delta^{18}O_Q$ (Fig. 2) because of the damping of the precipitation signal due to mixing and dispersion within the catchment. Temperature dependence caused more depleted (i.e. more negative) $\delta^{18}O_P$ in winter than in summer (Fig. 2).

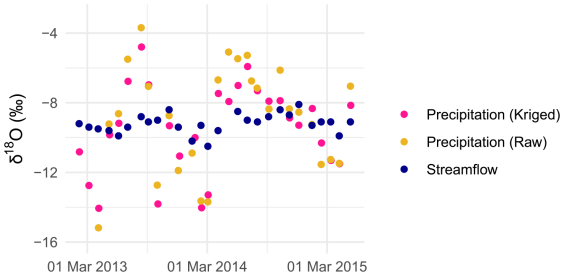

Figure 2. Data of δ^{18}O in precipitation (kriged values as pink dots and raw values as yellow dots) and streamflow (blue dots).

3 Methods

3.1 Catchment-scale transport model

In this study, we used the *tran*-SAS model (Benettin and Bertuzzo, 2018a) for describing the catchment-scale water mixing and solute transport based on SAS functions. The catchment was conceptualized as a single storage $S(t)$ (mm), whose water-age balance can be expressed as follows (Benettin and Bertuzzo, 2018a):

$$S(t) = S_0 + V(t) \tag{1}$$

$$\frac{\partial S_T(T,t)}{\partial t} + \frac{\partial S_T(T,t)}{\partial T} = P(t) - Q(t)\cdot\Omega_Q(S_T,t) - \mathrm{ET}(t)\cdot\Omega_{\mathrm{ET}}(S_T,t), \tag{2}$$

$$\text{with an initial condition of } S_T(T,t=0) = S_{T_0}(T) \tag{3}$$

$$\text{and a boundary condition of } S_T(0,t) = 0. \tag{4}$$

Here, S_0 (mm) is the initial storage; $V(t)$ (mm) represents the storage variations; $P(t)$ (mm d^{-1}), $Q(t)$ (mm d^{-1}), and ET(t) (mm d^{-1}) are precipitation, discharge, and evapotranspiration, respectively; $S_T(T,t)$ (mm) is the age-ranked storage; $S_{T_0}(T)$ (mm) is the initial age-ranked storage; and $\Omega_Q(S_T,t)$ (–) and $\Omega_{\mathrm{ET}}(S_T,t)$ (–) are the cumulative SAS functions for Q and ET, respectively.

By definition, the TTD of streamflow $p_Q(T,t)$ (d^{-1}) is calculated as follows (Benettin and Bertuzzo, 2018a):

$$p_Q(T,t) = \frac{\partial \Omega_Q(S_T,t)}{\partial S_T} \cdot \frac{\partial S_T}{\partial T}. \quad (5)$$

The isotopic signature in streamflow $C_Q(t)$ (‰) can be obtained as follows (Benettin and Bertuzzo, 2018a):

$$C_Q(t) = \int_0^{+\infty} C_S(T,t) \cdot p_Q(T,t) \cdot dT, \quad (6)$$

where $C_S(T,t)$ (‰) is the isotopic signature of a water parcel in storage. Equations (5) and (6) also apply for ET.

In this study, we tested three SAS parameterizations: the power law time-invariant (PLTI; Eq. 7, Queloz et al., 2015), power law time-variant (PLTV; Eq. 8, Benettin et al., 2017), and beta time-invariant (BETATI; Eq. 9, Drever and Hrachowitz, 2017) distributions. Here, they are expressed as probability density functions in terms of the normalized age-ranked storage $P_S(T,t)$ (–), also known as fractional SAS functions (fSAS):

$$\omega(P_S(T,t),t) = k \cdot (P_S(T,t))^{k-1}, \quad (7)$$

$$\omega(P_S(T,t),t) = k(t) \cdot (P_S(T,t))^{k(t)-1}, \quad (8)$$

$$\omega(P_S(T,t),t) = \frac{(P_S(T,t))^{\alpha-1} \cdot (1-P_S(T,t))^{\beta-1}}{B(\alpha,\beta)}. \quad (9)$$

The parameters k, α, and β determine the catchment's water-age preference for outflows, while $B(\alpha,\beta)$ is the two-parameter beta function. If $k<1$, or if $\alpha<1$ and $\beta>1$, the system tends to discharge young water. If $k>1$, or if $\alpha>1$ and $\beta<1$, the catchment preferably releases old water. The case of $k=1$ or $\alpha=\beta=1$ describes no selection preference (i.e. complete water mixing). PLTV is characterized by $k(t)$ varying linearly over time between two extremes, k_1 and k_2, as a function of the catchment wetness wi (–), i.e. $\mathrm{wi}(t) = (S(t)-S_{\min})/(S_{\max}-S_{\min})$, where $S_{\min}$ and $S_{\max}$ are the respective minimum and maximum storage values over the entire period.

3.2 Interpolation techniques for $\delta^{18}O$ in precipitation

We tested the model with two spatial representation and two temporal interpolation methods for $\delta^{18}O_P$ to explore the impact of input tracer data on model performance, results, and uncertainty. To evaluate the effect of spatial representation, we firstly used single-point $\delta^{18}O_P$ measurements, which we refer to in the following as raw $\delta^{18}O_P$. These measurements, obtained from Lutz et al. (2018), were taken at the catchment outlet. The selection of $\delta^{18}O_P$ at the outlet assumes a precipitation collector close to the stream gauge at the outlet, which is a common occurrence in many catchments for logistical reasons. Indeed, the outlet, where in-stream $\delta^{18}O$ is sampled, serves as the location where all precipitation inputs across the catchment are integrated. For convenience, precipitation monitoring is also often conducted at or near the gauging station at the outlet. Secondly, we used spatially interpolated $\delta^{18}O_P$ with kriging based on multiple locations. The spatial interpolation was conducted in Lutz et al. (2018) using raw $\delta^{18}O_P$ from 24 precipitation collectors spread over the larger Bode region and using altitude as external drift. In a further step, the kriged $\delta^{18}O_P$ data were weighted with spatially distributed monthly precipitation to obtain representative estimates for the study catchment. In our study, the kriged $\delta^{18}O_P$ resulted in slightly more negative values than the raw $\delta^{18}O_P$ from the catchment outlet (Fig. 2) because of the inclusion of more depleted $\delta^{18}O_P$ values from locations with higher altitudes during the kriging process. By considering these two options for the spatial representation of $\delta^{18}O_P$, we intend to assess the influence of spatial variability and uncertainty in the simulated outputs between two opposing cases i.e. raw isotopes representing the simplest approach and kriged isotopes derived from a more sophisticated method. While there are other possibilities for the spatial representation of $\delta^{18}O_P$, our choice allows us to effectively address our research question regarding the effects on SAS models of tracer data in precipitation collected at a single location within the catchment or spatially interpolated from multiple sites.

SAS model results are sensitive to the choice of the temporal resolution of input tracer data, and a finer resolution is generally recommended to achieve a satisfactory level of detail (Benettin and Bertuzzo, 2018a). Additionally, a forward Euler scheme was employed to solve Eq. (2), whose precision increases with high-frequency time steps. For these reasons, we reconstructed daily $\delta^{18}O_P$ estimates from monthly values with two interpolation schemes. First, we used a step function in which the values between two consecutive samples assumed the value of the last sample. Second, we used a sine interpolation due to the fact that $\delta^{18}O_P$ samples typically exhibit pronounced seasonal variations with more depleted values in winter than in summer (Fig. 2). The sine-wave function has been used in several studies to describe temporal variation in $\delta^{18}O_P$ (McGuire and McDonnel, 2006; Feng et al., 2009; Allen et al., 2019). The seasonal pattern of $\delta^{18}O_P$ values over a period of 1 year can be described as follows (Kirchner, 2016):

$$\delta^{18}O_P(t) = a_P \cdot \cos(2\cdot\pi\cdot f\cdot t) + b_P \cdot \sin(2\cdot\pi\cdot f\cdot t) + k_P, \quad (10)$$

where a and b are regression coefficients (–), t is the time (decimal years), f is the frequency (yr^{-1}), and k is the vertical offset of the isotope signal (‰). The coefficients a and b were estimated by fitting Eq. (10) to monthly $\delta^{18}O_P$ values using the iteratively re-weighted least-squares (IRLS) estimation (von Freyberg et al., 2018). In our study, we reproduced the daily frequency isotopic data through the estimated regression coefficients of Eq. (10). Figure 3 displays the daily kriged and raw $\delta^{18}O_P$ values simulated via step function and sine interpolation; by employing step function and sine interpolation as techniques to reconstruct tracer data in precip-

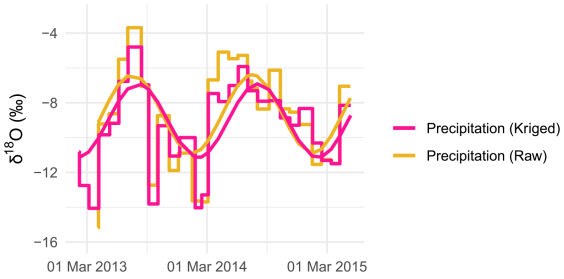

Figure 3. Predicted δ^{18}O in precipitation (kriged values as pink lines and raw values as yellow lines) via step function and sine interpolation.

itation, we aim to analyze the effects on SAS-based results from two relatively simple, rather opposing approaches: one focusing on individual measurements and the other on seasonality.

3.3 Experimental design

In this study, different scenarios were used to quantify uncertainty in the modeled results. We tested 12 setups composed of three SAS functions (PLTI, PLTV, and BETATI), two temporal interpolations (step and sine function), and two spatial representations (raw and kriged values) of $\delta^{18}O_P$ (Table 1). For each setup, we performed a Monte Carlo experiment by running the model with 10 000 parameter sets generated by Latin hypercube sampling (LHS; McKay et al., 1979). Model parameters and their search ranges are shown in Table 2. A 5-year warm-up period (i.e. repetition of the input data) from February 2008 to January 2013 was performed to reduce the impact of model initialization. The period from February 2013 to May 2015 was used to infer behavioral parameters (i.e. parameter sets giving acceptable predictions) and, subsequently, to interpret model results. The initial concentration of δ^{18}O in storage was set to 9.2 ‰, coinciding with the mean $\delta^{18}O_Q$ over the study period.

The informal likelihood of the Sequential Uncertainty Fitting (SUFI-2; Abbaspour et al., 2004) procedure was applied to account for uncertainty in the parameter sets and resulting modeled estimates. In SUFI-2, the uncertainty is represented by a uniform distribution, which is gradually reduced until a specific criterion is reached. In our study, we calibrated the values of model parameters until the predicted output matched the measured $\delta^{18}O_Q$ to a satisfactory level, defined by an objective function. As the objective function, we employed the Kling–Gupta efficiency (KGE; Gupta et al., 2009), and once the criterion of KGE ≥ 0.5 was satisfied, we defined a set of behavioral solutions for each model setup. However, as the aim of this study is to investigate the impact of various sources of uncertainty on simulated outputs, rather than to determine the best model setup, we decided to set a fixed sample size and narrow down those solutions generated by SUFI-2 in the previous step. Setting a fixed sample size ensures the comparability of results across the setups, as different sample sizes could influence the uncertainty analysis (i.e. the greater the number of behavioral solutions, the wider the uncertainty band). By fixing the sample size, we can still meet the requirement of a minimum acceptable KGE value (i.e. KGE ≥ 0.5). In this study, we determined the final behavioral solutions by using a fixed sample size that corresponds to the best 5 % parameter sets and modeled results in terms of the KGE.

Table 1. List of model setups.

Setup	Interpolation	SAS function
a	step function	PLTI
b	kriged $\delta^{18}O_P$	PLTV
c		BETATI
d	step function	PLTI
e	raw $\delta^{18}O_P$	PLTV
f		BETATI
g	sine function	PLTI
h	kriged $\delta^{18}O_P$	PLTV
i		BETATI
j	sine function	PLTI
k	raw $\delta^{18}O_P$	PLTV
l		BETATI

To assess the range of possible behavioral solutions and understand the level of uncertainty associated with it, we calculated the 95 % confidence interval (CI) derived by computing the 2.5 % and 97.5 % percentile values of the cumulative distribution in the parameters and time series of output variables (Abbaspour et al., 2004). These percentile values represent the lower and upper bounds of the CI, respectively. In our experimental setup, the main output variables were the in-stream δ^{18}O signature and backward median transit time (TT_{50}, in days, i.e. the time it takes for half of the water particles to leave the system as streamflow at the catchment outlet). Time series of TT_{50} were extracted directly from daily TTDs (Eq. 5) and used as a metric for the streamflow age. This was done because TTDs are typically skewed with long tails (Kirchner et al., 2001); hence, the median is often a more suitable metric than, for example, the MTT, as it is less impacted by the poor identifiability of the older water components (Benettin et al., 2017).

4 Results

4.1 Simulated δ^{18}O in streamflow and model performance

Modeled δ^{18}O values in streamflow ($\delta^{18}O_Q$) represented by the 95 % confidence interval (CI) in the ensemble solu-

Table 2. Model parameters and search ranges.

SAS parameter	Symbol	Unit	Lower bound	Upper bound
Discharge SAS parameter	k_Q	–	0.1	2
	k_{Q1}	–	0.1	2
	k_{Q2}	–	0.1	2
	α	–	0.1	2
	β	–	0.1	2
Evapotranspiration SAS parameter	k_{ET}	–	0.1	2
Initial storage	S_0	mm	300	3000

tion are displayed in Fig. 4. The results reveal how the predicted $\delta^{18}O_Q$ values enveloped the measured isotopic signature by reproducing its seasonal fluctuations, with depleted (i.e. more negative) values in winter and enriched (i.e. less negative) values in summer. Although the behavioral parameter sets were able to capture the seasonal isotopic trend, they poorly reproduced the exact values; therefore, the ensemble simulations are characterized by a non-negligible uncertainty.

Figure 4 shows the distinct effects of the interpolated input tracer data and model parameterization on the simulated $\delta^{18}O_Q$ values. The step function interpolation generated an erratic isotopic signature in streamflow with flashy fluctuations (Fig. 4a–f). On the other hand, sine interpolation of $\delta^{18}O_P$ values yielded a smooth response in the simulated $\delta^{18}O_Q$ values (Fig. 4g–l). No significant visual distinction was found between kriged (Fig. 4a–c) and raw (Fig. 4d–f) $\delta^{18}O_P$ samples when the step function interpolation was used, except for a slightly larger uncertainty observed with raw $\delta^{18}O_P$ samples. Furthermore, when employing the sine interpolation and raw $\delta^{18}O_P$ values (Fig. 4j–l), the simulations overestimated the in-stream measurements in comparison with kriged values (Fig. 4g–i). Finally, distinct SAS parameterizations did not produce remarkable differences in the simulated $\delta^{18}O_Q$ values, although PLTV generally yielded simulations that better enveloped the measured isotopic signature (Fig. 4b, e, h, k).

Despite the differences in the predicted $\delta^{18}O_Q$ values, all simulations can be considered satisfactory given the KGE values ranging between 0.55 and 0.72 across all tested setups (Fig. 5). This aforementioned model performance can be classified as intermediate (Thiemig et al., 2013) to good (Andersson et al., 2017; Sutanudjaja et al., 2018). When considering the best fit, the combination of step function interpolation and raw $\delta^{18}O_P$ values performed best. Additionally, PLTV generally yielded slightly better KGE values than PLTI or BETATI when grouping the setups with the same spatiotemporal interpolation of $\delta^{18}O_P$. Differences in the mean KGEs were statistically insignificant (t test with p values > 0.05) only between setups a–g, c–i–k, and j–l (Table 1), as the mean KGE values were nearly identical; this largely agrees with the visual analysis (Fig. 5). Contrarily, the differences in the mean KGE values of the remaining setups were statistically significant (p values < 0.05), indicating that the a priori methodological choices (i.e. interpolation techniques of $\delta^{18}O_P$ values and/or SAS parameterization) strongly impact the overall results. Nonetheless, this does not mean that we can clearly identify the most suitable setup, but there is a need to carefully analyze the multiple potential choices with respect to SAS parameterization and tracer data interpolations as well as to evaluate the uncertainty range in modeled predictions.

Ranges of the behavioral SAS parameters for the tested setups are summarized in Table S1 in the Supplement. Parameters for the SAS functions of Q (i.e. k_Q, k_{Q1}, k_{Q2}, α, and β) were different across the setups, although they were generally relatively narrow and well identified. However, the behavioral parameters were better constrained when using the step function interpolation, as their 95 % CI was, on average, 34 % narrower than that provided by the sine interpolation, across all the SAS parameterizations. The parameters k_{Q1} and α were also better identified than k_{Q2} and β, as their 95 % CI was, on average, 56 % narrower, across all tested setups. Conversely, there was no clear difference in the parameter ranges when using kriged or raw $\delta^{18}O_P$ values. The evapotranspiration parameter (i.e. k_{ET}) was poorly identified in all setups, as any value in the search range provided equally good results. The initial storage (i.e. S_0) was only partially constrained, as any value between 335 and 2895 mm was considered acceptable.

4.2 Simulated transit times and model uncertainty

Figure 6 illustrates the 95 % CI of the behavioral solutions for the predicted median transit time (TT_{50}). The results show that the model simulated largely different ranges of TT_{50} based on the tested setups. When using PLTI and BETATI (Fig. 6a, c, d, f, g, i, j, l), the 95 % CI was relatively stable with smaller fluctuations throughout the simulation period compared with PLTV (Fig. 6b, e, h, k). However, minor differences emerged across the simulated TT_{50} as a result of the distinct interpolation techniques used for $\delta^{18}O_P$. The 95 % CI of TT_{50} was, on average, 37 % larger, across all tested se-

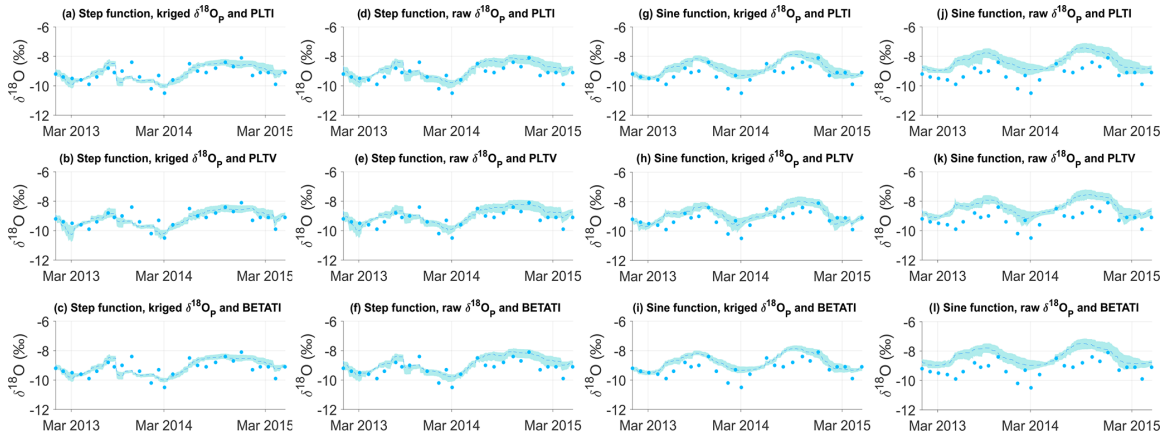

Figure 4. Predicted δ^{18}O values in streamflow. The dark blue filled circles represent the observed data, and the dashed light blue lines and shaded areas represent the ensemble mean of all possible solutions and their range according to the 95 % CI, respectively.

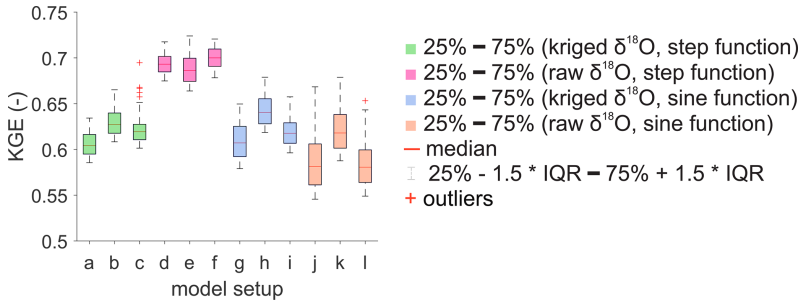

Figure 5. Box plots of model performance ranges in behavioral solutions. The letters on the x axis refer to the model setup type according to Table 1. Box plots filled with the same colors represent model setups characterized by the same interpolation scheme in space and time. On each box, the central red line indicates the median, and the bottom and top edges of the box indicate the 25th and 75th percentiles, respectively, namely the interquartile range (IQR). The whiskers extend to the most extreme data points not considered outliers, which are the 25th percentile $- 1.5 \times$ IQR and the 75th percentile $+ 1.5 \times$ IQR, respectively. The outliers are plotted individually using the red "+" markers.

tups, when using raw $\delta^{18}O_P$ (Fig. 6d–f and j–l) rather than kriged $\delta^{18}O_P$ (Fig. 6a–c and g–i). This was especially visible when the step function was used (Fig. 6a–f). Moreover, the sine interpolation generated a 95 % CI of TT_{50} that was, on average, 62 % narrower across all tested setups (Fig. 6g–l) with respect to the step function (Fig. 6a–f). These differences were more evident for high-flow conditions where the 95 % CI of TT_{50} showed a significant reduction. In addition, the behavioral solutions obtained with the sine interpolation (Fig. 6g–l) were more skewed towards shorter mean TT_{50} values, across all tested setups, than those of the step function (Fig. 6a–f).

Behavioral solutions obtained with PLTV revealed a similar pattern regardless of the interpolation employed (Fig. 6b, e, h, k). Nonetheless, there was a noticeable difference in the 95 % CI of TT_{50} under distinct flow regimes. During low flows and dry periods (i.e. summer and autumn), the time series of predicted TT_{50} showed large uncertainties ranging at most between 259 and 1009 d across the different setups (Fig. 6e). Conversely, during high flows (i.e. winter and spring), the 95 % CI was much narrower and varied at least between 126 and 154 d (Fig. 6h). The large 95 % CI and the notable differences across the tested setups highlight the sensitivity and, in turn, the uncertainty in the predicted TT_{50} to the model parameterization, temporal interpolation of input data, hydrologic conditions, and nonspatially interpolated $\delta^{18}O_P$.

In general, the variability in the predicted TT_{50} was controlled by the hydrological state of the system (Fig. 6). High-discharge events reduced the TT_{50} values, whereas low-flow periods were associated with a longer estimated TT_{50}. This is expected, as streamflow during high (low) flows is dominated

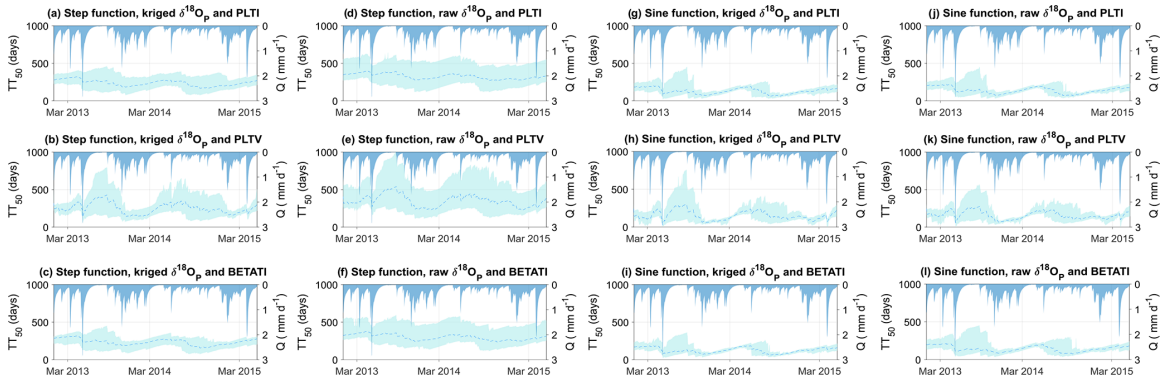

Figure 6. Predicted TT_{50} of streamflow. The dashed light blue lines and shaded areas represent the ensemble mean of all possible solutions and their range according to the 95 % CI, respectively.

by near-surface runoff (groundwater) with shallow (deep) flow paths leading to a shorter (longer) TT_{50}. Such differences were particularly visible with PLTV (Fig. 6b, e, h, k), as the exponent $k_Q(t)$ shifts the water selection preference over time as a function of the wet/dry conditions. This resulted in the variability in TT_{50} being more pronounced than that of PLTI and BETATI, whose SAS parameters for Q are constant over time.

4.3 Catchment-scale water release

SAS functions provided valuable insights into the catchment-scale water release dynamics. Figure 7 presents the behavioral solutions releasing water of different ages and also shows that the catchment generally experienced a stronger affinity for releasing young water (i.e. $k_Q < 1$, or $\alpha < 1$ and $\beta > 1$), rather than old water (i.e. $k_Q > 1$, or $\alpha > 1$ and $\beta < 1$). These findings are in agreement with other studies in the upper Selke catchment (Winter et al., 2020; Nguyen et al., 2021). Nonetheless, there were differences in the water release scheme when comparing various combinations of SAS functions and spatiotemporal interpolation techniques of isotopes. The use of PLTV resulted in a substantial number of solutions, approximately 50 % of all behavioral solutions, suggesting a preference for both young and old water. On the other hand, only a few solutions showed affinity for old-water release, and this was more prominent when using the sine interpolation, raw $\delta^{18}O_P$ values, and PLTI across all tested setups.

5 Discussion

5.1 Uncertainty in TTD modeling

In this study, we characterized the TTD uncertainty arising from some significant and critical aspects for the SAS modeling. These aspects are also the most directly linked to the data interpolation and SAS parameterization that we explored in this work. The uncertainty analysis was carried out across the 12 tested setups corresponding to different combinations of spatiotemporal data interpolation techniques and SAS parameterizations. Our results show that the uncertainty (i.e. 95 % CI) of the simulated TT_{50} (Fig. 6) was firmly dependent on the choice of model setup, as the 95 % CI was primarily sensitive to the type of SAS function, temporal interpolation, and spatial representation of $\delta^{18}O_P$.

Uncertainty in the simulated TT_{50} differed considerably between time-invariant (i.e. PLTI and BETATI; Fig. 6a, c, d, f, g, i, j, l) and time-variant (i.e. PLTV; Fig. 6b, e, h, k) SAS functions; thus, a large sensitivity is associated with the choice of the SAS parameterization. For example, PLTI and BETATI explicitly assume constant water selection preference over time, as these functions do not consider the temporal variability in the catchment wetness. As a consequence, the resulting TT_{50} had a moderately stable 95 % CI with smaller fluctuations compared with those of PLTV. On the other hand, including an explicit time dependence in the SAS function strongly affected the 95 % CI of TT_{50}. Notably, PLTV produced a wider 95 % CI during low-flow conditions, which can hinder the TTDs ability to provide robust insights into flow and solute transport behaviors in the study area during low-flow conditions. This highlights the need to further constrain PLTV with additional data, which could involve obtaining tracer data at a finer resolution or additional information on the evapotranspiration and initial storage. In addition, the exceptionally old flow components associated with a very large 95 % CI of TT_{50} might be a distortion of the actual TT_{50} values, which can usually be more reliably estimated using radioactive tracers than with stable isotopes (Visser et al., 2019). Hence, PLTV-based TT_{50} greater than the observed period (828 d) should be interpreted carefully. It is important to note that we discussed the fractional SAS (fSAS) functions in this study, but another form of the SAS

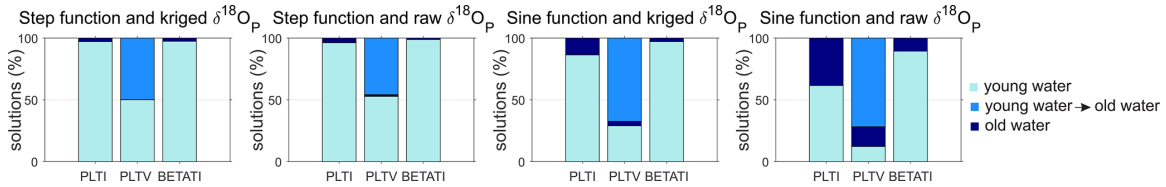

Figure 7. Percentage of behavioral solutions releasing water of different ages.

functions, such as the rank SAS (rSAS) functions, may have different uncertainty. This is mainly due to the difference in how the storage is considered: fSAS functions are expressed as function of the normalized age-ranked storage, which is equal to the cumulative residence time, whereas rSAS functions depend on the age-ranked storage, which is the volume of water in storage ranked from youngest to oldest (Harman, 2015).

Likewise, the high-frequency reconstruction of $\delta^{18}O_P$ from monthly samples via interpolation created further uncertainty. The sine interpolation effectively captured the dominant features of the observed $\delta^{18}O_P$, such as seasonality. Consequently, sine interpolation successfully reproduced the seasonal trend in in-stream $\delta^{18}O$, although simulations overestimated the measurements (Fig. 4g–l). On the other hand, sine interpolation poorly reproduced rainfall isotopes during short-term flashy events and missed detailed characteristics of the tracer dataset by smoothing the variability in the observed $\delta^{18}O_P$ (Fig. 3). As a result, high values of $\delta^{18}O_P$ are underestimated, whereas low values are overestimated. It is critical to recognize these limitations when interpreting modeling results, as uncertainty in the simulated $\delta^{18}O_P$ may conceal a more pronounced hydrological response of the system (Dunn et al., 2008; Birkel et al., 2010; Hrachowitz et al., 2011). Contrarily, step function interpolation preserved the maxima in the monthly observed $\delta^{18}O_P$ values by capturing their variation correctly (Fig. 3). Simulations showed a better fit with measured in-stream $\delta^{18}O$ (Fig. 4a–f) and higher model performance (Fig. 5). However, combining step function with raw $\delta^{18}O_P$ resulted in larger uncertainty in the simulated TT_{50} (Fig. 6d–f). This reflects the need for a comprehensive exploration of the uncertainty range, rather than relying solely on the goodness of fit. Overall, the choice between step function and sine interpolation largely affected the reconstructed input data (Fig. 3), leading to significant differences in the simulated TT_{50} and associated uncertainty. It is important to note that alternative methods, such as generalized additive models (GAMs; Buzacott et al., 2020), offer other options for interpolating tracer data. We conducted further tests with the SAS model using a GAM to reconstruct both kriged and raw $\delta^{18}O_P$ using smoothing functions; this provides a more sophisticated approach than the intuitive methods used in this study. However, the results, available in the Supplement, show that while a GAM provided more detailed reconstructed input tracer data (Fig. S1), it did not significantly alter the SAS-based results (Figs. S2, S3) or yield any new insights or conclusions about uncertainty with respect to using step function and sine interpolation. Therefore, we conclude that, while highly resolved input data may seem appealing, they do not necessarily lead to substantial benefits for the SAS-based output, supposedly due to the conceptual simplifications in the SAS model.

The spatial representation of $\delta^{18}O_P$ values had limited impact on the overall pattern of simulated TT_{50}, as the time series were comparable with both kriged (Fig. 6a–c and g–i) and raw (Fig. 6d–f and j–l) $\delta^{18}O_P$. Nonetheless, the spatial interpolation of $\delta^{18}O_P$ from different locations resulted in a reduction in the uncertainty in the TT_{50}, which was particularly evident with the step function (Fig. 6a–f). This difference may be attributed to the fact that the upper Selke is a large (mesoscale) catchment with a substantial gradient in elevation, and, as a consequence, measurement for $\delta^{18}O_P$ from only one location may be generally overly simplistic. This finding highlights the importance of considering not only the model performance (Fig. 5; raw values with a step function interpolation produced higher KGE values) but also the uncertainty range in predicted TT_{50}.

Finally, we found that the uncertainty was larger under dry conditions when lower flow and longer TT_{50} were observed. This was especially visible when using the time-variant SAS function (Fig. 6b, e, h, k). It might be due to the fact that, under wet conditions, there is a high level of hydrologic connectivity within the catchment (Ambroise, 2004; Blume and van Meerveld, 2015; Hrachowitz et al., 2016), which results in nearly all flow paths being active and contributing to the streamflow. This, ultimately, may make TT_{50} values easier to constrain. Conversely, under dry conditions, when usually only longer flow paths carrying older water are active (Soulsby and Tetzlaff, 2008; Jasechko et al., 2017), water partially flows through a drier soil zone where flow is more erratic (i.e. flow directions and patterns can vary widely) as the conductivity is controlled by soil moisture. As a result, wet areas can be patchy and water flows preferentially at certain locations only, as opposed to spatially uniform flow through the soil matrix; this might make it more challenging to constrain older water ages. Similarly, Benettin et al. (2017) found higher uncertainty in the simulated SAS-based median water ages during drier periods, potentially due to

higher uncertainty in the total storage. Moreover, non-SAS function studies have observed major uncertainties and deviations from observations in lumped modeled results during low-flow conditions (Kumar et al., 2010). This was primarily due to the lack of spatial variability in the catchment characteristics in lumped models, which is a critical factor controlling low-flow regimes in rivers.

The dissimilarities in the simulated TT_{50} across the tested setups underline the importance of accounting for uncertainty in model-based TTDs. The uncertainty analysis with SUFI-2 performed in this study was essential to best describe the parameter identifiability and bounds of the behavioral solutions of each output variable. Furthermore, our results highlight the importance of gaining tracer datasets of good quality (i.e. tracer data with a finer temporal resolution), considering the spatial variability in the isotopic composition in precipitation, and, possibly, employing a model parameterization that best describes the catchment-specific storage and release dynamics. The last point can be defined according to a precise conceptual knowledge of the catchment's functioning and information from previous studies in similar catchments.

5.2 TTD modeling: advantages and limitations

Our results provide visually plausible seasonal fluctuations in the predicted $\delta^{18}O_Q$ samples (Fig. 4) and satisfactory KGE values (Fig. 5), despite the uncertainty arising from model inputs, structure, and parameters. The good match with observations provides confidence in the simulated TT_{50} for the upper Selke catchment. The magnitude of the uncertainty resulting from different setups cannot be generalized, but the overall approach for uncertainty assessment presented here could be extended to other areas and TTD studies. However, we recognize some limitations and indicate below possible reasons and, in turn, improvements that future work could achieve.

First, the limited length of the $\delta^{18}O$ time series might not describe the system accurately; hence, implementing longer time series could improve the parameter identifiability and provide a more accurate estimation of the TTDs. Second, this study relied on stable water isotopes, which might underestimate the tails of the TTDs (Stewart et al., 2010; Seeger and Weiler, 2014), although recent works have contested this (Wang et al., 2022). Possible advancements could be reached by using decaying tracers varying over a longer timescale than stable water isotopes (e.g. tritium; Stewart et al., 2012; Morgenstern et al., 2015) and imparting more information on old water. Next, future work should retrieve more information on the evapotranspiration ET and initial storage S_0, whose parameters were poorly identified. However, this issue is common in transport studies that rely on measurements of in-stream stable water isotopes (Benettin et al., 2017; Buzacott et al., 2020). As a way forward, information on the ET isotopic compositions might help better constrain ET parameters and assess their affinity for young/old water. Regarding constraining the range of S_0, further information can be gained from geophysical surveys in the study areas or groundwater modeling as well as by using decaying isotopes (Visser et al., 2019).

5.3 Implications of TTD uncertainties

This study characterized the uncertainty in TTDs, which summarize the catchment's hydrologic transport behavior and, therefore, comprise decisive information for water managers. The value of TT_{50} has relevant implications for both water quantity and quality, as does its uncertainty. The larger the 95 % CI in the simulated TT_{50}, the greater the difference in the TT_{50} values, which, ultimately, implies distinct hydrological processes, water availability, groundwater recharge, and solute export dynamics (McDonnel et al., 2010).

For example, knowing the TTD and its uncertainty may be crucial for characterizing the catchment's response to climatic change (Wilusz et al., 2017). Considering the increasing severity of droughts in the past decades (Dai, 2013), a catchment with a shorter TT_{50} and a dominant release of young water might be more affected by droughts than a catchment with a longer TT_{50}, which means that its stream is fed by relatively old water sources. Therefore, a short TT_{50} reveals a low drought resilience of the catchment and limited water availability, which could limit streamflow generation processes and change the in-stream water quality status during drought periods (Winter et al., 2023). Likewise, TTD uncertainty may affect the understanding of the water infiltration rate, hydrological processes, and aquifer recharge, as a shorter TT_{50} suggests that water is quickly routed to the catchment outlet rather than infiltrating deeply into the groundwater. Finally, TTD uncertainty can have an impact on the quantification of the modern groundwater age, i.e. groundwater younger than 50 years (Bethke and Johnson, 2008). According to Jasechko (2019), the correct identification of modern groundwater abundance and distribution can help determine its renewal (Le Gal La Salle et al., 2001; Huang et al., 2017), groundwater wells and depths most likely to contain contaminants (Visser et al., 2013; Opazo et al., 2016), and the part of the aquifer flushed more rapidly.

Uncertainty in TTDs also impacts on assessing the fate of dissolved solutes, such as nitrates (X. Yang et al., 2018; Nguyen et al., 2021, 2022; Lutz et al., 2022), pesticides (Holvoet et al., 2007; Lutz et al., 2017), and chlorides (Kirchner et al., 2000; Benettin et al., 2013). These solutes constitute a crucial source of diffuse water pollution in agricultural areas (Jiang et al., 2014; Kumar et al., 2020), as they are spread on the soil in large quantities, especially during the growing season. The exposure time of solutes with the soil matrix has strong consequences for biogeochemical reactions, such as denitrification in the case of nitrates (Kolbe et al., 2019; Kumar et al., 2020). A short TT_{50} suggests that water can be rapidly conveyed to the stream network

(Kirchner et al., 2001), with limited time for denitrification. This explains the elevated in-stream concentration and short-term impact of nitrate export compared with that of a longer TT_{50}, which is typically associated with old-water release and a low nitrate concentration (Nguyen et al., 2021). Similarly, pesticide transport is highly affected by the TTD uncertainty, as a long TT_{50} suggests little pesticide degradation due to decreased microbial activity along deeper flow paths (Rodríguez-Cruz et al., 2006). In other cases, a shorter TT_{50} may limit the time for degradation, causing a peak in the in-stream concentration (Leu et al., 2004). Overall, a longer TT_{50} can delay or buffer the catchment's reactive solute response at the outlet (Dupas et al., 2016; Van Meter et al., 2017). This creates a long-term effect of hydrological legacies and a continuous problem with diffuse pollution of nitrates (Ehrhardt et al., 2019; Winter et al., 2020) and pesticides (Lutz et al., 2013), which can persist in the catchment for several years. Finally, TTD uncertainties also play an important role in chloride transport, although chlorides are commonly known to be conservative (Svensson et al., 2012). A short TT_{50} may indicate rapid chloride mobilization, whereas a long TT_{50} implies chloride persistence in groundwater; therefore, chloride accumulates and is released at lower rates, with impacts on the ecosystem functions, vegetation uptake, and metabolism (Xu et al., 1999).

Understanding the uncertainty in TTDs is crucial for the aforementioned implications. While previous studies have used only a specific SAS function and/or specific tracer data interpolation technique in time and space, here we show that there could be a wide range of different results in terms of water ages, model performance, and parameter uncertainty. This is due to the specific choice regarding SAS parameterization and tracer data interpolation. With this, we want to convey that uncertainty is omnipresent in TTD-based models, and we need to recognize it, especially when dealing with sparse tracer data and multiple choices for model parameterization. Therefore, we want to encourage future studies to explore these uncertainties in other catchments and different geophysical settings, with the final aim to investigate whether these uncertainties may affect the conclusions of water quantity and quality studies for management purposes.

6 Conclusions

This study explored the uncertainty in TTDs of streamflow, resulting from 12 model setups obtained from different SAS parameterizations (i.e. PLTI, PLTV, and BETATI), and reconstruction of the precipitation isotopic signature in time and space via interpolation (step function vs. sine fit and raw vs. kriged values).

We found satisfactory KGE values, whose differences across the tested setups were statistically significant, meaning that the choice of the setup matters. As a consequence, distinct setups led to considerably different simulated TT_{50} values. The choice between using time-variant or time-invariant SAS functions was crucial, as the time-invariant functions generated moderate fluctuations in the 95 % CI of the estimated TT_{50} because of the constant water selection preference over time. On the other hand, the time-variant SAS function captured the dynamics of the catchment wetness, resulting in more pronounced fluctuations in TT_{50}. However, the time-variant SAS function also produced a larger 95 % CI in TT_{50}, notably during drier periods, which might indicate the need to constrain the function with additional data (e.g. finer tracer data resolution and/or information on evapotranspiration and storage). Significant differences in TT_{50} were observed depending on the employed temporal interpolations. Results from the sine interpolation produced a smaller uncertainty in TT_{50}, with the time series skewed towards smaller values. However, such results must be interpreted carefully, as the sine interpolation poorly reproduced flashy events in precipitation, thus indicating that some more dynamic transport processes were not fully considered. Conversely, the step function interpolation resulted in a larger uncertainty in the TT_{50}, but it was able to better reproduce the measured $\delta^{18}O_P$ data by capturing the peak values, as opposed to the sine interpolation. Dry conditions were another reason for uncertainty, as indicated by the high variance in the simulated TT_{50} values, which is potentially attributed to the water preferentially moving at certain locations, making wet areas patchy, so it may be more challenging to accurately constrain older water ages. Finally, there was comparable pattern in the modeled results when using kriged vs. raw isotopes, but the kriged values yielded an uncertainty reduction in TT_{50}. This highlights the potential advantage of spatially interpolated values over a single measurement representative of the entire area, particularly in a mesoscale catchment that varies with respect to elevation.

These findings provide new insights into TTD uncertainty when high-frequency tracer data are missing and the SAS framework is used. Regardless of the degree of efficiency or uncertainty, the decision on which setup is more plausible depends on the best conceptual knowledge of the catchment functioning. We consider the presented approach to be potentially applicable to other studies to enable a better characterization of TTD uncertainty, improve TTD simulations and, ultimately, inform water management. These aspects are particularly crucial in view of increasingly extreme climatic conditions and worsening water pollution under global change.

Code and data availability. The version of the model used in this study (v1.0) and its documentation are available at https://github.com/pbenettin/tran-SAS (last access: August 2020) and https://doi.org/10.5281/zenodo.1203600 (Benettin and Bertuzzo, 2018b). The iteratively re-weighted least-squares (IRLS) method used to obtain the modeled daily kriged and raw isotope ($\delta^{18}O$) in precipitation information with the sine interpolation

is presented at https://doi.org/10.5194/hess-22-3841-2018 (von Freyberg et al., 2018). The hydroclimatic time series, δ^{18}O data, and interpolated δ^{18}O time series can be accessed at https://doi.org/10.5281/zenodo.8121108 (Borriero, 2022).

Supplement. The supplement related to this article is available online at: https://doi.org/10.5194/hess-27-2989-2023-supplement.

Author contributions. AB conducted the model simulations, carried out the analysis, interpreted the results, and wrote the original draft of the paper. SRL and RK designed and conceptualized the study and provided data for model simulations. TVN provided technical support for modeling and helped organize the structure and content of the paper. AB, SRL, RK, and TVN conceived the methodology and experimental design. All co-authors helped AB interpret the results. All authors contributed to the review, final writing, and finalization of this work.

Competing interests. At least one of the (co-)authors is a member of the editorial board of *Hydrology and Earth System Sciences*. The peer-review process was guided by an independent editor, and the authors also have no other competing interests to declare.

Disclaimer. Publisher's note: Copernicus Publications remains neutral with regard to jurisdictional claims in published maps and institutional affiliations.

Acknowledgements. The authors thank the Helmholtz Centre for Environmental Research – UFZ of the Helmholtz Association for funding this study; the German Weather Service and the mHM model team for providing the necessary input data; and the developers of the *tran*-SAS model and IRLS code for making them publicly available.

Financial support. The article processing charges for this open-access publication were covered by the Helmholtz Centre for Environmental Research – UFZ.

Review statement. This paper was edited by Laurent Pfister and reviewed by Ciaran Harman and one anonymous referee.

References

Abbaspour, K. C., Johnson, C. A., and van Genuchten, M. T.: Estimating uncertain flow and transport parameters using a sequential uncertainty fitting procedure, Vadose Zone J., 3, 1340–1352, https://doi.org/10.2136/vzj2004.1340, 2004.

Ajami, N. K., Duan, Q., and Sorooshian, S.: An integrated hydrologic Bayesian multimodel combination framework: Confronting input, parameter, and model structural uncertainty in hydrologic prediction, Water Resour. Res., 43, W01403, https://doi.org/10.1029/2005WR004745, 2007.

Allen, S. T., Jasechko, S., Berghuijs, W. R., Welker, J. M., Goldsmith, G. R., and Kirchner, J. W.: Global sinusoidal seasonality in precipitation isotopes, Hydrol. Earth Syst. Sci., 23, 3423–3436, https://doi.org/10.5194/hess-23-3423-2019, 2019.

Ambroise, B.: Variable "active" versus "contributing" areas or periods: a necessary distinction, Hydrol. Process., 18, 1149–1155, https://doi.org/10.1002/hyp.5536, 2004.

Andersson, J. C. M., Arheimer, B., Traoré, F., Gustafsson, D., and Ali, A.: Process refinements improve a hydrological model concept applied to the Niger River basin, Hydrol. Process., 31, 4540–4554, https://doi.org/10.1002/hyp.11376, 2017.

Asadollahi, M., Stumpp, C., Rinaldo, A., and Benettin, P.: Transport and water age dynamics in soils: A comparative study of spatially integrated and spatially explicit models, Water Resour. Res., 56, e2019WR025539, https://doi.org/10.1029/2019WR025539, 2020.

Benettin, P. and Bertuzzo, E.: tran-SAS v1.0: a numerical model to compute catchment-scale hydrologic transport using StorAge Selection functions, Geosci. Model Dev., 11, 1627–1639, https://doi.org/10.5194/gmd-11-1627-2018, 2018a.

Benettin, P. and Bertuzzo, E.: tran-SAS v1.0 (1.0), Zenodo [code], https://doi.org/10.5281/zenodo.1203600, 2018b.

Benettin, P., van der Velde, Y., van der Zee, S. E. A. T. M., Rinaldo, A., and Botter, G.: Chloride circulation in a lowland catchment and the formulation of transport by travel time distributions, Water Resour. Res., 49, 4619–4632, https://doi.org/10.1002/wrcr.20309, 2013.

Benettin, P., Bailey, S. W., Campbell, J. L., Green, M. B., Rinaldo, A., Likens, G. E., McGuire, J. K., and Botter, G.: Linking water age and solute dynamics in streamflow at the Hubbard Brook Experimental Forest, NH, USA, Water Resour. Res., 51, 9256–9272, https://doi.org/10.1002/2015WR017552, 2015a.

Benettin, P., Kirchner, J. W., Rinaldo, A., and Botter, G.: Modeling chloride transport using travel time distributions at Plynlimon, Wales, Water Resour. Res., 51, 3259–3276, https://doi.org/10.1002/2014WR016600, 2015b.

Benettin, P., Soulsby, C., Birkel, C., Tetzlaff, D., Botter, G., and Rinaldo, A.: Using SAS functions and high-resolution isotope data to unravel travel time distributions in headwater catchments, Water Resour. Res., 53, 1864–1878, https://doi.org/10.1002/2016WR020117, 2017.

Bethke, C. M. and Johnson, T. M.: Groundwater age and groundwater age dating, Annu. Rev. Earth Planet. Sci., 36, 121–152, https://doi.org/10.1146/annurev.earth.36.031207.124210, 2008.

Beven, K.: A manifesto for the equifinality thesis, J. Hydrol., 320, 18–36, https://doi.org/10.1016/j.jhydrol.2005.07.007, 2006.

Beven, K. and Freer, J.: Equifinality, data assimilation, and uncertainty estimation in mechanistic modelling of complex environmental systems using the GLUE methodology, J. Hydrol., 249, 11–29, https://doi.org/10.1016/S0022-1694(01)00421-8, 2001.

Birkel, C. and Soulsby, C.: Advancing tracer-aided rainfall-runoff modelling: A review of progress, problems and unrealised potential, Hydrol. Process., 29, 5227–5240, https://doi.org/10.1002/hyp.10594, 2015.

Birkel, C., Dunn, S. M., Tetzlaff, D., and Soulsby, C.: Assessing the value of high-resolution isotope tracer data in the stepwise development of a lumped conceptual rainfall–runoff model, Hy-

drol. Process., 24, 2335–2348, https://doi.org/10.1002/hyp.7763, 2010.

Blume, T. and van Meerveld, H. J.: From hillslope to stream: methods to investigate subsurface connectivity, WIREs Water, 2, 177–198, https://doi.org/10.1002/wat2.1071, 2015.

Borriero, A.: Hydroclimatic and isotope data – Upper Selke, Zenodo [data set], https://doi.org/10.5281/zenodo.8121108, 2022.

Botter, G., Bertuzzo, E., Bellin, A., and Rinaldo, A.: On the Lagrangian formulations of reactive solute transport in the hydrologic response, Water Resour. Res., 41, W04008, https://doi.org/10.1029/2004WR003544, 2005.

Botter, G., Bertuzzo, E., and Rinaldo, A.: Transport in the hydrologic response: Travel time distributions, soil moisture dynamics, and the old water paradox, Water Resour. Res., 46, W03514, https://doi.org/10.1029/2009WR008371, 2010.

Botter, G., Bertuzzo, E., and Rinaldo, A.: Catchment residence and travel time distributions: The master equation, Geophys. Res. Lett., 38, L11403, https://doi.org/10.1029/2011GL047666, 2011.

Buzacott, A. J. V., van der Velde, Y., Keitel, C., and Vervoort, R. W.: Constraining water age dynamics in a southeastern Australian catchment using an age-ranked storage and stable isotope approach, Hydrol. Process., 34, 4384–4403, https://doi.org/10.1002/hyp.13880, 2020.

Dai, A.: Erratum: Increasing drought under global warming in observations and models, Nat. Clim. Change, 3, 171, https://doi.org/10.1038/nclimate1811, 2013.

Danesh-Yazdi, M., Foufoula-Georgiou, E., Karwan, D. L., and Botter, G.: Inferring changes in water cycle dynamics of intensively managed landscapes via the theory of time-variant travel time distributions, Water Resour. Res., 52, 7593–7614, https://doi.org/10.1002/2016WR019091, 2016.

Danesh-Yazdi, M., Klaus, J., Condon, L. E., and Maxwell, R. M.: Bridging the gap between numerical solutions of travel time distributions and analytical storage selection functions, Hydrol. Process., 32, 1063–1076, https://doi.org/10.1002/hyp.11481, 2018.

Drever, M. C. and Hrachowitz, M.: Migration as flow: using hydrological concepts to estimate the residence time of migrating birds from the daily counts, Methods Ecol. Evol., 8, 1146–1157, https://doi.org/10.1111/2041-210X.12727, 2017.

Dunn, S. M., Bacon, J. R., Soulsby, C., Tetzlaff, D., Stutter, M. I., Waldron, S., and Malcolm, I. A.: Interpretation of homogeneity in δ^{18}O signatures of stream water in a nested sub-catchment system in north-east Scotland, Hydrol. Process., 22, 4767–4782, https://doi.org/10.1002/hyp.7088, 2008.

Dupas, R., Jomaa, S., Musolff, A., Borchardt, D., and Rode, M.: Disentangling the influence of hydroclimatic patterns and agricultural management on river nitrate dynamics from sub-hourly to decadal time scales, Sci. Total Environ., 571, 791–800, https://doi.org/10.1016/j.scitotenv.2016.07.053, 2016.

Dupas, R., Musolff, A., Jawitz, J. W., Rao, P. S. C., Jäger, C. G., Fleckenstein, J. H., Rode, M., and Borchardt, D.: Carbon and nutrient export regimes from headwater catchments to downstream reaches, Biogeosciences, 14, 4391–4407, https://doi.org/10.5194/bg-14-4391-2017, 2017.

Ehrhardt, S., Kumar, R., Fleckenstein, J. H., Attinger, S., and Musolff, A.: Trajectories of nitrate input and output in three nested catchments along a land use gradient, Hydrol. Earth Syst. Sci., 23, 3503–3524, https://doi.org/10.5194/hess-23-3503-2019, 2019.

Feng, X., Faiia, A. M., and Posmentier, E. S.: Seasonality of isotopes in precipitation: A global perspective, J. Geophys. Res, 114, D08116, https://doi.org/10.1029/2008JD011279, 2009.

Gupta, H. V., Kling, H., Yilmaz, K. K., and Martinez, G. F.: Decomposition of the mean squared error and NSE performance criteria: Implications for improving hydrological modelling, J. Hydrol., 377, 80–91, https://doi.org/10.1016/j.jhydrol.2009.08.003, 2009.

Harman, C. J.: Time-variable transit time distributions and transport: Theory and application to storage-dependent transport of chloride in a watershed, Water Resour. Res., 51, 1–30, https://doi.org/10.1002/2014WR015707, 2015.

Harman, C. J.: Age-Ranked Storage-Discharge Relations: A Unified Description of Spatially Lumped Flow and Water Age in Hydrologic Systems, Water Resour. Res., 55, 7143–7165, https://doi.org/10.1029/2017WR022304, 2019.

Heidbüchel, I., Troch, P. A., and Lyon, S. W.: Separating physical and meteorological controls of variable transit times in zero-order catchments, Water Resour. Res., 49, 7644–7657, https://doi.org/10.1002/2012WR013149, 2013.

Heidbüchel, I., Yang, J., Musolff, A., Troch, P., Ferré, T., and Fleckenstein, J. H.: On the shape of forward transit time distributions in low-order catchments, Hydrol. Earth Syst. Sci., 24, 2895–2920, https://doi.org/10.5194/hess-24-2895-2020, 2020.

Holvoet, K. M. A., Seuntjens, P., and Vanrolleghem, P. A.: Monitoring and modeling pesticide fate in surface waters at the catchment scale, Ecol. Model., 209, 53–64, https://doi.org/10.1016/j.ecolmodel.2007.07.030, 2007.

Hrachowitz, M., Soulsby, C., Tetzlaff, D., Malcolm, I. A., and Schoups, G.: Gamma distribution models for transit time estimation in catchments: Physical interpretation of parameters and implications for time-variant transit time assessment, Water Resour. Res., 46, W10536, https://doi.org/10.1029/2010WR009148, 2010.

Hrachowitz, M., Soulsby, C., Tetzlaff, D., and Malcolm, I. A.: Sensitivity of mean transit time estimates to model conditioning and data availability, Hydrol. Process., 25, 980–990, https://doi.org/10.1002/hyp.7922, 2011.

Hrachowitz, M., Savenije, H., Bogaard, T. A., Tetzlaff, D., and Soulsby, C.: What can flux tracking teach us about water age distribution patterns and their temporal dynamics?, Hydrol. Earth Syst. Sci., 17, 533–564, https://doi.org/10.5194/hess-17-533-2013, 2013.

Hrachowitz, M., Benettin, P., van Breukelen, B. M., Fovet, O., Howden, N. J. K., Ruiz, L van der Velde, Y., and Wade, A. J.: Transit times – the link between hydrology and water quality at the catchment scale, WIREs Water, 3, 629–657, https://doi.org/10.1002/wat2.1155, 2016.

Huang, T., Pang, Z., Li, J., Xiang, Y., and Zhao, Z.: Mapping groundwater renewability using age data in the Baiyang alluvial fan, NW, China, Hydrogeol. J., 25, 743–755, https://doi.org/10.1007/s10040-017-1534-z, 2017.

Jasechko, S.: Global isotope hydrogeology – review, Rev. Geophys., 57, 835–965, https://doi.org/10.1029/2018RG000627, 2019.

Jasechko, S., Wassenaar, L. I., and Mayer, B.: Isotopic evidence for widespread cold-season-biased groundwater recharge and young streamflow across central Canada, Hydrol. Process., 31, 2196–2209, https://doi.org/10.1002/hyp.11175, 2017.

Jiang, S., Jomaa, S., and Rode, M.: Modelling inorganic nitrogen leaching in nested mesoscale catchments in central Germany,

Ecohydrol., 7, 1345–1362, https://doi.org/10.1002/eco.1462, 2014.

Jing, M., Heße, F., Kumar, R., Kolditz, O., Kalbacher, T., and Attinger, S.: Influence of input and parameter uncertainty on the prediction of catchment-scale groundwater travel time distributions, Hydrol. Earth Syst. Sci., 23, 171–190, https://doi.org/10.5194/hess-23-171-2019, 2019.

Kim, M. and Troch, P. A.: Transit time distributions estimation exploiting flow-weighted time: Theory and proof-of-concept, Water Resour. Res., 56, e2020WR027186, https://doi.org/10.1029/2020WR027186, 2020.

Kim, M., Pangle, L. A., Cardoso, C., Lora, M., Volkmann, T. H. M., Wang, Y., Harman, C. J., and Troch, P. A.: Transit time distributions and StorAge Selection functions in a sloping soil lysimeter with time-varying flow paths: Direct observation of internal and external transport variability, Water Resour. Res., 52, 7105–7129, https://doi.org/10.1002/2016WR018620, 2016.

Kirchner, J. W.: Getting the right answers for the right reasons: Linking measurements, analyses, and models to advance the science of hydrology, Water Resour. Res., 42, W03S04, https://doi.org/10.1029/2005WR004362, 2006.

Kirchner, J. W.: Aggregation in environmental systems – Part 1: Seasonal tracer cycles quantify young water fractions, but not mean transit times, in spatially heterogeneous catchments, Hydrol. Earth Syst. Sci., 20, 279–297, https://doi.org/10.5194/hess-20-279-2016, 2016.

Kirchner, J. W.: Quantifying new water fractions and transit time distributions using ensemble hydrograph separation: theory and benchmark tests, Hydrol. Earth Syst. Sci., 23, 303–349, https://doi.org/10.5194/hess-23-303-2019, 2019.

Kirchner, J. W., Feng, X., and Neal, C.: Fractal stream chemistry and its implications for contaminant transport in catchments, Nature, 403, 524–527, https://doi.org/10.1038/35000537, 2000.

Kirchner, J. W., Feng, X., and Neal, C.: Catchment-scale advection and dispersion as a mechanism for fractal scaling in stream tracer concentrations, J. Hydrol., 254, 82–101, https://doi.org/10.1016/S0022-1694(01)00487-5, 2001.

Kirchner, J. W., Feng, X., Neal, C., and Robson, A. J.: The fine structure of water-quality dynamics: the (high-frequency) wave of the future, Hydrol. Process., 18, 1353–1359, https://doi.org/10.1002/hyp.5537, 2004.

Kolbe, T., de Dreuzy, J. R., Abbot, B. W., Aquilina, L., Babey, T., Green, C. T., Fleckenstein, J. H., Labasque, T., Laverman, A. M., Marçais, J., Peiffer, S., Thomas, Z., and Pinay, G.: Stratification of reactivity determines nitrate removal in groundwater, P. Natl. Acad. Sci. USA, 116, 2494–2499, https://doi.org/10.1073/pnas.1816892116, 2019.

Kumar, R., Samaniego, L., and Attinger, S.: The effects of spatial discretization and model parameterization on the prediction of extreme runoff characteristics, J. Hydrol., 392, 54–69, https://doi.org/10.1016/j.jhydrol.2010.07.047, 2010.

Kumar, R., Samaniego, L., and Attinger, S.: Implications of distributed hydrologic model parameterization on water fluxes at multiple scales and locations, Water Resour. Res., 49, 360–379, https://doi.org/10.1029/2012WR012195, 2013.

Kumar, R., Heße, F., Rao, P. S. C., Musolff, A., Jawitz, J. W., Sarrazin, F., Samaniego, L., Fleckenstein, J. H., Rakovec, O., Thober, S., and Attinger, S.: Strong hydroclimatic controls on vulnerability to subsurface nitrate contamination across Europe, Nat. Commun., 11, 6302, https://doi.org/10.1038/s41467-020-19955-8, 2020.

Le Gal La Salle, C., Marlin, C., Leduc, C., Taupin, J. D., Massault, M., and Favreau, G.: Renewal rate estimation of groundwater based on radioactive tracers (^{3}H, ^{14}C) in an unconfined aquifer in a semi-arid area, Iullemeden Basin, Niger, J. Hydrol., 254, 145–156, https://doi.org/10.1016/S0022-1694(01)00491-7, 2001.

Leu, C., Singer, H., Stamm, C., Muller, S. R., and Schwarzenbach, R. P.: Simultaneous Assessment of Sources, Processes, and Factors Influencing Herbicide Losses to Surface Waters in a Small Agricultural Catchment, Environ. Sci. Technol., 38, 3827–3834, https://doi.org/10.1021/es0499602, 2004.

Lutz, S. R., van Meerveld, H. J., Waterloo, M. J., Broers, H. P., and van Breukelen, B. M.: A model-based assessment of the potential use of compound-specific stable isotope analysis in river monitoring of diffuse pesticide pollution, Hydrol. Earth Syst. Sci., 17, 4505–4524, https://doi.org/10.5194/hess-17-4505-2013, 2013.

Lutz, S. R., Velde, Y. V. D., Elsayed, O. F., Imfeld, G., Lefrancq, M., Payraudeau, S., and van Breukelen, B. M.: Pesticide fate on catchment scale: conceptual modelling of stream CSIA data, Hydrol. Earth Syst. Sci., 21, 5243–5261, https://doi.org/10.5194/hess-21-5243-2017, 2017.

Lutz, S. R., Krieg, R., Müller, C., Zink, M., Knöller, K., Samaniego, L., and Merz, R.: Spatial patterns of water age: using young water fractions to improve the characterization of transit times in contrasting catchments, Water Resour. Res., 54, 4767–4784, https://doi.org/10.1029/2017WR022216, 2018.

Lutz, S. R., Ebeling, P., Musolff, A., Nguyen, T. V., Sarrazin, F. J., Van Meter, K. J., Basu, N. B., Fleckenstein, J. H., Attinger, S., and Kumar, R.: Pulling the rabbit out of the hat: Unravelling hidden nitrogen legacies in catchment-scale water quality models, Hydrol. Processes, 36, e14682, https://doi.org/10.1002/hyp.14682, 2022.

McDonnell, J. J., McGuire, K., Aggarwal, P., Beven, K. J., Biondi, D., Destouni, G., Dunn, S., James, A., Kirchner, J., Kraft, P., Lyon, S., Maloszewski, P., Newman, B., Pfister, L., Rinaldo, A., Rodhe, A., Sayama, T., Seibert, J., Solomon, K., Soulsby, C., Stewart, M., Tetzlaff, D., Tobin, C., Troch, P., Weiler, M., Western, A., Wörman, A., and Wrede, S.: How old is streamwater? Open questions in catchment transit time conceptualization, modelling and analysis, Hydrol. Process., 24, 1745–1754, https://doi.org/10.1002/hyp.7796, 2010.

McGuire, K. J. and McDonnel, J. J.: A review and evaluation of catchment transit time modeling, J. Hydrol., 330, 543–563, https://doi.org/10.1016/j.jhydrol.2006.04.020, 2006.

McKay, M. D., Beckman, R. J., and Conover, W. J.: A Comparison of Three Methods for Selecting Values of Input Variables in the Analysis of Output from a Computer Code, Technometrics, 21, 239–245, https://doi.org/10.2307/1268522, 1979.

Morgenstern, U., Daughney, C. J., Leonard, G., Gordon, D., Donath, F. M., and Reeves, R.: Using groundwater age and hydrochemistry to understand sources and dynamics of nutrient contamination through the catchment into Lake Rotorua, New Zealand, Hydrol. Earth Syst. Sci., 19, 803–822, https://doi.org/10.5194/hess-19-803-2015, 2015.

Nguyen, T. V., Kumar, R., Lutz, S. R., Musolff, A., Yang, J., and Fleckenstein, J. H.: Modeling Nitrate Export From a Mesoscale Catchment Using StorAge Selec-

tion Functions, Water Resour. Res., 57, e2020WR028490, https://doi.org/10.1029/2020WR028490, 2021.

Nguyen, T. V., Sarrazin, F. J., Ebeling, P., Musolff, A., Fleckenstein, J. H., and Kumar, R.: Toward Understanding of Long-Term Nitrogen Transport and Retention Dynamics Across German Catchments, Geophys. Res. Lett., 49, e2022GL100278, https://doi.org/10.1029/2022GL100278, 2022.

Niemi, A. J.: Residence time distributions of variable flow processes, Int. J. Appl. Radiat. Is., 28, 855–860, https://doi.org/10.1016/0020-708X(77)90026-6, 1977.

Opazo, T., Aravena, R., and Parker, B.: Nitrate distribution and potential attenuation mechanisms of a municipal water supply bedrock aquifer, Appl. Geochem., 73, 157–168, https://doi.org/10.1016/j.apgeochem.2016.08.010, 2016.

Queloz, P., Carraro, L., Benettin, P., Botter, G., Rinaldo, A., and Bertuzzo, E.: Transport of fluorobenzoate tracers in a vegetated hydrologic control volume: 2. Theoretical inferences and modeling, Water Resour. Res, 51, 2793–2806, https://doi.org/10.1002/2014WR016508, 2015.

Rinaldo, A. and Marani, M.: Basin Scale Model of Solute Transport, Water Resour. Res., 23, 2107–2118, https://doi.org/10.1029/WR023i011p02107, 1987.

Rinaldo, A., Botter, G., Bertuzzo, E., Uccelli, A., Settin, T., and Marani, M.: Transport at basin scales: 1. Theoretical framework, Hydrol. Earth Syst. Sci., 10, 19–29, https://doi.org/10.5194/hess-10-19-2006, 2006.

Rinaldo, A., Benettin, P., Harman, C. J., Hrachowitz, M., McGuire, K. J., ven der Velde, Y., Bertuzzo, E., and Botter, G.: Storage selection functions: A coherent framework for quantifying how catchments store and release water and solutes, Water Resour. Res., 51, 4840–4847, https://doi.org/10.1002/2015WR017273, 2015.

Rodriguez, N. B., McGuire, K. J., and Klaus, J.: Time-Varying Storage–Water Age Relationships in a Catchment With a Mediterranean Climate, Water Resour. Res., 54, 3988–4008, https://doi.org/10.1029/2017WR021964, 2018.

Rodriguez, N. B., Pfister, L., Zehe, E., and Klaus, J.: A comparison of catchment travel times and storage deduced from deuterium and tritium tracers using StorAge Selection functions, Hydrol. Earth Syst. Sci., 25, 401–428, https://doi.org/10.5194/hess-25-401-2021, 2021.

Rodríguez-Cruz, M. S., Jones, J. E., and Bending, G. D.: Field-scale study of the variability in pesticide biodegradation with soil depth and its relationship with soil characteristics, Soil Biol. Biochem., 38, 2910–2918, https://doi.org/10.1016/j.soilbio.2006.04.051, 2006.

Samaniego, L., Kumar, R., and Attinger, S.: Multiscale parameter regionalization of a grid-based hydrologic model at the mesoscale, Water Resour. Res., 46, W05523, https://doi.org/10.1029/2008WR007327, 2010.

Schoups, G., van de Giesen, N. C., and Savenije, H. H. G.: Model complexity control for hydrologic prediction, Water Resour. Res., 44, W00B03, https://doi.org/10.1029/2008WR006836, 2008.

Seeger, S. and Weiler, M.: Reevaluation of transit time distributions, mean transit times and their relation to catchment topography, Hydrol. Earth Syst. Sci., 18, 4751–4771, https://doi.org/10.5194/hess-18-4751-2014, 2014.

Soulsby, C. and Tetzlaff, D.: Towards simple approaches for mean residence time estimation in ungauged basins using tracers and soil distributions, J. Hydrol., 363, 60–74, https://doi.org/10.1016/j.jhydrol.2008.10.001, 2008.

Stewart, M. K., Morgenstern, U., and McDonnell, J. J.: Truncation of stream residence time: How the use of stable isotopes has skewed our concept of streamwater age and origin, Hydrol. Process., 24, 1646–1659, https://doi.org/10.1002/hyp.7576, 2010.

Stewart, M. K., Morgenstern, U., McDonnell, J. J., and Pfister, L.: The "hidden streamflow" challenge in catchment hydrology: A call to action for stream water transit time analysis, Hydrol. Process., 26, 2061–2066, https://doi.org/10.1002/hyp.9262, 2012.

Stockinger, M. P., Lücke, A., McDonnell, J. J., Diekkrüger, B., Vereecken, H., and Bogena, H. R.: Interception effects on stable isotope driven streamwater transit time estimates, Geophys. Res. Lett., 42, 5299–5308, https://doi.org/10.1002/2015GL064622, 2015.

Sutanudjaja, E. H., van Beek, R., Wanders, N., Wada, Y., Bosmans, J. H. C., Drost, N., van der Ent, R. J., de Graaf, I. E. M., Hoch, J. M., de Jong, K., Karssenberg, D., López López, P., Peßenteiner, S., Schmitz, O., Straatsma, M. W., Vannametee, E., Wisser, D., and Bierkens, M. F. P.: PCR-GLOBWB 2: a 5 arcmin global hydrological and water resources model, Geosci. Model Dev., 11, 2429–2453, https://doi.org/10.5194/gmd-11-2429-2018, 2018.

Svensson, T., Lovett, G. M., and Likens, G. E.: Is chloride a conservative ion in forest ecosystems?, Biogeochemistry, 107, 125–134, https://doi.org/10.1007/s10533-010-9538-y, 2012.

Tetzlaff, D., Piovano, T., Ala-Aho, P., Smith, A., Carey, S. K., Marsh, P., Wookey, P. A., Street, L. E., and Soulsby, C.: Using stable isotopes to estimate travel times in a data-sparse Arctic catchment: Challenges and possible solutions, Hydrol. Process., 32, 1936–1952, https://doi.org/10.1002/hyp.13146, 2018.

Thiemig, V., Rojas, R., Zombrano-Bigiarini, M., and De Roo, A.: Hydrological evaluation of satellite-based rainfall estimates over the Volta and Baro-Akobo Basin, J. Hydrol., 499, 324–338, https://doi.org/10.1016/j.jhydrol.2013.07.012, 2013.

Van der Velde, Y., De Rooij, G. H., Rozemeijer, J. C., Van Geer, F. C., and Broers, H. P.: Nitrate response of a lowland catchment: On the relation between stream concentration and travel time distribution dynamics, Water Resour. Res., 46, W11534, https://doi.org/10.1029/2010WR009105, 2010.

van der Velde, Y., Torfs, P. J. J. F., van der Zee, S. E. A. T. M., and Uijlenhoet, R.: Quantifying catchment-scale mixing and its effect on time-varying travel time distributions, Water Resour. Res., 48, W06536, https://doi.org/10.1029/2011WR011310, 2012.

Van Meter, K. J., Basu, N. B., and Van Cappellen, P.: Two centuries of nitrogen dynamics: legacy sources and sinks in the Mississippi and Susquehanna River Basins, Global Biogeochem. Cy., 31, 2–23, https://doi.org/10.1002/2016GB005498, 2017.

Visser, A., Broers, H. P., Purtschert, R., Sültenfuß, J., and de Jonge, M.: Groundwater age distributions at a public drinking water supply well field derived from multiple age tracers (^{85}Kr, ^{3}H / ^{3}He, and ^{39}Ar), Water Resour. Res., 49, 7778–7796, https://doi.org/10.1002/2013WR014012, 2013.

Visser, A., Thaw, M., Deinhart, A., Bibby, R., Safeeq, M., Conklin, M., Esser, B., and van der Velde, Y.: Cosmogenic isotopes unravel the hydrochronology and water storage dynamics of the Southern Sierra critical zone, Water Resour. Res., 55, 1429–1450, https://doi.org/10.1029/2018WR023665, 2019.

von Freyberg, J., Studer, B., and Kirchner, J. W.: A lab in the field: high-frequency analysis of water quality and stable isotopes in stream water and precipitation, Hydrol. Earth Syst. Sci., 21, 1721–1739, https://doi.org/10.5194/hess-21-1721-2017, 2017.

von Freyberg, J., Allen, S. T., Seeger, S., Weiler, M., and Kirchner, J. W.: Sensitivity of young water fractions to hydro-climatic forcing and landscape properties across 22 Swiss catchments, Hydrol. Earth Syst. Sci., 22, 3841–3861, https://doi.org/10.5194/hess-22-3841-2018, 2018.

von Freyberg, J., Rücker, A., Zappa, M., Schlumpf, A., Studer, B., and Kirchner, J. W.: Four years of daily stable water isotope data in stream water and precipitation from three Swiss catchments, Sci. Data, 9, 46, https://doi.org/10.1038/s41597-022-01148-1, 2022.

Wang, S., Hrachowitz, M., Schoups, G., and Stumpp, C.: Stable water isotopes and tritium tracers tell the same tale: No evidence for underestimation of catchment transit times inferred by stable isotopes in SAS function models, Hydrol. Earth Syst. Sci. Discuss. [preprint], https://doi.org/10.5194/hess-2022-400, in review, 2022.

Wilusz, D. C., Harman, C. J., and Ball, W. P.: Sensitivity of Catchment Transit Times to Rainfall Variability Under Present and Future Climates, Water Resour. Res., 53, 10231–10256, https://doi.org/10.1002/2017WR020894, 2017.

Winter, C., Lutz, S. R., Musolff, A., Kumar, R. Weber, M., and Fleckenstein, J. H.: Disentangling the Impact of Catchment Heterogeneity on Nitrate Export Dynamics From Event to Long-Term Time Scales, Water Resour. Res., 57, e2020WR027992, https://doi.org/10.1029/2020WR027992, 2020.

Winter, C., Nguyen, T. V., Musolff, A., Lutz, S. R., Rode, M., Kumar, R., and Fleckenstein, J. H.: Droughts can reduce the nitrogen retention capacity of catchments, Hydrol. Earth Syst. Sci., 27, 303–318, https://doi.org/10.5194/hess-27-303-2023, 2023.

Wollschläger, U., Attinger, S., Borchardt, D., Brauns, M., Cuntz, M., Dietrich, P., Fleckenstein, J. H., Friese, K., Friesen, J., Harpke, A., Hildebrandt, A., Jäckel, G., Kamjunke, N., Knöller, K., Kögler, S., Kolditz, O., Krieg, R., Kumar, R., Lausch, A., Liess, M., Marx, A., Merz, R., Mueller, C., Musolff, A., Norf, H., Oswald, S. E., Rebmann, C., Reinstorf, F., Rode, M., Rink, K., Rinke, K., Samaniego, L., Vieweg, M., Vogel, H. J., Weitere, M., Werban, U., Zink, M., and Zacharias, S.: The Bode hydrological observatory: a platform for integrated, interdisciplinary hydro-ecological research within the TERENO Harz/-Central German Lowland Observatory, Environ. Earth Sci., 76, 29, https://doi.org/10.1007/s12665-016-6327-5, 2017.

Xu, G., Magen, H., Tarchitzky, J., and Kafkafi, U.: Advances in Chloride Nutrition of Plants, Adv. Agron., 68, 97–150, https://doi.org/10.1016/S0065-2113(08)60844-5, 1999.

Yang, J., Heidbüchel, I., Musolff, A., Reinstorf, F., and Fleckenstein, J. H.: Exploring the Dynamics of Transit Times and Subsurface Mixing in a Small Agricultural Catchment, Water Resour. Res., 54, 2317–2335, https://doi.org/10.1002/2017WR021896, 2018.

Yang, X., Seifeddine, J., Zink, M., Fleckenstein, J. H., Borchardt, D., and Rode, M.: A New Fully Distributed Model of Nitrate Transport and Removal at Catchment Scale, Water Resour. Res., 54, 5856–5877, https://doi.org/10.1029/2017WR022380, 2018.

Zink, M., Kumar, R., Cuntz, M., and Samaniego, L.: A high-resolution dataset of water fluxes and states for Germany accounting for parametric uncertainty, Hydrol. Earth Syst. Sci., 21, 1769–1790, https://doi.org/10.5194/hess-21-1769-2017, 2017.

Supplement of Hydrol. Earth Syst. Sci., 27, 2989–3004, 2023
https://doi.org/10.5194/hess-27-2989-2023-supplement

Hydrology and Earth System Sciences
Open Access
EGU

Supplement of

Uncertainty in water transit time estimation with StorAge Selection functions and tracer data interpolation

Arianna Borriero et al.

Correspondence to: Arianna Borriero (arianna.borriero@ufz.de)

1 Supplement

Table S1. 95% confidence interval of the behavioral SAS parameter ranges for each tested setup.

Interpolation	SAS parameters	k_Q [-]	k_{Q1} or α [-]	k_{Q2} or β [-]	k_{ET} [-]	S_0 [mm]
step function kriged $\delta^{18}O_P$	PLTI	0.42 - 1.00	-	-	0.34 - 1.93	590 - 2875
	PLTV	-	0.31 - 0.86	0.56 - 1.80	0.39 - 1.94	575 - 2754
	BETATI	-	0.49 - 1.00	0.26 - 1.98	0.35 - 1.95	783 - 2847
step function raw $\delta^{18}O_P$	PLTI	0.50 - 1.01	-	-	0.18 - 1.92	600 - 2894
	PLTV	-	0.40 - 0.95	0.53 - 1.8	0.20 - 1.95	618 - 2875
	BETATI	-	0.55 - 0.99	1.01 - 1.97	0.20 - 1.93	788 - 2875
sine function kriged $\delta^{18}O_P$	PLTI	0.36 - 1.56	-	-	0.18 - 1.93	335 - 1688
	PLTV	-	0.19 - 1.02	0.62 - 1.96	0.19 - 1.95	335 - 1441
	BETATI	-	0.41 - 1.06	0.84 - 1.99	0.24 - 1.96	411 - 2362
sine function raw $\delta^{18}O_P$	PLTI	0.49 - 1.83	-	-	0.21 - 1.96	335 - 1087
	PLTV	-	0.24 - 1.47	0.81 - 1.97	0.22 - 1.94	353 - 1110
	BETATI	-	0.51 - 1.68	0.25 - 1.98	0.22 - 1.95	347 - 1781

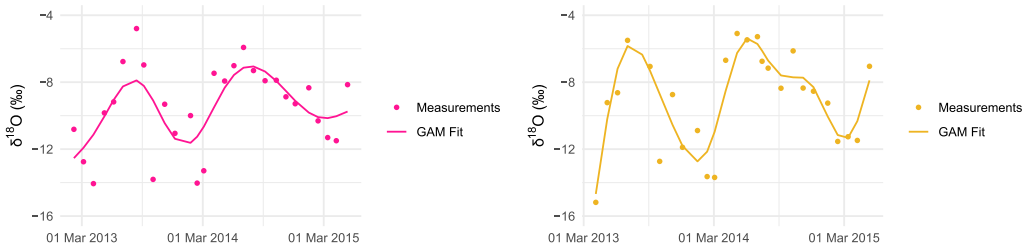

Figure S1. Measured (dots) and predicted (line) $\delta^{18}O_P$ via GAM with kriged (pink) and raw (yellow) data.

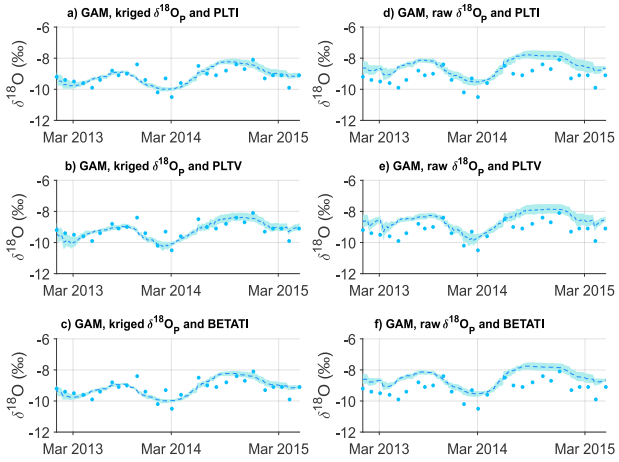

Figure S2. Predicted $\delta^{18}O$ values in streamflow. The dark blue filled circles represent the observed data, and the dashed light blue lines and shaded areas represent the ensemble mean of all possible solutions and their range according to the 95% CI, respectively.

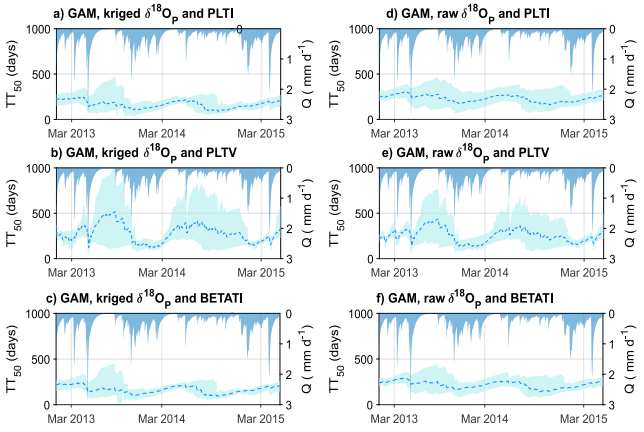

Figure S3. Predicted TT_{50} of streamflow. The dashed light blue lines and shaded areas represent the ensemble mean of all possible solutions and their range according to the 95% CI, respectively.

Journal of Hydrology 645 (2024) 132238

Contents lists available at ScienceDirect

Journal of Hydrology

journal homepage: www.elsevier.com/locate/jhydrol

Research papers

Can the young water fraction reduce predictive uncertainty in water transit time estimations?

Arianna Borriero [a,*], Tam V. Nguyen [a], Stefanie R. Lutz [b], Jan H. Fleckenstein [a,c], Andreas Musolff [a], Rohini Kumar [d]

[a] Department of Hydrogeology, Helmholtz-Centre for Environmental Research - UFZ, Leipzig, Germany
[b] Copernicus Institute of Sustainable Development, Department of Environmental Sciences, Utrecht University, Utrecht, The Netherlands
[c] Bayreuth Centre of Ecology and Environmental Research, University of Bayreuth, Bayreuth, Germany
[d] Department of Computational Hydrosystems, Helmholtz-Centre for Environmental Research - UFZ, Leipzig, Germany

ARTICLE INFO

This manuscript was handled by S. Sally Elizabeth Thompson, Editor-in-Chief, with the assistance of Kyle Blount, Associate Editor.

Dataset link: http://www.hydroshare.org/resource/796d45e9b43c45f1abf4dd243dd559d1

Keywords:
Young water fraction
Transit time distribution
SAS functions
Uncertainty

ABSTRACT

Transit time distributions (TTDs) of streamflow are informative descriptors of catchment hydrological functioning and solute transport mechanisms. Conventional methods for estimating TTDs generally require model calibration against extensive tracer data time series, which are often limited to well-studied experimental catchments. We challenge this limitation and propose an alternative approach that uses the young water fraction (F_{yw}^{obs}), an increasingly used water age metric which represents the proportion of streamflow with a transit time younger than 2–3 months, and that can be robustly estimated with sparsely measured tracer data. To this end, we conducted a proof of concept study by modeling TTDs using StorAge Selection (SAS) functions with oxygen isotopes ($\delta^{18}O$) measurements for 23 diverse catchments in Germany. In a Monte-Carlo approach, we computed the (averaged) marginal TTDs of a prior parameter distribution and derived a model-based F_{yw} (F_{yw}^{sim}). We compared F_{yw}^{sim} with F_{yw}^{obs}, obtained from $\delta^{18}O$ measurements, and constrained the prior SAS parameters distribution. Subsequently, we derived a posterior distribution of parameters and resulting model simulations. Our findings showed that using F_{yw}^{obs} to constrain the model effectively reduced parameter equifinality and simulation uncertainty. However, the value of F_{yw}^{obs} on reducing model uncertainty varied across sites, with larger values ($F_{yw}^{obs} \geq 0.10$) leading to simulations with a narrower uncertainty band and higher model efficiency, whilst smaller values ($F_{yw}^{obs} \leq 0.05$) had limited influence on reducing model output uncertainty. We discussed the potential and limitations of combining SAS functions with F_{yw}^{obs}, and considered broader implications of this approach for enhancing our understanding of catchment functioning and water quality status.

1. Introduction

The streamflow water age, commonly referred to as water transit time (TT), describes the time elapsed between the entry of a water parcel into a catchment and its exit via outflows (i.e. evapotranspiration or streamflow). As there are multiple flowpaths in catchments with different characteristics, the water transit time distribution (TTD) is used to describe the entirety of water TTs in the outflows (Botter et al., 2010). The TTD provides valuable insights into a catchment's hydrological behavior (Rinaldo and Marani, 1987), including water sources, flowpath characteristics, and water mixing in streamflow (Kirchner et al., 2000; McGuire et al., 2005; McGuire and McDonnel, 2006; Berghuijs and Kirchner, 2017) across different environments (Botter et al., 2022). Understanding these aspects is relevant for many purposes, such as water resources management and protection, water supply (Seager et al., 2007; Berghuijs et al., 2014), water quality status (Benettin et al., 2015a), and vulnerability assessment (Kumar et al., 2020).

As TTDs are not directly measurable, they have been simulated with models based on non-stationary assumptions, resulting in time-variant TTDs (Benettin et al., 2013; Engdahl et al., 2016; Kumar et al., 2020; Heidbüchel et al., 2020). The time-variant nature of TTDs is due to the variability of the meteorological forcing (Botter et al., 2010; Heidbüchel et al., 2012; Harman, 2015), and the activation/deactivation of flowpaths under different hydrological conditions (Ambroise, 2004; Heidbüchel et al., 2013). In recent years, StorAge Selection (SAS) functions have emerged as a novel way to represent time-variant TTDs (Botter et al., 2011; van der Velde et al., 2012; Rinaldo et al., 2015), as they describe the relationship between

* Corresponding author.
E-mail address: arianna.borriero@ufz.de (A. Borriero).

https://doi.org/10.1016/j.jhydrol.2024.132238
Received 17 July 2023; Received in revised form 14 August 2024; Accepted 7 October 2024
Available online 24 October 2024

the water ages distribution in storage and outflows (Harman, 2019). SAS functions describe the evolution of water balance depending on water inputs, outputs and aging within the catchment (Benettin et al., 2022), enabling the exploration of various water release patterns. Due to these advantages, SAS functions have been implemented in many water quantity and quality studies across different settings (Lutz et al., 2017; Wilusz et al., 2020; Zhang et al., 2020; Nguyen et al., 2022; Li et al., 2024).

SAS functions can be seen as catchment functioning properties describing how water within the catchment contributes to streamflow or evapotranspiration fluxes, thus determining the preference for young or old water-age selection in the outflows. SAS functions rely on intrinsic parameters and connecting them to catchment-scale processes is crucial. Because the values of these parameters are unknown, their calibration is necessary. Current approaches involve calibrating SAS parameters to the time series of tracer data, such as stable water isotopes, which provide valuable insights on water transport and storage (Jasechko, 2019). Calibration against stable water isotopes allows the link of the SAS parameters with the catchment-scale processes which, ultimately, control hydrological and solute export dynamics (Kaandorp et al., 2018; Smith et al., 2018; Rodriguez and Klaus, 2019; Lapides et al., 2022; Sprenger et al., 2022).

In data-rich experimental catchments, stable water isotopes in precipitation serve as model input data. They show variability at both seasonal and event scales, which can be more or less pronounced depending on climate conditions, geographical location, and evaporation and condensation processes. Instead, instream stable water isotopes are used to evaluate model simulations. They are also characterized by seasonal variability which is, however, more damped and phase-shifted compared to that of stable water isotopes in precipitation. The more pronounced the seasonal variation in instream isotopes is, the younger the water being discharged, whereas the more damped the seasonal variation in instream isotopes is, the older the water being released. Such contrast in variability between stable water isotopes in precipitation and streamflow allows us to distinguish, via SAS functions, stream water from precipitation events that have occurred over different timescales.

Recent research has demonstrated the possibility of deriving metrics for TTDs directly from tracer data without the need to calibrate models. Relevant examples are the mean water transit time (MTT; i.e. the average time for water to leave the catchment) and the young water fraction (F_{yw}; Kirchner (2016a)). F_{yw} has been shown to be less susceptible to aggregation bias caused by the heterogeneity and nonstationarity of real-world catchments, unlike MTT (Kirchner, 2016a,b). F_{yw} represents the proportion of streamflow with a transit time younger than approximately 2–3 months (Kirchner, 2016a), and it has been increasingly reported as a useful proxy for fast hydrological and solute transport dynamics (Benettin et al., 2017a). F_{yw} is commonly derived from the ratio of the seasonal tracer amplitudes in precipitation and streamflow, and can be readily estimated from sparsely sampled tracers spanning at least 2–3 years (Benettin et al., 2022). Given its advantages, F_{yw} has been widely applied in several studies to quantify water age contribution to runoff and perform catchments inter-comparison (Jasechko et al., 2016; Song et al., 2017; Lutz et al., 2018; von Freyberg et al., 2018; Gentile et al., 2023).

The global availability of F_{yw} data was significantly enhanced by the study of Jasechko et al. (2016), who calculated F_{yw} in 254 catchments worldwide using $\delta^{18}O$ values. Their findings revealed a correlation between F_{yw} and topographic gradient, thus providing valuable insights for F_{yw} across different regions and climates. In our view, such an analysis can offer potential for regionalizing F_{yw} values, so that corresponding estimates can be possibly derived for other (ungauged) areas. This is similar to $\delta^{18}O$ precipitation data whose values can be derived through spatial interpolation methods using $\delta^{18}O$ measurements from nearby monitoring stations (Bowen and Revenaugh, 2003). In addition, with the advent of large datasets such as Allen et al. (2019), it is possible to estimate F_{yw} for catchments lacking local tracer measurements in precipitation. This knowledge can potentially help address lack of tracer data in areas with limited monitoring (Tetzlaff et al., 2018), since long-term, high-frequency $\delta^{18}O$ data are often restricted to well-equipped experimental catchments (von Freyberg et al., 2022), due to cost and logistical constraints.

In this study, we hypothesize that F_{yw} estimates, derived from fitting seasonal isotopic cycles, can contain useful information to constrain the predictions of a SAS-based transit time model, especially in catchments where detailed information of instream $\delta^{18}O$ data may not be available. This work serves as a "proof of concept" study for exploring the potential and effectiveness of incorporating F_{yw} – as an abstract metric that robustly encapsulates the input and output isotopic relationship – into a SAS-based transit time model. Along with utilizing low-frequency time series of instream $\delta^{18}O$ data for estimating F_{yw}, we used them for cross-validation of model results. To this end, we applied a SAS-based transit time model to multiple catchments within the Bode River Basin, Germany, and employed estimates of F_{yw} to constrain a prior SAS parameters distribution. With this approach, we derived a posterior distribution of SAS parameters and generated posterior model simulations, such as for the TTDs. We discussed the implications of employing F_{yw} as a constraint for SAS-based transit time models, by exploring the trend in the reduction from the prior to the posterior SAS parameters and resulting model simulations. We highlighted potential benefits and associated challenges of the use of F_{yw} in SAS-based transit time models, and made broader considerations for enhancing our understanding of catchments functioning and water quality status.

2. Materials

2.1. Study site

We conducted our analysis in the Bode River Basin and 22 sub-catchments (Fig. 1), for a total of 23 catchments explored. These catchments are characterized by diversity in size, land use, vegetation, soil, geology and climate (Lutz et al., 2018). The Bode River Basin is a mesoscale catchment with an area of 3178 km^2 at Staßfurt gauging station. The catchment extends from the Harz Mountains to the Central German Lowlands, and it is an intensively studied region within the TERENO network (TERrestrial ENvironmental Observatories; Wollschläger et al. (2017)). The size of the sub-catchments ranges between 0.11 km^2 and 200 km^2, without considering the Bode catchment at Staßfurt. The altitude varies from 14 to 1139 m above mean sea level (m.a.s.l.), while the mean slope ranges from 2% to 19%. The headwater region is largely dominated by coniferous and broadleaf forest, while the lowland areas are mainly used for agriculture. The soil consists of Cambisols, Luvisols, Leptosols and Gleysols in the Harz Mountains, and Chernozems in the central lowland (Wollschläger et al., 2017). The geology is characterized by Palaeozoic rocks in the mountainous catchments (Fruhauf and Schwab, 2008), whereas the lowlands are dominated by Mesozoic and late Palaeozoic rocks covered by Tertiary and Quaternary sediments (Schuberth, 2008).

2.2. Data

We used hydroclimatic and tracer data for model simulations. Daily precipitation (P) data for each catchment were interpolated data based on the German Weather Service, while daily streamflow (Q) and evapotranspiration (ET) time series were simulated with the mesoscale Hydrologic Model (mHM; Samaniego et al. (2010), Kumar et al. (2013) and Zink et al. (2017)) as continuous measurements were not available for all the given catchment outlets and study period. Time series of Q and ET were calibrated and evaluated across multiple stations in the Bode region (see Mueller et al. (2016) for more details). Additionally, the performance of the mHM model simulations for past measurements

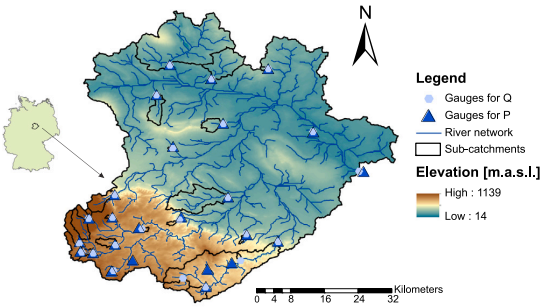

Fig. 1. Location of the Bode region in Germany (left); Bode region with its sub-catchments (black polygons), river network (blue lines), streamwater (light blue dots) and precipitation sampling locations (blue triangles), and elevation in meters above sea level as colored map (right). Not all sub-catchments are visible on the map due to their very small size (e.g. 0.2 km^2).

has been largely assessed (Yang et al., 2018; Nguyen et al., 2021), and the use of time series of simulated Q ensured the water balance closure. Average annual P, ET and Q across the study sites are 795 (542–1311), 610 (494–802) and 202 (52–601) mm, respectively, with annual P and Q being higher in the mountainous catchments compared to the lowland areas.

Monthly δ^{18}O in precipitation and streamflow were based on monthly grab samples mostly collected during non-event flow conditions (Lutz et al., 2018). The δ^{18}O in precipitation were sampled with 24 precipitation collectors and spatially interpolated using kriging with altitude as external drift. These data were then weighted with spatially distributed monthly precipitation to obtain areal monthly instream δ^{18}O for each catchment. Further details underlying the processing of the isotope dataset can be found in Lutz et al. (2018).

3. Methodology

This study explores the use of F_{yw} as a constraint in a SAS-based transit time model. To this end, we first derived estimates of F_{yw} by fitting seasonal isotopic cycles in precipitation and streamflow. Then, using SAS functions, we simulated TTDs with prior (unconstrained) model parameters. Next, from the simulated TTDs we derived the averaged (marginal) distribution and calculated the simulated F_{yw}. We compared the simulated F_{yw} with F_{yw}, obtained from fitting the δ^{18}O measurements, and constrained the prior SAS parameters distribution by deriving a posterior distribution of parameters and resulting model simulations. Lastly, we assessed the effectiveness of F_{yw} in constraining the SAS model by evaluating model performance in matching the instream δ^{18}O values for cross-validation, and simulations uncertainty. Below, we provide a detailed description of each step.

3.1. Model description

3.1.1. Young water fraction estimation

The values of young water fraction obtained by fitting seasonal isotopic cycles in precipitation and streamflow (referred in this study as F_{yw}^{obs}), were estimated for each catchment according to Kirchner (2016a). The time series of δ^{18}O in precipitation ($\delta^{18}O_P$) and streamflow ($\delta^{18}O_Q$) were fitted with sinusoids as follows:

$$\delta^{18}O_P(t) = a_P \cdot cos(2 \cdot \pi \cdot f \cdot t) + b_P \cdot sin(2 \cdot \pi \cdot f \cdot t) + k_P \quad (1)$$

$$\delta^{18}O_Q(t) = a_Q \cdot cos(2 \cdot \pi \cdot f \cdot t) + b_Q \cdot sin(2 \cdot \pi \cdot f \cdot t) + k_Q \quad (2)$$

where a [-] and b [-] are the cosine and sine coefficients of the sinusoids, f [T^{-1}] is the cycle frequency, and k [M] is the vertical displacement of the sinusoid. The values for a and b were determined using the iteratively reweighted least squares regression, which is commonly employed to limit the influence of outliers (Stockinger et al., 2016; Lutz et al., 2018; von Freyberg et al., 2018). Values of δ^{18}O in precipitation were volume-weighted by their corresponding precipitation rates to reduce the impact of small precipitation events (von Freyberg et al., 2018). Finally, F_{yw}^{obs} was calculated as the ratio of the amplitude of the seasonal cycles in the isotopes in precipitation (A_P) and streamflow (A_Q):

$$F_{yw}^{obs} = \frac{A_Q}{A_P} = \frac{\sqrt{a_Q^2 + b_Q^2}}{\sqrt{a_P^2 + b_P^2}}. \quad (3)$$

The uncertainty in the estimated F_{yw}^{obs} values was expressed as standard error (SE), calculated from a Gaussian error propagation (von Freyberg et al., 2018).

3.2. SAS-based transit time model

The transit time distribution (TTD) of streamflow was simulated using the *tran-SAS v1.0* model (Benettin and Bertuzzo, 2018) based on StorAge Selection (SAS) functions. In this study, we conceptualized each study catchment as a single storage $S(t)$ [L^3], for which the governing water-age balance equations are as follows (Botter et al., 2011):

$$S(t) = S_0 + V(t) \quad (4)$$

$$\frac{\partial S_T(T,t)}{\partial t} + \frac{\partial S_T(T,t)}{\partial T} = P(t) - Q(t) \cdot \Omega_Q(S_T(T,t),t) - ET(t) \cdot \Omega_{ET}(S_T(T,t),t) \quad (5)$$

$$\text{Initial condition: } S_T(T, t=0) = S_{T_0}(T) \quad (6)$$

$$\text{Boundary condition: } S_T(0,t) = 0 \quad (7)$$

where S_0 [L^3] is the initial storage; $V(t)$ [L^3] are the storage variations at each time step t obtained from the hydrological balance equation $dV(t)/dt = P(t) - ET(t) - Q(t)$; $P(t)$ [L^3/T], $Q(t)$ [L^3/T], and $ET(t)$ [L^3/T] are precipitation, streamflow and evapotranspiration fluxes, respectively; $S_T(T,t)$ [L^3] is the age-ranked storage with an age T; $S_{T0}(T)$ [L^3] is the initial age-ranked storage; and $\Omega_Q(S_T,t)$ [-] and $\Omega_{ET}(S_T,t)$ [-] are the cumulative SAS functions for Q and ET, respectively.

By solving Eq. (5), the main output of our study was derived, namely the TTD of streamflow [T^{-1}] and the instream isotopic signature $\delta^{18}O_Q$ [ML^{-3}]. The TTD was calculated as:

$$p_Q(T,t) = \frac{\partial \Omega_Q(S_T,t)}{\partial S_T} \cdot \frac{\partial S_T}{\partial T}. \quad (8)$$

The instream isotopic signature $\delta^{18}O_Q$ [ML^{-3}] was obtained from:

$$\delta^{18}O_Q(t) = \int_0^{+\infty} \delta^{18}O_S(T,t) \cdot p_Q(T,t) \cdot dT \quad (9)$$

where $\delta^{18}O_S(T,t)$ [ML^{-3}] is the isotopic signature of a water parcel in storage. The same equations apply to the ET flux.

SAS functions for Q and ET are approximated using probability distributions. In this work, the SAS function for Q and ET was approximated by the time-invariant beta function (van der Velde et al., 2012; Drever and Hrachowitz, 2017), and time-invariant power law (Queloz et al., 2015; Benettin et al., 2017b; Asadollahi et al., 2020), respectively. They are expressed below as probability density function in terms of the normalized age-ranked storage $P_S(T,t)$ [-] (van der Velde et al., 2012):

$$\omega_Q(P_S(T,t),t) = \frac{(P_S(T,t))^{\alpha-1} \cdot (1 - P_S(T,t))^{\beta-1}}{B(\alpha,\beta)} \quad (10)$$

$$\omega_{ET}(P_S(T,t),t) = k \cdot (P_S(T,t))^{k-1} \quad (11)$$

Table 1
Summary of the model parameters and their initial ranges.

SAS parameter	Symbol	Unit	Lower bound	Upper bound
Q parameter	α	[–]	0.1	5
Q parameter	β	[–]	0.1	5
ET parameter	k_{ET}	[–]	0.1	1
Initial storage	S_0	[mm]	1000	5000

where $B(\alpha, \beta)$ is the beta function with two shape parameters α and β, and k is the power-law parameter. Time-invariant SAS functions assume that SAS parameters are not coupled with any catchment state variable (e.g. catchment wetness index parameter).

Finally, the model-based F_{yw} (F_{yw}^{sim}) was simulated by time-averaging the ensemble distribution of all TTDs previously obtained from Eq. (8) (Benettin et al., 2022), after editing the SAS model code with the following equation:

$$\langle p_Q(T) \rangle = \frac{1}{t} \int_0^t p_Q(T,t) \cdot dt \tag{12}$$

Eq. (12) represents the so-called marginal TTD (Botter et al., 2010; Heidbüchel et al., 2012), as it is analogous to the concept of marginalization in statistics. The averaging in Eq. (12) was done using daily flows as weights to obtain a flow-weighted age distribution. By computing the marginal TTD, we compared the SAS model with the observational estimates of F_{yw}^{obs} (see Section 3.3.2 for more details). Indeed, the link between F_{yw}^{obs} and TTD is challenged by the fact that F_{yw}^{obs} is stationary (a single value) while the TTDs simulated with SAS functions are time-variant (a series of values). Given that the marginal TTD represents an ensemble of time-averaged TTDs, we translate the time-variant TTDs towards steady-state conditions, hence aligning with the stationary nature of F_{yw}^{obs} derived from measured isotopes.

3.3. Model setup

3.3.1. Prior model solution

We executed the SAS-based transit time model as a Monte-Carlo experiment generating 10,000 uniform parameter sets with Latin Hypercube Sampling (McKay et al., 1979). This yielded a prior solution (i.e. the solution before the application of a constraint) characterized by prior parameters, whose values and search ranges are given in Table 1. The prior parameters covered a wide range, chosen based on other studies in the region (Nguyen et al., 2021, 2022) and elsewhere (Benettin et al., 2017b), indicating a lack of prior knowledge about the SAS parameters and catchment storage. Additionally, by using a uniform prior parameter distribution, we avoided introducing preferences, biases, or outliers into the parameters values.

The values of α and β determine the selection preference for streamflow imposed by the beta SAS function (Eq. (10)). In this work, a wide chosen range of values in the prior SAS parameters allows both old and young water to be selected; the beta SAS parameters either assume $\alpha<1$ and $\beta\geq1$ (i.e. preferably young water), or $\alpha\geq1$ and $\beta<1$ (i.e. preferably old water). The power law SAS parameter k_{ET} (Eq. (11)) assumes $k_{ET}\leq1$, considering that *ET* is likely to be sampled from shallow, root-accessible soil layers where young water ages usually prevail (Buzacott et al., 2020; Thaw et al., 2021). The initial storage (S_0) is difficult to estimate without knowing the catchment's physical characteristics and volume of older water (Benettin et al., 2017b; Benettin and Bertuzzo, 2018); hence, S_0 was also calibrated within a prior range based on similar studies in the same area (Nguyen et al., 2021, 2022) and elsewhere (Benettin et al., 2017b).

3.3.2. Posterior model solution

To compare F_{yw}^{obs} with the SAS model results, we utilized the marginal TTD (Eq. (12)). For each set of prior parameters, we derived the corresponding prior F_{yw}^{sim} value from the prior marginal TTD. This approach is based on the principle that F_{yw} can be generally viewed as the cumulative marginal TTD evaluated at $T = \tau_{yw}$ (Benettin et al., 2022), where τ_{yw} is the young water threshold in streamflow. According to Kirchner (2016a), τ_{yw} can be approximated based on the shape parameter α of the assumed gamma TTD:

$$\tau_{yw} = 0.0949 + 0.1065 \cdot \alpha - 0.0126 \cdot \alpha^2 \tag{13}$$

The typical range for α varies between α = [0.2–2] (Kirchner, 2016a), corresponding to τ_{yw} = [42–94 days]. Consequently, we evaluated the cumulative marginal TTD over T = [42–94 days], to account for the entire range associated with τ_{yw}. Then, we selected the posterior solution (i.e. the solution after the application of a constraint) based on the condition that the prior cumulative marginal TTD at T = [42–94 days] matches the values within the range of F_{yw}^{obs}±SE. This allowed us to derive a set of posterior parameters and output variables, corresponding to the so-called posterior solution.

The main output variables included the instream $\delta^{18}O$ (Eq. (9)) and backward median transit time (TT_{50}; i.e. the time over which half of the water that has entered the catchment via precipitation has left at the catchment outlet). The TT_{50} time series are widely used in hydrological studies (Kirchner, 2016a), and were extracted directly as the median (i.e. 50% probability) of the cumulative TTDs (Eq. (8)) calculated for each day of the study period (Kumar et al., 2020). We explored TT_{50} for the many advantages it offers. Unlike MTT, TT_{50} is less affected by the poor identifiability of old water (Benettin et al., 2017b), typically associated with long-tailed TTDs. Additionally, unlike TTD, which is a distribution function, TT_{50} is an abstract measure (median value) of that distribution, represented as a time series. This allows for a more effective interpretation of the effects of changing hydrometeorological conditions on TT_{50}, thus providing insights that may not be so straightforward to visualize when examining a distribution. The individual steps in this methodology are summarized in Fig. 2.

After defining a posterior solution, we assessed its uncertainty (Beven and Binley, 1992) based on the 95% prediction uncertainty (95PPU) calculated from the 2.5% and 97.5% confidence intervals of the cumulative distribution in the time series of the output variables (Abbaspour et al., 2004). We quantified the difference between the prior and posterior solution of model parameters and output variables in terms of the reduction percentage in the 95PPU.

Finally, in a "proof of concept" study, we explored the potential and effectiveness of incorporating F_{yw}^{obs} estimates in a SAS-based transit time model by using measured instream $\delta^{18}O$ data for cross-validation of $\delta^{18}O$ simulations. To this aim, we evaluated the Kling–Gupta efficiency (KGE; Gupta et al. (2009)), which quantifies the difference between the observed and simulated instream $\delta^{18}O$ before (i.e. prior solution) and after (i.e. posterior solution) the calibration against F_{yw}^{obs}. The analysis of prior KGE values aligns with the classical modeling approach that directly optimizes SAS-based transit time models with instream tracer observations. Overall, we used 28 observed data points of instream $\delta^{18}O$ signatures to evaluate the KGE.

3.3.3. Data processing and initial conditions

Model simulations were run at daily time step. Since we obtained monthly data for $\delta^{18}O$ in precipitation after kriging of the monthly composite samples from Lutz et al. (2018), we disaggregated them to daily scale using a step function. Therefore, the missing daily values between two consecutive samples matched the value of the more recent sample. To minimize the impact of model initialization, the model was run with a warm-up period (June 1999–January 2013) consisting of repeated input data of available records. This warm-up period was followed by the actual simulation from February 2013 to May 2015. Initial values of instream $\delta^{18}O$ were set equal to the mean instream $\delta^{18}O$ of each catchment throughout the study period.

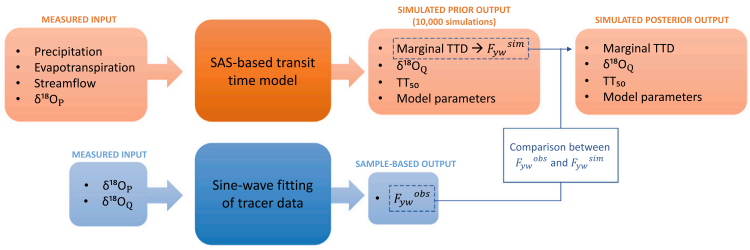

Fig. 2. Flowchart of the methodology conceptualization.

4. Results

In the following, we first present our results based on the analysis of F_{yw}^{obs} derived from the sine-wave fitting approach (Section 4.1), and simulated F_{yw}^{sim} as well as marginal TTDs derived from the SAS-based transit time model (Section 4.2). Second, we explore the identifiability of SAS parameters (Section 4.3). Third, we assess the model fit of posterior simulations to individual $\delta^{18}O$ measurements, which serve as cross-validation to demonstrate the effectiveness of F_{yw}^{obs} as a model constraint (Section 4.4). Finally, we evaluate the predictive uncertainty in the TT_{50} time series (Section 4.5).

4.1. Young water fractions

The sample-based young water fractions (F_{yw}^{obs}), derived by fitting the isotope cycles with sine-waves, are shown in Fig. 3; the corresponding standard errors (SE) and the fitting of $\delta^{18}O$ values in precipitation and streamflow with sine-waves are presented in the Supplement (Table S1 and Fig. S1). The results exhibit a wide range of F_{yw}^{obs} across the study sites, varying from 0.02 to 0.26 (mean of 0.12). This means that 2%–26% of the streamflow is water that entered the catchments in the past 2–3 months. F_{yw}^{obs} values vary across the study area based on hydroclimatic conditions and land cover. Smaller values were found in mountainous catchments having higher *P*, *Q* and forest cover fraction (id 9, 14, 23 and 26 in Fig. 3), while larger values were located mostly at lower altitudes (id 20, 79, 81 and 111 in Fig. 3). These values of F_{yw}^{obs} are similar to those of Lutz et al. (2018), who examined F_{yw}^{obs} at the same sites with a comparable approach (see Lutz et al. (2018) for more details).

The sine-wave fitting of $\delta^{18}O$ values indicated a pronounced seasonal amplitude in precipitation, with more negative (or positive) values in winter (or summer). In contrast, the seasonal amplitude of instream $\delta^{18}O$ data was more damped and the sine-waves were phase-shifted. Larger values of F_{yw}^{obs} (e.g. id 20, 79, 81 and 111) were associated with less damped amplitudes in the sine-waves. The goodness of fit of the sine-wave for $\delta^{18}O$ values was assessed using Pearson's correlation coefficient, which ranged between 0.58 and 0.77 (mean of 0.66) for $\delta^{18}O$ in precipitation, and with *p*-value < 0.001 across all 23 catchments. Conversely, the fit of instream $\delta^{18}O$ values was lower, with Pearson's correlation coefficient ranging between 0 and 0.62 (mean of 0.36), and *p*-value < 0.001 in all 23 catchments.

4.2. Marginal transit time distributions

The model-based young water fraction (F_{yw}^{sim}), derived from the cumulative marginal TTD of streamflow, was compared with F_{yw}^{obs} to constrain the prior parameter distribution and obtain a posterior solution for various output variables. To further support the idea that stationary TTDs, like the gamma function, can represent the marginal TTD, thereby making the comparison between the marginal TTD and F_{yw}^{obs} more robust, we fit the marginal TTD with a gamma function.

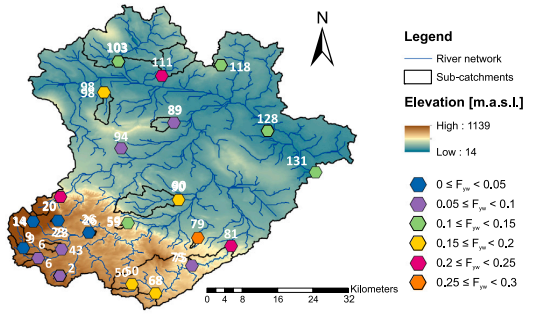

Fig. 3. F_{yw}^{obs} values obtained from the sine-wave approach in 23 catchments (black polygons) with their corresponding identification number, the river network (blue lines), and elevation in meters above sea level (colored map). (For interpretation of the references to color in this figure legend, the reader is referred to the web version of this article.)

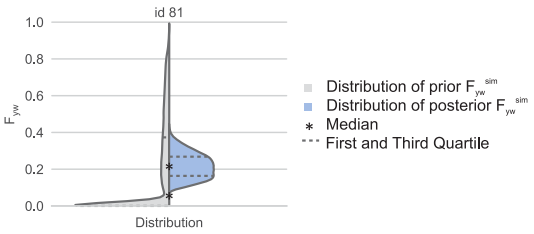

Fig. 4. Violin boxplot with F_{yw}^{sim} distribution for one example catchment obtained before (i.e. prior; left, gray) and after (i.e. posterior; right, blue) applying F_{yw}^{obs}±SE as a model constraint. (For interpretation of the references to color in this figure legend, the reader is referred to the web version of this article.)

We obtained mean values of α = [0.28–0.78] in all study areas, thus in the range of α = [0.2–2] defined by Kirchner (2016a).

The prior F_{yw}^{sim} consists of 10,000 different values for each catchment, with each value corresponding to a specific prior parameters set. By constraining the prior F_{yw}^{sim} using F_{yw}^{obs}±SE, a narrower posterior F_{yw}^{sim} was obtained at all sites. Fig. 4 displays the prior (gray) and posterior (blue) F_{yw}^{sim} for one catchment; plots for all catchments are available in the Supplement (Fig. S2). The reduction in the range of F_{yw}^{sim} between prior and posterior solution was from 43% to 87% across the 23 catchments. Notably, no significant correlation was observed between the magnitude of reduction and factors such as land use, land cover, size, elevation, area, and mean slope.

Constraining the model with F_{yw}^{obs}±SE yielded a posterior solution for the cumulative marginal TTD. Fig. 5 illustrates the 95PPU of the

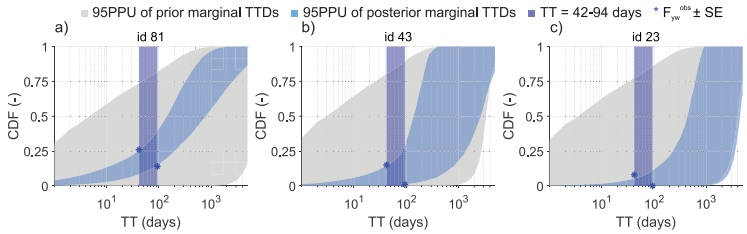

Fig. 5. 95PPU of the marginal TTDs as a cumulative density function (CDF) obtained with the prior (gray) and posterior (blue) parameter sets for three representative catchments categorized into good (a), moderate (b), and poor (c) clusters; the thick blue vertical area represents the range of T = [42–94 days], with the two blue asterisks indicating the upper and lower limits defined by F_{yw}^{obs}±SE. The *x*-axis is shown in a logarithmic scale.

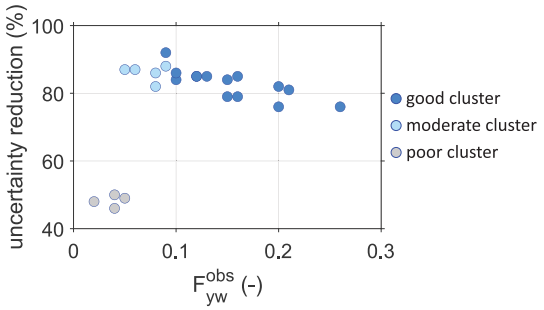

Fig. 6. Relation between the percentage reduction in the 95PPU of prior solution (i.e. uncertainty reduction) and F_{yw}^{obs}, where each dot represents one catchment.

prior (gray) and posterior (blue) marginal TTD, expressed as a cumulative density function (CDF), for three analyzed catchments; figures for all the study sites are given in the Supplement (Fig. S3). It can be seen that F_{yw}^{obs} did not uniformly constrained the prior marginal TTD across the three catchments; instead, there is a relation between the reduction in the 95PPU and the value of F_{yw}^{obs}, as shown in Fig. 6. Overall, F_{yw}^{obs}±SE reduced the 95PPU of the prior marginal TTD from 46% to 92% (mean of 77%). The most substantial reduction (from 76% to 92%) occurred when $0.10 \leq F_{yw}^{obs} \leq 0.26$, whilst for $F_{yw}^{obs} \leq 0.05$ the constraining effect was smaller (from 46% to 50%). Based on the value of F_{yw}^{obs} and the constraining effect on the prior marginal TTD, the 23 catchments were grouped into three clusters: good, moderate and poor. These clusters are those illustrated by the example catchments in Fig. 5.

The good cluster includes 14 out of 23 sites with $F_{yw}^{obs} \geq 0.10$ (Table S1). In this cluster, the 95PPU of posterior marginal TTDs was well constrained (Fig. 6), and indicated preference for younger water age release typically associated with a larger F_{yw}^{obs} (see example in Fig. 5a). The moderate cluster consists of 5 out of 23 sites with $0.05 \leq F_{yw}^{obs} \leq 0.09$ (Table S1). Despite the reduced number of simulations in the posterior solution (Fig. 6), the posterior marginal TTDs showed a relatively large 95PPU (see example in Fig. 5b). The poor cluster is composed of the remaining 4 catchments with $F_{yw}^{obs} \leq 0.05$ (Table S1). The posterior solution for this cluster was only loosely constrained (Fig. 6), resulting in widely spread posterior marginal TTDs (Fig. 5c), and a substantial contribution of older water ages, typically related to a small F_{yw}^{obs} (see example in Fig. 5c).

4.3. SAS model parameters

Fig. 7 compares the prior (black diagonal lines) and posterior (colored lines) CDFs of the SAS parameters. Each colored line is the posterior SAS parameter CDF for a given study catchment. The closer the colored lines to the black lines, the less constrained the SAS parameter is.

The SAS parameters for Q (α and β) were generally well identified (Fig. 7a–d) as the use of F_{yw}^{obs}±SE reduced the parameter range by 65% and 33% for α and β respectively, across all catchments. The posterior α and β give information about the water storage dynamics of the study sites: most of the catchments (15 out of 23) had a majority of posterior simulations indicating preference for young water release. We found a significant positive (or negative) correlation (Pearson correlation coefficient r = 0.78, *p*-value < 0.0001) between F_{yw}^{obs} and the percentage of posterior solution with a greater affinity for younger (or older) water ages, meaning that the larger (or smaller) F_{yw}^{obs}, the more parameter sets suggest preference for younger (or older) water. These results provide evidence in favor of F_{yw}^{obs}±SE for constraining model parameters in the "right direction".

On the other hand, the parameter for ET (k_{ET}) and the initial storage (S_0) were poorly identified in all catchments, with a modest average reduction between prior and posterior parameter range of only 5% and 7%, respectively (Fig. 7e–f). This indicates that the values of F_{yw}^{obs} did not significantly constrain these model parameters, suggesting the relative model insensitivity to changes in the ET flux and S_0. This highlights the need for additional data to better constrain these parameters (see Section 5.2 for further discussion).

The simulations of instream $\delta^{18}O$ and TT_{50} time series explored in this study were dependent on the posterior SAS parameters described above. These simulations are classified and interpreted into the three clusters – good, moderate, and poor – in the following sections.

4.4. Simulated instream isotopes

Fig. 8 illustrates the prior and posterior instream $\delta^{18}O$ for the three catchments of the good (Fig. 8a), moderate (Fig. 8b), and poor (Fig. 8c) cluster. Figures for all catchments are shown in the Supplement (Fig. S4). The impact of F_{yw}^{obs}±SE on the reduction in the prior 95PPU of instream $\delta^{18}O$ varied across the clusters. By visually analyzing Fig. 8, it is seen that in the good cluster (Fig. 8a), the posterior 95PPU was notably reduced compared to the prior one, and successfully captured the seasonality in the measured $\delta^{18}O$, with more negative values in winter and less negative values in summer. However, the peaks of the measured $\delta^{18}O$ were only partially captured. In the moderate cluster (Fig. 8b), the posterior 95PPU of instream $\delta^{18}O$ were not appreciably reduced compared to the prior 95PPU. In the poor cluster (Fig. 8c), the posterior instream $\delta^{18}O$ exhibited a wide 95PPU, indicating that smaller F_{yw}^{obs} values apparently resulted in a considerable uncertainty and equifinality of the posterior solution.

Differences between the measured and simulated instream $\delta^{18}O$ were evaluated with the Kling–Gupta efficiency (KGE) in a cross-validation. Fig. 9 displays the reduction in KGE, represented as the respective kernel density distributions, of the prior and posterior solution for the three representative catchments. Results for all catchments

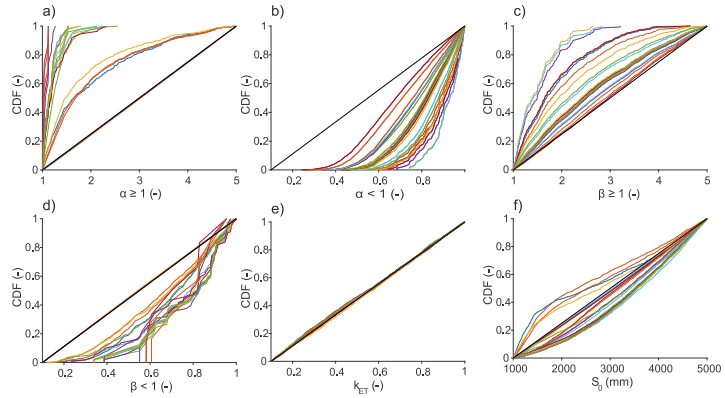

Fig. 7. CDFs of the SAS parameters; black diagonal lines are the CDFs of the prior SAS parameters, while colored lines are the catchment specific CDFs of the SAS posterior parameters. SAS functions either assume values of $\alpha < 1$ and $\beta \geq 1$ (younger water release), or $\alpha \geq 1$ and $\beta < 1$ (older water release).

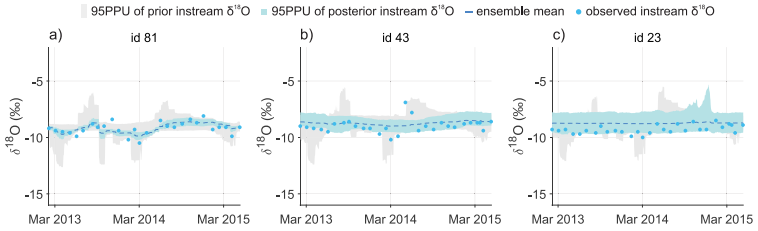

Fig. 8. 95PPU of instream $\delta^{18}O$ obtained with the prior (gray) and posterior (blue) parameter sets for three representative catchments categorized into good (a), moderate (b), and poor (c) clusters; dark blue circles represent observed data, and the light blue dashed line represents the ensemble mean of all solutions. (For interpretation of the references to color in this figure legend, the reader is referred to the web version of this article.)

are shown in the Supplement (Fig. S5). The gray distributions represent the initial 10,000 Monte-Carlo simulations, while the blue distributions correspond to the posterior simulations after constraining with F_{yw}^{obs}. The distributions highlight the range and density of model performance from best (upper part of the distribution with values closer to 1) to worst (lower part of the distribution with values closer to $-\infty$).

Similar to the findings regarding the reduction in the 95PPU of the marginal TTD and instream $\delta^{18}O$ in the three clusters, we observed consistent behaviors in the KGE values within the same cluster classification. For example, applying F_{yw}^{obs}±SE improved the KGE values in 19 out of 23 catchments (i.e. good and moderate cluster), yielding a maximum posterior KGE ranging between 0.07 and 0.67 across all study sites. The maximum median KGE at these 19 sites increased from −0.04 to 0.52 after constraining the model with F_{yw}^{obs}±SE. On the other hand, in 4 out of 23 study sites (i.e. poor cluster), the KGE values diminished, resulting in a decreased maximum median KGE from −0.15 to −0.23 after using F_{yw}^{obs}±SE.

We found a significant positive correlation between F_{yw}^{obs} and the median posterior KGE (Pearson correlation coefficient r = 0.74, *p*-value < 0.0001), meaning that the larger F_{yw}^{obs}, the better the model performances were (i.e. good cluster), whilst the smaller F_{yw}^{obs}, the worse the model performances were (i.e. poor cluster). However, even in the good cluster, fitting individual $\delta^{18}O$ measurements remained challenging, as the posterior solution captured the overall seasonality of the measurements but missed some individual values. For example, when examining catchment id 103 in Fig. S4, we observed simulations during the second half of the study period that consistently underestimated the measured data. It is important to acknowledge this uncertainty, especially when dealing with low-frequency tracer data.

4.5. Median transit time

Fig. 10 shows the posterior simulated median transit times (TT_{50}) of streamflow representative of the good (Fig. 10a), moderate (Fig. 10b) and poor (Fig. 10c) clusters. Figures for all catchments are illustrated in the Supplement (Fig. S6). Figures comparing the TT_{50} time series between the prior and posterior solution are also given in the Supplement (Fig. S7).

The simulated TT_{50} time series were relatively constant with moderate temporal fluctuations as a function of Q (Fig. 10 and S6). In the good cluster (Fig. 10a), the simulated TT_{50} time series were skewed towards smaller values (e.g. lower bound of TT_{50} in Fig. 10a ranges between 2.3 and 7.3 months), typically associated with a larger F_{yw}^{obs}. The 95PPU of TT_{50} was relatively narrow (mean 95PPU of all catchments in the good cluster is 3 years) compared to the moderate and poor clusters. Conversely, in the moderate (Fig. 10b) and poor (Fig. 10c) clusters, the TT_{50} values were comparably large (e.g. upper bound of TT_{50} in Fig. 10c is up to 12.5 years), which reflects the smaller F_{yw}^{obs}. These clusters exhibited a wider 95PPU (mean 95PPU of all catchments in the moderate and poor cluster is 8 years) and flatter TT_{50} time series compared to the good cluster. From these results, we argue that the model simulated distinct ranges of 95PPU depending on the specific F_{yw}^{obs} value. This is reflected in a significant negative correlation (Pearson correlation coefficient r = 0.84, *p*-value < 0.00001) between F_{yw}^{obs} and the mean 95PPU across the simulated period for each site. The larger (or smaller) F_{yw}^{obs}, the narrower (or wider) the 95PPU for TT_{50} and, in turn, the smaller (or greater) the uncertainty in the model outputs were.

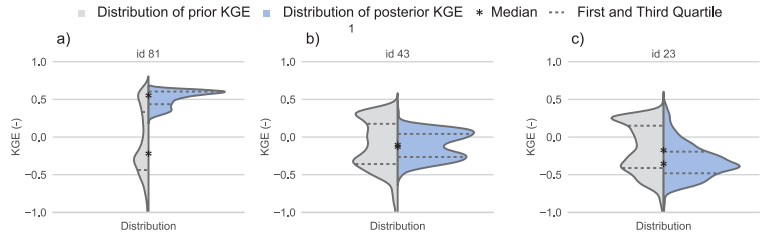

Fig. 9. Violin boxplot with the distribution of KGE for instream $\delta^{18}O$ obtained with the prior (left, gray) and posterior (right, blue) parameter sets for three representative catchments categorized into good (a), moderate (b), and poor (c) clusters. (For interpretation of the references to color in this figure legend, the reader is referred to the web version of this article.)

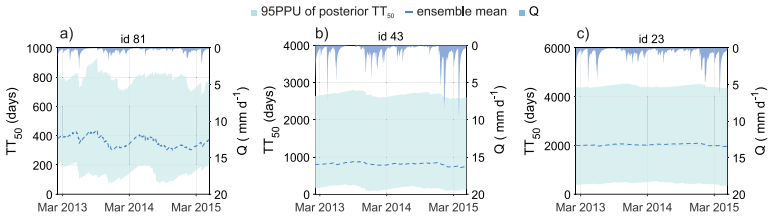

Fig. 10. 95PPU of TT_{50} in streamflow obtained with the posterior (light blue) parameter sets for three representative catchments categorized into good (a), moderate (b), and poor (c) clusters; the light blue dashed line represents the ensemble mean of all solutions, and the dark blue area is the streamflow time series. (For interpretation of the references to color in this figure legend, the reader is referred to the web version of this article.)

5. Discussions

5.1. Young water fraction and water transit time in the Bode River Basin

This study explores the calibration of a SAS-based transit time model to advance the understanding of water ages in the Bode River Basin. Previous works have also explored water ages using tracer-aided models and SAS functions (Benettin et al., 2015b; Wilusz et al., 2017; Remondi et al., 2018; Kim and Harman, 2022), focusing on modeling seasonal trends in instream isotope data over long time scales (e.g. years). Like our study, these works aimed to understand the dynamics of tracer transport and water movement across catchments from inflow to outflow, thus revealing the pore water velocity represented by water transit time. This approach is in contrast with studies on hydrograph separation, which primarily focused on the speed of pressure pulses during streamflow events (e.g. hours) to understand runoff generation from precipitation. However, unlike these studies on transit time-based modeling, our approach uniquely applies F_{yw}^{obs}, derived from fitting seasonal cycles of $\delta^{18}O$, and SAS functions, with the goal to gain meaningful insights into water age dynamics across diverse catchments.

The values of F_{yw}^{obs} estimates, SAS parameters, $\delta^{18}O$ and TT_{50} time series serve as proxies for physical processes and water age dynamics within the study areas. We found that catchments with $F_{yw}^{obs} \leq 0.05$ were characterized by SAS parameters with greater affinity for old water release (Fig. 7a–d), exhibited damped instream $\delta^{18}O$ compared to precipitation (Fig. 8c, S1 and S4), and had a longer TT_{50} up to 12.5 years (Fig. 10c and S6). This likely indicates the presence of deep and long flowpaths within the catchments, releasing water retained in the subsoil for more than a decade (Soulsby and Tetzlaff, 2008; Hrachowitz et al., 2010; Jasechko et al., 2017). The smallest F_{yw}^{obs} coupled with SAS parameters favoring old water release, were mainly observed in the mountainous catchments with high precipitation and streamflow rates. These findings align with previous studies which employed F_{yw}^{obs} to explore water ages contribution (Jasechko et al., 2016), and perform catchments intercomparison (Song et al., 2017; Lutz et al., 2018). However, this might also contradict the fast water transmission observed in some mountainous sites (Clow et al., 2018; Zhang et al., 2018), where larger F_{yw}^{obs} values would be expected. Nonetheless, smaller F_{yw}^{obs} values and SAS parameters indicating preference for old water release associated to high-elevated catchments could be attributed to the highly permeable soil of the Harz mountains. The permeability might enhance rapid vertical water infiltration (Tetzlaff et al., 2009b), triggering the activation of deep flowpaths (Jasechko et al., 2016). Through these flowpaths, there can be a significant old water supply also during a precipitation event (Botter et al., 2010), indicating a plug-flow regime, i.e. old water export activated by precipitation that just entered the system (Kirchner, 2013), or slow catchment drainage with long-term memory of past inputs (de Lavenne et al., 2022). From a water quality perspective, this can result in a lagged solute export response (Dupas et al., 2016; Van Meter et al., 2017).

On the other hand, we found that catchments with $0.10 \leq F_{yw}^{obs} \leq 0.26$ had SAS parameters revealing greater preference towards discharging young water (Fig. 7a–d), and a shorter TT_{50} (Fig. 10a and S6). This likely indicates the activation of fast flowpaths such as lateral flow via macropores (Tromp-van Meerveld and McDonnell, 2006), which can route water to the outlet more quickly (Berghuijs and Allen, 2019). This implies a short-term responsiveness of the catchment associated with a rapid transmission of solutes. The largest F_{yw}^{obs} values were observed in the lower-altitude mountainous catchments, where there can be rapid runoff via shallow flowpaths caused by wet conditions and soil saturation (Lutz et al., 2018; Sprenger et al., 2019). Additionally, larger F_{yw}^{obs} values were observed in the lowland areas where faster runoff to the stream could be triggered by artificial drainage (Musolff et al., 2015; Danesh-Yazdi et al., 2016; Lutz et al., 2018).

Exploring multiple heterogeneous catchments with different F_{yw}^{obs} values using the SAS-based transit time model revealed highly different water release behaviors. Some catchments predominantly discharged younger water to the outlet, while others released water retained in the subsurface for longer. This was elucidated by the SAS parameters which enabled us to infer varying physical processes governing catchment's connectivity, influencing water quantity and quality dynamics. In the study sites, we found varying degrees of hydrological

connectivity (Blume and van Meerveld, 2015), driven by the catchment's spatio-temporal hydro-meteorological forcing and arrangement of contributing source area (Tetzlaff et al., 2007, 2009a; Kim et al., 2016).

5.2. Challenges and recommendations for using the Young water fraction in TTD modeling

The use of F_{yw}^{obs} in the SAS-based transit time model helped reduce uncertainty in model parameters and simulations for catchments with $F_{yw}^{obs} \geq 0.10$. Most study sites demonstrated improved model performance, as indicated by higher posterior KGE values than the prior ones (Fig. S5). The posterior KGEs were constrained to positive values up to 0.67, indicative of good simulations (Sutanudjaja et al., 2018; Knoben et al., 2019; Towner et al., 2019). These results provide further evidence to support the validity of F_{yw}^{obs} as a model constraint. In addition, we used a relatively wide range for the young water threshold in streamflow τ_{yw} = [42–94 days] in the marginal TTD analysis (see Section 3.3.2), as opposed to using a single value. Nonetheless, we recognize some limitations and indicate possible reasons and recommendations for future work.

The poor cluster, characterized by small values of F_{yw}^{obs} and long values of TT_{50}, exhibited large 95PPU (Figs. S3, S4 and S6) and poor model performance (Fig. S5). However, the prior solution of the poor cluster also failed to accurately capture $\delta^{18}O$ measurements (see gray 95PPU in Fig. 8 and S4, and distribution in Fig. 9 and S5). This may be attributed to the inherent difficulty of accurately representing old water components, which are prominent in the catchments of the poor cluster. The strong attenuation in instream tracer concentration (Fig. 8) results in a uniform signal which makes it challenging to fit with sine-waves (Fig. S1), hence to quantify old water ages (Benettin et al., 2017b). The use of radioactive tracers (e.g. tritium; Michel et al. (2015), Morgenstern et al. (2015) and Visser et al. (2019)) may be more favorable to model TTDs over longer time scales (Duvert et al., 2016; Rodriguez et al., 2021).

Similar to the poor cluster, the moderate cluster showed relatively large 95PPUs (Figs. S3, S4 and S6), despite the reduced number of simulations in the posterior solution (Fig. 6). This highlights how uncertainty also likely exists due to parameter combinations influencing output variables (Beven and Freer, 2001). Nevertheless, it is important to note that in most catchments (i.e. 19 out of 23), the high values in the distribution of the KGE values (Fig. 9 and S5) are indicative of good model performance and, hence, demonstrate the robustness of the SAS-based transit time model. In other words, this means that posterior parameter sets found in this study can realistically simulate $\delta^{18}O$ measurements.

Another noteworthy limitation is that monthly grab samples during non-event flow conditions may have underestimated F_{yw}^{obs}, particularly in those mountain catchments classified into the poor cluster. This is because mountainous catchments are typically associated with high streamflow variability (Arnell, 1989), therefore there is limited opportunity to sample young water ages during rapid events (Gallart et al., 2020). The limited number of samples may contribute to the high uncertainty found in the catchments of the poor cluster. However, our analysis found comparable coefficients of variation of streamflow (CV; i.e. the ratio of the standard deviation to the mean) between the daily streamflow simulated with the mHM model for the entire study period (CV = 1.14) and the streamflow simulated with the mHM model on the dates when monthly grab-samples were collected (CV = 1.11), for the poor cluster catchments. Additionally, a t-test revealed no significant differences (p-value > 0.1) in mean values between daily streamflow for the entire study period and streamflow at the day of the monthly sampling in all catchments. These findings indicate that the sampled streamflow and thus F_{yw}^{obs} are likely representative of the variability of the whole study period. While we acknowledge that high-frequency data hold more information than low-frequency measurements, the more widespread availability of low-frequency data makes it crucial to leverage their potential. Similarly, while an automated logging scheme is more ideal for accurately capturing various hydrological flow conditions, its cost and implementation remain challenging. Until such systems are widely available, grab sampling data, such as those used in this study, remain the best option.

Additionally, parameters related to ET (k_{ET}) and initial storage (S_0) were poorly constrained (Fig. 7e–f) using F_{yw}^{obs} derived from instream tracer concentrations. Retrieving measurements of ET tracers could help improve the identifiability of k_{ET}, whilst conducting geophysical surveys in the study areas or groundwater modeling could address the poor identification of S_0. However, poor identifiability of S_0 is quite common in other SAS-based studies (Benettin et al., 2017b; Nguyen et al., 2021; Borriero et al., 2022).

Furthermore, we recognize that constraining the model with F_{yw}^{obs} may exclude some simulations that can accurately represent instream $\delta^{18}O$ measurements and yield high KGE values. To explore this, we evaluated the percentage of non-behavioral solution (i.e. that ignored by F_{yw}^{obs}) that produced a positive KGE in the good cluster catchments (Table S2). This percentage ranged from 13% to 33% (average of 23%). In contrast, the percentage of posterior solution within the good cluster that produced positive KGE values ranged from 28% to 100% (average of 87%), being significantly higher than the non-behavioral solution. This suggests that while F_{yw}^{obs} may neglect some good simulations, the posterior solution consists mostly or entirely of simulations that accurately reproduce instream $\delta^{18}O$ values, rather than including simulations that they do not.

Regardless of the aforementioned challenges, our results highlight the potential of F_{yw}^{obs} in conveying crucial information through model calibration. Despite the limited data availability in our study, the use of F_{yw}^{obs} to constrain the model produced reliable simulations at most study sites, giving confidence that we are modeling the right processes for the right reason (Kirchner, 2006). This approach is particularly beneficial at locations and periods when continuous high-frequency data are lacking.

5.3. Broader considerations on the potential use of the Young water fraction

It is widely recognized that hydrology heavily relies on measurement techniques (Beven, 2006), because underlying processes, which determine variations in water fluxes, are reflected in the measured sampled data (Knapp et al., 2019). As a consequence, it is important to determine how much sampled data is sufficient for an accurate representation of the estimates of F_{yw}^{obs} and the underlying hydrological process. This is especially crucial when considering that collecting high-frequency water samples can be expensive and that not all catchments worldwide may be well equipped to collect high-frequency measurements.

In our study, it was not possible to explore the impact of sampling frequency due to limited $\delta^{18}O$ measurements in the catchments. However, the impact of sampling frequency and tracer data series length on hydrological behavior have been extensively discussed in other studies (Hrachowitz et al., 2011; McGuire and McDonnel, 2006; Timbe et al., 2014; Stockinger et al., 2016; Stevenson et al., 2021; Benettin et al., 2022), some of which have shown that isotope sampling frequencies affect the estimated TTD and F_{yw}^{obs}. Additionally, F_{yw}^{obs} is a derived metric based on observed $\delta^{18}O$ data rather than a direct measurement, which may have uncertainties due to its derivation through sine-wave fitting (Fig. S1). Despite these drawbacks, F_{yw}^{obs} is the only metric that can be calculated when limited tracer data are available and has been reported as a robust method for estimating some water age statistics (Benettin et al., 2022). Future studies should explore the effects of $\delta^{18}O$ sampling frequencies on F_{yw}^{obs} used as a constraint for a SAS-based transit time model, and understand how potential errors and biases arising from sampling, analytical techniques, or interpretation models can affect its reliability.

Overall, F_{yw}^{obs} can represent a practical and cost-effective tool particularly useful in data-scarce regions where there is absence of intensive monitoring campaigns, ultimately leading to a lack of high-frequency tracer data. Therefore, compared with methods that rely on high-frequency measurements, F_{yw}^{obs} has the potential to be more widely applicable across broad spatial domains. Furthermore, the potential regionalization of F_{yw}^{obs} may help to derive corresponding estimates for some (ungauged) areas, hypothetically contributing to modeling experiments in regions lacking extensive data. The establishment of a database containing derived F_{yw}^{obs}, similar to isotopic seasonal cycles datasets (Allen et al., 2019), coupled with SAS-functions, can facilitate catchment inter-comparison and improve our understanding of hydrological processes.

Additionally, similar to previous studies highlighting the benefits of incorporating F_{yw}^{obs} as an additional constraint in the calibration of transit-time based models (Lutz et al., 2018; Çallı et al., 2023), our work showed, in a "proof of concept", the general benefit of using F_{yw}^{obs} as the sole constraint in SAS-based transit time models. In this way, we were able to provide a unique perspective on F_{yw}^{obs} capacity to constrain model parameters independently of previous calibration targets, and fully explore F_{yw}^{obs} potentials and limitations in modeling outcomes. As demonstrated in this study, utilizing F_{yw}^{obs} to constrain model calibration helps distinguish the most informative model outputs from prior Monte-Carlo simulations.

In terms of water quality, the use of SAS-based transit time modeling along with F_{yw}^{obs} has potential to assist water managers in solving water chemistry issues. Due to the link between hydrology and water quality (Hrachowitz et al., 2016), biogeochemical processes affecting solute transport are partially controlled by the amount of time water spends and interacts within the subsoil (Li et al., 2021). By reducing uncertainty in simulated TTDs, we can improve prediction of, for example, nitrate (Yang et al., 2018; Ehrhardt et al., 2019; Winter et al., 2020; Lutz et al., 2022; Li et al., 2024) and pesticide (Holvoet et al., 2007; Lutz et al., 2013) transport. Catchments with a larger F_{yw}^{obs} and shorter transit times generally indicate pollution-prone catchments with high water quality vulnerability, as there is less time for natural attenuation of contaminants (Ocampo et al., 2006; Rivett et al., 2008; Otero et al., 2009; Jawitz et al., 2020; Kumar et al., 2020). On the other hand, catchments with a smaller F_{yw}^{obs} and larger transit times, combined with continuous solute input, might be prone to legacy effects (Ascott et al., 2021; Basu et al., 2022; Lutz et al., 2022). Our results are promising considering that uncertainty in model parameters and simulations has been largely reduced at sites with shorter transit times. Therefore, combining an elaborated transit time model such as those based on SAS functions and F_{yw}^{obs}, derived from the relatively simple sine-wave fitting approach, can improve the understanding of water quantity and quality status, intended to support planning, design, and/or operational decisions for land management at local and regional scale.

6. Conclusions

This study serves as a "proof of concept" to assess the effectiveness of using F_{yw}^{obs}, derived from fitting seasonal isotopic cycles, in constraining SAS-based transit time models. We applied this approach to 23 diverse catchments in Central Germany, using instream $\delta^{18}O$ time series for cross-validation purpose. Our results showed that using F_{yw}^{obs} as the sole model constraint effectively reduced parameters equifinality and simulation uncertainty, as evidenced by a narrowing of the prior 95PPU of the simulated outputs (e.g. marginal TTDs, instream $\delta^{18}O$ and water ages) in most catchments. The effectiveness of F_{yw}^{obs} was further supported by an overall improvement in maximum median KGE values for instream $\delta^{18}O$ increasing from −0.04 to 0.52, after constraining the model with this metric. However, F_{yw}^{obs} did not consistently reduce the uncertainty across all sites, as $F_{yw}^{obs} \geq 0.10$ yielded a narrower 95PPU in the output variables and higher model efficiency, whilst $F_{yw}^{obs} \leq 0.05$ was less effective in constraining model output due to a lower reduction in the 95PPU and limited model efficiency.

These results highlight the advantages of using F_{yw}^{obs}, particularly with the increasing availability of seasonal isotopic time series and F_{yw}^{obs} values for catchments across the globe. The potential regionalization of these values provides an opportunity to derive them in ungauged areas, where detailed data on $\delta^{18}O$ may be lacking. While this study demonstrates the effectiveness of F_{yw}^{obs} in constraining a SAS-based transit time model, it is important to acknowledge some limitations such as the reduced capacity of $F_{yw}^{obs} \leq 0.05$ in constraining model simulations. For this reason, further research is needed to explore the broader applicability of F_{yw}^{obs}, especially in other catchments and different geophysical settings. Overall, the combination of SAS models, which describe water movement and storage, and F_{yw}^{obs}, a metric for young water age, can effectively characterize water age dynamics. This knowledge is crucial to address catchment management challenges and develop water management strategies in an era of increasing hydroclimatic risk and water quality problems.

CRediT authorship contribution statement

Arianna Borriero: Conceptualization, Data curation, Formal analysis, Investigation, Methodology, Validation, Visualization, Writing – original draft, Writing – review & editing. **Tam V. Nguyen:** Conceptualization, Methodology, Supervision, Writing – review & editing. **Stefanie R. Lutz:** Conceptualization, Methodology, Supervision, Writing – review & editing. **Jan H. Fleckenstein:** Conceptualization, Funding acquisition, Methodology, Supervision, Writing – review & editing. **Andreas Musolff:** Conceptualization, Methodology, Supervision, Writing – review & editing. **Rohini Kumar:** Conceptualization, Methodology, Supervision, Writing – review & editing.

Declaration of competing interest

The authors declare that they have no known competing financial interests or personal relationships that could have appeared to influence the work reported in this paper.

Acknowledgments

Funding for this study was provided by the Helmholtz-Centre for Environmental Research of the Helmholtz Association, Germany. Source codes of the tran-SAS v1.0 model used in this study is presented at https://doi.org/10.5194/gmd-11-1627-2018. Input data for this study, such as hydroclimatic timeseries, $\delta^{18}O$ measurements in precipitation and streamflow as well as catchments characteristics can be accessed at http://www.hydroshare.org/resource/796d45e9b43c45f1abf4dd243dd559d1. The authors thank the German Weather Service, the mHM model team for providing the necessary input data, and the developers of the tran-SAS v1.0 model for making it publicly available.

Appendix A. Supplementary data

Supplementary material related to this article can be found online at https://doi.org/10.1016/j.jhydrol.2024.132238.

Data availability

Input data for this study (e.g. hydroclimatic and tracer data, catchments characteristics) can be accessed at http://www.hydroshare.org/resource/796d45e9b43c45f1abf4dd243dd559d1.

References

Abbaspour, K.C., Johnson, C.A., van Genuchten, M.T., 2004. Estimating uncertain flow and transport parameters using a sequential uncertainty fitting procedure. Vadose Zone J. 3, 1340–1352. http://dx.doi.org/10.2136/vzj2004.1340.

Allen, S.T., Jasechko, S., Berghuijs, W.R., Welker, J.M., Goldsmith, G.R., Kirchner, J.W., 2019. Global sinusoidal seasonality in precipitation isotopes. Hydrol. Earth Syst. Sci. 23, 3423–3436. http://dx.doi.org/10.5194/hess-23-3423-2019.

Ambroise, B., 2004. Variable 'active' versus 'contributing' areas or periods: a necessary distinction. Hydrol. Process. 18, 1149–1155. http://dx.doi.org/10.1002/hyp.5536.

Arnell, N., 1989. Humid temperate sloping land. In M. Falkenmark and T. Chapman (Eds.), comparative hydrology: An ecological approach to land and water resources. Proc. Natl. Acad. Sci. USA 163–207, 163–207, doi:Paris, France: The UNESCO, Press. ISBN: 92-3-102571-6.

Asadollahi, M., Stumpp, C., Rinaldo, A., Benettin, P., 2020. Transport and water age dynamics in soils: A comparative study of spatially integrated and spatially explicit models. Water Resour. Res. 56, e2019WR025539. http://dx.doi.org/10.1029/2019WR025539.

Ascott, M.J., Gooddy, D.C., Fenton, O., Vero, S., Ward, R.S., Basu, N.B., Worrall, F., Van Meter, K., Surridge, B.W.J., 2021. The need to integrate legacy nitrogen storage dynamics and time lags into policy and practice. Sci. Total Environ. 781, 146698. http://dx.doi.org/10.1016/j.scitotenv.2021.146698.

Basu, N.B., Van Meter, K.J., Byrnes, D.K., Van Cappellen, P., Brouwer, R., Jacobsen, B.H., Jarsjö, J., Rudolph, D.L., Cunha, M.C., Nelson, N., Bhattacharya, R., Destouni, G., Olsen, S.B., 2022. Managing nitrogen legacies to accelerate water quality improvement. Sci. Total Environ. 15 (2), 97–105. http://dx.doi.org/10.1038/s41561-021-00889-9.

Benettin, P., Bailey, S.W., Campbell, J.L., Green, M.B., Rinaldo, A., Likens, G.E., J., M.K., Botter, G., 2015a. Linking water age and solute dynamics in streamflow at the hubbard brook experimental forest, NH, USA. Water Resour. Res. 51, 9256–9272. http://dx.doi.org/10.1002/2015WR017552.

Benettin, P., Bailey, W., S., Rinaldo, A., Likens, G.E., McGuire, K.J., Botter, G., 2017a. Young runoff fractions control streamwater age and solute concentration dynamics. Hydrol. Process. 31, 2982–2986. http://dx.doi.org/10.1002/hyp.11243.

Benettin, P., Bertuzzo, E., 2018. tran-SAS v1.0: a numerical model to compute catchment-scale hydrologic transport using StorAge selection functions. Geosci. Model Dev. 11, 1627–1639. http://dx.doi.org/10.5194/gmd-11-1627-2018.

Benettin, P., Kircher, J.W., Rinaldo, A., Botter, G., 2015b. Modeling chloride transport using travel time distributions at Plynlimon, Wales. Water Resour. Res. 51, 3259–3276. http://dx.doi.org/10.1002/2014WR016600.

Benettin, P., Rodriguez, N.B., Sprenger, M., Kim, M., Klaus, C.J., der Velde, Y., Hrachowitz, M., Botter, G., McGuire, K.J., Kirchner, J., Rinaldo, A., McDonnell, J.J., 2022. Transit time estimation in catchments: Recent developments and future directions. Water Resour. Res. 58, e2022WR033096. http://dx.doi.org/10.1029/2022WR033096.

Benettin, P., Soulsby, C., Birkel, C., Tetzlaff, D., Botter, G., Rinaldo, A., 2017b. Using SAS functions and high-resolution isotope data to unravel travel time distributions in headwater catchments. Water Resour. Res. 53, 1864–1878. http://dx.doi.org/10.1002/2016WR020117.

Benettin, P., van der Velde, Y., van der Zee, S.E.A.T.M., Rinaldo, A., Botter, G., 2013. Chloride circulation in a lowland catchment and the formulation of transport by travel time distributions. Water Resour. Res. 49, 4619–4632. http://dx.doi.org/10.1002/wrcr.20309.

Berghuijs, W.R., Allen, S.T., 2019. Waters flowing out of systems are younger than the waters stored in those same systems. Hydrol. Process. 33, 3251–3254. http://dx.doi.org/10.1002/hyp.13569.

Berghuijs, W.R., Kirchner, J.W., 2017. The relationship between contrasting ages of groundwater and streamflow. Geophys. Res. Lett. 44 (17), 8925–8935. http://dx.doi.org/10.1002/2017GL074962.

Berghuijs, W.R., Woods, R.A., Hrachowitz, M., 2014. A precipitation shift from snow towards rain leads to a decrease in streamflow. Nature Clim. Change 4, 583–586. http://dx.doi.org/10.1038/nclimate2246.

Beven, K., 2006. A manifesto for the equifinality thesis. J. Hydrol. 320 (1–2), 18–36. http://dx.doi.org/10.1016/j.jhydrol.2005.07.007.

Beven, K., Binley, A., 1992. The future of distributed models: Model calibration and uncertainty prediction. Hydrol. Process. 6, 279–298. http://dx.doi.org/10.1002/hyp.3360060305.

Beven, K., Freer, J., 2001. Equifinality, data assimilation, and uncertainty estimation in mechanistic modelling of complex environmental systems using the GLUE methodology. J. Hydrol. 249, 11–29. http://dx.doi.org/10.1016/S0022-1694(01)00421-8.

Blume, T., van Meerveld, H.J., 2015. From hillslope to stream: methods to investigate subsurface connectivity. WIREs Water 2, 177–198. http://dx.doi.org/10.1002/wat2.1071.

Borriero, A., Kumar, R., Nguyen, T.V., Fleckenstein, J.H., Lutz, S.R., 2022. Uncertainty in water transit time estimation with StorAge selection functions and tracer data interpolation. Hydrol. Earth Syst. Sci. Discuss. http://dx.doi.org/10.5194/hess-2022-222, [preprint]. in review.

Botter, G., Benettin, P., Soulsby, C., 2022. Using water age to explore hydrological processes in contrasting environments. Hydrol. Process. 36, e14524. http://dx.doi.org/10.1002/hyp.14524.

Botter, G., Bertuzzo, E., Rinaldo, A., 2010. Transport in the hydrologic response: Travel time distributions, soil moisture dynamics, and the old water paradox. Water Resour. Res. 46, W03514. http://dx.doi.org/10.1029/2009WR008371.

Botter, G., Bertuzzo, E., Rinaldo, A., 2011. Catchment residence and travel time distributions: The master equation. Geophys. Res. Lett. 38, L11403. http://dx.doi.org/10.1029/2011GL047666.

Bowen, G.J., Revenaugh, J., 2003. Interpolating the isotopic composition of modern meteoric precipitation. Proc. Natl. Acad. Sci. USA 39, 1299. http://dx.doi.org/10.1029/2003WR002086.

Buzacott, A.J.V., van der Velde, Y., Keitel, C., Vervoort, R.W., 2020. Constraining water age dynamics in a south-eastern Australian catchment using an age-ranked storage and stable isotope approach. Hydrol. Process. 34, 4384–4403. http://dx.doi.org/10.1002/hyp.13880.

Çallı, K.O., Bittner, D., Liu, Y., Çallı, S.S., Mielsen, V., Hartmann, A., 2023. Revealing the positive influence of young water fractions derived from stable isotopes on the robustness of karst water resources predictions. J. Hydrol. 621, 129549. http://dx.doi.org/10.1016/j.jhydrol.2023.129549.

Clow, D.W., Mast, M.A., Sickman, J.O., 2018. Linking transit times to catchment sensitivity to atmospheric deposition of acidity and nitrogen in mountains of the western United States. Hydrol. Process. 32, 2456–2470. http://dx.doi.org/10.1002/hyp.13183.

Danesh-Yazdi, M., Foufoula-Georgiou, E., Karwan, D.L., Botter, G., 2016. Inferring changes in water cycle dynamics of intensively managed landscapes via the theory of time-variant travel time distributions. Water Resour. Res. 52, 7593–7614. http://dx.doi.org/10.1002/2016WR019091.

de Lavenne, A., Andréassian, V., Crochemore, L., Lindström, G., Arheimer, B., 2022. Quantifying multi-year hydrological memory with catchment forgetting curves. Hydrol. Earth Syst. Sci. 26, 2715–2732. http://dx.doi.org/10.5194/hess-26-2715-2022.

Drever, M.C., Hrachowitz, M., 2017. Migration as flow: using hydrological concepts to estimate the residence time of migrating birds from the daily counts. Methods Ecol. Evol. 8, 1146–1157. http://dx.doi.org/10.1111/2041-210X.12727.

Dupas, R., Jomaa, S., Musolff, A., Borchardt, D., Rode, M., 2016. Disentangling the influence of hydroclimatic patterns and agricultural management on river nitrate dynamics from sub-hourly to decadal time scales. Sci. Total Environ. 571, 791–800. http://dx.doi.org/10.1016/j.scitotenv.2016.07.053.

Duvert, C., Stewart, M.K., Cendón, D.I., Raiber, M., 2016. Time series of tritium, stable isotopes and chloride reveal short-term variations in groundwater contribution to a stream. Hydrol. Earth Syst. Sci. 20, 257–277. http://dx.doi.org/10.5194/hess-20-257-2016.

Ehrhardt, S., Kumar, R., Fleckenstein, J.H., Attinger, S., Musolff, A., 2019. Trajectories of nitrate input and output in three nested catchments along a land use gradient. Hydrol. Earth Syst. Sci. 23, 3503–3524. http://dx.doi.org/10.5194/hess-23-3503-2019.

Engdahl, N.B., McCallum, J.L., Massoudieh, A., 2016. Transient age distributions in subsurface hydrologic systems. J. Hydrol. 543, 88–100. http://dx.doi.org/10.1002/2014WR016247.

Fruhauf, M., Schwab, M., 2008. 5.6.2 landschaftscharakter und oberflachengestalt. In: Bachmann, G.H., et al. (Eds.), Geologie von Sachsen-Anhalt.

Gallart, F., Valiente, M., Llorens, P., Cayuela, C., Sprenger, M., Latron, J., 2020. Investigating young water fractions in a small mediterranean mountain catchment: Both precipitation forcing and sampling frequency matter. Hydrol. Process. 34, 3618–3634. http://dx.doi.org/10.1002/hyp.13806.

Gentile, A., Canone, D., Ceperley, N., Gisolo, D., Previati, M., Zuecco, G., Schaefli, B., Ferraris, S., 2023. Towards a conceptualization of the hydrological processes behind changes of young water fraction with elevation: a focus on mountainous alpine catchments. Hydrol. Earth Syst. Sci. 27, 2301–2323. http://dx.doi.org/10.5194/hess-27-2301-2023.

Gupta, H.V., Kling, H., Yilmaz, K.K., Martinez, G.F., 2009. Decomposition of the mean squared error and NSE performance criteria: Implications for improving hydrological modelling. J. Hydrol. 377, 80–91. http://dx.doi.org/10.1016/j.jhydrol.2009.08.003.

Harman, C.J., 2015. Time-variable transit time distributions and transport: Theory and application to storage-dependent transport of chloride in a watershed. Water Resour. Res. 51, 1–30. http://dx.doi.org/10.1002/2014WR015707.

Harman, C.J., 2019. Age-ranked storage-discharge relations: A unified description of spatially lumped flow and water age in hydrologic systems. Water Resour. Res. 55, 7143–7165. http://dx.doi.org/10.1029/2017WR022304.

Heidbüchel, I., Troch, P.A., Lyon, S.W., 2013. Separating physical and meteorological controls of variable transit times in zero-order catchments. Water Resour. Res. 49, 7644–7657. http://dx.doi.org/10.1002/2012WR013149.

Heidbüchel, I., Troch, P.A., Lyon, S.W., Wiler, M., 2012. The master transit time distribution of variable flow systems. Water Resour. Res. 48, W06520. http://dx.doi.org/10.1029/2011WR011293.

Heidbüchel, I., Yang, J., Musolff, A., Troch, P., Ferré, T., Fleckenstein, J.H., 2020. On the shape of forward transit time distributions in low-order catchments. Hydrol. Earth Syst. Sci. 24, 2895–2920. http://dx.doi.org/10.5194/hess-24-2895-2020.

Holvoet, K.M., Seuntjens, P., Vanrolleghem, P.A., 2007. Monitoring and modeling pesticide fate in surface waters at the catchment scale. Ecol. Model. 209, 53–64. http://dx.doi.org/10.1016/j.ecolmodel.2007.07.030.

Hrachowitz, M., Benettin, P., van Breukelen, B.M., Fovet, O., Howden, N.J.K., Ruiz, L., van der Velde, Y., Wade, A.J., 2016. Transit times — the link between hydrology and water quality at the catchment scale. WIREs Water 3, 629–657. http://dx.doi.org/10.1002/wat2.1155.

Hrachowitz, M., Soulsby, C., Tetzlaff, D., Malcolm, I.A., 2011. Sensitivity of mean transit time estimates to model conditioning and data availability. Hydrol. Process. 25, 980–990. http://dx.doi.org/10.1002/hyp.7922.

Hrachowitz, M., Soulsby, C., Tetzlaff, D., Malcolm, I.A., Schoups, G., 2010. Gamma distribution models for transit time estimation in catchments: Physical interpretation of parameters and implications for time-variant transit time assessment. Water Resour. Res. 46, W10536. http://dx.doi.org/10.1029/2010WR009148.

Jasechko, S., 2019. Global isotope hydrogeology—review. Rev. Geophys. 57, 835–965. http://dx.doi.org/10.1029/2018RG000627.

Jasechko, S., Kirchner, J.W., Welker, J.M., McDonnell, J.J., 2016. Substantial proportion of global streamflow less than three months old. Nat. Geosci. 9, 126–129. http://dx.doi.org/10.1038/ngeo2636.

Jasechko, S., Wassenaar, L.I., Mayer, B., 2017. Isotopic evidence for widespread cold-season-biased groundwater recharge and young streamflow across central Canada. Hydrol. Process. 31, 2196–2209. http://dx.doi.org/10.1002/hyp.11175.

Jawitz, J., Desormeaux, A.M., Annable, M.D., Borchardt, D., Dobberfuhl, D., 2020. Disaggregating landscape-scale nitrogen attenuation along hydrological flow paths. JGR Biosci. 15, e2019JG005229. http://dx.doi.org/10.1029/2019JG005229.

Kaandorp, V.P., de Louw, P.G.B., van der Velde, Y., Broers, H.P., 2018. Transient groundwater transit time distributions and age-ranked storage–discharge relationships of three lowland catchments. Water Resour. Res. 54, 4519–4536. http://dx.doi.org/10.1029/2017WR022461.

Kim, M., Harman, C.J., 2022. Transit times and StorAge selection functions in idealized hillslopes with steady infiltration. Water Resour. Res. 58, e2019WR025917. http://dx.doi.org/10.1029/2019WR025917.

Kim, M., Pangle, L.A., Cardoso, C., Lora, M., Volkmann, T.H.M., Wang, Y., Harman, C.J., Troch, P.A., 2016. Transit time distributions and StorAge selection functions in a sloping soil lysimeter with time-varying flow paths: Direct observation of internal and external transport variability. Water Resour. Res. 52, 7105–7129. http://dx.doi.org/10.1002/2016WR018620.

Kirchner, J.W., 2006. Getting the right answers for the right reasons: Linking measurements, analyses, and models to advance the science of hydrology. Water Resour. Res. 42, W03S04. http://dx.doi.org/10.1029/2005WR004362.

Kirchner, J.W., 2013. A double paradox in catchment hydrology and geochemistry. Hydrol. Process. 17, 871–874. http://dx.doi.org/10.1002/hyp.5108.

Kirchner, J.W., 2016a. Aggregation in environmental systems – part 1: Seasonal tracer cycles quantify young water fractions, but not mean transit times, in spatially heterogeneous catchments. Hydrol. Earth Syst. Sci. 20, 279–297. http://dx.doi.org/10.5194/hess-20-279-2016.

Kirchner, J.W., 2016b. Aggregation in environmental systems – part 2: Catchment mean transit times and young water fractions under hydrologic nonstationarity. Hydrol. Earth Syst. Sci. 20, 299–328. http://dx.doi.org/10.5194/hess-20-299-2016.

Kirchner, J.W., Feng, X., Neal, C., 2000. Fractal stream chemistry and its implications for contaminant transport in catchments. Nature 403, 524–527. http://dx.doi.org/10.1038/35000537.

Knapp, J.L.A., Neal, C., Schlumpf, A., Neal, M., Kirchner, J.W., 2019. New water fractions and transit time distributions at plynlimon, Wales, estimated from stable water isotopes in precipitation and streamflow. Hydrol. Earth Syst. Sci. 23, 4367–4388. http://dx.doi.org/10.5194/hess-23-4367-2019.

Knoben, W.J.M., Freer, J.E., Woods, R.A., 2019. Technical note: Inherent benchmark or not? Comparing Nash–Sutcliffe and Kling–Gupta efficiency scores. Hydrol. Earth Syst. Sci. 23, 4323–4331. http://dx.doi.org/10.5194/hess-23-4323-2019.

Kumar, R., Heße, F., Rao, P.S.C., Musolff, A., Jawitz, J.W., Sarrazin, F., Samaniego, L., Fleckenstein, J.H., Rakovec, O., Thober, S., Attinger, S., 2020. Strong hydroclimatic controls on vulnerability to subsurface nitrate contamination across Europe. Nature Commun. 11, 6302. http://dx.doi.org/10.1038/s41467-020-19955-8.

Kumar, R., Samaniego, L., Attinger, S., 2013. Implications of distributed hydrologic model parameterization on water fluxes at multiple scales and locations. Water Resour. Res. 49, 360–379. http://dx.doi.org/10.1029/2012WR012195.

Lapides, D.A., Hahm, W.J., Rempe, D.M., Dietrich, W.E., Dralle, D.N., 2022. Controls on stream water age in a saturation overland flow-dominated catchment. Water Resour. Res. 58, e2021WR031665. http://dx.doi.org/10.1029/2021WR031665.

Li, W., Nguyen, T.V., Cheng, X., Zhu, D., Kumar, R., 2024. Toward representing the subsurface nitrate legacy through a coupled StorAge selection function and hydrological model (SWAT-SAS). J. Hydrol. 637, http://dx.doi.org/10.1016/j.jhydrol.2024.131386.

Li, P., Subramani, K.T., Srinivasamoorthy, K., 2021. Sources and consequences of groundwater contamination. Arch. Environ. Contam. Toxicol. 80, 1–10. http://dx.doi.org/10.1007/s00244-020-00805-z.

Lutz, S.R., Ebeling, P., Musolff, A., Nguyen, T.V., Sarrazin, F.J., Van Meter, K.J., Basu, N.B., Fleckenstein, J.H., Attinger, S., Kumar, R., 2022. Pulling the rabbit out of the hat: Unravelling hidden nitrogen legacies in catchment-scale water quality models. Hydrol. Process. 36, e14682. http://dx.doi.org/10.1002/hyp.14682.

Lutz, S.R., Krieg, R., Müller, C., Zink, M., Knöller, K., Samaniego, L., Merz, R., 2018. Spatial patterns of water age: using young water fractions to improve the characterization of transit times in contrasting catchments. Water Resour. Res. 54, 4767–4784. http://dx.doi.org/10.1029/2017WR022216.

Lutz, S.R., van der Velde, Y., Elsayed, O.F., Imfeld, G., Lefrancq, M., Payraudeau, S., van Breukelen, B.M., 2017. Pesticide fate on catchment scale: conceptual modelling of stream CSIA data. Hydrol. Earth Syst. Sci. 21, 5243–5261. http://dx.doi.org/10.5194/hess-21-5243-2017.

Lutz, S.R., van Meerveld, H.J., Waterloo, M.J., Broers, H.P., van Breukelen, B.M., 2013. A model-based assessment of the potential use of compound-specific stable isotope analysis in river monitoring of diffuse pesticide pollution. Hydrol. Earth Syst. Sci. 17, 4505–4524. http://dx.doi.org/10.5194/hess-17-4505-2013.

McGuire, K.J., McDonnel, J.J., 2006. A review and evaluation of catchment transit time modeling. J. Hydrol. 330, 543–563. http://dx.doi.org/10.1016/j.jhydrol.2006.04.020.

McGuire, K.J., McDonnell, J.J., Weiler, M., Kendall, C., McGlynn, B.L., Welker, J.M., Seibert, J., 2005. The role of topography on catchment-scale water residence time. Water Resour. Res. 41, W05002. http://dx.doi.org/10.1029/2004WR003657.

McKay, M.D., Beckman, R.J., Conover, W.J., 1979. A comparison of three methods for selecting values of input variables in the analysis of output from a computer code. Technometrics 21, 239–245. http://dx.doi.org/10.2307/1268522.

Michel, R.L., Aggarwal, P., Araguas-Araguas, L., Kurttas, K., Newman, B.D., Vitvar, T., 2015. A simplified approach to analysing historical and recent tritium data in surface waters. Hydrol. Process. 29, 572–578. http://dx.doi.org/10.1002/hyp.10174.

Morgenstern, U., Daughney, C.J., Leonard, G., Gordon, D., Donath, F.M., Reeves, R., 2015. Using groundwater age and hydrochemistry to understand sources and dynamics of nutrient contamination through the catchment into lake Rotorua, New Zealand. Hydrol. Earth Syst. Sci. 19, 803–822. http://dx.doi.org/10.5194/hess-19-803-2015.

Mueller, C., Zink, M., Samaniego, L., Krieg, E., Merz, R., Rode, M.., Knöller, K., 2016. Discharge driven nitrogen dynamics in a mesoscale river basin as constrained by stable isotope patterns. Environ. Sci. Technol. 50, 17, 9187–9196. http://dx.doi.org/10.1021/acs.est.6b01057.

Musolff, A., Schmidt, C., Selle, B., Fleckenstein, J.H., 2015. Catchment controls on solute export. Adv. Water Resour. 86, 133–146. http://dx.doi.org/10.1016/j.advwatres.2015.09.026.

Nguyen, T.V., Kumar, R., Lutz, S.R., Musolff, A.J., Fleckenstein, J.H., 2021. Modeling nitrate export from a mesoscale catchment using StorAge selection functions. Water Resour. Res. 57, e2020WR028490. http://dx.doi.org/10.1029/2020WR028490.

Nguyen, T.V., Kumar, R., Musolff, A., Lutz, S.R., Sarrazin, F., Attinger, S., Fleckenstein, J.H., 2022. Disparate seasonal nitrate export from nested heterogeneous subcatchments revealed with StorAge selection functions. Water Resour. Res. 58, e2021WR030797. http://dx.doi.org/10.1029/2021WR030797.

Ocampo, C.J., Oldham, C.E., Sivapalan, M., 2006. Nitrate attenuation in agricultural catchments: Shifting balances between transport and reaction. Water Resour. Res. 42, W01408. http://dx.doi.org/10.1029/2004WR003773.

Otero, N., Torrentó, C., Solerb, A., Menció, A., Mas-Pla, J., 2009. Monitoring groundwater nitrate attenuation in a regional system coupling hydrogeology with multi-isotopic methods: The case of Plana de Vic (Osona, Spain). Agric. Ecosyst. Environ. 133, 103–113. http://dx.doi.org/10.1016/j.agee.2009.05.007.

Queloz, P., Carraro, L., Benettin, P., Botter, G., Rinaldo, A., Bertuzzo, E., 2015. Transport of fluorobenzoate tracers in a vegetated hydrologic control volume: 2. Theoretical inferences and modeling. Water Resour. Res. 51, 2793–2806. http://dx.doi.org/10.1002/2014WR016508.

Remondi, F., Kirchner, J.W., Burlando, P., Fatichi, S., 2018. Water flux tracking with a distributed hydrological model to quantify controls on the spatio-temporal variability of transit time distributions. Water Resour. Res. 54, 3081–3099. http://dx.doi.org/10.1002/2017WR021689.

Rinaldo, A., Benettin, P., Harman, C.J., Hrachowitz, M., McGuire, K.J., van der Velde, Y., et al., 2015. Storage selection functions: A coherent framework for quantifying how catchments store and release water and solutes. Water Resour. Res. 51, 4840–4847. http://dx.doi.org/10.1002/2015WR017273.

Rinaldo, A., Marani, M., 1987. Basin scale model of solute transport. Water Resour. Res. 23, 2107–2118. http://dx.doi.org/10.1029/WR023i011p02107.

Rivett, M.O., Buss, S.R., Morgan, P., Smith, J.W.N., Bemment, C.D., 2008. Nitrate attenuation in groundwater: A review of biogeochemical controlling processes. Water Res. 42, 4215–4232. http://dx.doi.org/10.1016/j.watres.2008.07.020.

Rodriguez, N.B., Klaus, J., 2019. Catchment travel times from composite StorAge selection functions representing the superposition of streamflow generation processes. Water Resour. Res. 11, 9292–9314. http://dx.doi.org/10.1029/2019WR024973.

Rodriguez, N.B., Pfister, L., Zehe, E., Klaus, J., 2021. A comparison of catchment travel times and storage deduced from deuterium and tritium tracers using StorAge selection functions. Hydrol. Earth Syst. Sci. 25, 401–428. http://dx.doi.org/10.5194/hess-25-401-2021.

Samaniego, L., Kumar, R., Attinger, S., 2010. Multiscale parameter regionalization of a grid-based hydrologic model at the mesoscale. Water Resour. Res. 46, W05523. http://dx.doi.org/10.1029/2008WR007327.

Schuberth, K., 2008. 2 geomorphologischer überblick. In: Bachmann, G.H., et al. (Eds.), Geologie von Sachsen-Anhalt. p. 689.

Seager, R., Ting, M., Held, I., Kushnir, Y., Lu, J., Vecchi, G., Huang, H.P., Harnik, N., Leetmaa, A., Lau, N.C., Li, C., Velez, J., Naik, N., 2007. Model projections of an imminent transition to a more arid climate in southwestern North America. Science 316, 1181–1184. http://dx.doi.org/10.1126/science.1139601.

Smith, A., Tetzlaff, D., Soulsby, C., 2018. On the use of StorAge selection functions to assess time-variant travel times in lakes. Water Resour. Res. 54, 5163–5185. http://dx.doi.org/10.1029/2017WR021242.

Song, C., Wang, G., Liu, G., Mao, T., Sun, X., Chen, X., 2017. Stable isotope variations of precipitation and streamflow reveal the young water fraction of a permafrost watershed. Hydrol. Process. 31, 935–947. http://dx.doi.org/10.1002/hyp.11077.

Soulsby, C., Tetzlaff, D., 2008. Towards simple approaches for mean residence time estimation in ungauged basins using tracers and soil distributions. J. Hydrol. 363, 60–74. http://dx.doi.org/10.1016/j.jhydrol.2008.10.001.

Sprenger, M., Llorens, P., Gallart, F., Benettin, P., Allen, S.T., Latron, J., 2022. Precipitation fate and transport in a Mediterranean catchment through models calibrated on plant and stream water isotope data. Hydrol. Earth Syst. Sci. 26, 4093–4410. http://dx.doi.org/10.5194/hess-26-4093-2022.

Sprenger, M., Stumpp, C., Weiler, M., Aeschbach, W., Allen, S.T., Benettin, P., Dubbert, M., Hartmann, A., Hrachowitz, M., Kirchner, J.W., McDonnell, J.J., Orlowski, N., Penna, D., Pfahl, S., Rinderer, M., Rodriguez, N., Schmidt, M., Werner, C., 2019. The demographics of water: a review of water ages in the critical zone. Rev. Geophys. 57, 800–834. http://dx.doi.org/10.1029/2018RG000633.

Stevenson, J.L., Birkel, C., Neill, A.J., Tetzlaff, D., Soulsby, C., 2021. Effects of stream-flow isotope sampling strategies on the calibration of a tracer-aided rainfall-runoff model. Hydrol. Process. 35, e14223. http://dx.doi.org/10.1002/hyp.14223.

Stockinger, M.P., Bogena, H.R., Lücke, A., Diekkrüger, B., Cornelissen, T., Vereecken, H., 2016. Tracer sampling frequency influences estimates of young water fraction and streamwater transit time distribution. J. Hydrol. 541, 952–964. http://dx.doi.org/10.1016/j.jhydrol.2016.08.007.

Sutanudjaja, E.H., Van Beek, R., Wanders, N., Wada, Y., Bosmans, J.H.C., et al., 2018. PCR-GLOBWB 2: a 5 arcmin global hydrological and water resources model. Geosci. Model Dev. 11, 2429–2453. http://dx.doi.org/10.5194/gmd-11-2429-2018.

Tetzlaff, D., Malcolm, I.A., Soulsby, C., 2007. Influence of forestry, environmental change and climatic variability on the hydrology. J. Hydrol. 346, 93–111. http://dx.doi.org/10.1016/j.jhydrol.2007.08.016.

Tetzlaff, D., Piovano, T., A., P., Smith, A., K., C.S., Marsh, P., Wookey, P.A., Street, L.E., Soulsby, C., 2018. Using stable isotopes to estimate travel times in a data-sparse arctic catchment: Challenges and possible solutions. Hydrol. Process. 32, 1936–1952. http://dx.doi.org/10.1002/hyp.13146.

Tetzlaff, D., Seibert, J., McGuire, K.J., Laudon, H., Burn, D.A., Dunn, S.M., Soulsby, C., 2009a. How does landscape structure influence catchment transit time across different geomorphic provinces? Hydrol. Process. 23, 945–953. http://dx.doi.org/10.1002/hyp.7240.

Tetzlaff, D., Seibert, J., Soulsby, C., 2009b. Inter-catchment comparison to assess the influence of topography and soils on catchment transit times in a geomorphic province; the Cairngorm mountains, Scotland. Hydrol. Process. 23, 1874–1886. http://dx.doi.org/10.1002/hyp.7318.

Thaw, M., Visser, A., Bibby, R., Deinhart, A., Oerter, E., Conklin, M., 2021. Vegetation water sources in california's sierra nevada (USA) are young and change over time, a multi-isotope ($\delta^{18}O$, $\delta^{2}H$,^{3}H) tracer approach. Hydrol. Process. 35, e14249. http://dx.doi.org/10.1002/hyp.14249.

Timbe, E., Windhorst, D., Crespo, P., Frede, H.G., Feyen, J., L., B., 2014. Understanding uncertainties when inferring mean transit times of water trough tracer-based lumped-parameter models in Andean tropical montane cloud forest catchments. Hydrol. Earth Syst. Sci. 18, 1503–1523. http://dx.doi.org/10.5194/hess-18-1503-2014.

Towner, J., Cloke, H.L., Zsoter, E., Flamig, Z., Hoch, J.M., Bazo, J., Coughlan de Perez, E., Stephens, E.M., 2019. Assessing the performance of global hydrological models for capturing peak river flows in the Amazon basin. Hydrol. Earth Syst. Sci. 23, 3057–3080. http://dx.doi.org/10.5194/hess-23-3057-2019.

Tromp-van Meerveld, H.J., McDonnell, J.J., 2006. Threshold relations in subsurface stormflow: 1. A storm analysis of the Panola hillslope. Water Resour. Res. 42, W02410. http://dx.doi.org/10.1029/2004WR0037780.

van der Velde, Y., Torfs, P.J.J.F., van der Zee, S.E.A.T.M., Uijlenhoet, R., 2012. Quantifying catchment-scale mixing and its effect on time-varying travel time distributions. Water Resour. Res. 48, W06536. http://dx.doi.org/10.1029/2011WR011310.

Van Meter, K.J., Basu, N.B., Van Cappellen, P., 2017. Two centuries of nitrogen dynamics: legacy sources and sinks in the Mississippi and Susquehanna river basins. Glob. Biogeochem. Cycles 31, 2–23. http://dx.doi.org/10.1002/2016GB005498.

Visser, A., Thaw, M., Deinhart, A., Bibby, R., Safeeq, M., Conklin, M., Esser, B., van der Velde, Y., 2019. Cosmogenic isotopes unravel the hydrochronology and water storage dynamics of the southern sierra critical zone. Water Resour. Res. 55, 1429–1450. http://dx.doi.org/10.1029/2018WR023665.

von Freyberg, J., Allen, S.T., Seeger, S., Weiler, M., Kirchner, J.W., 2018. Sensitivity of young water fractions to hydro-climatic forcing and landscape properties across 22 Swiss catchments. Hydrol. Earth Syst. Sci. 22, 3841–3861. http://dx.doi.org/10.5194/hess-22-3841-2018.

von Freyberg, J., Rücker, A., Zappa, M., Schlumpf, A., Studer, B., Kirchner, J.W., 2022. Four years of daily stable water isotope data in stream water and precipitation from three swiss catchments. Sci. Data 9, 46. http://dx.doi.org/10.1038/s41597-022-01148-1.

Wilusz, D.C., Harman, C.J., Ball, W.P., 2017. Sensitivity of catchment transit times to rainfall variability under present and future climates. Hydrol. Process. 53, 10231–10256. http://dx.doi.org/10.1002/2017WR020894.

Wilusz, D.C., Harman, C.J., Ball, W.P., Maxwell, R.M., Buda, A.R., 2020. Using PARTICLE tracking to understand flow paths, age distributions, and the paradoxical origins of the inverse storage effect in an experimental catchment. Water Resour. Res. 54, e2019WR025140. http://dx.doi.org/10.1029/2019WR025140.

Winter, C., Lutz, S.R., Musolff, A., Kumar, R., Weber, M., Fleckenstein, J.H., 2020. Disentangling the impact of catchment heterogeneity on nitrate export dynamics from event to long-term time scales. Water Resour. Res. 57, e2020WR027992. http://dx.doi.org/10.1029/2020WR027992.

Wollschläger, U., Attinger, S., Borchardt, D., Brauns, M., Cuntz, M., Dietrich, P., Fleckenstein, J.H., Friese, K., Friesen, J., Harpke, A., Hildebrandt, A., Jäckel, G., Kamjunke, N., Knöller, K., Kögler, S., Kolditz, O., Krieg, R., Kumar, R., Lausch, A., Liess, M., Marx, R., Mueller, C., Musolff, A., Norf, H., Oswald, S.E., Rebmann, C., Reinstorf, F., Rode, M., Rink, K., Rinke, K., Samaniego, L., Vieweg, M., Vogel, H.J., Weitere, M., Werban, U., M., Z., Zacharias, S., 2017. The bode hydrological observatory: a platform for integrated, interdisciplinary hydro-ecological research within the TERENO harz/central german lowland observatory. Environ. Earth Sci. 76, 29. http://dx.doi.org/10.1007/s12665-016-6327-5.

Yang, X., Jomaa, S., Zink, M., Fleckenstein, J.H., Borchardt, D., Rode, M., 2018. A new fully distributed model of nitrate transport and removal at catchment scale. Water Resour. Res. 54, 5856–5877. http://dx.doi.org/10.1029/2017WR022380.

Zhang, Z., Che, X., Cheng, Q., Soulsby, C., 2020. Using StorAge selection (SAS) functions to understand flow paths and age distributions in contrasting karst groundwater systems. Hydrol. Process. 34, 3156–3174. http://dx.doi.org/10.1002/hyp.13829.

Zhang, Q., Knowles, J.F., Barnes, R.T., Cowie, R.M., Rock, N., Williams, M.W., 2018. Surface and subsurface water contributions to streamflow from a mesoscale watershed in complex mountain terrain. Hydrol. Process. 31, 954–967. http://dx.doi.org/10.1002/hyp.11469.

Zink, M., Kumar, R., Cuntz, M., Samaniego, L., 2017. A high-resolution dataset of water fluxes and states for Germany accounting for parametric uncertainty. Hydrol. Earth Syst. Sci. 21, 1769–1790. http://dx.doi.org/10.5194/hess-21-1769-2017.

Table 1: Identification number of the sub-catchments, values of the young water fractions and standard errors from the sine-wave approach, as well as the cluster to which the sub-catchments belong.

catchment	$F_{yw}^{obs} \pm SE$	cluster	
id 2	0.09 ± 0.04	moderate	
id 6	0.08 ± 0.06	moderate	
id 9	0.04 ± 0.06	poor	
id 14	0.05 ± 0.06	poor	
id 20	0.21 ± 0.09	good	
id 23	0.02 ± 0.06	poor	
id 26	0.04 ± 0.06	poor	
id 43	0.08 ± 0.07	moderate	
id 50	0.16 ± 0.06	good	c c c
id 59	0.13 ± 0.06	good	
id 68	0.15 ± 0.06	good	
id 75	0.09 ± 0.05	good	
id 79	0.26 ± 0.10	good	
id 81	0.20 ± 0.06	good	
id 89	0.05 ± 0.04	moderate	
id 90	0.15 ± 0.07	good	
id 94	0.06 ± 0.05	moderate	
id 98	0.16 ± 0.08	good	
id 103	0.10 ± 0.06	good	
id 111	0.20 ± 0.09	good	
id 118	0.10 ± 0.05	good	
id 128	0.12 ± 0.05	good	
id 131	0.12 ± 0.05	good	

Table 2: Identification number of the sub-catchments and number of posterior solutions after constraining the SAS-based transit time model against values of the young water fractions.

catchment	posterior solution
id 2	842
id 6	1390
id 9	4989
id 14	5128
id 20	1915
id 23	5154
id 26	5362
id 43	1817
id 50	1541
id 59	1523
id 68	1561
id 75	1185
id 79	2405
id 81	1832
id 89	1304
id 90	2058
id 94	1327
id 98	2093
id 103	1574
id 111	2420
id 118	1438
id 128	1499
id 131	1490

3

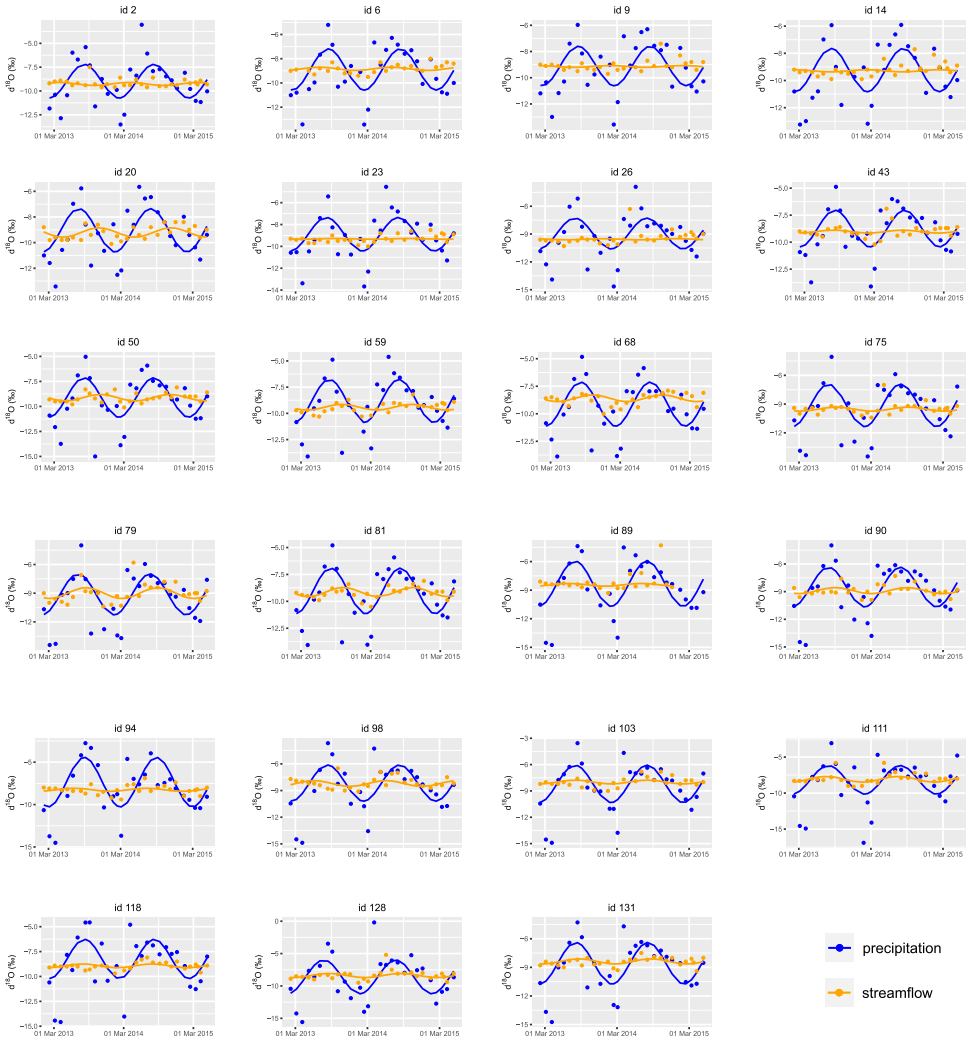

Figure 1: Sine-wave fitting of δ^{18}O data in precipitation and streamflow. Values of δ^{18}O were fitted to sine-waves using the iteratively reweighted least squares regression.

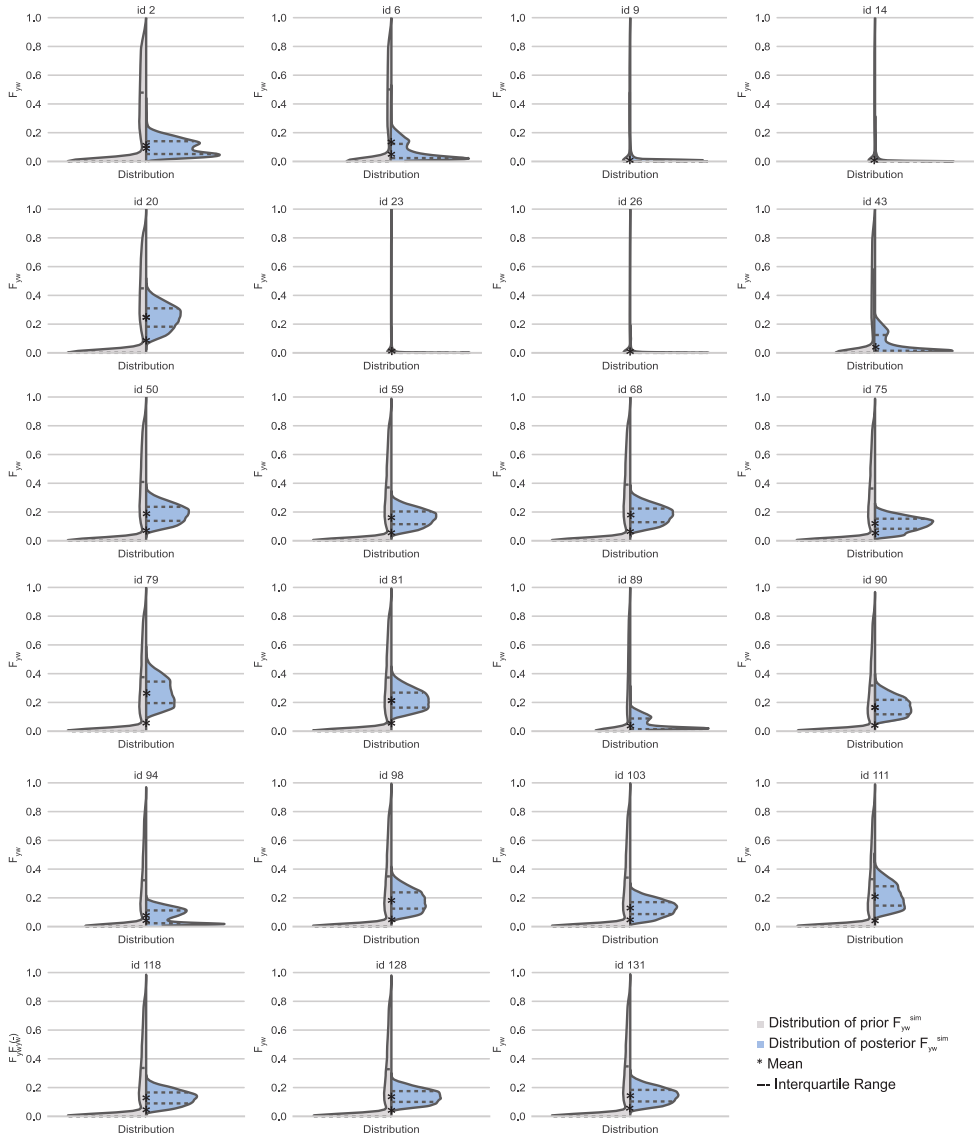

Figure 2: Violin boxplot with the distribution of F_{yw} simulated from the marginal TTD computed via SAS functions (i.e. $F_{yw}{}^{sim}$) obtained before (i.e. prior; grey) and after (i.e. posterior; blue) applying $F_{yw}{}^{obs}$±SE from the sine-wave approach as a model constraint.

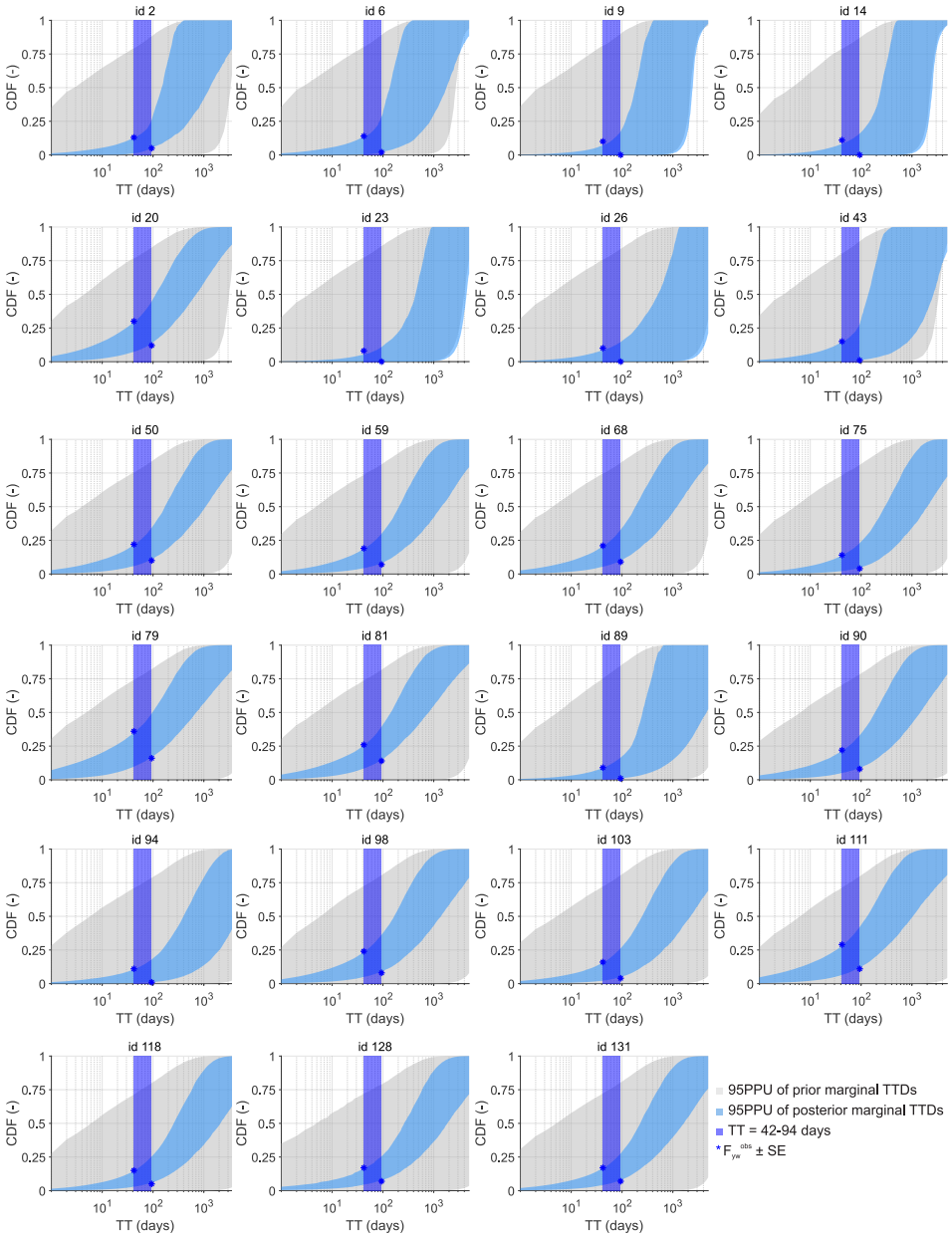

Figure 3: 95PPU of the marginal TTDs obtained with the prior (gray) and posterior (blue) parameter sets; the thick blue vertical area represents the range of T=[42-94 day], with two blue asterisks indicating the upper and lower limits defined by F_{yw}^{obs}±SE. The x-axis is shown in a logarithmic scale.

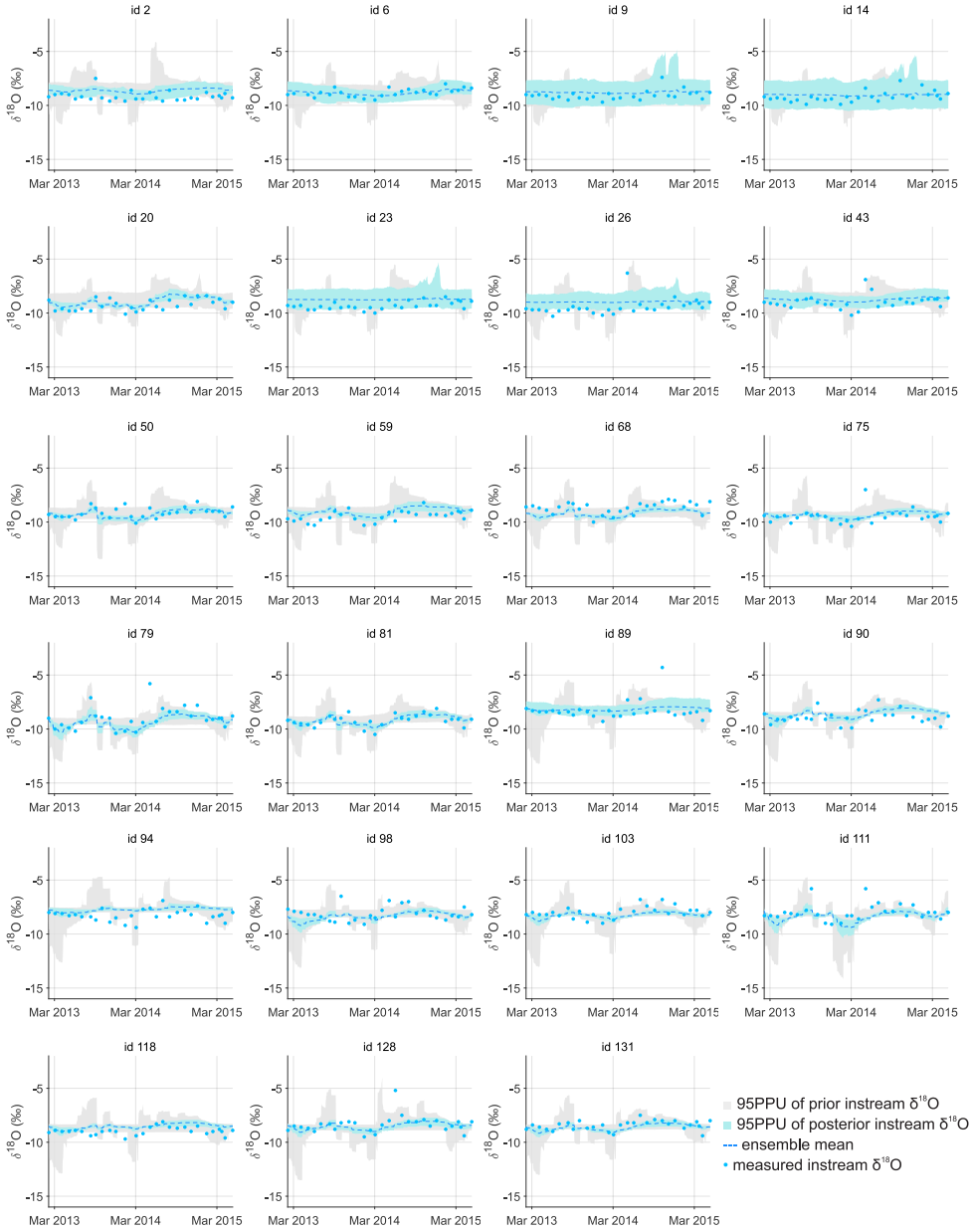

Figure 4: 95PPU of instream δ^{18}O obtained with the prior (grey) and posterior (blue) parameter sets, dark blue filled circles represent the observed data and the light blue dashed line represents the ensemble mean of all possible solution.

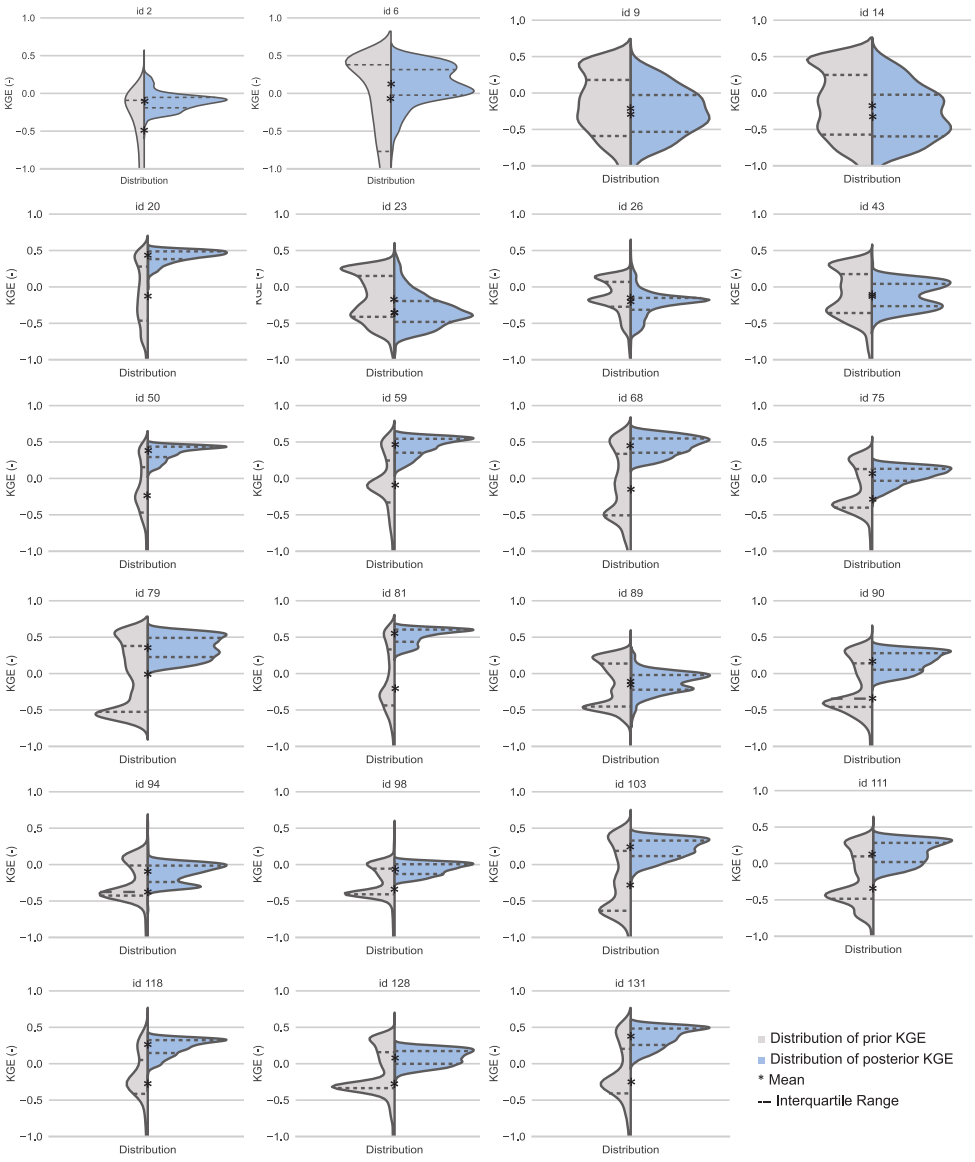

Figure 5: Violin boxplot with the distribution of KGE obtained before (i.e. prior; grey) and after (i.e. posterior; blue) applying $F_{yw}{}^{obs}$±SE from the sine-wave approach as a model constrained.

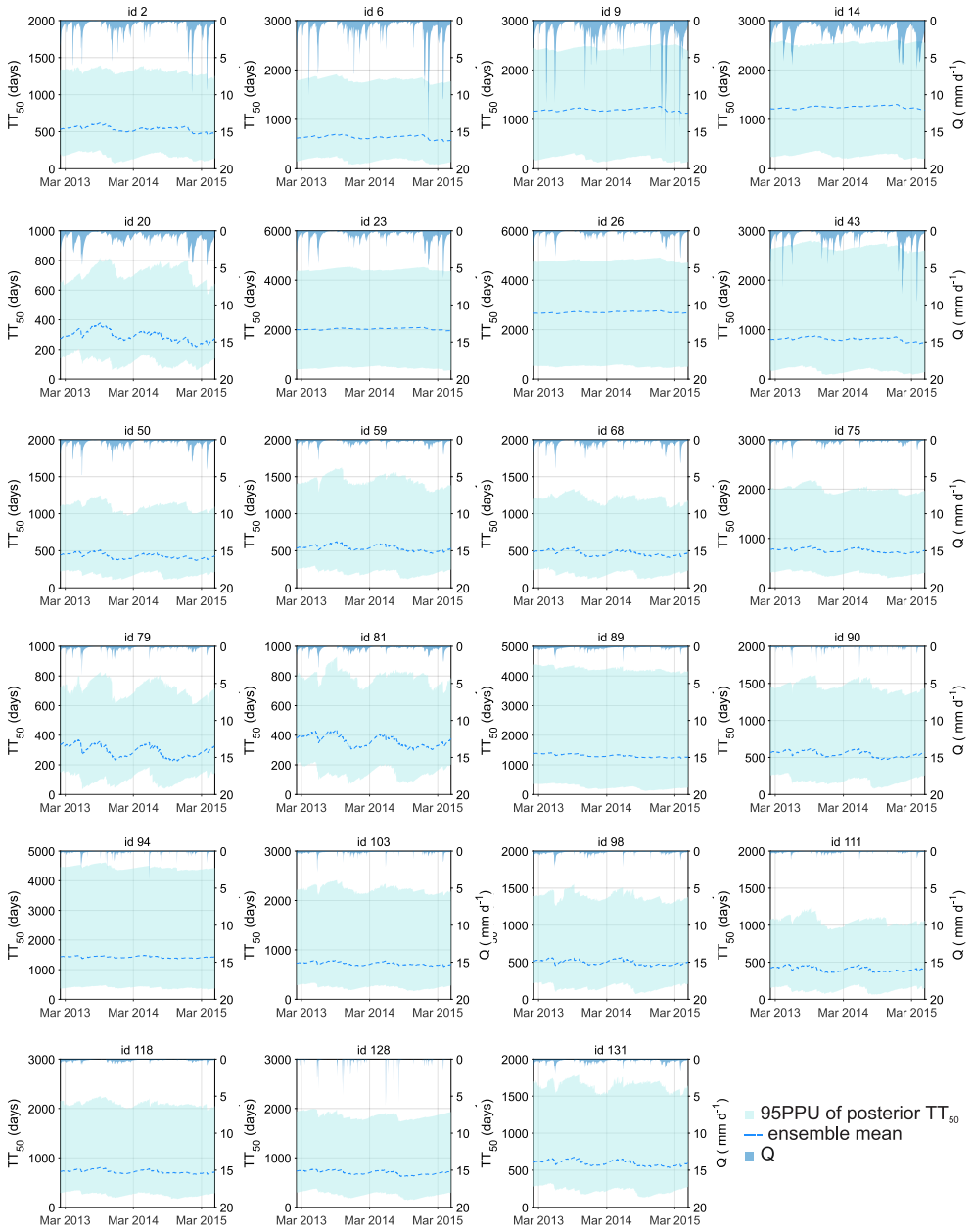

Figure 6: 95PPU of TT_{50} in streamflow obtained with the posterior (blue) parameter sets; light blue dashed line represents the ensemble mean of all possible solution, and dark blue area is the streamflow time series.

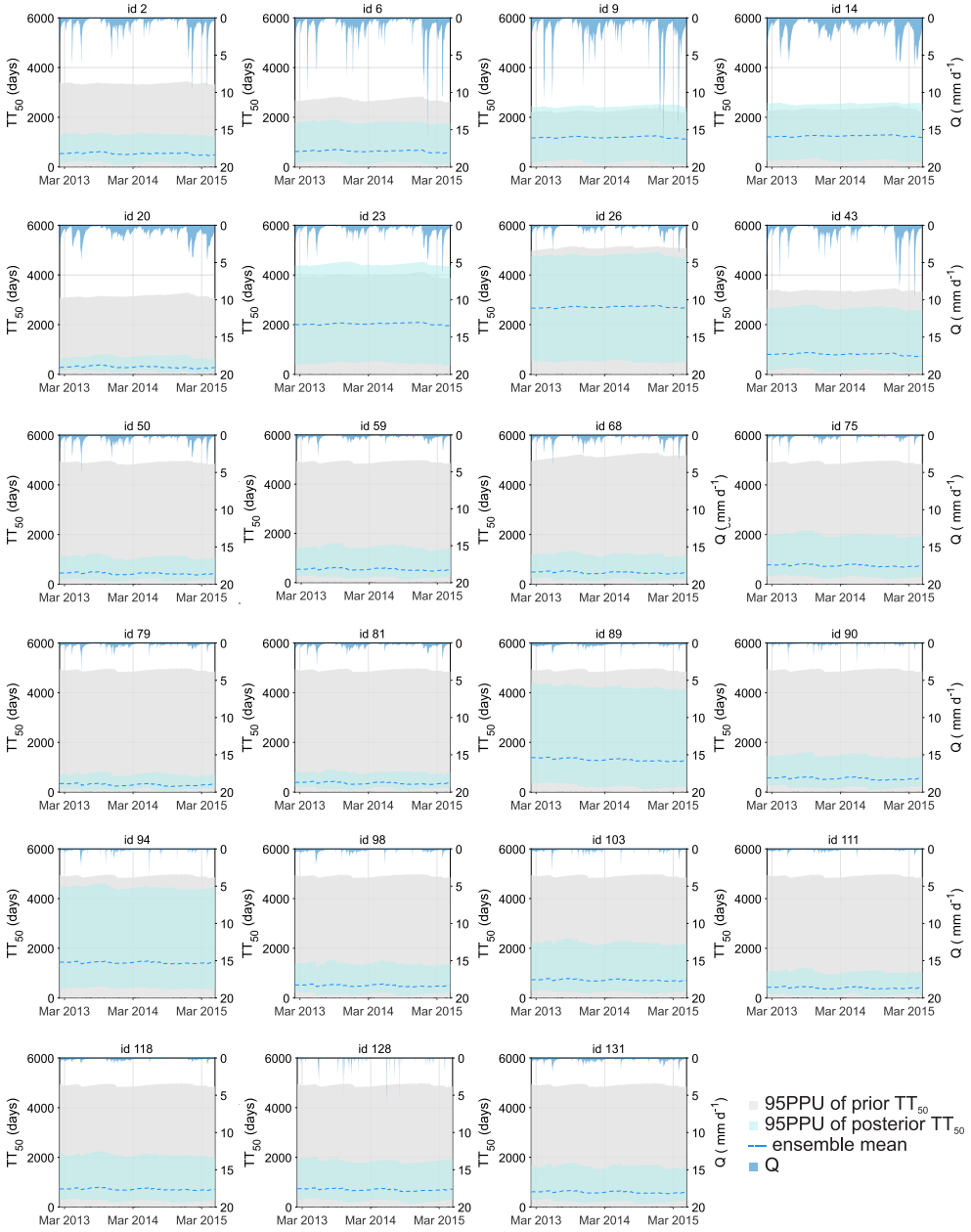

Figure 7: 95PPU of TT_{50} in streamflow obtained with the prior (grey) and posterior (blue) parameter sets; light blue dashed line represents the ensemble mean of all possible solution, and dark blue area is the streamflow time series.

Received: 6 November 2023 | Revised: 21 March 2024 | Accepted: 8 April 2024

DOI: 10.1002/hyp.15154

RESEARCH ARTICLE

WILEY

The value of instream stable water isotope and nitrate concentration data for calibrating a travel time-based water quality model

A. Borriero[1] | A. Musolff[1] | R. Kumar[2] | J. H. Fleckenstein[1,3] | S. R. Lutz[4] | T. V. Nguyen[1]

[1]Department of Hydrogeology, Helmholtz-Centre for Environmental Research—UFZ, Leipzig, Germany

[2]Department of Computational Hydrosystems, Helmholtz-Centre for Environmental Research—UFZ, Leipzig, Germany

[3]Bayreuth Centre of Ecology and Environmental Research, University of Bayreuth, Bayreuth, Germany

[4]Copernicus Institute of Sustainable Development, Department of Environmental Sciences, Utrecht University, Utrecht, The Netherlands

Correspondence
A. Borriero and T. V. Nguyen, Department of Hydrogeology, Helmholtz-Centre for Environmental Research—UFZ, Leipzig, Germany.
Email: arianna.borriero@ufz.de and tam.nguyen@ufz.de

Abstract

Transit time-based water quality models using StorAge Selection (SAS) functions are crucial for nitrate (NO_3^-) management. However, relying solely on instream NO_3^- concentration for model calibration can result in poor parameter identifiability. This is due to the interaction, or correlation, between transport parameters, such as SAS function parameters, and denitrification rate, which challenges accurate parameters identification and description of catchment-scale hydrological processes. To tackle this issue, we conducted three Monte-Carlo experiments for a German mesoscale catchment by calibrating a SAS-based model with daily instream NO_3^- concentrations (Experiment 1), monthly instream stable water isotopes (e.g. $\delta^{18}O$) (Experiment 2) and both datasets (Experiment 3). Our findings revealed comparable ranges of SAS transport parameters and median water transit times (TT_{50}) across the experiments. This suggests that, despite their distinct reactive or conservative nature, and sampling strategies, the NO_3^- and $\delta^{18}O$ time series offer similar information for calibration. However, the absolute values of transport parameters and TT_{50} time series, as well as the degree of parameter interaction differed. Experiment 1 showed greater interaction between certain transport parameters and denitrification rate, leading to greater equifinality. Conversely, Experiment 3 yielded reduced parameters interaction, which enhanced transport parameters identifiability and decreased uncertainty in TT_{50} time series. Hence, even a modest effort to incorporate only monthly $\delta^{18}O$ values in model calibration for highly frequent NO_3^-, improved the description of hydrological transport. This study showcased the value of combining NO_3^- and $\delta^{18}O$ model results to improve transport parameter identifiability and model robustness, which ultimately enhances NO_3^- management strategies.

KEYWORDS
nitrate transport, stable water isotopes, StorAge Selection functions, transit time distribution

1 | INTRODUCTION

Today's global food production heavily relies on the intensive use of synthetic fertilizers and animal manure in agriculture (Bouraoui & Grizzetti, 2014; Lu & Tian, 2017; Steffen et al., 2015). This practice results in high nutrient enrichment in the landscape, particularly nitrogen (N), which can be converted by soil bacteria into nitrate. Elevated nitrate concentrations can cause eutrophication of fresh and marine waters (Boeykens et al., 2017; Le Moal et al., 2019; Rabalais et al., 2002), and hypoxic dead zones in coastal oceans (Diaz & Rosenberg, 2008). Several initiatives have attempted to regulate agricultural fertilizer inputs such as the Nitrate Directive (EU Commission, 1991) and the Water Framework Directive (EU Commission, 2020). Despite these efforts, high nitrate concentrations still impact water quality (Bodirsky et al., 2014; Bouraoui & Grizzetti, 2014; Van Meter et al., 2023) due to legacy effects, that is, accumulation of N in the soil and long transport times of nitrate through soil and groundwater (Lutz et al., 2022; Nguyen, Sarrazin et al., 2022; Van Meter & Basu, 2017). This situation can create time delays between implemented measures and actual improvements (Kopáček et al., 2013; Puckett et al., 2011; Van Meter et al., 2016), and calls for further actions to enhance water quality status (Solomon et al., 2015) and protect drinking water supplies (Carrard et al., 2019).

The aforementioned lag times are related to the transit time distribution (TTD) of streamflow, the probability distribution of the time elapsed between the entry of a water parcel into the catchment as precipitation and its exit via streamflow (Benettin et al., 2022; Botter et al., 2010; McGuire & McDonnell, 2006; Rinaldo et al., 2011). Environmental tracers, such as stable water isotopes, have been widely employed for determining TTDs through various modelling approaches. More specifically, by integrating stable water isotopes in TTD-based models, we can effectively differentiate between the pressure pulse progression speed (i.e., celerity), and the pore water flow velocity (Birkel & Soulsby, 2015; Ilampooranan et al., 2019; Yang, Tetzlaff, et al., 2021). This distinction is a crucial step in improving the realism of solute transport modelling (Hrachowitz et al., 2016; Lutz et al., 2022). Recent advancements in TTD-based models have acknowledged the time-variant nature of TTDs (Benettin et al., 2013; Kaandorp et al., 2018; Kim et al., 2016) due to meteorological variability (Harman, 2019; Heidbüchel et al., 2020) and temporal dynamics of flow paths partitioning (Ambroise, 2004; Heidbüchel et al., 2012; Jencso et al., 2009). This development has led to the concept of Stor-Age Selection (SAS) functions (Rinaldo et al., 2015; van der Velde et al., 2012), a novel way to link water age in storage and outflows (Harman, 2019). SAS functions have significantly advanced our understanding of catchment hydrology and have been applied in several water and solute transport process studies (Benettin et al., 2015; Kim et al., 2016; Yang, Heidbüchel, et al., 2018).

In addition to hydrological transport, biogeochemical processes, such as plant uptake (Wang et al., 2012) and denitrification (Ocampo et al., 2006), control the fate of nitrate within the catchment. Such processes cause changes in nitrate concentration as nitrate travels from diffuse and point-source inputs to the outlet. Water quality models are employed to analyse these changes and predict future nitrate trajectories under changing climate and land use (Beck, 1987; Burigato Costa et al., 2019; Wang et al., 2013). Water quality models such as the Soil Water Assessment Tool (SWAT; Arnold et al., 1998), the Hydrological Predictions for the Environment (HYPE; Lindström et al., 2010) and the Integrated Catchment model (INCA; Wade et al., 2002) are widely used for simulating nitrate concentration (Wellen et al., 2015). However, the hydrological transport of these models is based on celerity rather than pore water flow velocity, which may lead to challenges in representing longer time delays in nitrate (Hrachowitz et al., 2016; Ilampooranan et al., 2022; Lutz et al., 2022). Nonetheless, incorporating TTDs into water quality models to describe hydrological transport based on pore water flow water velocity remains largely unexplored. For example, van der Velde et al. (2010) revealed that TTD dynamics explain nitrate and chloride concentration fluctuations in a small agricultural catchment. Similarly, Kaandorp et al. (2021) coupled groundwater TTDs and tritium, chloride and nitrate concentrations in a lowland stream, and found how different groundwater pathways contributed to seasonal and long-term fluctuations in instream solute concentration. Van Meter et al. (2017) simulated nitrate transport and retention with a TTD-based approach for the entire Mississippi and Susquehanna River basins. Yang, Heidbüchel, et al. (2018) found lower nitrate concentration in correspondence of older streamflow water ages in an agricultural headwater catchment, due to greater nitrate denitrified along deeper flow paths. Nguyen et al. (2021) and Nguyen, Kumar, et al. (2022) explored nitrate concentration using a TTD-based nitrate transport model and incorporating SAS functions in a mesoscale catchment with mixed land use. More recently, Yu et al. (2023) integrated a SAS-based water age modelling with chloride measurements, and analysis of nitrate and oxygen isotopes of nitrate in a tile-drained corn-soybean field. In this study, they revealed nitrate export characterized by a chemostatic regime. Overall, TTD-based water quality models for nitrate can be beneficial for management activities, tracking old or new N releases and introducing a robust mechanistic framework for catchment-scale nitrate description (Lutz et al., 2022).

When modelling nitrate with a TTD-based approach using SAS functions, specific model parameters need to be assigned to account for both hydrological and biogeochemical processes. However, relying solely on instream nitrate concentration for calibration can lead to interaction between transport and reaction parameters (Beven, 2005, 2006; Beven & Freer, 2001), thus yielding transport parameters (i.e., SAS parameters affecting the water age selection preference for streamflow and subsequently the TTD) that are misleading due to compensation by reaction parameters (i.e., first-order denitrification rate). Parameter interaction refers to the correlation between parameters, which makes them difficult to identify. This is a common problem in hydrological and water quality models (Beven, 2006; Nguyen et al., 2021). Disentangling hydrological and biogeochemical processes by calibrating models with both nitrate concentration and stable water

isotope can ensure that good results for nitrate concentration also correspond to a reasonable representation of hydrological transport. While some studies have used time-variant TTDs in nitrate simulations (Kumar et al., 2020; Nguyen et al., 2021; Nguyen, Kumar, et al., 2022; van der Velde et al., 2012; Yang et al., 2022; Yang, Heidbüchel, et al., 2021; Yang, Jomaa, et al., 2018; Yang, Tetzlaff, et al., 2021), a comprehensive analysis of the specific interaction between model parameters that define hydrological and biogeochemical processes in nitrate simulations is still missing. This understanding is critical for effective water and nitrate management at local and regional scales, necessitating the use of a mechanistically plausible model.

This study aims to test whether nitrate concentration can offer comparable insights into catchment-scale transport processes as stable water isotopes. Here, for the first time, we compared TTDs of streamflow derived from model calibration with instream nitrate concentrations and stable water isotope values. We aimed to identify potential interaction between transport and biogeochemical parameters affecting parameter identifiability and model's robustness in describing hydrological processes. With this objective, we used the mesoscale Hydrologic Model (mHM) and the SAS function, namely the mHM-SAS transport model (Nguyen et al., 2021), in a central German mesoscale catchment. We conducted three experiments by calibrating (i) transport and reaction parameters with daily nitrate values, (ii) only transport parameters with monthly instream isotope values and (iii) transport and reaction parameters with both datasets. Our analysis explored the differences and similarities among experiments not only in terms of using calibration targets of distinct nature (reactive vs. conservative) but also in contrasting sampling strategies (daily vs. monthly). We evaluated the ability to calibrate model parameters and simulate water ages by improving the understanding of hydrological and biogeochemical processes in the study catchment, and ultimately offering insights for enhancing catchment-scale nitrate management.

2 | DATA AND METHODS

2.1 | Study site

The Upper Selke catchment (Figure 1) is located in the north-eastern region of the Harz Mountains in Central Germany, as part of the larger Bode catchment. This region represents a well-studied area integrated within the TERrestrial ENvironmental Observatories network (TERENO; Wollschläger et al., 2016). The catchment covers a total area of 184 km^2, with elevation ranging between 184 and 594 m above mean sea level and a mean slope of 7.65%. The study area has an average annual precipitation (*P*), actual evapotranspiration (ET) and streamflow (*Q*) of 613, 437 and 171 mm, respectively. Forest is the most dominant land use, accounting for 72% of the entire area, followed by agricultural land use, constituting 21% of the landscape. The soils, primarily consisting of cambisols, and overlaying schist and

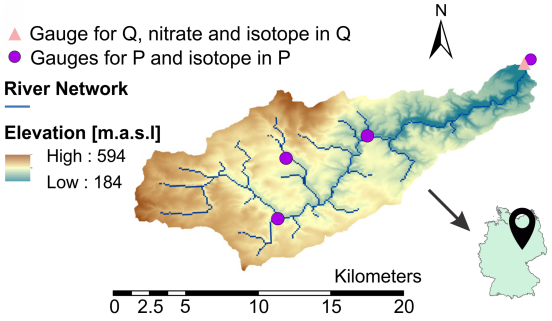

FIGURE 1 Upper Selke catchment with precipitation (purple dots) and streamflow sampling points (pink triangle), the river network (blue lines) and the elevation gradient (coloured map). The location of the Upper Selke catchment in Germany is shown in the lower right corner.

claystone layers, exhibit relatively high permeability. This results in a shallow groundwater system with relatively fast flow paths (Jiang et al., 2014; Yang, Jomaa, et al., 2018).

2.2 | Data

As input data for model simulations, we used daily hydroclimatic time series covering the period from February 2013 to December 2022. Daily P and actual ET time series were supplied from the German Weather Service, while Q time series were simulated with the (mHM; Kumar et al., 2013; Samaniego et al., 2010) model based on raw Q data provided by the State Office of Flood Protection and Water Management of Saxony-Anhalt. Simulated *Q* was used to ensure a closure of the water mass balance. A thorough evaluation of mHM performance for past measurements has been conducted in previous studies (Nguyen et al., 2021; Yang, Jomaa, et al., 2018; Zink et al., 2017).

As data for model calibration, we utilized datasets with different sampling frequency, length of time series and natural characteristics (conservative vs. reactive). Firstly, we used daily instream nitrate concentrations from February 2013 to December 2022, obtained with an in situ ultraviolet-visible probe used in other studies in the same region (Nguyen, Kumar, et al., 2022; Rode et al., 2016; Winter et al., 2022). Secondly, we used monthly isotope data in precipitation and streamflow from the study by Lutz et al. (2018), spanning the period from February 2013 to May 2015. Instream isotope samples were grab samples collected at the catchment outlet during low-flow conditions, while precipitation isotope data were sampled at different locations in the broader Bode region and integrated at a monthly time scale. Precipitation isotope data were subsequently spatially interpolated using kriging with altitude as external drift and weighted with spatially distributed monthly precipitation of the Upper Selke.

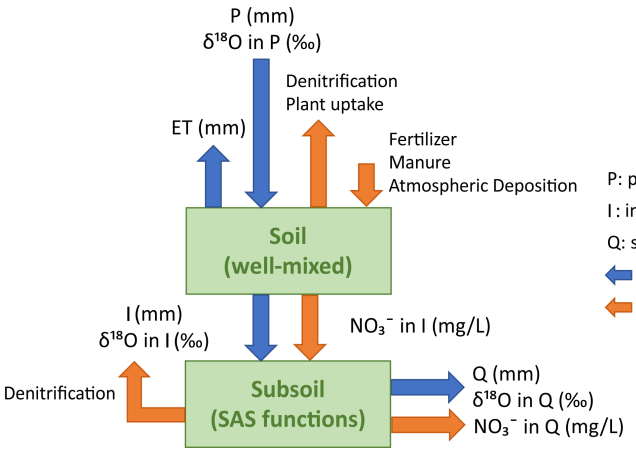

FIGURE 2 Representation of the mHM-SAS model with its two hydrological compartments (soil and subsoil), and the associated hydrological and solute/tracer data time series. mHM, mesoscale hydrologic; SAS, StorAge Selection.

2.3 | The mHM-SAS model

The mHM-SAS model (Nguyen et al., 2021) consists of a spatially distributed N model in the well-mixed soil (i.e., root zone) and a lumped transport model for nitrate in the entire subsoil compartment of the whole catchment (i.e., unsaturated zone and groundwater). The model is based on (i) the mHM model to simulate the hydrological processes accounting for variability of catchment properties; (ii) the mHM-Nitrate model (Yang, Jomaa, et al., 2018) to describe the fate of N in the soil through spatially explicit representation of agricultural practices and (iii) the SAS functions (Botter et al., 2011; Rinaldo et al., 2015; van der Velde et al., 2012) to represent the TTD-based nitrate transport in the subsoil along with denitrification.

The mHM-Nitrate model incorporates N inputs from atmospheric deposition, fertilizer, manure application and plant residues. It also accounts for N removal processes including denitrification and plant uptake, and transformations such as degradation, dissolution (i.e., conversion of active solid organic N to dissolved organic N), and mineralization within distinct pools, designed for dissolved inorganic N, dissolved organic N, active organic N and inactive organic N. Land-use dependent parameters, adapted spatially and temporally based on environmental conditions such as soil moisture and temperature, regulate N transformations within the pools and denitrification rate. The model assumes that dissolved inorganic N is exclusively nitrate (NO_3^-), which can be transported to the subsoil and, eventually, to the stream. In the subsoil, NO_3^- denitrification and transport are described with SAS functions.

In this study, we employed a simplified version of the mHM-SAS model, by utilizing a pre-calibrated mHM-Nitrate model for the soil for which optimal parameters for mineralization, dissolution and denitrification were selected based on their fit to observed instream NO_3^- (Nguyen, Kumar, et al., 2022; Nguyen, Sarrazin, et al., 2022). Hence, we focused on the subsoil only where water potentially contaminated with NO_3^- can reach water supply wells. Previous studies in the Upper Selke have demonstrated the significance of subsoil denitrification (Nguyen et al., 2021; Winter et al., 2021). Notably, the calibrated parameters used in this study (see Section 2.4.1 for parameters calibration) are among those affecting most of the instream NO_3^- dynamics in the original mHM-SAS model (see Nguyen et al. (2021) and Nguyen, Kumar, et al. (2022) for parameter sensitivity).

The mHM-SAS model employed in this work is depicted in Figure 2. We used a lumped version of the transport model in the subsoil, thereby applying the SAS function to the entire compartment. Time series of percolation flux (I) and NO_3^- concentration (NO_3^- in I) from the soil to the subsoil were simulated with the mHM and mHM-Nitrate model. Both I and NO_3^- in I were spatially lumped over the entire catchment. The $\delta^{18}O$ signature in I ($\delta^{18}O$ in I) was calculated from an isotopic balance in the soil as outlined below in Equations (8) and (9).

Here, we provide a technical description for the subsoil within the mHM-SAS model. The water-age balance based on SAS functions is expressed as (Benettin & Bertuzzo, 2018; Botter et al., 2011; Harman, 2015; van der Velde et al., 2012):

$$S^{sub}(t) = S_0{}^{sub} + V(t), \tag{1}$$

$$\frac{\partial S_T{}^{sub}(T,t)}{\partial t} + \frac{\partial S_T{}^{sub}(T,t)}{\partial T} = I(t) - Q(t) \times \Omega_Q(T,t), \tag{2}$$

$$\text{Initial conditions}: S_T{}^{sub}(T, t=0) = S_{T_0}{}^{sub}(T), \tag{3}$$

$$\text{Boundary conditions}: S_T{}^{sub}(T=0) = 0, \tag{4}$$

where $S^{sub}(t)$ [L^3] is the subsoil storage at time t [T]; T [T] is the water age; $S_0{}^{sub}$ [L^3] is the initial subsoil storage; V [L^3] is the subsoil storage variations obtained from the mHM model; $I(t)$ [L^3T^{-1}] and $Q(t)$ [L^3T^{-1}] are the percolation and streamflow fluxes entering and leaving the subsoil, respectively; $S_T{}^{sub}(T, t)$ [L^3] is the age-ranked subsoil storage at time t; and Ω_Q [−] is the cumulative SAS function for Q.

In this study, we assumed that the SAS function for Q is time-invariant and follows the beta function (Drever & Hrachowitz, 2017),

which is expressed below as the probability density function of the normalized age-ranked storage $P_s(T, t)$ (van der Velde et al., 2012):

$$\omega_Q(P_s(T,t),t) = \frac{P_s(T,t)^{\alpha-1} \times (1-P_S(T,t))^{\beta-1}}{B(\alpha,\beta)}, \quad (5)$$

where B(α, β) is the beta function characterized by the shape (α) and scale (β) parameters, representing the transport parameters of our modelling scheme.

From Equation (2), we derived the TTD of streamflow [T^{-1}] and the instream isotopic signature [−] as (Benettin & Bertuzzo, 2018):

$$p_Q(T,t) = \frac{\partial \Omega_Q\left(S_T^{sub}(T,t),t\right)}{\partial S_T^{sub}(T,t)} \times \frac{S_T^{sub}(T,t)}{\partial T}, \quad (6)$$

$$C^Q_{\delta^{18}O}(t) = \int_{T=0}^{\infty} C^{sub}_{\delta^{18}O}(T,t) \times p_Q(T,t) \times dT, \quad (7)$$

where $C^{sub}{}_{\delta}{}^{18}{}_{O}$ [−] is the isotopic signature of a water parcel in the subsoil carried by the percolation flux from the soil compartment (Figure 2). The value of $C^{sub}{}_{\delta}{}^{18}{}_{O}$ is derived from the following isotope balance in the soil, assuming that the soil is well-mixed and there is no isotope fractionation:

$$\frac{\partial S^{soil}(t)}{\partial t} = P(t) - ET(t) - I(t), \quad (8)$$

$$\frac{\partial M_{\delta^{18}O}{}^{soil}(t)}{\partial t} = C_{\delta^{18}O}{}^{P}(t) \times P(t) - C_{\delta^{18}O}{}^{soil}(t) \times (I(t) + \mathrm{ET}(t)), \quad (9)$$

where $S^{soil}(t)$ [L^3] is the water storage at time t [T] provided by the mHM model (initially S^{soil} ($t = 0$) = S_0^{soil}); $P(t)$ [L^3T^{-1}] is the precipitation flux; ET(t) [L^3T^{-1}] is the actual evapotranspiration; $M^{soil}{}_{\delta}{}^{18}{}_{O}(t)$ [L] is the isotopic signature integrated with the soil storage; and $C^{P}{}_{\delta}{}^{18}{}_{O}(t)$ [−] is the isotopic signature in precipitation. $C^{soil}{}_{\delta}{}^{18}{}_{O}(t)$ is the isotope signature in soil storage and in the percolation flux (due to the well-mixed assumption), therefore, $C^{soil}{}_{\delta}{}^{18}{}_{O}(t) = C^{sub}{}_{\delta}{}^{18}{}_{O}(t-T)$ of Equation (7) (e.g. Queloz et al. 2015).

Finally, we simulated the concentration of NO_3^- in the subsoil undergoing denitrification, which is expressed with a first-order reaction. Hence, the instream NO_3^- concentration [ML^{-3}] is calculated as (Nguyen et al., 2021):

$$C^Q{}_{NO_3^-}(t) = \int_0^{\infty} C^{sub}{}_{NO_3^-}(T,t) \times e^{-k \times T} \times p_Q(T,t) \times dT, \quad (10)$$

where $C^{sub}{}_{NO_3^-}$ [ML^{-3}] represents the NO_3^- concentration in the subsoil and k [T^{-1}] is the first-order denitrification rate parameter in the subsoil.

2.4 | Experimental design

In this study, we calibrated the mHM-SAS model against (i) instream NO_3^- concentrations, (ii) instream $\delta^{18}O$ values and (iii) both datasets. These three experiments aim to explore simulated TTDs, calibrated parameters and their correlations, when using different calibration targets. In all experiments, we did not re-simulate the hydrological fluxes (i.e., Q and I), and the NO_3^- leaching flux (i.e., NO_3^- in I) with the mHM model, but instead we took the best simulation from a prior study by Nguyen, Kumar, et al. (2022), Nguyen, Sarrazin, et al. (2022) for the same area. We selected the simulation of Q, I and NO_3^- in I with the highest efficiency for observed Q and instream NO_3^- concentrations, ensuring the most accurate representation of hydrological and water quality processes for our study. Hence, in this study, we calibrated only the transport parameters in the subsoil (see Table 1 in 2.4.3).

2.4.1 | Experiment 1

In Experiment 1, we calibrated the model against daily instream NO_3^- concentrations using 100 000 parameter sets generated in a Monte-Carlo experiment with Latin hypercube sampling (LHS; McKay et al., 1979). Model parameters and their initial ranges can be found in Table 1. Initial ranges for model parameters were chosen based on other studies in the region (Nguyen et al., 2021; Nguyen, Kumar, et al., 2022) and elsewhere (Benettin et al., 2017; Van Meter et al., 2017). Nonetheless, the selected parameter ranges were wide, implying no prior knowledge regarding the SAS functions, catchment storage and denitrification within the catchment. The SAS parameters α and β assume values that determine the catchment's preference for realizing young water (i.e., $\alpha < 1$ and $\beta \geq 1$), old water (i.e., $\alpha \geq 1$ and $\beta < 1$), complete mixing (i.e., $\alpha = \beta = 1$), or both young and old water (i.e., $\alpha > 0$ and $\beta < 1$), hence representing transport processes. The model parameters were calibrated from February 2013 to December 2022. The initial NO_3^- concentration in the subsoil, corresponding to the value of $C^{sub}{}_{NO_3^-}$ in Equation (10) at the first model iteration, was 1.6 mg N-NO_3^-/L (i.e., mass of N in NO_3^-) and matched the mean instream NO_3^- observed throughout the study period.

The output of the Monte-Carlo simulations is detailed in Table 2, which, for Experiment 1, is instream NO_3^- concentration

TABLE 1 Summary of the calibrated model parameters and their respective initial search ranges used for calibration.

Calibrated parameter	Symbol & unit	Lower bound	Upper bound	Use
SAS parameter	α (–)	0.1	3	Experiments 1, 2 and 3
SAS parameter	β (–)	0.1	3	Experiments 1, 2 and 3
Denitrification rate	k (d^{-1})	6×10^{-6}	1×10^{-1}	Experiments 1 and 3
Initial soil storage	$S^{soil}{}_0$ (mm)	300	500	Experiments 2 and 3
Initial subsoil storage	$S^{sub}{}_0$ (mm)	500	1000	Experiments 1, 2 and 3

TABLE 2 Summary of the simulated model outputs.

Simulated parameter	Symbol & unit	Use
Instream nitrate concentration	NO_3^- (mg/L)	Experiments 1 and 3
Instream stable water isotopes value	$\delta^{18}O$ (‰)	Experiments 2 and 3
Median transit time	TT_{50} (d)	Experiments 1, 2 and 3

(Equation 10) and backward median transit time (TT_{50}; i.e., the time it takes for half of the water to leave the catchment as streamflow at the outlet). The TT_{50} of streamflow was calculated as the 50th percentile (i.e., median) of the TTDs for each day of the study period (Equation 6). Therefore, it approximates the TT of water after it has reached the stream and excludes the TT of water that has not yet reached the stream. The TT_{50} is often used as it overcomes the poor identifiability of old water especially in the case of long-tailed TTDs (Benettin et al., 2017).

After running the 100 000 simulations corresponding to 100 000 random parameter sets, we selected behavioural simulations based on the Kling–Gupta efficiency (KGE; Gupta et al., 2009), quantifying the difference between the observed and simulated instream NO_3^-. We employed 2980 data points of observed instream NO_3^- concentrations to evaluate KGE, having a coefficient of variation (CV; the ratio between the standard deviation to the mean) of 0.8. We selected model parameters from the simulations, which yielded KGE ≥0.4 for NO_3^-, indicative of satisfactory model efficiency. We assessed model output uncertainty with the 95% prediction uncertainty (95PPU) by calculating the 2.5% and 97.5% percentiles within the cumulative distribution of the time series of the output variables (Abbaspour et al., 2004).

2.4.2 | Experiment 2

In Experiment 2, we calibrated 100 000 parameter sets in a Monte-Carlo analysis against $\delta^{18}O$ data. The initial range of model parameters corresponds to the lower and upper bound of Table 1. In Experiment 2, we simulated instream $\delta^{18}O$ (Equation 7) and TT_{50} of streamflow. Model simulations covered the period from February 2013 to May 2015 for $\delta^{18}O$ values and from February 2013 to December 2022 for TT_{50} time series. The initial concentration of $\delta^{18}O$ in the soil, corresponding to the value of $C^{soil}{}_{\delta}{}^{18}{}_{O}$ and $C^{sub}{}_{\delta}{}^{18}{}_{O}$ in Equations (7) and (9), respectively at the first model iteration, was set to −9.2 ‰, corresponding to the mean instream $\delta^{18}O$ during the study period. We followed the procedure of Experiment 1 for the uncertainty assessment and model performance evaluation by analysing model parameters and results based on KGE ≥0.4 for $\delta^{18}O$ values. We assessed model performance using 27 observed instream $\delta^{18}O$ values, resulting in a CV of 0.05.

2.4.3 | Experiment 3

In Experiment 3, we conducted a Monte-Carlo analysis with 100 000 parameter sets calibrated against both NO_3^- and $\delta^{18}O$ data. We simulated instream NO_3^- concentration (Equation 10), instream $\delta^{18}O$ values (Equation 7) and TT_{50} of streamflow. The initial parameter ranges correspond to the lower and upper bound given in Table 1. Model simulations covered the time period from February 2013 to December 2022 for NO_3^- and TT_{50} simulations, and from February 2013 to May 2015 for $\delta^{18}O$ simulations. The initial values of NO_3^- concentration in the subsoil and $\delta^{18}O$ data in the soil were 1.6 mg N-NO_3^-/L and − 9.2 ‰, respectively. We followed the procedure of Experiments 1 and 2 for uncertainty assessment and model performance evaluation, analysing model parameters and results with KGE ≥0.4 for both NO_3^- and $\delta^{18}O$ values. The KGE was calculated separately for NO_3^- and $\delta^{18}O$ to ensure that they were equally weighted.

3 | RESULTS

The calibration of the mHM-SAS model within Experiments 1, 2 and 3, with the criterion of KGE ≥0.4, resulted in 1332, 1706 and 315 model parameters set out of 100 000, respectively. The corresponding simulated output variables are described below.

3.1 | Instream nitrate concentrations

The 95PPU of simulated daily instream NO_3^- concentrations from Experiments 1 and 3 is illustrated in Figure 3. Comparison between instream NO_3^- concentration and NO_3^- in *I* is reported in Figure S1. The simulated NO_3^- were similar between the experiments, and seasonal and event-scale variations in the measured daily NO_3^- were well reproduced. The model yielded satisfactory performance with KGE values in the range of [0.40–0.68] across the 1332 and 315 simulations of Experiments 1 and 3. Additionally, the 95PPU covered approximately 63% and 58% of the measured data (*p*-factor = 0.64 and 0.58) for Experiments 1 and 3.

In both experiments, the model accurately reproduced higher NO_3^- during high-flow conditions in winter and spring and predicted lower NO_3^- during low-flow periods in summer and early autumn. We further compared the simulated and observed NO_3^- under different flow conditions, specifically during low flow ($Q < Q_{10\%}$ percentile) and high flow ($Q > Q_{95\%}$) periods (Kumar et al., 2010; Smakhtin, 2001). The mean simulated NO_3^- during high flows was 2.64 and 2.88 mg N-NO_3^-/L for Experiments 1 and 3, whereas the mean measured NO_3^- during high flows was 3.94 mg N-NO_3^-/L. During low flows, Experiments 1 and 3 had mean simulated NO_3^- of 0.77 mg N-NO_3^-/L and 0.85 mg N-NO_3^-/L, whereas the mean measured NO_3^- during low flows was 0.45 mg N-NO_3^-/L. Relation between simulated NO_3^- and *Q* throughout the study period was further supported by a mean Spearman's rank correlation coefficient of

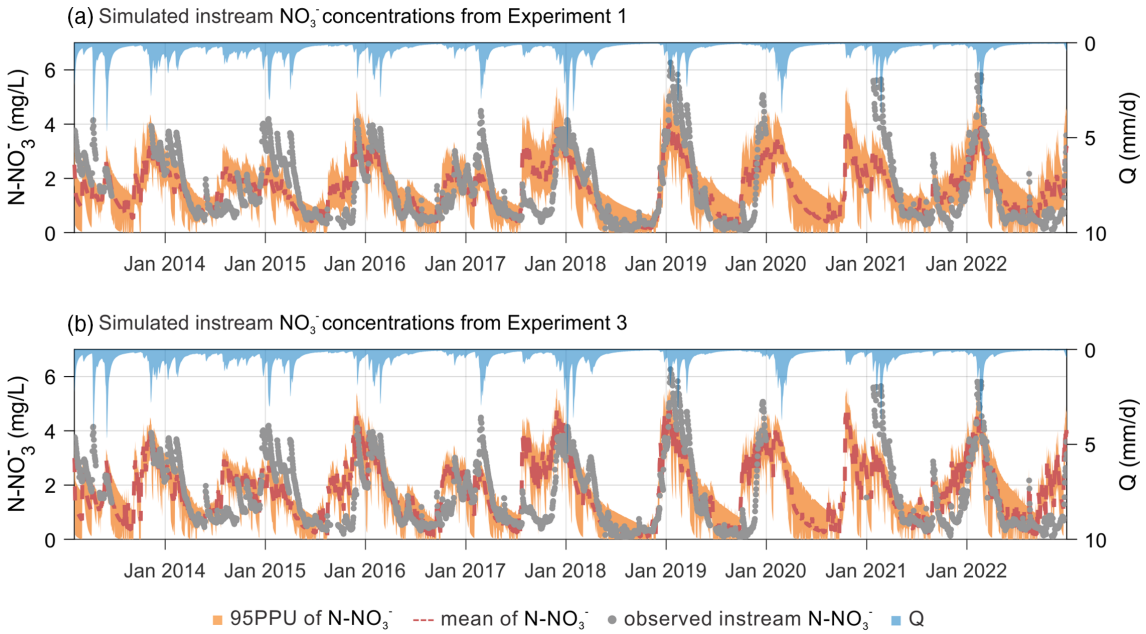

FIGURE 3 95PPU of simulated daily instream NO_3^- for (a) Experiment 1 with 1332 simulations and (b) Experiment 3 with 315 simulations; the grey circles are the observed data; the dashed line is the ensemble mean derived from all solutions; the dark blue area is the streamflow time series.

$\rho = 0.64$ for Experiment 1 and $\rho = 0.56$ for Experiment 3. The correlation between measured NO_3^- and Q was $\rho = 0.85$.

The 95PPU of NO_3^- exhibited a relatively narrow band over the simulation period, particularly in the first half, while the 95PPU increased in the second half of the simulations, coinciding with the exceptional drought in 2018–2019. The deviation of the simulated NO_3^- from the mean value, represented as the ratio of the 95PPU range to the mean value of simulated NO_3^- concentration, showed a significant negative correlation with Q, with a mean Pearson correlation coefficient of $r = -0.48$ and $r = -0.37$ for Experiments 1 and 3. A narrower 95PPU was observed during high flows, with mean 95PPU values of 0.50 and 0.46 mg $N\text{-}NO_3^-$/L for Experiments 1 and 3, and a wider range during low flows, with mean 95PPU values of 2.29 and 2.96 mg $N\text{-}NO_3^-$/L for Experiments 1 and 3. A summary of all the statistical characteristics for NO_3^- discussed in this subsection is given in Table S1.

3.2 | Instream isotope signatures

The simulated monthly instream $\delta^{18}O$ values from Experiments 2 and 3, represented as the 95PPU of the ensemble solutions, are presented in Figure 4. Simulations for Experiments 2 and 3 were nearly identical and characterized by a notably narrower 95PPU compared to that of NO_3^- (Figure 3). In both experiments, the simulated $\delta^{18}O$ captured the isotopic seasonality but did not precisely match the observed monthly measurements, which is characterized by depleted (i.e., more negative) values in winter and enriched (i.e., less negative) values in summer.

Simulated $\delta^{18}O$ values could not capture individual observations, which could be due to uncertainty in the observed data (e.g. noise, measurement errors). However, despite the $\delta^{18}O$ time series spans a relatively short period (February 2013–May 2025) and the observations may not be perfectly simulated, we highlight the importance of employing a modelling approach to accurately reproduce $\delta^{18}O$ seasonality, as detailed in Text S1. This is in contrast with relying solely on a straight-line simulation for instream $\delta^{18}O$ data. In addition, it is important to note the significant influence of $\delta^{18}O$ values and their inherent seasonality on the model results, as elaborated in Text S2 and illustrated in Figure S2 and S3.

3.3 | Median transit times

The 95PPU for the simulated TT_{50} of streamflow of Experiments 1, 2 and 3 are presented in Figure 5. The 95PPU values ranged approximately from 0 to 15 months in Experiment 1 (Figure 5a), and from 0 to 11 months in Experiments 2 (Figure 5b) and 3 (Figure 5c) throughout the study period. Hence, the 95PPU of TT_{50} time series in Experiments 2 and 3 (Figure 5b,c) was narrower than in Experiment 1 (Figure 5a).

All three experiments exhibited pronounced seasonality in TT_{50} values, linked to the catchment's hydrological conditions. There was a

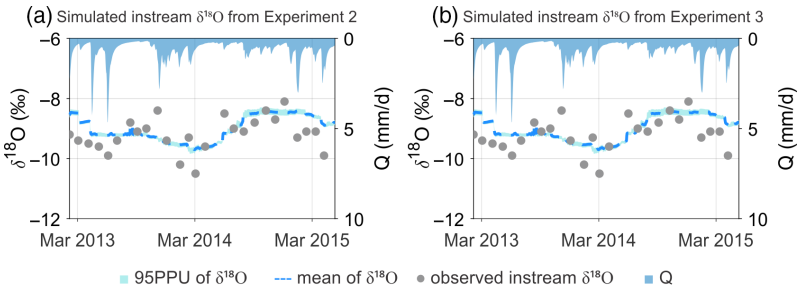

FIGURE 4 95PPU of simulated monthly instream $\delta^{18}O$ for (a) Experiment 2 with 1706 simulations and (b) Experiment 3 with 315 simulations; the grey circles correspond to observed data; the dashed line is the ensemble mean derived from all solutions; the dark blue area is the streamflow time series.

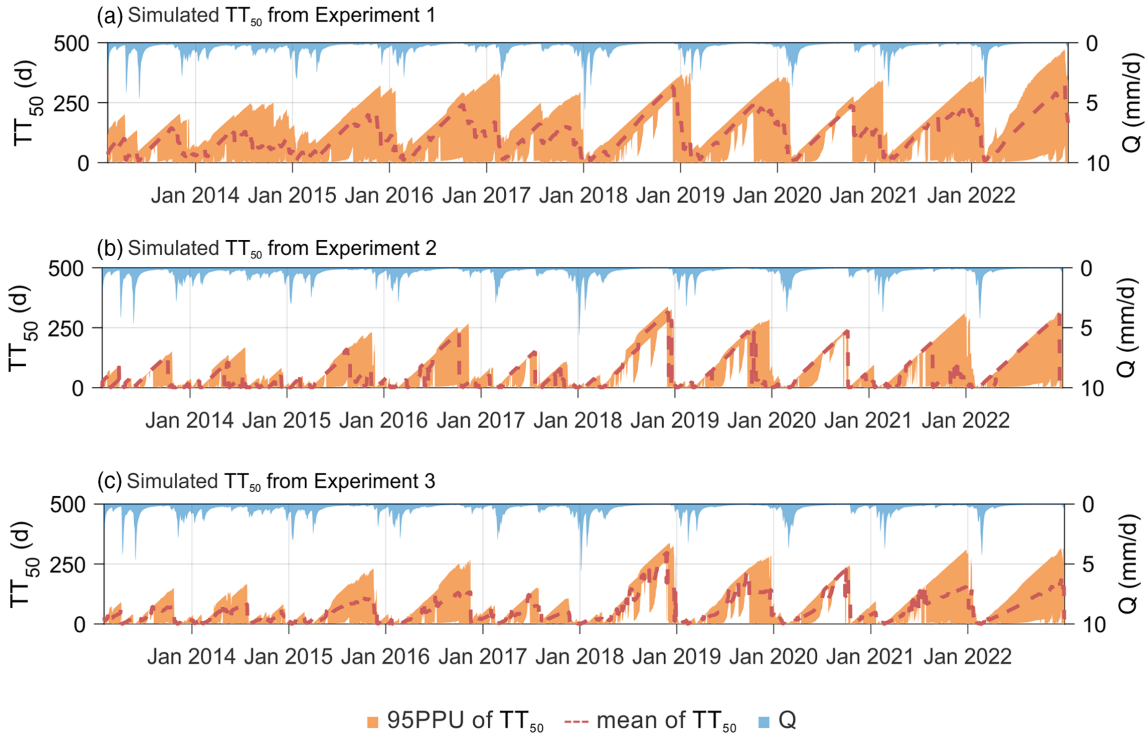

FIGURE 5 95PPU of simulated TT_{50} of streamflow for (a) Experiment 1 with 1332 simulations, (b) Experiment 2 with 1706 simulations and (c) Experiment 3 with 315 simulations; the dashed line is the ensemble mean derived from all solutions; the dark blue area is the streamflow time series.

strong difference in the TT_{50} values between high- and low-flow periods; during high flows, as outlined in 3.1, TT_{50} values sharply decreased to a mean value of 17, 13 and 4 days for Experiments 1, 2 and 3. Conversely, during low flows, TT_{50} values were characterized by a gradual increase and their mean value was approximately 8 months for all experiments. The impact of the drought in 2018–2019 was clearly visible, with a prominent peak in TT_{50} values corresponding to these years and the onward period, which was characterized by very dry summers. In support of this, the maximum TT_{50} values in the period before the 2018–2019 drought reached 12.4 months for Experiment 1, and 8.8 months Experiments 2 and 3. Conversely, after the years 2018–2019, TT_{50} values exhibited a peak of 15.5, months for Experiment 1, and 11.1 months for Experiments 2 and 3. A summary of the statistical characteristics of NO_3^- and TT_{50} in the experiments is given in Table S2.

3.4 | mHM-SAS parameters

Ranges of model parameters calibrated in all experiments are presented as kernel distributions in Figure 6, with mean, minimum, and maximum values detailed in Table S3. Kernel distributions of the

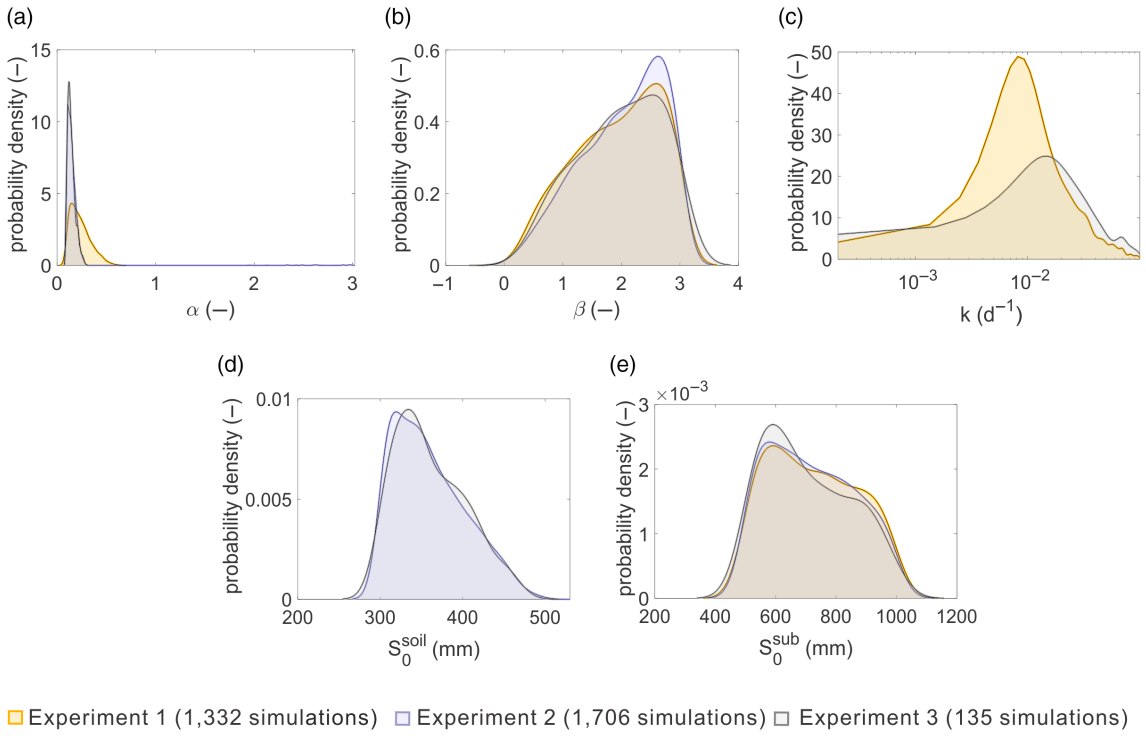

FIGURE 6 Kernel distribution of mHM-SAS parameters. The *x*-axis for *k* in the subsoil (panel c) is expressed in a logarithmic scale for better displaying small values. The *y*-axis represents the probability per unit value of the mHM-SAS parameters. Note that the kernel probability on the *x*-axis extends beyond the dataset limits due to the sum effect of individual Gaussian probability distributions applied to each value in the dataset. mHM, mesoscale hydrologic; SAS, StorAge Selection.

100 000 parameter sets, which are uniform distributions, are displayed in Figure S4. Within all experiments, the parameter α (Figure 6a) was strongly constrained to smaller values. Notably, values for α in Experiments 2 and 3 were more constrained and similar to each other compared to Experiment 1. This difference is supported by statistically different mean α values (Kruskal-Wallis test, *p*-value <0.00001) and distributions of α (two-sample Kolmogorov–Smirnov test, *p*-value <0.00001) in Experiments 2 and 3 versus Experiment 1. The parameter β (Figure 6b) was well constrained to greater values across all experiments (Figure 6b). Overall, low values of α and high values of β indicate that the catchment predominantly discharges younger water throughout the study period (i.e., $\alpha < 1$ and $\beta \geq 1$).

The subsoil denitrification rate *k* in Experiments 1 and 3 was well constrained towards larger values [10^{-3}–10^{-4} d^{-1}] than the initial range [10^{-2}–10^{-7} d^{-1}] (Figure 6c). Significant differences were found between Experiments 1 and 3 in terms of mean values of *k* (Kruskal-Wallis test, *p*-value <0.05) and distribution of *k* (two-sample Kolmogorov–Smirnov test, *p*-value <0.05), with a more pronounced peak of *k* in Experiment 1 in contrast to the flatter distribution in Experiment 3. The initial soil storage employed in Experiments 2 and 3 exhibited moderate constraints towards smaller values (Figure 6d). The initial subsoil storage was loosely constrained towards smaller values in all three experiments (Figure 6e).

For gaining an in-depth understanding into the interactions between model parameters, we examined the Pearson correlation coefficients among parameters within the same experiment. Results are available in Table S4. Experiment 1 showed a negative correlation with $r = -0.43$ (*p*-value <0.0001) between α and *k* (Table S4). However, in Experiment 3, this correlation decreased to $r = -0.23$ (*p*-value <0.0001), and this result is visually supported by Figure 7. Also, a correlation existed between α and β in Experiments 1, 2 and 3 with $r = 0.41$ (*p*-value <0.00001), $r = 0.34$ (*p*-value <0.00001) and $r = 0.38$ (*p*-value <0.00001), respectively (Table S4 and Figure S4).

3.5 | Damköhler number

To reveal which driver between riverine transport and denitrification controls NO_3^- export from the catchment, we calculated the Damköhler number (Da) as the dimensionless ratio between the flow path transit time and NO_3^- reaction time. In our study, we used TT_{50} [*T*] and 1/*k* [*T*] as representative transport and reaction time scales

respectively, resulting in the calculation of Da_{50}. While we are aware that Da represents a distribution, we chose Da_{50} as a single metric to describe the interaction between transport and reaction in our work. When $Da_{50} < 1$, transport processes dominate NO_3^- export, whereas $Da_{50} > 1$ indicates the primary influence of reaction processes. In this study, the Da_{50} analysis focused on the subsoil, hence on the release of NO_3^- to the stream.

Figure 8 illustrates the 95PPU for Da_{50} obtained from Experiments 1 and 3. Da_{50} values exhibited a mean value of 2.2 in both Experiments 1 and 3. Oscillations in the Da_{50} number clearly depended on the catchment's hydrological state, with $Da_{50} < 1$ during high-flow periods and $Da_{50} > 1$ during low-flow or dry periods.

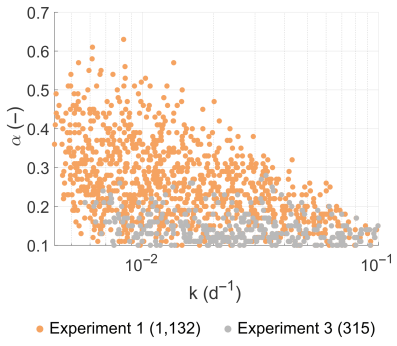

FIGURE 7 Relation between α and k in Experiment 1 with 1332 simulations and Experiment 3 with 315 simulations.

During high-flow periods, as outlined in 3.1, Da_{50} had a mean value of 0.23 and 0.12 across all simulations for Experiment 1 and 3. Conversely, during low-flow periods, Da_{50} exhibited a mean value of 5.2 and 7.1 across all simulations for Experiments 1 and 3. A summary of the statistical characteristics of Da_{50} in the experiments is provided in Table S5.

4 | DISCUSSION

4.1 | Comparative analysis among the experiments

This study explored how model parameters and TTDs of a SAS-based water quality model are constrained with daily NO_3^- and monthly $\delta^{18}O$ data separately (i.e., Experiments 1 and 2) and simultaneously (i.e., Experiment 3). While previous studies have simulated NO_3^- concentrations using SAS functions (Nguyen et al., 2021; Nguyen, Kumar, et al., 2022; van der Velde et al., 2012), our focus is on understanding the interaction between transport and reaction parameters when using distinct calibration targets, sampling frequencies and length of time series. This exploration has implications for interpreting catchment functioning and NO_3^- export dynamics.

Experiments 1 and 3 produced closely aligned NO_3^- simulations (Figure 3), thus indicating the validity of combining $\delta^{18}O$ and NO_3^- data for describing NO_3^- dynamics. Across all the experiments, TT_{50} patterns were comparable (Figure 5) and calibrated parameter ranges were similar (Figure 6). However, there were differences in the absolute values of TT_{50} time series (Figure 5) and transport parameter α

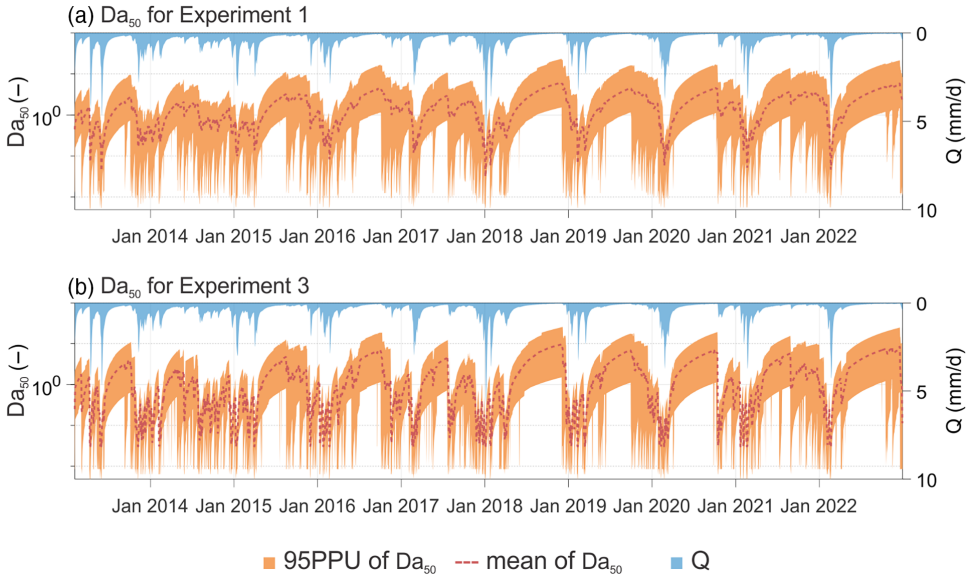

FIGURE 8 95PPU of simulated Da_{50} number obtained from (a) Experiment 1 with 1332 simulations and (b) Experiment 3 with 315 simulations; the dashed line is the ensemble mean derived from all solutions; the dark blue area is the streamflow time series; left y-axis is expressed in logarithmic scale.

(Figure 6a) between Experiments 2 and 3 versus Experiment 1. In Experiments 2 and 3, the range of the parameter α was narrower than in Experiment 1 (Figure 6a), indicating the capacity of instream $\delta^{18}O$ values to better constrain the parameter. This was also evident by the decreased correlation between parameters α and k in Experiment 3 ($r = -0.23$) compared to Experiment 1 ($r = -0.43$). Nonetheless, a correlation is expected due to the inverse relationship between TT_{50} and denitrification (Hrachowitz et al., 2016). Hence, α and k are better constrained in Experiment 3 compared to Experiment 1. A better constraint on the parameter α corresponded to a narrower 95PPU of the TT_{50} time series in Experiment 3 (Figure 5c) compared to Experiment 1 (Figure 5a). This is because α is one of the determining factors influencing water age selection preference (Nguyen, Kumar, et al., 2022; Nguyen, Sarrazin, et al., 2022), thus affecting both the TTD and TT_{50}. We also found a correlation between α and β in Experiment 1 ($r = 0.41$), which decreased in Experiment 2 ($r = 0.34$) and 3 ($r = 0.38$). This yielded a narrower range in α in Experiments 2 and 3 compared to Experiment 1 (Figure S1).

Given that our results were generally consistent across the experiments, the parameter interactions outlined in Table S1 did not severely impact TTDs and the α parameter. This suggests that monthly $\delta^{18}O$ and daily NO_3^- time series hold similar information content to constrain the hydrological transport in the study catchment. The subsequent subsections examine details of the model parameters in the three experiments.

4.1.1 | Water release dynamics

Parameters α and β (Figure 6a,b) showed a convergence towards the same values across the experiments, indicating that the catchment predominantly discharged young water (i.e., $\alpha < 1$ and $\beta \geq 1$) during the study period. This release of young water, associated with a sharp decrease in TT_{50} values during precipitation events (Figure 5), suggests that precipitation quickly turns into runoff via fast, shallow flow paths (Tetzlaff et al., 2007; Tromp-van Meerveld & McDonnell, 2006), activated by wet conditions and soil saturation which enhance connectivity within the catchment (Ambroise, 2004; Blume & van Meerveld (Ilja), 2015). Rapid water routing to the outlet limits water interaction with the subsoil, where NO_3^- may be retained or denitrified. Consequently, fast water movement results in a quick mobilization and transport of solutes during storm events, contributing to the catchment short-term responsiveness (Berghuijs & Allen, 2019) and limiting time for denitrification. Ultimately, this leads to elevated instream NO_3^- concentrations in streamflow (Figure 3).

While the catchment primarily releases young water, it is crucial to recognize the seasonal variations in TT_{50} values (Figure 5), which increase (or decrease) during low (or high) flows. During low flows, TT_{50} values gradually increase (Figure 5), and suggest that streamflow is likely sustained by older water from deeper groundwater via long flow paths established between rainfall events (Jasechko et al., 2016; Soulsby & Tetzlaff, 2008). This condition is due to limited connectivity within the catchment caused by less or no saturation, unlike during precipitation events. Longer TT_{50} values correspond to prolonged exposure time of water with the soil matrix, facilitating denitrification and leading to smaller NO_3^- concentrations in streamflow (Figure 3). Nonetheless, longer TT_{50} values can also result in a significantly delayed response of solute export to input changes (Dupas et al., 2016; Van Meter et al., 2017), thus inducing legacies and long-term problems associated with diffuse NO_3^- pollution persisting in the subsoil, provided that denitrification is limited (Basu et al., 2022; Kumar et al., 2020; Lutz et al., 2022). Overall, the water release dynamics observed in the Upper Selke catchment are consistent with prior work conducted in the region (Borriero et al., 2023; Nguyen et al., 2021; Winter et al., 2021).

4.1.2 | Catchment storage

Calibrated initial soil storage had similarly and relatively well-constrained values in Experiments 2 and 3 (Figure 6d); hence, soil storage was well constrained by the instream $\delta^{18}O$ time series. In contrast, the initial subsoil storage in all experiments was more loosely constrained (Figure 6e). Given the substantial impact of catchment storage on water and NO_3^- transport times, it is critical to improve subsoil storage estimation from other methods. For example, groundwater modelling could help better understand the catchment's physical characteristics and the older water volume, both useful for inferring the storage. Nonetheless, difficulty in estimating the subsoil storage is common in other works based on SAS functions (Benettin et al., 2017; Borriero et al., 2023; Buzacott et al., 2020; Nguyen et al., 2021).

4.1.3 | Denitrification processes

The calibrated denitrification rate in the subsoil was well constrained in both Experiments 1 and 3 (Figure 6c). However, when the density distribution is more uniform, a parameter tends to be less identifiable. Hence, while the denitrification rate generally falls within the same range between Experiments 1 and 3, it appears less identifiable in Experiment 3 compared to Experiment 1. Overall, the accuracy of these values cannot be verified as the 'true' shape of the parameter's posterior density distribution is unknown. Nonetheless, values for the denitrification rate found in this study are within the ranges of other studies conducted in the same region (Nguyen et al., 2021; Nguyen, Kumar, et al., 2022; Yang, Heidbüchel, et al., 2018) and elsewhere (Van Meter et al., 2017; Yu et al., 2023). The mass of denitrified N in the subsoil, along with its balance in the subsoil, is reported in Table S6, while for the N balance in the soil, we refer to the original studies of Nguyen et al. (2021); Nguyen, Sarrazin, et al. (2022).

Previous work comparing the Upper Selke catchment with downstream areas, such as the Lower Selke catchment, showed that denitrification is a key factor of NO_3^- removal in the Upper Selke. For example, Nguyen, Sarrazin, et al. (2022) and Winter et al. (2021) found higher denitrification rates in the Upper Selke than in the Lower Selke

based on NO_3^- model applications. The subsoil hydrochemical conditions of the Upper Selke allow for more effective denitrification than the Lower Selke. Despite showing a generally smaller TT50 than the Lower Selke (Nguyen, Sarrazin, et al., 2022; Winter et al., 2021), the Upper Selke is characterized by a significant TT50 variability (Figure 5), which allows denitrification under low-flow conditions (see Da50 number in Figure 8). In contrast, the Lower Selke, has a more stable TT50 time series and, although having a generally longer TT50 than the Upper Selke, the transport time scale is still shorter than the very long reaction time scale due to very low denitrification rates. As a consequence, denitrification is limited (Nguyen, Sarrazin, et al., 2022; Winter et al., 2021). Additionally, Hannappel et al. (2018) showed a clear sign of ongoing denitrification in the Upper Selke based on groundwater samples. Considering that denitrification is the only process leading to permanent NO_3^- removal (Boyer et al., 2006; Burgin & Hamilton, 2007), there is a highly relevant role of denitrification in the Upper Selke for natural attenuation of water pollution (Otero et al., 2009; Singleton et al., 2007; Smith et al., 2009).

4.2 | Interplay between hydrological and biogeochemical processes

Addressing NO_3^- pollution in water and understanding the fate of NO_3^-, that is, its transport and retention within and export from the catchment, requires a comprehensive exploration of hydrological and biogeochemical processes across different catchment compartments at various time scales (Bouwman et al., 2013; Kumar et al., 2020; Liao et al., 2012). In this regard, the Damköhler number offers insights into the primary driver of NO_3^- removal (Lansdown et al., 2015), that is, hydrological transport or denitrification (Ebeling et al., 2021; Minaudo et al., 2019; Musolff et al., 2015, 2021). Our results for Da_{50} number (Figure 8) revealed that during high-flow periods (i.e., $Da_{50} < 1$), transport processes predominantly controlled the fate of NO_3^-. Hence, denitrification played a limited role in NO_3^- removal, and NO_3^- and $\delta^{18}O$ time series likely conveyed similar information in the study area. In further support of this conclusion, we found a significant positive correlation ($r = 0.81$; p-value <0.0001) among KGE values for Experiments 1, 2 and 3, which indicates that when the SAS parameters perform well for $\delta^{18}O$, the same parameters, when coupled with the denitrification rate, are equally effective for NO_3^-. On the other hand, during low-flow periods (i.e., $Da_{50} > 1$) denitrification became primarily responsible for NO_3^- removal from the catchment (Benettin et al., 2020). Our results for the Da_{50} number clearly show the continuous switch between the dominance of transport and denitrification in NO_3^- export dynamics, depending on the flow conditions.

The relationship between Q and solute concentration is often explored through streamflow-concentration (C–Q) relationships, revealing patterns in solute export dynamics (Godsey et al., 2009; Musolff et al., 2017, 2021). Our results indicate that, generally, during high Q periods, NO_3^- concentration peaks, suggesting a chemodynamic accretion pattern in the Upper Selke (Godsey et al., 2009). This pattern can be influenced by the activation of source areas for NO_3^- during storm events, resulting in a rapid release of NO_3^- into the stream network (Ambroise, 2004; Blume & van Meerveld (Ilja), 2015; Jencso et al., 2009). Furthermore, this suggests that NO_3^- is more likely stored in shallow subsoil zones rather than deeper within the catchment (Musolff et al., 2021; Rozemeijer & Broers, 2007; Tiemeyer et al., 2008).

4.3 | Towards improved representation of nitrate transport modelling

Acknowledging the importance of modelling NO_3^- with TTDs (Benettin et al., 2020; Kumar et al., 2020; Nguyen et al., 2021; Nguyen, Kumar, et al., 2022; Nguyen, Sarrazin, et al., 2022; van der Velde et al., 2010), our study demonstrates that evaluating NO_3^- transport models against $\delta^{18}O$ data can improve the identifiability of transport parameter α and reduce the 95PPU of TT_{50} time series, thus enhancing the description of hydrological transport. This is critical for environmental policies and decision-making aimed at enhancing NO_3^- management strategies and regulating fertilizer applications (Basu et al., 2022; Bouraoui & Grizzetti, 2014; Van Meter et al., 2023).

Our findings in the Upper Selke suggested that during high flow conditions, NO_3^- export was primarily driven by hydrological transport, and associated with a main release of young water. Additionally, our results demonstrated that the insights derived from calibrating the model against the time series of NO_3^- concentrations closely mirrored the information gained by the corresponding time series of $\delta^{18}O$ values. Indeed, despite the interaction between transport parameter α and reaction parameter k (Table S4), there were small differences in time series of TT_{50} and posterior distribution of α (Figures 5 and 6a) when derived using daily NO_3^- and monthly $\delta^{18}O$ separately (i.e., Experiments 1 and 2) or simultaneously (i.e., Experiment 3). This highlights the value of both NO_3^- and $\delta^{18}O$ in understanding the hydrological processes in the Upper Selke catchment. However, these results may be site-specific and not readily apply to all catchments. For example, in a recent study by Yu et al. (2023) conducted in a tile-drained agricultural field, SAS functions were calibrated using chlorides, revealing a significant preference for young water more pronounced during wetter conditions, as observed in our study. Instead, the NO_3^- export regime was classified as chemostatic (i.e., NO_3^- concentrations remain stable over time) based on C–Q relationships, which was attributed to a substantial mixing volume and the absence of a pronounced vertical contrast in NO_3^- levels. Therefore, our results may be particularly relevant to catchments with hydrological conditions and solute export regimes similar to the Upper Selke, that is, the preferential release of young water along with the mobilization of solutes during precipitation events. Whereas, the information derived from NO_3^- concentration in terms of hydrological processes might differ from that derived from $\delta^{18}O$ values at other sites. For this reason, a systematic assessment of water quality models for NO_3^- against TTDs inferred from $\delta^{18}O$ values is needed across diverse catchments.

Our study demonstrated successfully constrained model parameters (Figure 6) and simulated TT_{50} time series (Figure 5) with even a few years of monthly $\delta^{18}O$ observations. This aligns with a recent study in the region that used a different transport model to simulate instream $\delta^{18}O$ values and TT50 time series using monthly $\delta^{18}O$ values in the same region (Borriero et al., 2023). In addition, incorporating low-frequency $\delta^{18}O$ values into model calibration alongside high-frequency NO_3^- concentrations proved beneficial in further constraining model simulations, as highlighted by the narrower 95PPU of most of the model results in Experiment 3 as compared to those in Experiment 1. This emphasizes the significance of low-frequency, short-term observations in providing useful information about the underlying hydrological processes.

Nonetheless, we advocate for richer datasets of high-frequency $\delta^{18}O$ values (e.g. daily or sub-daily) that may provide valuable insights into underlying processes. However, collecting high-frequency water samples can be expensive. Hence, it is crucial to know whether this expense is justified in terms of better representation of the hydrological process. Yet, in this study, we could not test the effect of $\delta^{18}O$ sampling on the modelled results due to insufficient $\delta^{18}O$ observations. Stockinger et al. (2016) showed that isotope sampling frequencies affect the estimated TTD and related metrics (i.e., young water fraction). Therefore, future studies should explore the effects of $\delta^{18}O$ sampling frequencies on the water age selection preference and TTD with a SAS-based modelling approach, and the sampling frequency of $\delta^{18}O$ data that can provide useful information for NO_3^- transport modelling.

Overall, our results demonstrated that constraining NO_3^- transport models with sparse $\delta^{18}O$ data can serve as a validation tool for water quality models. This allows for easy reproducibility in other regions with different hydrological and geophysical settings. Ultimately, this can facilitate a systematic evaluation across multiple catchments, to assess how using different target variables for model calibration may impact the simulation of water transport dynamics. Improving the realism of our modelling approaches is particularly crucial in view of increasingly extreme weather conditions and increased water pollution due to global change.

5 | CONCLUSIONS

This study calibrated an NO_3^- transport model using instream NO_3^- and $\delta^{18}O$ values to determine whether both data sources provide equivalent insights into catchment-scale transport processes. To this aim, different Monte-Carlo experiments were conducted using SAS functions and by calibrating model parameters with instream NO_3^- only (Experiment 1), instream $\delta^{18}O$ only (Experiment 2) and with both datasets (Experiment 3).

Our results showed similar transport parameters regardless of the calibrated data used in the experiments. In addition, our findings displayed a similar temporal dynamic of the simulated TT_{50} among the experiments, suggesting that NO_3^- and $\delta^{18}O$ values contain similar information for model calibration, despite their differing nature (reactive vs. conservative) and contrasting sampling frequencies (daily vs. monthly). However, we identified interaction between transport parameter α and reaction parameter k in Experiment 1, which was reduced when incorporating monthly $\delta^{18}O$ values in Experiment 3. This reduction was beneficial as it improved the description of hydrological transport by reducing the uncertainty in the transport parameters α and TT_{50} time series. Notably, these interactions did not significantly affect the overall model outcomes, given their general similarities across the experiments.

We attributed the general similarity in transport mechanisms between NO_3^- and $\delta^{18}O$ values to the chemo-dynamic accretion pattern for solute export behaviour, characterized by rapid NO_3^- release during storm events. This highlighted the dominance of transport as the driving force for NO_3^- export during high flows, supported by $Da_{50} < 1$. Hence, in the Upper Selke where NO_3^- export is primarily transport-driven during high flows, simulated TT_{50} and calibrated transport parameters derived from NO_3^- concentration will likely align with those derived from $\delta^{18}O$ values. However, these results may not readily apply to all catchments, as simulated TT_{50} and calibrated transport parameters might differ when using NO_3^- and $\delta^{18}O$ data at other sites.

This study explored the relationship between hydrology and biogeochemistry governing solute export from catchments, and highlighted how validation of NO_3^- transport models with a coarse dataset of $\delta^{18}O$ values can enhance the robustness of transport description. This ultimately can improve NO_3^- management strategies under changing environmental conditions.

ACKNOWLEDGEMENTS

A. Borriero conducted the model simulations, carried out the analysis, interpreted the results, prepared the figures and wrote the original draft of the paper. A. Borriero, A. Musolff, T. V. Nguyen and R. Kumar designed and conceptualized the study. T. V. Nguyen provided support for modelling. A. Musolff, T. V. Nguyen, R. Kumar and SRL provided data for model simulations. A. Borriero, A. Musolff, T. V. Nguyen and R. Kumar conceived the methodology and experimental design. All co-authors helped A. Borriero interpret the results. All authors contributed to the review, final writing and finalization of this work.

The research was supported by TERENO (TERrestrial ENvironmental Observatories), funded by the Helmholtz-Centre for Environmental Research of the Helmholtz Association, and the Federal Ministry of Education and Research (BMBF). The authors thank the German Weather Service and State Office of Flood Protection and Water Management of Saxony-Anhalt for providing the necessary input raw data to set up the mHM-SAS model. The authors would like to thank Michael Rode and Uwe Kiwel for providing the in situ nitrate-N data. Open Access funding enabled and organized by Projekt DEAL.

CONFLICT OF INTEREST STATEMENT

The authors have no competing interests to declare.

DATA AVAILABILITY STATEMENT

Source codes of the mHM-SAS model are available at https://git.ufz.de/nguyenta/mhm-sas (Nguyen et al., 2021) and https://git.ufz.de/yangx/mHM-Nitrate (X. Yang et al., 2018).Values of stable water isotope data in precipitation and streamflow are available at https://doi.org/10.1029/2017WR022216 (Lutz et al., 2018).

ORCID

T. V. Nguyen https://orcid.org/0000-0001-9111-4393

REFERENCES

Abbaspour, K. C., Johnson, C. A., & van Genuchten, M. T. (2004). Estimating uncertain flow and transport parameters using a sequential uncertainty fitting procedure. *Vadose Zone Journal*, *3*(4), 1340–1352. https://doi.org/10.2136/vzj2004.1340

Ambroise, B. (2004). Variable 'active' versus 'contributing' areas or periods: A necessary distinction. *Hydrological Processes*, *18*(6), 1149–1155. https://doi.org/10.1002/hyp.5536

Arnold, C. J., Srinivasan, R., Muttiah, R. S., & Williams, J. R. (1998). Large area hydrologic modeling and assessment part I: Model development 1. *Journal of the American Water Resources Association*, *34*(1), 73–89.

Basu, N. B., Van Meter, K. J., Byrnes, D. K., Van Cappellen, P., Brouwer, R., Jacobsen, B. H., Jarsjö, J., Rudolph, D. L., Cunha, M. C., Nelson, N., Bhattacharya, R., Destouni, G., & Olsen, S. B. (2022). Managing nitrogen legacies to accelerate water quality improvement. *Nature Geoscience*, *15*(2), 97–105. https://doi.org/10.1038/s41561-021-00889-9

Beck, M. B. (1987). Water quality modeling: A review of the analysis of uncertainty. *Water Resources Research*, *23*(8), 1393–1442. https://doi.org/10.1029/WR023i008p01393

Benettin, P., & Bertuzzo, E. (2018). Tran-SAS v1.0: A numerical model to compute catchment-scale hydrologic transport using StorAge selection functions. *Geoscientific Model Development*, *11*(4), 1627–1639. https://doi.org/10.5194/gmd-11-1627-2018

Benettin, P., Fovet, O., & Li, L. (2020). Nitrate removal and young stream water fractions at the catchment scale. *Hydrological Processes*, *34*(12), 2725–2738. https://doi.org/10.1002/hyp.13781

Benettin, P., Kirchner, J. W., Rinaldo, A., & Botter, G. (2015). Modeling chloride transport using travel time distributions at Plynlimon, Wales. *Water Resources Research*, *51*(5), 3259–3276. https://doi.org/10.1002/2014WR016600

Benettin, P., Rodriguez, N. B., Sprenger, M., Kim, M., Klaus, J., Harman, C. J., van der Velde, Y., Hrachowitz, M., Botter, G., McGuire, K. J., Kirchner, J. W., Rinaldo, A., & McDonnell, J. J. (2022). Transit time estimation in catchments: Recent developments and future directions. *Water Resources Research*, *58*(11), e2022WR033096. https://doi.org/10.1029/2022WR033096

Benettin, P., Soulsby, C., Birkel, C., Tetzlaff, D., Botter, G., & Rinaldo, A. (2017). Using SAS functions and high-resolution isotope data to unravel travel time distributions in headwater catchments. *Water Resources Research*, *53*(3), 1864–1878. https://doi.org/10.1002/2016WR020117

Benettin, P., van der Velde, Y., van der Zee, S. E. A. T. M., Rinaldo, A., & Botter, G. (2013). Chloride circulation in a lowland catchment and the formulation of transport by travel time distributions. *Water Resources Research*, *49*(8), 4619–4632. https://doi.org/10.1002/wrcr.20309

Berghuijs, W. R., & Allen, S. T. (2019). Waters flowing out of systems are younger than the waters stored in those same systems. *Hydrological Processes*, *33*(25), 3251–3254. https://doi.org/10.1002/hyp.13569

Beven, K. (2005). On the concept of model structural error. *Water Science and Technology*, *52*(6), 167–175. https://doi.org/10.2166/wst.2005.0165

Beven, K. (2006). A manifesto for the equifinality thesis. *Journal of Hydrology*, *320*(1), 18–36. https://doi.org/10.1016/j.jhydrol.2005.07.007

Beven, K., & Freer, J. (2001). Equifinality, data assimilation, and uncertainty estimation in mechanistic modelling of complex environmental systems using the GLUE methodology. *Journal of Hydrology*, *249*(1), 11–29. https://doi.org/10.1016/S0022-1694(01)00421-8

Birkel, C., & Soulsby, C. (2015). Advancing tracer-aided rainfall–runoff modelling: A review of progress, problems and unrealised potential. *Hydrological Processes*, *29*(25), 5227–5240. https://doi.org/10.1002/hyp.10594

Blaen, P. J., Khamis, K., Lloyd, C., Comer-Warner, S., Ciocca, F., Thomas, R. M., MacKenzie, A. R., & Krause, S. (2017). High-frequency monitoring of catchment nutrient exports reveals highly variable storm event responses and dynamic source zone activation. *Journal of Geophysical Research: Biogeosciences*, *122*(9), 2265–2281. https://doi.org/10.1002/2017JG003904

Blume, T., & van Meerveld (Ilja), H. J. (2015). From hillslope to stream: Methods to investigate subsurface connectivity. *WIREs Water*, *2*(3), 177–198. https://doi.org/10.1002/wat2.1071

Bodirsky, B. L., Popp, A., Lotze-Campen, H., Dietrich, J. P., Rolinski, S., Weindl, I., Schmitz, C., Müller, C., Bonsch, M., Humpenöder, F., Biewald, A., & Stevanovic, M. (2014). Reactive nitrogen requirements to feed the world in 2050 and potential to mitigate nitrogen pollution. *Nature Communications*, *5*(1), 3858. https://doi.org/10.1038/ncomms4858

Boeykens, S. P., Piol, M. N., Samudio Legal, L., Saralegui, A. B., & Vázquez, C. (2017). Eutrophication decrease: Phosphate adsorption processes in presence of nitrates. *Journal of Environmental Management*, *203*, 888–895. https://doi.org/10.1016/j.jenvman.2017.05.026

Borriero, A., Kumar, R., Nguyen, T. V., Fleckenstein, J. H., & Lutz, S. R. (2023). Uncertainty in water transit time estimation with StorAge selection functions and tracer data interpolation. *Hydrology and Earth System Sciences*, *27*(15), 2989–3004. https://doi.org/10.5194/hess-27-2989-2023

Botter, G., Bertuzzo, E., & Rinaldo, A. (2010). Transport in the hydrologic response: Travel time distributions, soil moisture dynamics, and the old water paradox. *Water Resources Research*, *46*(3), W03514. https://doi.org/10.1029/2009WR008371

Botter, G., Bertuzzo, E., & Rinaldo, A. (2011). Catchment residence and travel time distributions: The master equation. *Geophysical Research Letters*, *38*(11), L11403. https://doi.org/10.1029/2011GL047666

Bouraoui, F., & Grizzetti, B. (2014). Modelling mitigation options to reduce diffuse nitrogen water pollution from agriculture. *Science of the Total Environment*, *468–469*, 1267–1277. https://doi.org/10.1016/j.scitotenv.2013.07.066

Bouwman, A. F., Bierkens, M. F. P., Griffioen, J., Hefting, M. M., Middelburg, J. J., Middelkoop, H., & Slomp, C. P. (2013). Nutrient dynamics, transfer and retention along the aquatic continuum from land to ocean: Towards integration of ecological and biogeochemical models. *Biogeosciences*, *10*(1), 1–22. https://doi.org/10.5194/bg-10-1-2013

Boyer, E. W., Alexander, R. B., Parton, W. J., Li, C., Butterbach-Bahl, K., Donner, S. D., Skaggs, R. W., & Del Grosso, S. J. (2006). Modeling denitrification in terrestrial and aquatic ecosystems at regional scales. *Ecological Applications*, *16*(6), 2123–2142. https://doi.org/10.1890/1051-0761(2006)016[2123:MDITAA]2.0.CO;2

Burgin, A. J., & Hamilton, S. K. (2007). Have we overemphasized the role of denitrification in aquatic ecosystems? A review of nitrate removal pathways. *Frontiers in Ecology and the Environment*, *5*(2), 89–96. https://doi.org/10.1890/1540-9295(2007)5[89:HWOTRO]2.0.CO;2

Burigato Costa, C. M. d. S., da Silva Marques, L., Almeida, A. K., Leite, I. R., & de Almeida, I. K. (2019). Applicability of water quality models around the world—A review. *Environmental Science and Pollution Research*, *26*(36), 36141–36162. https://doi.org/10.1007/s11356-019-06637-2

Buzacott, A. J. V., van der Velde, Y., Keitel, C., & Vervoort, R. W. (2020). Constraining water age dynamics in a south-eastern Australian catchment using an age-ranked storage and stable isotope approach. *Hydrological Processes*, *34*(23), 4384–4403. https://doi.org/10.1002/hyp.13880

Carrard, N., Foster, T., & Willetts, J. (2019). Groundwater as a source of drinking water in Southeast Asia and the Pacific: A multi-country review of current reliance and resource concerns. *Water*, *11*(8), 1605. https://doi.org/10.3390/w110816

Diaz, R. J., & Rosenberg, R. (2008). Spreading dead zones and consequences for marine ecosystems. *Science*, *321*(5891), 926–929. https://doi.org/10.1126/science.1156401

Drever, M. C., & Hrachowitz, M. (2017). Migration as flow: Using hydrological concepts to estimate the residence time of migrating birds from the daily counts. *Methods in Ecology and Evolution*, *8*(9), 1146–1157. https://doi.org/10.1111/2041-210x.12727

Dupas, R., Jomaa, S., Musolff, A., Borchardt, D., & Rode, M. (2016). Disentangling the influence of hydroclimatic patterns and agricultural management on river nitrate dynamics from sub-hourly to decadal time scales. *Science of the Total Environment*, *571*, 791–800. https://doi.org/10.1016/j.scitotenv.2016.07.053

Ebeling, P., Kumar, R., Weber, M., Knoll, L., Fleckenstein, J. H., & Musolff, A. (2021). Archetypes and controls of riverine nutrient export across German catchments. *Water Resources Research*, *57*(4), e2020WR028134. https://doi.org/10.1029/2020WR028134

EU Commission. (1991). Directive 91/676/EEC. Council directive of 12 December 1991 concerning the protection of waters against pollution caused by nitrates from agricultural sources. *Official Journal of European Community*, *L375*, 1–8.

EU Commission. (2020). Directive 2000/60/EC of the European Parliament and of the council of 23 October 2000 on establishing a framework for community action in the field of water policy. *Official Journal of European Community*, *L327*, 1–72.

Godsey, S. E., Kirchner, J. W., & Clow, D. W. (2009). Concentration–discharge relationships reflect chemostatic characteristics of US catchments. *Hydrological Processes*, *23*(13), 1844–1864. https://doi.org/10.1002/hyp.7315

Gupta, H. V., Kling, H., Yilmaz, K. K., & Martinez, G. F. (2009). Decomposition of the mean squared error and NSE performance criteria: Implications for improving hydrological modelling. *Journal of Hydrology*, *377*(1), 80–91. https://doi.org/10.1016/j.jhydrol.2009.08.003

Hannappel, S., Köpp, C., & Bach, T. (2018). Charakterisierung des Nitratabbauvermögens der Grundwasserleiter in Sachsen-Anhalt. *Grundwasser*, *23*(4), 311–321. https://doi.org/10.1007/s00767-018-0402-7

Harman, C. J. (2015). Time-variable transit time distributions and transport: Theory and application to storage-dependent transport of chloride in a watershed. *Water Resources Research*, *51*(1), 1–30. https://doi.org/10.1002/2014WR015707

Harman, C. J. (2019). Age-ranked storage-discharge relations: A unified description of spatially lumped flow and water age in hydrologic systems. *Water Resources Research*, *55*(8), 7143–7165. https://doi.org/10.1029/2017WR022304

Heidbüchel, I., Troch, P. A., Lyon, S. W., & Weiler, M. (2012). The master transit time distribution of variable flow systems. *Water Resources Research*, *48*(6), W06520. https://doi.org/10.1029/2011WR011293

Heidbüchel, I., Yang, J., Musolff, A., Troch, P., Ferré, T., & Fleckenstein, J. H. (2020). On the shape of forward transit time distributions in low-order catchments. *Hydrology and Earth System Sciences*, *24*(6), 2895–2920. https://doi.org/10.5194/hess-24-2895-2020

Hrachowitz, M., Benettin, P., van Breukelen, B. M., Fovet, O., Howden, N. J. K., Ruiz, L., van der Velde, Y., & Wade, A. J. (2016). Transit times—The link between hydrology and water quality at the catchment scale. *WIREs Water*, *3*(5), 629–657. https://doi.org/10.1002/wat2.1155

Ilampooranan, I., Van Meter, K. J., & Basu, N. B. (2019). A race against time: Modeling time lags in watershed response. *Water Resources Research*, *55*(5), 3941–3959. https://doi.org/10.1029/2018WR023815

Ilampooranan, I., van Meter, K. J., & Basu, N. B. (2022). Intensive agriculture, nitrogen legacies, and water quality: Intersections and implications. *Environmental Research Letters*, *17*(3), 35006. https://doi.org/10.1088/1748-9326/ac55b5

Jasechko, S., Kirchner, J. W., Welker, J. M., & McDonnell, J. J. (2016). Substantial proportion of global streamflow less than three months old. *Nature Geoscience*, *9*(2), 126–129. https://doi.org/10.1038/ngeo2636

Jencso, K. G., McGlynn, B. L., Gooseff, M. N., Wondzell, S. M., Bencala, K. E., & Marshall, L. A. (2009). Hydrologic connectivity between landscapes and streams: Transferring reach- and plot-scale understanding to the catchment scale. *Water Resources Research*, *45*(4), W04428. https://doi.org/10.1029/2008WR007225

Jiang, S., Jomaa, S., & Rode, M. (2014). Modelling inorganic nitrogen leaching in nested mesoscale catchments in central Germany. *Ecohydrology*, *7*(5), 1345–1362. https://doi.org/10.1002/eco.1462

Kaandorp, V. P., Broers, H. P., van der Velde, Y., Rozemeijer, J., & de Louw, P. G. B. (2021). Time lags of nitrate, chloride, and tritium in streams assessed by dynamic groundwater flow tracking in a lowland landscape. *Hydrology and Earth System Sciences*, *25*, 3691–3711. https://doi.org/10.5194/hess-25-3691-2021

Kaandorp, V. P., de Louw, P. G. B., van der Velde, Y., & Broers, H. P. (2018). Transient groundwater travel time distributions and age-ranked storage-discharge relationships of three lowland catchments. *Water Resources Research*, *54*(7), 4519–4536. https://doi.org/10.1029/2017WR022461

Kim, M., Pangle, L. A., Cardoso, C., Lora, M., Volkmann, T. H. M., Wang, Y., Harman, C. J., & Troch, P. A. (2016). Transit time distributions and StorAge selection functions in a sloping soil lysimeter with time-varying flow paths: Direct observation of internal and external transport variability. *Water Resources Research*, *52*(9), 7105–7129. https://doi.org/10.1002/2016WR018620

Kopáček, J., Hejzlar, J., & Posch, M. (2013). Factors controlling the export of nitrogen from agricultural land in a large central European catchment during 1900–2010. *Environmental Science & Technology*, *47*(12), 6400–6407. https://doi.org/10.1021/es400181m

Kumar, R., Heße, F., Rao, P. S. C., Musolff, A., Jawitz, J. W., Sarrazin, F., Samaniego, L., Fleckenstein, J. H., Rakovec, O., Thober, S., & Attinger, S. (2020). Strong hydroclimatic controls on vulnerability to subsurface nitrate contamination across Europe. *Nature. Communications*, *11*(1), 6302. https://doi.org/10.1038/s41467-020-19955-8

Kumar, R., Livneh, B., & Samaniego, L. (2013). Toward computationally efficient large-scale hydrologic predictions with a multiscale regionalization scheme. *Water Resources Research*, *49*(9), 5700–5714. https://doi.org/10.1002/wrcr.20431

Kumar, R., Samaniego, L., & Attinger, S. (2010). The effects of spatial discretization and model parameterization on the prediction of extreme runoff characteristics. *Journal of Hydrology*, *392*(1), 54–69. https://doi.org/10.1016/j.jhydrol.2010.07.047

Lansdown, K., Heppell, C. M., Trimmer, M., Binley, A., Heathwaite, A. L., Byrne, P., & Zhang, H. (2015). The interplay between transport and reaction rates as controls on nitrate attenuation in permeable, streambed sediments. *Journal of Geophysical Research: Biogeosciences*, *120*(6), 1093–1109. https://doi.org/10.1002/2014JG002874

Le Moal, M., Gascuel-Odoux, C., Ménesguen, A., Souchon, Y., Étrillard, C., Levain, A., Moatar, F., Pannard, A., Souchu, P., Lefebvre, A., & Pinay, G. (2019). Eutrophication: A new wine in an old bottle? *Science of the Total Environment*, *651*, 1–11. https://doi.org/10.1016/j.scitotenv.2018.09.139

Liao, L., Green, C. T., Bekins, B. A., & Böhlke, J. K. (2012). Factors controlling nitrate fluxes in groundwater in agricultural areas. *Water Resources Research*, *48*(6), W00L09. https://doi.org/10.1029/2011WR011008

Lindström, G., Pers, C., Rosberg, J., Strömqvist, J., & Arheimer, B. (2010). Development and testing of the HYPE (hydrological predictions for the environment) water quality model for different spatial scales. *Hydrology Research*, *41*(3–4), 295–319. https://doi.org/10.2166/nh.2010.007

Lu, C., & Tian, H. (2017). Global nitrogen and phosphorus fertilizer use for agriculture production in the past half century: Shifted hot spots and nutrient imbalance. *Earth System Science Data*, *9*(1), 181–192. https://doi.org/10.5194/essd-9-181-2017

Lutz, S. R., Ebeling, P., Musolff, A., Van Nguyen, T., Sarrazin, F. J., Van Meter, K. J., Basu, N. B., Fleckenstein, J. H., Attinger, S., & Kumar, R. (2022). Pulling the rabbit out of the hat: Unravelling hidden nitrogen legacies in catchment-scale water quality models. In *Hydrological Processes* (Vol. 3610). John Wiley and Sons Ltd. https://doi.org/10.1002/hyp.14682

Lutz, S. R., Krieg, R., Müller, C., Zink, M., Knöller, K., Samaniego, L., & Merz, R. (2018). Spatial patterns of water age: Using young water fractions to improve the characterization of transit times in contrasting catchments. *Water Resources Research*, *54*(7), 4767–4784. https://doi.org/10.1029/2017WR022216

McGuire, K. J., & McDonnell, J. J. (2006). A review and evaluation of catchment transit time modeling. *Journal of Hydrology*, *330*(3), 543–563. https://doi.org/10.1016/j.jhydrol.2006.04.020

McKay, M. D., Beckman, R. J., & Conover, W. J. (1979). A comparison of three methods for selecting values of input variables in the analysis of output from a computer code. *Technometrics*, *21*(2), 239–245. https://doi.org/10.2307/1268522

Minaudo, C., Dupas, R., Gascuel-Odoux, C., Roubeix, V., Danis, P.-A., & Moatar, F. (2019). Seasonal and event-based concentration-discharge relationships to identify catchment controls on nutrient export regimes. *Advances in Water Resources*, *131*, 103379. https://doi.org/10.1016/j.advwatres.2019.103379

Musolff, A., Fleckenstein, J. H., Rao, P. S. C., & Jawitz, J. W. (2017). Emergent archetype patterns of coupled hydrologic and biogeochemical responses in catchments. *Geophysical Research Letters*, *44*(9), 4143–4151. https://doi.org/10.1002/2017GL072630

Musolff, A., Schmidt, C., Selle, B., & Fleckenstein, J. H. (2015). Catchment controls on solute export. *Advances in Water Resources*, *86*, 133–146. https://doi.org/10.1016/j.advwatres.2015.09.026

Musolff, A., Zhan, Q., Dupas, R., Minaudo, C., Fleckenstein, J. H., Rode, M., Dehaspe, J., & Rinke, K. (2021). Spatial and temporal variability in concentration-discharge relationships at the event scale. *Water Resources Research*, *57*(10), e2020WR029442. https://doi.org/10.1029/2020WR029442

Nguyen, T. V., Kumar, R., Lutz, S. R., Musolff, A., Yang, J., & Fleckenstein, J. H. (2021). Modeling nitrate export from a mesoscale catchment using StorAge selection functions. *Water Resources Research*, *57*(2), e2020WR028490. https://doi.org/10.1029/2020WR028490

Nguyen, T. V., Kumar, R., Musolff, A., Lutz, S. R., Sarrazin, F., Attinger, S., & Fleckenstein, J. H. (2022). Disparate seasonal nitrate export from nested heterogeneous subcatchments revealed with StorAge selection functions. *Water Resources Research*, *58*(3), e2021WR030797. https://doi.org/10.1029/2021WR030797

Nguyen, T. V., Sarrazin, F. J., Ebeling, P., Musolff, A., Fleckenstein, J. H., & Kumar, R. (2022). Toward understanding of long-term nitrogen transport and retention dynamics across German catchments. *Geophysical Research Letters*, *49*(24), e2022GL100278. https://doi.org/10.1029/2022GL100278

Ocampo, C. J., Oldham, C. E., Sivapalan, M., & Turner, J. V. (2006). Hydrological versus biogeochemical controls on catchment nitrate export: A test of the flushing mechanism. *Hydrological Processes*, *20*(20), 4269–4286. https://doi.org/10.1002/hyp.6311

Otero, N., Torrentó, C., Soler, A., Menció, A., & Mas-Pla, J. (2009). Monitoring groundwater nitrate attenuation in a regional system coupling hydrogeology with multi-isotopic methods: The case of plana de Vic (Osona, Spain). *Agriculture, Ecosystems & Environment*, *133*(1), 103–113. https://doi.org/10.1016/j.agee.2009.05.007

Puckett, L. J., Tesoriero, A. J., & Dubrovsky, N. M. (2011). Nitrogen contamination of surficial aquifers—A growing legacy. *Environmental Science & Technology*, *45*(3), 839–844. https://doi.org/10.1021/es1038358

Queloz, P., Carraro, L., Benettin, P., Botter, G., Rinaldo, A., & Bertuzzo, E. (2015). Transport of fluorobenzoate tracers in a vegetated hydrologic control volume: 2. Theoretical inferences and modeling. *Water Resources Research*, *51*(4), 2793–2806. https://doi.org/10.1002/2014wr016508

Rabalais, N. N., Turner, R. E., Dortch, Q., Justic, D., Bierman, V. J., & Wiseman, W. J. (2002). Nutrient-enhanced productivity in the northern Gulf of Mexico: Past, present and future. In E. Orive, M. Elliott, & V. N. de Jonge (Eds.), *Nutrients and eutrophication in estuaries and coastal waters: Proceedings of the 31st symposium of the estuarine and coastal sciences association (ECSA), held in Bilbao, Spain, 3–7 July 2000* (Vol. 475, pp. 39–63). Springer Netherlands. https://doi.org/10.1007/978-94-017-2464-7_4

Rinaldo, A., Benettin, P., Harman, C. J., Hrachowitz, M., McGuire, K. J., van der Velde, Y., Bertuzzo, E., & Botter, G. (2015). Storage selection functions: A coherent framework for quantifying how catchments store and release water and solutes. *Water Resources Research*, *51*(6), 4840–4847. https://doi.org/10.1002/2015WR017273

Rinaldo, A., Beven, K. J., Bertuzzo, E., Nicotina, L., Davies, J., Fiori, A., Russo, D., & Botter, G. (2011). Catchment travel time distributions and water flow in soils. *Water Resources Research*, *47*(7), W07537. https://doi.org/10.1029/2011WR010478

Rode, M., Halbedel Née Angelstein, S., Anis, M. R., Borchardt, D., & Weitere, M. (2016). Continuous in-stream assimilatory nitrate uptake from high-frequency sensor measurements. *Environmental Science & Technology*, *50*(11), 5685–5694. https://doi.org/10.1021/acs.est.6b00943

Rozemeijer, J. C., & Broers, H. P. (2007). The groundwater contribution to surface water contamination in a region with intensive agricultural land use (Noord-Brabant, The Netherlands). *Environmental Pollution*, *148*(3), 695–706. https://doi.org/10.1016/j.envpol.2007.01.028

Samaniego, L., Kumar, R., & Attinger, S. (2010). Multiscale parameter regionalization of a grid-based hydrologic model at the mesoscale. *Water Resources Research*, *46*(5), W05523. https://doi.org/10.1029/2008WR007327

Singleton, M. J., Esser, B. K., Moran, J. E., Hudson, G. B., McNab, W. W., & Harter, T. (2007). Saturated zone denitrification: Potential for natural attenuation of nitrate contamination in shallow groundwater under dairy operations. *Environmental Science & Technology*, *41*(3), 759–765. https://doi.org/10.1021/es061253g

Smakhtin, V. U. (2001). Low flow hydrology: A review. *Journal of Hydrology*, *240*(3), 147–186. https://doi.org/10.1016/S0022-1694(00)00340-1

Smith, J. W. N., Surridge, B. W. J., Haxton, T. H., & Lerner, D. N. (2009). Pollutant attenuation at the groundwater–surface water interface: A classification scheme and statistical analysis using national-scale nitrate data. *Journal of Hydrology*, *369*(3), 392–402. https://doi.org/10.1016/j.jhydrol.2009.02.026

Solomon, C. T., Jones, S. E., Weidel, B. C., Buffam, I., Fork, M. L., Karlsson, J., Larsen, S., Lennon, J. T., Read, J. S., Sadro, S., & Saros, J. E. (2015). Ecosystem consequences of changing inputs of terrestrial dissolved organic matter to lakes: Current knowledge and future challenges. *Ecosystems*, *18*(3), 376–389. https://doi.org/10.1007/s10021-015-9848-y

Soulsby, C., & Tetzlaff, D. (2008). Towards simple approaches for mean residence time estimation in ungauged basins using tracers and soil distributions. *Journal of Hydrology*, *363*(1), 60–74. https://doi.org/10.1016/j.jhydrol.2008.10.001

Steffen, W., Richardson, K., Rockström, J., Cornell, S. E., Fetzer, I., Bennett, E. M., Biggs, R., Carpenter, S. R., de Vries, W., de Wit, C. A., Folke, C., Gerten, D., Heinke, J., Mace, G. M., Persson, L. M., Ramanathan, V., Reyers, B., & Sörlin, S. (2015). Planetary boundaries: Guiding human development on a changing planet. *Science*, *347*(6223), 1259855. https://doi.org/10.1126/science.1259855

Stockinger, M. P., Bogena, H. R., Lücke, A., Diekkrüger, B., Cornelissen, T., & Vereecken, H. (2016). Tracer sampling frequency influences estimates of young water fraction and streamwater transit time distribution. *Journal of Hydrology*, *541*, 952–964. https://doi.org/10.1016/j.jhydrol.2016.08.007

Tetzlaff, D., Soulsby, C., Waldron, S., Malcolm, I. A., Bacon, P. J., Dunn, S. M., Lilly, A., & Youngson, A. F. (2007). Conceptualization of runoff processes using a geographical information system and tracers in a nested mesoscale catchment. *Hydrological Processes*, *21*(10), 1289–1307. https://doi.org/10.1002/hyp.6309

Tiemeyer, B., Lennartz, B., & Kahle, P. (2008). Analysing nitrate losses from an artificially drained lowland catchment (north-eastern Germany) with a mixing model. *Agriculture, Ecosystems & Environment*, *123*(1), 125–136. https://doi.org/10.1016/j.agee.2007.05.006

Tromp-van Meerveld, H. J., & McDonnell, J. J. (2006). Threshold relations in subsurface stormflow: 1. A 147-storm analysis of the Panola hillslope. *Water Resources Research*, *42*(2), W02410. https://doi.org/10.1029/2004WR003778

van der Velde, Y., de Rooij, G. H., Rozemeijer, J. C., van Geer, F. C., & Broers, H. P. (2010). Nitrate response of a lowland catchment: On the relation between stream concentration and travel time distribution dynamics. *Water Resources Research*, *46*(11), W11534. https://doi.org/10.1029/2010WR009105

van der Velde, Y., Torfs, P. J. J. F., van der Zee, S. E. A. T. M., & Uijlenhoet, R. (2012). Quantifying catchment-scale mixing and its effect on time-varying travel time distributions. *Water Resources Research*, *48*(6), W06536. https://doi.org/10.1029/2011WR011310

Van Meter, K. J., & Basu, N. B. (2017). Time lags in watershed-scale nutrient transport: An exploration of dominant controls. *Environmental Research Letters*, *12*(8), 084017. https://doi.org/10.1088/1748-9326/aa7bf4

Van Meter, K. J., Basu, N. B., & Van Cappellen, P. (2017). Two centuries of nitrogen dynamics: Legacy sources and sinks in the Mississippi and Susquehanna River basins. *Global Biogeochemical Cycles*, *31*(1), 2–23. https://doi.org/10.1002/2016GB005498

Van Meter, K. J., Basu, N. B., Veenstra, J. J., & Burras, C. L. (2016). The nitrogen legacy: Emerging evidence of nitrogen accumulation in anthropogenic landscapes. *Environmental Research Letters*, *11*(3), 035014. https://doi.org/10.1088/1748-9326/11/3/035014

Van Meter, K. J., Byrnes, D. K., & Basu, N. B. (2023). Memory and management: Competing controls on long-term nitrate trajectories in U.S, Rivers. *Global Biogeochemical Cycles*, *37*(4), e2022GB007651. https://doi.org/10.1029/2022GB007651

Wade, A. J., Durand, P., Beaujouan, V., Wessel, W. W., Raat, K. J., Whitehead, P. G., Butterfield, D., Rankinen, K., & Lepisto, A. (2002). A nitrogen model for European catchments: INCA, new model structure and equations. *Hydrology and Earth System Sciences*, *6*(3), 559–582. https://doi.org/10.5194/hess-6-559-2002

Wang, Q., Li, S., Jia, P., Qi, C., & Ding, F. (2013). A review of surface water quality models. *The Scientific World Journal*, *2013*, 231768. https://doi.org/10.1155/2013/231768

Wang, Z., Liu, F., Kang, S., & Jensen, C. R. (2012). Alternate partial root-zone drying irrigation improves nitrogen nutrition in maize (Zea mays L.) leaves. *Environmental and Experimental Botany*, *75*, 36–40. https://doi.org/10.1016/j.envexpbot.2011.08.015

Wellen, C., Kamran-Disfani, A.-R., & Arhonditsis, G. B. (2015). Evaluation of the current state of distributed watershed nutrient water quality modeling. *Environmental Science & Technology*, *49*(6), 3278–3290. https://doi.org/10.1021/es5049557

Winter, C., Lutz, S. R., Musolff, A., Kumar, R., Weber, M., & Fleckenstein, J. H. (2021). Disentangling the impact of catchment heterogeneity on nitrate export dynamics from event to long-term time scales. *Water Resources Research*, *57*(1), e2020WR027992. https://doi.org/10.1029/2020WR027992

Winter, C., Tarasova, L., Lutz, S. R., Musolff, A., Kumar, R., & Fleckenstein, J. H. (2022). Explaining the variability in high-frequency nitrate export patterns using long-term hydrological event classification. *Water Resources Research*, *58*(1), e2021WR030938. https://doi.org/10.1029/2021WR030938

Wollschläger, U., Attinger, S., Borchardt, D., Brauns, M., Cuntz, M., Dietrich, P., Fleckenstein, J. H., Friese, K., Friesen, J., Harpke, A., Hildebrandt, A., Jäckel, G., Kamjunke, N., Knöller, K., Kögler, S., Kolditz, O., Krieg, R., Kumar, R., Lausch, A., … Zacharias, S. (2016). The Bode hydrological observatory: A platform for integrated, interdisciplinary hydro-ecological research within the TERENO Harz/central German lowland observatory. *Environmental Earth Sciences*, *76*(1), 29. https://doi.org/10.1007/s12665-016-6327-5

Yang, J., Heidbüchel, I., Musolff, A., Reinstorf, F., & Fleckenstein, J. H. (2018). Exploring the dynamics of transit times and subsurface mixing in a small agricultural catchment. *Water Resources Research*, *54*(3), 2317–2335. https://doi.org/10.1002/2017WR021896

Yang, J., Heidbüchel, I., Musolff, A., Xie, Y., Lu, C., & Fleckenstein, J. H. (2021). Using nitrate as a tracer to constrain age selection preferences in catchments with strong seasonality. *Journal of Hydrology*, *603*, 126889. https://doi.org/10.1016/j.jhydrol.2021.126889

Yang, J., Wang, Q., Heidbüchel, I., Lu, C., Xie, Y., Musolff, A., & Fleckenstein, J. H. (2022). Effect of topographic slope on the export of nitrate in humid catchments: A 3D model study. *Hydrology and Earth System Sciences*, *26*(19), 5051–5068. https://doi.org/10.5194/hess-26-5051-2022

Yang, X., Jomaa, S., Zink, M., Fleckenstein, J. H., Borchardt, D., & Rode, M. (2018). A new fully distributed model of nitrate transport and removal at catchment scale. *Water Resources Research*, *54*(8), 5856–5877. https://doi.org/10.1029/2017WR022380

Yang, X., Tetzlaff, D., Soulsby, C., Smith, A., & Borchardt, D. (2021). Catchment functioning under prolonged drought stress: Tracer-aided ecohydrological modeling in an intensively managed agricultural catchment. *Water Resources Research*, *57*(3), e2020WR029094. https://doi.org/10.1029/2020WR029094

Yu, Z., Hu, Y., Gentry, L. E., Yang, W. H., Margenot, A. J., Guan, K., Mitchell, C. A., & Hu, M. (2023). Linking water age, nitrate export regime, and nitrate isotope biogeochemistry in a tile-drained agricultural field. *Water Resources Research*, *59*, e2023WR034948. https://doi.org/10.1029/2023WR034948

Zink, M., Kumar, R., Cuntz, M., & Samaniego, L. (2017). A high-resolution dataset of water fluxes and states for Germany accounting for parametric uncertainty. *Hydrology and Earth System Sciences*, *21*(3), 1769–1790. https://doi.org/10.5194/hess-21-1769-2017

SUPPORTING INFORMATION

Additional supporting information can be found online in the Supporting Information section at the end of this article.

How to cite this article: Borriero, A., Musolff, A., Kumar, R., Fleckenstein, J. H., Lutz, S. R., & Nguyen, T. V. (2024). The value of instream stable water isotope and nitrate concentration data for calibrating a travel time-based water quality model. *Hydrological Processes*, *38*(5), e15154. https://doi.org/10.1002/hyp.15154

Supplementary Information

The Value of Stable Water Isotope and Nitrate Data for Calibrating a Travel Time based Water Quality Model

Authors: A. Borriero[1,*], A. Musolff[1], R. Kumar[2], J. H. Fleckenstein[1,3], S. R. Lutz[4], T. V. Nguyen[1,*]

[1] Department of Hydrogeology, Helmholtz-Centre for Environmental Research - UFZ, Leipzig, Germany.
[2] Department of Computational Hydrosystems, Helmholtz-Centre for Environmental Research - UFZ, Leipzig, Germany.
[3] Bayreuth Centre of Ecology and Environmental Research, University of Bayreuth, Bayreuth, Germany.
[4] Copernicus Institute of Sustainable Development, Department of Environmental Sciences, Utrecht University, Utrecht, the Netherlands.

***Corresponding author:** A. Borriero (arianna.borriero@ufz.de), Tam V. Nguyen (tam.nguyen@ufz.de);

Text S1: Importance of modeling to reproduce instream $\delta^{18}O$ observations

The observed $\delta^{18}O$ time series was not perfectly simulated in both Experiments 2 and 3. By examining Fig. 4 of the main text, it appears that a straight line could potentially fit the $\delta^{18}O$ data as well as the curved line. To explore this possibility, we conducted an experiment in which we assumed a constant value for the simulated $\delta^{18}O$ over time and calculated the corresponding KGE. For example, using a constant value of the simulated $\delta^{18}O$ of -9.2‰ (the average of the observed $\delta^{18}O$) resulted in a KGE of -0.41. In addition, we tested a range of 100,000 simulated $\delta^{18}O$ constant values within the range of observed $\delta^{18}O$ (-10.5‰ to 8.1‰) and found KGE values consistently between -0.41 and -0.42.

These KGE values were significantly lower than those obtained through the model calibration conducted in our study, which yielded a maximum KGE value of 0.68. Therefore, these results showcase the importance of using a modeling approach to accurately reproduce $\delta^{18}O$ seasonality, rather than relying solely on a straight line to simulate instream $\delta^{18}O$ data.

Text S2: Model's sensitivity to $\delta^{18}O$ values and their seasonality

We tested the sensitivity of the model to $\delta^{18}O$ values and their seasonality by calibrating the model parameters with a synthetic instream $\delta^{18}O$ data set, as a new iteration of Experiment 2. This synthetic time series lacks seasonality as it is derived from randomly selected values a with a normal distribution with a mean of -9.2‰ and a standard deviation of 0.55‰, reflecting the statistical properties of the observed instream $\delta^{18}O$ data. To ensure statistical robustness and generalize our results, we used three separate time series of randomly selected $\delta^{18}O$ values.

Our results highlight the significant influence of $\delta^{18}O$ values and their seasonal patterns on the model results. Calibration using non-seasonal synthetic $\delta^{18}O$ data resulted in inaccuracies, as the model could not accurately reproduce the synthetic instream $\delta^{18}O$ for the three-time series, achieving maximum KGE values of only 0.20, 0.06, and 0.27, respectively These values are well below the KGE of 0.68 obtained with the original $\delta^{18}O$ data set. Simulations based on the synthetic time series with KGE > 0 yielded a total of 945, 73, and 1,743 solutions out of 100,000, resulting in larger 95PPU (Fig. S2 a, b and c) compared to the narrow and seasonal 95PPU observed with the original $\delta^{18}O$ data (Fig S2 d).

Similarly, the calibrated model parameters showed discrepancies between the use of synthetic and original instream $\delta^{18}O$ (Fig. S3). For the three synthetic time series of $\delta^{18}O$, the SAS parameters α and β indicated greater release of old water (i.e. $\alpha \geq 1$ and $\beta < 1$), as shown by the green distribution in Fig. S3. Conversely, using the original $\delta^{18}O$ time series resulted in parameters indicating greater release of young water (i.e. $\alpha < 1$ and $\beta \geq 1$).

Table S1: Summary of the mean statistical characteristics of simulated NO_3^- among all solutions throughout the entire study period, high and low flows, for Experiments 1 and 3, and measurements; values in squared brackets represent the minimum and maximum.

	Experiment 1 (NO_3^-)	Experiment 3 (NO_3^- + $\delta^{18}O$)	Measured NO_3^-
Spearman's rank correlation coefficient [-] (NO_3^- vs. Q)	$\rho = 0.64$ [0.46 — 0.87]	$\rho = 0.56$ [0.46 — 0.69]	$\rho = 0.85$
p-factor of 95PPU [-]	0.64	0.58	-
NO_3^- in high flow [mg/L]	2.64 [0.27 — 5.66]	2.88 [0.27 — 5.66]	3.94 [1.93 — 6.27]
NO_3^- in low flow [mg/L]	0.77 [0 — 4.23]	0.85 [0 — 4.23]	0.45 [0.03 — 1.31]
95PPU in high flow [mg/L]	0.50 [0.3 — 0.95]	0.46 [0.29 — 1.27]	-
95PPU in low flow [mg/L]	2.29 [1.14 — 4.07]	2.96 [0.54 — 6.36]	-

Table S2: Summary of the mean statistical characteristics of TT_{50} among all solutions throughout the entire study period, high and low flows, for Experiments 1, 2, and 3; values in squared brackets represent the minimum and maximum.

	Experiment 1 (NO_3^-)	Experiment 2 ($\delta^{18}O$)	Experiment 3 (NO_3^- + $\delta^{18}O$)
Pearson coefficient [-] (TT_{50} vs. Q)	-0.52 [-0.59 — 0.37]	-0.47 [-0.57 — 0.19]	-0.47 [-0.57 — 0.37]
TT_{50} in study period [d]	116 [0 — 472]	81 [0— 339]	72 [1 — 338]
TT_{50} in high flow [d]	17 [0 — 349]	13 [0 — 28]	4 [0 — 28]
TT_{50} in low flow [d]	247 [0 — 472]	240 [0 — 339]	229 [0 — 337]
TT_{50} before drought [d]	92 [0— 376]	54 [0 — 267]	46 [0— 267]
TT_{50} after drought [d]	139 [0— 472]	108 [0 — 339]	97 [0— 338]

Table S3: Summary of the mean calibrated parameters of the mHM-SAS model utilized in this study for Experiments 1, 2, and 3; values in squared brackets represent the minimum and maximum.

	Experiment 1 (NO_3^-)	Experiment 2 ($\delta^{18}O$)	Experiment 3 ($NO_3^- + \delta^{18}O$)
α [-]	0.24 [0.10 — 0.48]	0.17 [0.10 — 0.25]	0.15 [0.10 — 0.24]
β [-]	1.93 [0.48 — 2.96]	2.01 [0.54 — 2.97]	1.97 [0. 56 — 2.98]
k [d^{-1}]	0.02 [0.005 — 0.07]	-	0.03 [0.007 — 0.09]
S^{soil}_0 [mm]	-	360 [302 — 455]	361 [302 — 453]
S^{sub}_0 [mm]	725 [510 — 982]	719 [509 — 982]	704 [510 — 973]

Table S4: Matrix of Pearson correlation coefficients between pairs of calibrated mHM-SAS parameters used in this study.

Exp. 1.	**α**	**β**	**k**	**S^{soil}_0**	**S^{sub}_0**
α	1	0.41	-0.43	0.005	-0.15
β	0.41	1	0.04	0.03	0.006
k	-0.43	-0.04	1	0.06	0.007
S^{soil}_0	0.005	0.03	0.06	1	0.04
S^{sub}_0	-0.15	0.006	0.007	0.04	1
Exp. 2	**α**	**β**	**k**	**S^{soil}_0**	**S^{sub}_0**
α	1	0.34	-	-0.39	-0.09
β	0.34	1	-	0.19	0.07
k	-	-	-	-	-
S^{soil}_0	-0.39	0.19	-	1	-0.1
S^{sub}_0	-0.09	0.07	-	-0.1	1
Exp. 3	**α**	**β**	**k**	**S^{soil}_0**	**S^{sub}_0**
α	1	0.38	-0.23	-0.37	-0.13
β	0.38	1	0.1	0.17	0.08
k	-0.23	0.01	1	0.18	0.07
S^{soil}_0	-0.37	0.17	0.18	1	-0.03
S^{sub}_0	-0.13	0.08	0.07	-0.03	1

Table S5: Summary of the mean statistical characteristics of Da_{50} among all solutions during high and low flows, for Experiments 1 and 3; values in squared brackets represent the minimum and maximum.

	Experiment 1 (NO_3^-)	Experiment 3 (NO_3^- + $\delta^{18}O$)
Da_{50} in the study period [-]	2.1 [0 — 23.2]	2.2 [0 — 28.3]
Da_{50} in high flow [-]	0.23 [0 — 3.9]	0.12 [0 — 2.5]
Da_{50} in low flow [-]	5.2 [0 — 23.2]	7.1 [0 — 28.3]
Spearman's rank correlation coefficient [-] (Da_{50} vs. Q)	-0.79 [-0.94 — -0.45]	-0.82 [-0.94 — -0.56]

Table S6: Summary of the mean statistical characteristics of N balance in the subsoils, for Experiments 1 and 3; values in squared brackets represent the minimum and maximum; negative values of changes of N storage indicate that final N in storage is less than initial N in storage.

	Experiment 1 (NO_3^-)	Experiment 3 (NO_3^- + $\delta^{18}O$)
N input from infiltration [kg/ha/year]	7.67	7.67
N denitrified [kg/ha/year]	4 [2.45 – 4.91]	3.64 [2.47 – 4.87]
N exported to stream [kg/ha/year]	3.7 [2.72 – 5.22]	4.02 [2.76 – 5.22]
N changes in storage [kg/ha]	-0.31 [-1.71 – 0.49]	0.09 [-0.9 – 0.49]

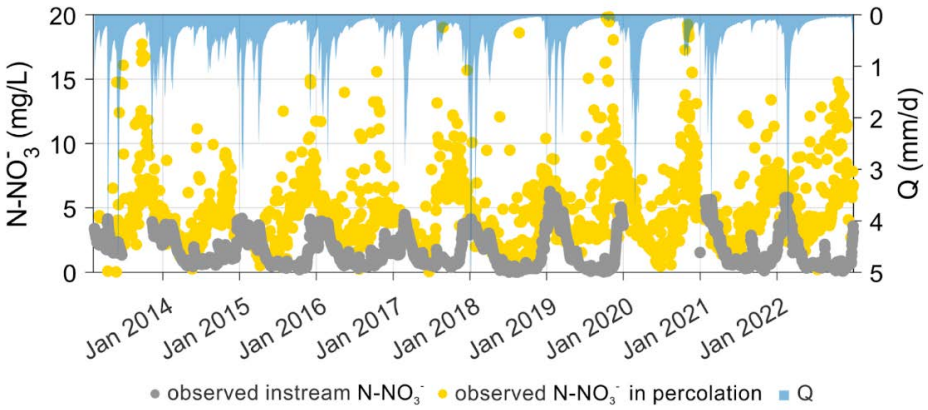

Fig. S1: Measured daily instream NO_3^- as grey circles and simulated daily NO_3^-, percolating from soil to subsoil, as yellow circles; the dark blue area is the streamflow time series.

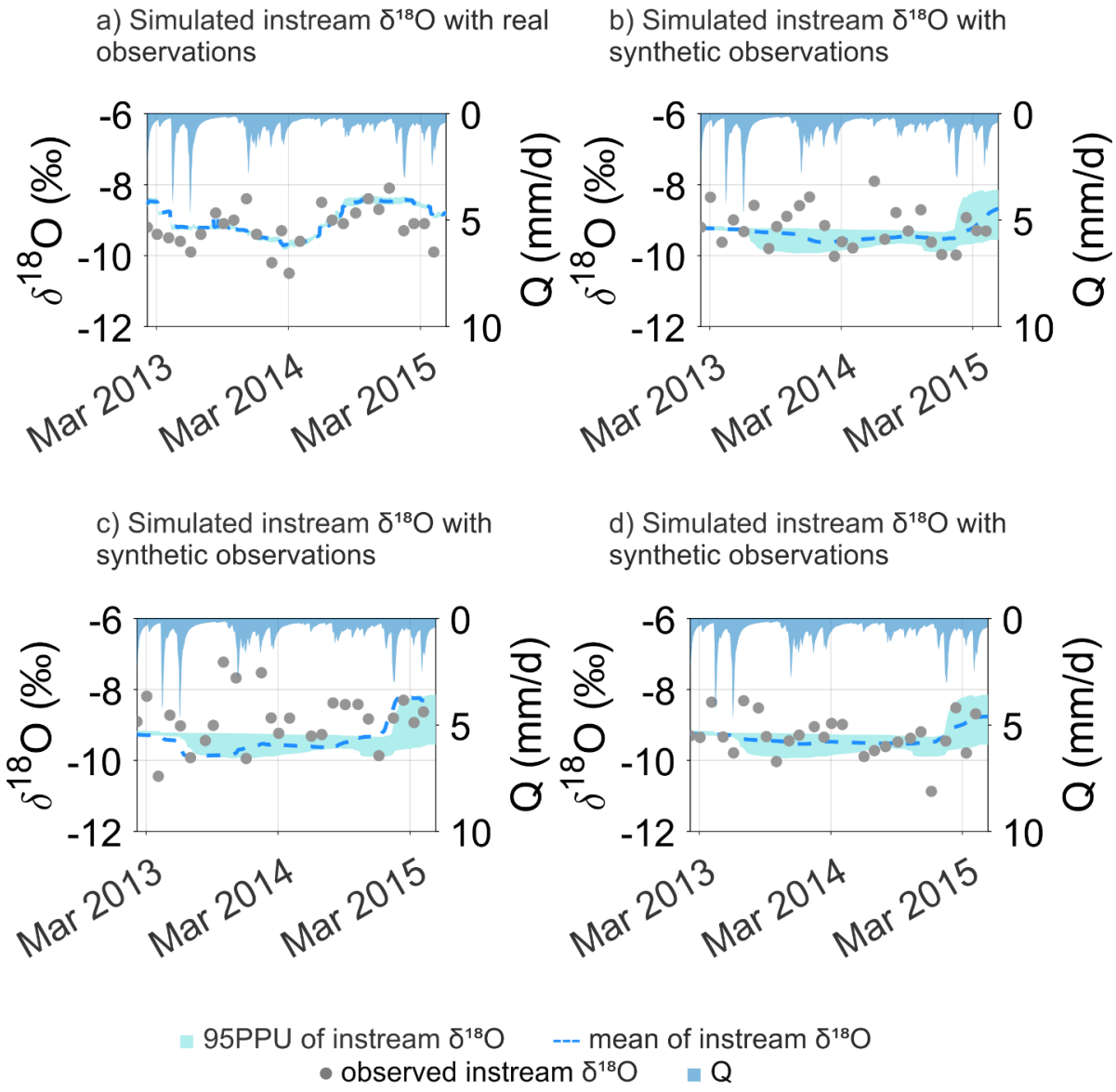

Fig S2: 95PPU of simulated monthly instream δ¹⁸O for Experiment 2: (a) 945, (b) 73, (c) 1,743, and (d) 1,706 simulations; grey circles represent synthetic (a, b, and c) and original (d) observed

instream $\delta^{18}O$ data; the dashed line is the ensemble mean derived from all solutions; the dark blue area is the streamflow time series.

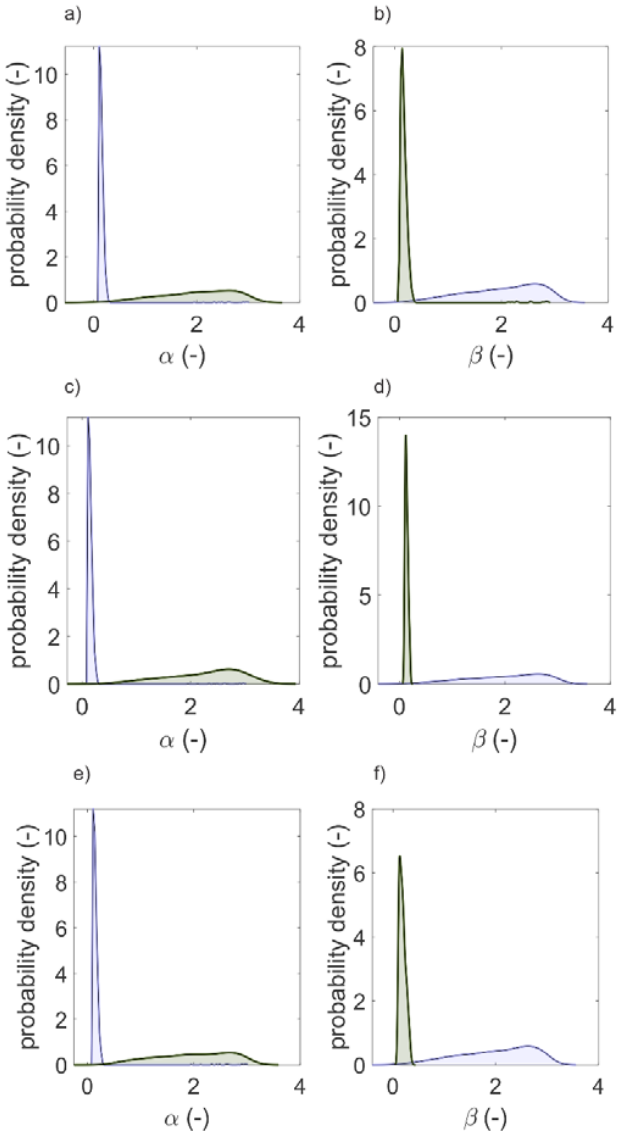

Fig S3: Kernel distributions of transport-related mHM-SAS parameters. Blue distributions stand for parameters calibrated using the original instream $\delta^{18}O$ data, while green distributions stand for synthetic $\delta^{18}O$ data. For the green distributions, panels (a)-(b) show results for 945 simulations, (c)-(d) for 73 simulations, and (e)-(f) for 1,743 simulations. The y-axis represents the probability per unit value of the mHM-SAS parameters. Note that the kernel probability on the x-axis extends

beyond the dataset limits due to the sum effect of individual Gaussian probability distributions applied to each value in the dataset.

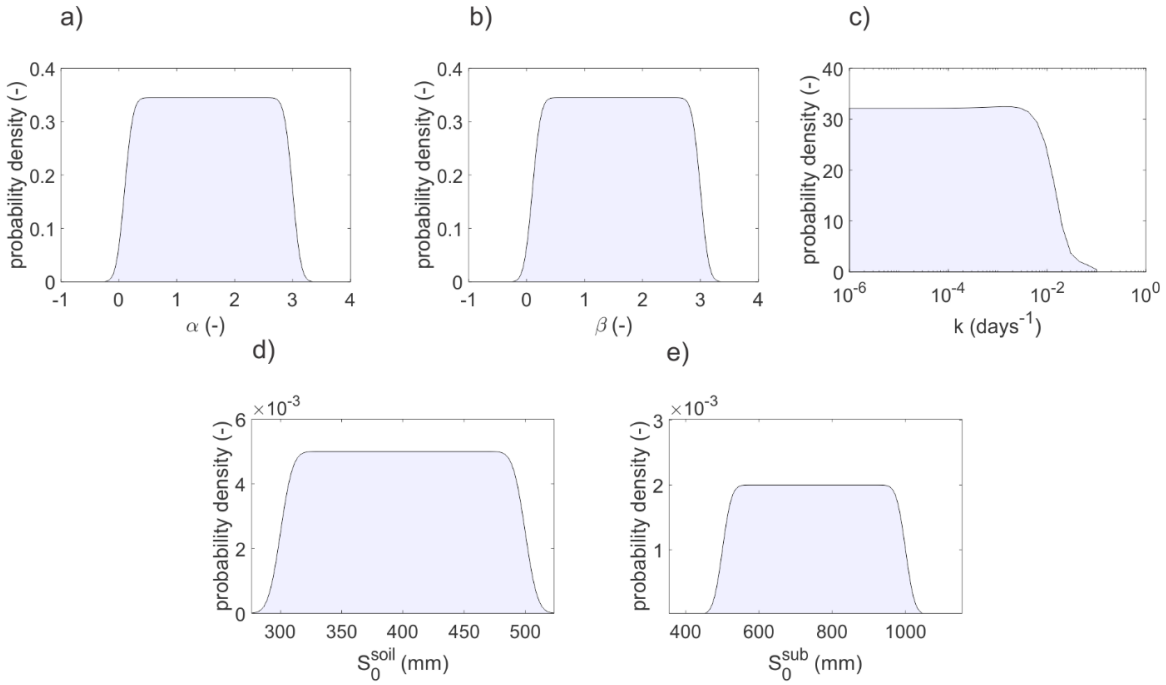

Fig. S4: Kernel distribution of the 100,000 mHM-SAS parameters, which are uniform distributions. The x-axis for k in the subsoil (panel c) is expressed in a logarithmic scale for better displaying small values. The y-axis represents the probability per unit value of the mHM-SAS parameters. Note that the kernel probability on the x-axis extends beyond the dataset limits due to the sum effect of individual Gaussian probability distributions applied to each value in the dataset.

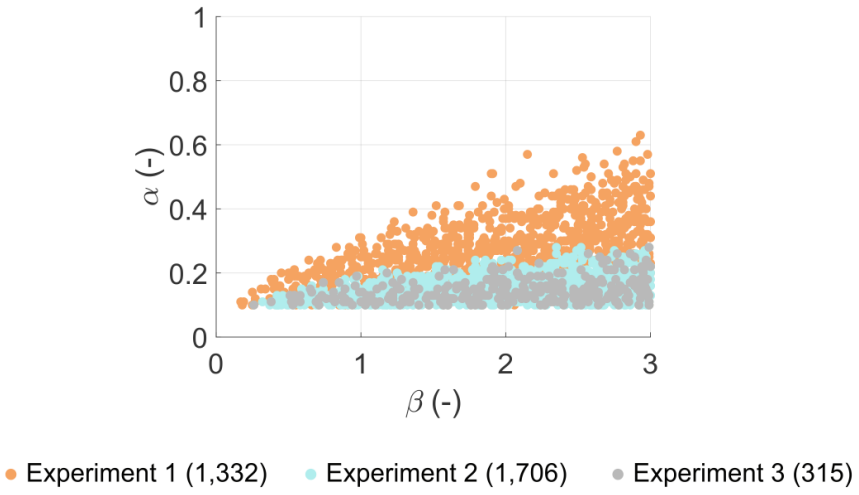

Fig. S5: Relation between α and β in Experiment 1, 2 and 3 with 1,332, 1,706 and 315 simulations, respectively.

List of publications

Publications included in this thesis

Borriero, A., Kumar, R., Nguyen, T. V., Fleckenstein, J. H., Lutz, S. R. (2023), 'Uncertainty in water transit time estimation with StorAge Selection functions and tracer data interpolation', *Hydrology and Earth System Sciences* 27, 2989–3004. https://doi.org/10.5194/hess-27-2989-2023

Borriero, A., Musolff, A., Kumar R., Fleckenstein, J. H., Lutz, S. R., Nguyen, T. V. (2024), 'The Value of Instream Stable Water Isotope and Nitrate Concentration Data for Calibrating a Travel-Time based Water Quality Model', *Hydrological Processes* 38, e15154. https://doi.org/10.1002/hyp.15154

Borriero, A., Nguyen, T. V., Lutz, S. R., Fleckenstein, J. H., Musolff, A., Lutz, S. R., Kumar R.(2024), 'Can the young water fraction reduce predictive uncertainty in water transit time estimations?', *Journal of Hydrology* 65, 132238. https://doi.org/10.1016/j.jhydrol.2024.132238

Data products published in repositories

Borriero, A, Kumar, R., Nguyen, T. V., Fleckenstein, J. H., Lutz, S. R. (2022), 'Hydroclimatic and isotope data - Upper Selke [Data set], Zenodo'. https://doi.org/10.5281/zenodo.8121108

(Eidesstattliche) Versicherungen und Erklärungen

(§ 8 Satz 2 Nr. 3 PromO Fakultät)

Hiermit versichere ich eidesstattlich, dass ich die Arbeit selbstständig verfasst und keine anderen als die von mir angegebenen Quellen und Hilfsmittel benutzt habe (vgl. Art. 97 Abs. 1 Satz 8 BayHIG).

(§ 8 Satz 2 Nr. 3 PromO Fakultät)

Hiermit erkläre ich, dass ich die Dissertation nicht bereits zur Erlangung eines akademischen Grades eingereicht habe und dass ich nicht bereits diese oder eine gleichartige Doktorprüfung endgültig nicht bestanden habe.

(§ 8 Satz 2 Nr. 4 PromO Fakultät)

Hiermit erkläre ich, dass ich Hilfe von gewerblichen Promotionsberatern bzw. –vermittlern oder ähnlichen Dienstleistern weder bisher in Anspruch genommen habe noch künftig in Anspruch nehmen werde.

(§ 8 Satz 2 Nr. 7 PromO Fakultät)

Hiermit erkläre ich mein Einverständnis, dass die elektronische Fassung der Dissertation unter Wahrung meiner Urheberrechte und des Datenschutzes einer gesonderten Überprüfung unterzogen werden kann.

(§ 8 Satz 2 Nr. 8 PromO Fakultät)

Hiermit erkläre ich mein Einverständnis, dass bei Verdacht wissenschaftlichen Fehlverhaltens Ermittlungen durch universitätsinterne Organe der wissenschaftlichen Selbstkontrolle stattfinden können.

…….
Ort, Datum, Unterschrift